PhD Thesis

Biomechanical study of the suture-affected area of the meniscal horn in the context of root detachment repairs

Doctoral Programme in:

Mechanical Engineering and Energy Efficiency

Technical School of Industrial Engineering

2024

Author

ALEJANDRO PEÑA TRABALÓN

Supervisors

MARÍA PRADO NÓVOA

ANA MARÍA PÉREZ DE LA BLANCA COBOS

University of Málaga

Department of Mechanical Engineering and Fluid Mechanics

PhD Thesis

2024

Biomechanical study of the suture-affected area of the meniscal horn in the context of root detachment repairs

THESIS

submitted in fulfillment of the requirements for the degree of

Doctor of Philosophy

in Mechanical Engineering and Energy Efficiency

Author: Alejandro Peña Trabalón

Supervisors: María Prado Nóvoa

Ana María Pérez de la Blanca Cobos

AUTOR: Alejandro Peña Trabalón

https://orcid.org/0000-0002-4291-317X

EDITA: Publicaciones y Divulgación Científica. Universidad de Málaga

DECLARACIÓN DE AUTORÍA Y ORIGINALIDAD DE LA TESIS PRESENTADA PARA OBTENER EL TÍTULO DE DOCTOR

D. Alejandro Peña Trabalón

Estudiante del programa de doctorado de Ingeniería Mecánica y Eficiencia Energética de la Universidad de Málaga, autor de la tesis, presentada para la obtención del título de doctor por la Universidad de Málaga, titulada *Biomechanical study of the suture-affected area of the meniscal horn in the context of root detachment repairs.*

Realizada bajo la tutorización de María Prado Nóvoa y dirección de María Prado Nóvoa y Ana María Pérez de la Blanca Cobos.

DECLARO QUE:

La tesis presentada es una obra original que no infringe los derechos de propiedad intelectual ni los derechos de propiedad industrial u otros, conforme al ordenamiento jurídico vigente (Real Decreto Legislativo 1/1996, de 12 de abril, por el que se aprueba el texto refundido de la Ley de Propiedad Intelectual, regularizando, aclarando y armonizando las disposiciones legales vigentes sobre la materia), modificado por la Ley 2/2019, de 1 de marzo.

Igualmente asumo, ante a la Universidad de Málaga y ante cualquier otra instancia, la responsabilidad que pudiera derivarse en caso de plagio de contenidos en la tesis presentada, conforme al ordenamiento jurídico vigente.

Doctorando:	Tutora:
Directoras:	

AUTORIZACIÓN DE LECTURA

Dª María Prado Nóvoa y Dª Ana María Pérez de la Blanca Cobos, Titulares de la Universidad de Málaga, en calidad de directores

CERTIFICAN:

Que las publicaciones que avalan la tesis de Alejandro Peña Trabalón, titulada *Biomechanical study of the suture-affected area of the meniscal horn in the context of root detachment repairs*, no han sido utilizadas en tesis anteriores; y que ha alcanzado los objetivos de investigación propuestos, estando debidamente cualificada para su defensa.

Directora y tutora de la tesis:	Directora de la tesis:

Málaga, a 17 de octubre de 2024

Acknowledgements

The completion of this work would not have been possible without the support and help of all the people I have shared these past few years with.

First of all, I would like to thank my thesis supervisors, María Prado and Ana Pérez, for all the support they have given me throughout this thesis. Both have been a source of inspiration with their immense dedication to research, as well as a wellspring of knowledge that illuminated the way when it was most needed. Thank you so much for all the hours you have spent helping this project move forward and for the confidence you had that everything would turn out well.

I would particularly like to thank Belén for her ability to always have a smile, to make laugh and to be ready to help when needed. I am looking forward to more skating sessions where we can skate for more than 5 minutes at a time!

Special thanks goes to thank Salvador for being an ideal companion on this journey called a thesis. Thank you so much for being there when I needed you and for all the support you have given me. I look forward to seeing what the future holds for us, and don't worry, I will keep asking you to help me making beautiful figures.

You both have been the best colleagues I could have asked for. Thank you for making the endless hours of lab testing more enjoyable and for creating a safe environment where there was no lack of laughter and trust, forging a beautiful friendship. Without you, I would not have made it through this process as well as I am now.

I would like to thank Fernando Nadal for his concern for our physical health, ensuring that we didn't spend all our time just sitting and waiting for a finite element model to produce coherent results. Thank you for all the "rutas" and "no rutas", and for the ones still to come. Don't worry, we'll always take a detour when needed to see some moss.

I also want to thank the rest of the members of the Mechanical Engineering Area who, at one time or another, contributed to the success of this thesis. A special mention goes to Juanma, for his ability to solve machine problems in seconds that would be impossible for the rest of us, and to Conchi, for her pleasant

morning chats before starting the experiments. Don't worry, we won't show you any human feet!

I would like to extend my thanks to Dr. Andreas Martin Seitz for welcoming me into his laboratory and allowing me to spend a productive and enriching international stay at the University of Ulm. This experience has been invaluable, both professionally and personally.

A big thank you to the team of orthopedic surgeons involved in BIOCLINA, especially Dr. Alejandro Espejo Baena and Dr. Alejandro Espejo Reina, whose ability to think of new challenges and research ideas to improve patients' quality of life is an endless source of inspiration. I also appreciate their willingness to come to the lab whenever necessary.

I would like to thank all my friends who have supported me over the years, and especially in these last few months, for making me laugh and helping me unwind when I needed it most.

And finally, I would like to dedicate this thesis to my family, especially my mother, for her trust, support and patience during this time, as well as for putting up with me in the hardest moments, when even I could not bear myself.

Summary

This thesis is developed within the PhD Program in Mechanical Engineering and Energy Efficiency, in its research line of Mechanical and Materials Engineering, and more specifically in the subline of New Surgical Methods Studies.

The development of the research has been framed within the project “Design of the fixation for meniscal transplantation without bone plugs and with natural biomechanics: NaturFix” (Grant agreement RTI2018-094339-B-IO0) funded by the Spanish State R+D+i Program Oriented to the Challenges of Society of the State Plan for Scientific and Technical Research and Innovation (PEICTI), and the project “Modeling the Sutured Meniscus Oriented to Meniscal Root Reconstruction” (Grant agreement UMA20-FEDERJA-116) funded by the Andalusian Plan for R+D+i in the Operational Programme FEDER Andalusia.

In addition, funding has been received from the Ministry of Science, Innovation and Universities of the Government of Spain through the University Teacher Training Programme (FPU) in the 2020 call for the formalization of a pre-doctoral contract (FPU20/05445) during the completion of this doctoral thesis.

The research described in Chapter 6 was conducted in collaboration with the Institute of Orthopaedic Research and Biomechanics at the University of Ulm (Germany) during the student's internship, under the supervision of PD Dr. Andreas Martin Seitz.

The work has been mainly carried out in the Clinical Biomechanics Laboratory of Andalusia (BIOCLINA), which has established a framework of collaboration between specialists from the Orthopedic Surgery and Traumatology Service of Clinica Espejo, the Vithas hospital group and the TEP-140 group (Mechanical Engineering Malaga) of the Andalusian Research Plan composed of members of the Mechanical Engineering Area of the University of Malaga.

Dr. Espejo's observations on the incidence of meniscal root tears and the need to improve the surgical technique motivated the interest in contributing to enhance the scientific knowledge on the mechanical behavior of the sutured meniscal horn subjected to physiological loads.

The menisci of the human knee are fibrocartilaginous structures, crescent-shaped in the axial plane with triangular cross section, that are located between the tibia and femur in the lateral and medial compartments. The meniscus plays a fundamental biomechanical role in the functioning and preservation of knee joint. Its presence reduces the contact pressure on the cartilages by distributing forces over larger contact articular surfaces, thus protecting the articular cartilage from excessive wear, and contribute to the knee stability. In addition, the menisci contribute to shock absorption, collaborate in the lubrication of the knee, and participate in its proprioceptive sensitivity.

The attachment of the meniscus occurs through ligamentous elements that retain it in the intraarticular area of the knee. Particularly, anterior and posterior meniscus endings, known as meniscal horns, are attached to the tibial plateau with ligamentous structures called meniscal roots compound of longitudinal fibers that continue circumferential meniscal body fibers.

There is a consensus that meniscal root detachment significantly alters knee biomechanics. These biomechanical changes mainly result in an increase in mean and maximum contact pressures and a decrease in tibiofemoral contact area, with changes in these magnitudes with respect to the healthy condition similar to those observed after total meniscectomy. From a clinical point of view, meniscal root detachments have been found to lead to the early development of some pathologies, such as arthritis and osteoarthritis. In general, the incidence of meniscal injuries leading to total or partial meniscectomy results in more than 1.7 million surgical interventions per year worldwide. Specifically, a direct link has been demonstrated between root injury and the development of osteoarthritis, which lead to knee arthroplasty when it degenerates, at an annual cost of €3,350/patient in end-stage or €8 billion in Europe for patients requiring total arthroplasty. This expenditure is expected to rise by up to 525% by 2030 in Europe. Given the well-documented association between meniscal root avulsion

and undesirable consequences for the knee, the importance of preserving their integrity is widely recognized. Indeed, the current paradigm shifts towards surgical repair. Although promising, the clinical results of these repairs are still not fully satisfactory.

As previously mentioned, surgical treatment has changed from total or partial meniscectomy to meniscal root repair. The repair is currently performed using different techniques that can be classified into two main approaches: transtibial fixation or *in situ* fixation. Both techniques involve suturing the meniscal horn, necessitating puncture of the horn to pass the surgical thread. Transtibial fixation chosen by many clinical specialists, shows moderate clinical results in the medium-long term regarding healing outcomes and proper bone insertion position. *In situ* fixation joins the meniscal horn with the native insertion of the meniscal root in the cortical bone of the tibial plateau using surgical thread and a secured anchor. There are several modifications to this technique, mainly based on the suture anchoring system on the cortical bone and the looping system on the meniscal tissue. The ability of these repairs to restore natural knee joint biomechanics depends on their capacity to maintain the meniscus in a position as close as possible to its anatomical location during the rehabilitation process until healing occurs. This avoids non-physiological displacements which could result in incorrect healing or a position far from the anatomical, making a realistic reconstruction of the meniscal root in its intact state impossible. According to studies assessing the average and maximum contact pressures and the contact area in the tibiofemoral joint compared with both the intact state and the root avulsion state, the biomechanics of the avulsion state are partially improved, although a complete recovery is not yet achieved.

In summary, current techniques for meniscal root repair share the requirement to puncture the meniscal horn to pass the surgical suture. After repair, this suture is responsible for restricting meniscal movement while being subjected to physiological loading, at least until the end of the healing period. At present, no technique has demonstrated the ability to completely restore knee joint biomechanics.

The meniscus-suture interface has been identified as a potentially determinant factor for improving the outcomes of surgical repair although the effects of suture traction directly applied to the tissue on the suture puncture are not well understood. Despite this gap in knowledge, very few studies have focused on analyzing the interaction between meniscal tissue and the suture thread at the suture hole site.

In vitro studies or computational techniques can be used to assess the biomechanical effectiveness of root reconstruction. Most in vitro studies compare specific repair techniques by analyzing differences in displacements, contact pressure distribution, or contact area under subcritical cyclic loading after repair, as well as the resistance of the resultant construct.

This thesis focuses on the comprehensive characterization of the mechanical properties of sutured meniscal horn tissue in the area affected by the suture. It begins with a thorough review of the anatomy, physiology and mechanics of human knee menisci, their connections to other joint elements with an especial focus on the meniscal roots, common meniscal root injuries, and their surgical repair techniques. A review of existing finite element models of the knee and more specially the meniscus is also conducted, highlighting various modelling approaches and the technologies applied in experimental studies used to characterize the models.

The overall objective of this thesis is to contribute to the scientific understanding of the biomechanics of the sutured human meniscal horn, with the specific aim of improving surgical treatments for meniscal root avulsions.

The thesis comprises specific objectives framed in three areas: methodological, proposing and validating experimental methods to quantify material properties of biological soft tissue and specimens; experimental, reporting the value of mechanical properties of meniscal specimens and tissue and evaluating the suitability of the most commonly used surrogate models for human menisci of young patients; and computational, assessing the impact on finite element simulations of the experimentally obtained values based on the proposed methodologies.

The specific objectives of this thesis are:

1. To develop a methodology, using a porcine model, for characterizing the resistance and deformation of sutured meniscal horns in the suture area in the early postoperative period when subjected to suture-induced traction in the direction of their circumferential fibers.

2. To determinate the tensile properties to describe the behavior of sutured meniscal horns around the suture area in the early postoperative period subjected to isolated suture-generated traction loads in the circumferential direction for three models: a human model including only menisci from donors within the age range typically eligible for meniscal root repair, a porcine model and an older human model, both of which are the most commonly used surrogates for the first.

3. To evaluate the impact of the age on the deformation and mechanical resistance of meniscal horn tissue in the suture-interface surroundings.

4. To assess the suitability of using porcine models and older human models as surrogates for human models of the age group routinely eligible for meniscal root repair, in the context of studies on surgical techniques for meniscal root repair.

5. To determine the compressive properties of sutured meniscal horn tissue around the suture area in a human model in the early postoperative period, under two loading conditions: pure axial compression, the standard testing method, and axial compression combined with circumferential traction, which represents the physiological stress state. Additionally, to analyze the impact of circumferential traction on the tissue's compressive properties.

6. To quantify, using a finite element model of a sutured human meniscal horn subjected to axial compression and suture-induced traction, the benefits of using material properties at the suture area derived from test conducted under the same physiological loading condition.

The first issue addressed in this research is the development of a robust methodology to mechanically characterize the sutured meniscal horns in the suture-affected area when subjected to circumferential tensile loads. The methodology is designed to quantify both tissue-level properties, such as the stress-strain curve at the hole area and the stress that initiates the cut-out, and specimen-level properties, such as the force required to initiate tearing at the suture hole. The methodology is initially applied to a porcine model with the twofold purposes: to validate the process and to obtain the mechanical properties of this commonly used surrogate for human meniscal models

Once the experimental methodology is fully developed, the thesis expands its scope to human specimens, specifically analyzing the impact of age on the mechanical properties of the sutured meniscal horn tissue and sutured meniscal specimens. Menisci are classified according to the age of the donors into three groups: young ($\leq$55 years old), middle-aged (between 56 and 75 years old), and older ($>$75 years old), and significant differences between groups are explored to investigate how age affects the mechanical response of the sutured meniscus, particularly in the context of surgical repair. This analysis aims to assess whether, from a biomechanical perspective, it would be advisable to routinely extend the age range of patients eligible for meniscal root repair beyond 55 years. This decision has recently been recommended by clinical researchers to prevent the well-known undesirable consequences of avulsion, though biomechanical data supporting the success of these interventions are currently lacking.

A comparison is also made between the mechanical properties in the suture-affected area of porcine and older human meniscal horns versus younger human menisci. This study aims to evaluate whether porcine or older human models can serve as effective surrogates for in vitro studying meniscal repair in younger patients. The use of these surrogate models is common in research because of their much greater availability, as well as cost reduction.

The second issue addressed in this thesis focuses on quantifying the axial compressive properties of the meniscal horn around the suture hole using unconfined indentation tests. Compressive properties are computed in two indentation test layouts: pure axial compression, the standard test method, and

compression combined with circumferential traction, which represents the physiological stress state. Compressive properties as the maximum force during indentation, the instantaneous modulus, the relaxation modulus and the stress relaxation percentage are computed, and the shift in these properties caused by the inclusion of circumferential loading in the test is assessed. Additionally, possible correlations between circumferential tensile and axial compressive properties are investigated.

Finally, a computational finite element model of a sutured meniscal horn is developed, incorporating the properties obtained experimentally. The model is developed to study the improvement in predictions that can be achieved by adjusting the axial compressive modulus to that obtained in indentation tests that reproduce the simulated loading conditions, specifically with or without the inclusion of circumferential traction combined with compressive loads.

The main conclusions derived from the experimental works performed by subjecting the menisci to traction load-to-failure tests in the direction of their circumferential fibers can be summarized as follows:

- At the tissue level, meniscal horns from individuals over 75 years old demonstrate increased elasticity and decreased tissue resistance to cut-out at the suture hole compared to those from younger specimens.

- At the specimen level, aging is associated with a thickening of the meniscal horns which may influence the overall mechanical performance of the menisci in the context of root surgical repair. Indeed, menisci from donors over 75 years old show comparable resistance to younger specimens, in terms of the force necessary to initiate tearing and the maximum force in a load-to-failure test, probably due to the fact that this age-related thickening compensates for the decreased tissue resistance.

Regarding the suitability of porcine or older human models as a surrogate for the human meniscus at the age considered routinely eligible for root surgical repair, this thesis has concluded that:

- Neither porcine nor cadaveric menisci from donors over 75 years old serve as an accurate overall model for replicating the behavior of the adult human meniscus under the age of 75. Differences in elasticity, thickness,

and resistance limit the ability of these models to accurately represent the mechanical properties of younger human menisci, and each model offers advantages depending on the study's objectives.

- The older human meniscus is a more appropriate surrogate for investigating the resistance of sutured meniscal root at the specimen level, particularly in relation to cut-out resistance.

- The porcine model provides a more accurate representation around the suture site of deformation-related properties at the tissue level.

After subjecting human meniscus samples to experimental pure unconfined indentation tests and indentation tests that included suture-induced tensile loads in the circumferential direction, it can be stated that:

- The compressive properties of the sutured human meniscal horns are significantly affected by the presence of circumferential tensile loads.

- The maximum force during relaxation, the instantaneous modulus, and the relaxation modulus more than double their values when suture-induced traction is involved in the test compared to the unloaded condition.

- No differences are observed in the compressive properties when suture-induced circumferential traction is applied at different load levels exceeding those corresponding to the toe region of the stress-strain curve obtained in traction load-to-failure tests in the direction of their circumferential fibers.

- No correlation is found between the compressive and tensile properties studied.

The main conclusions derived from the development and validation of the computational model of sutured meniscus can be summarised as follows:

- Computational simulations show that the compressive behavior of the tissue around the suture hole under combined axial compression and suture-generated circumferential traction, is more accurately predicted with material models that use compressive properties obtained from

indentation tests involving suture traction, rather than from pure axial compression tests.

Resumen

Esta tesis se desarrolla dentro del Programa de Doctorado en Ingeniería Mecánica y Eficiencia Energética, en su línea de investigación de Ingeniería Mecánica y de Materiales, y más concretamente en la sublínea de Estudios de Nuevos Métodos Quirúrgicos.

El desarrollo de la investigación se ha enmarcado dentro del proyecto «Diseño de la fijación para trasplante meniscal sin tapones óseos y con biomecánica natural: NaturFix» (Convenio de subvención RTI2018-094339-B-IO0) financiado por el Programa Estatal de I+D+i Orientada a los Retos de la Sociedad del Plan Estatal de Investigación Científica y Técnica y de Innovación (PEICTI), y el proyecto "Modelado del menisco suturado orientado a la reconstrucción de la raíz meniscal" (Convenio de subvención UMA20-FEDERJA-116) financiado por el Plan Andaluz de I+D+i del Programa Operativo FEDER Andalucía.

Además, se ha recibido financiación del Ministerio de Ciencia, Innovación y Universidades del Gobierno de España a través del Programa de Formación del Profesorado Universitario (FPU) en la convocatoria 2020 para la formalización de un contrato predoctoral (FPU20/05445) durante la realización de esta tesis doctoral.

La investigación descrita en el capítulo 6 se llevó a cabo en colaboración con el Instituto de Investigación Ortopédica y Biomecánica de la Universidad de Ulm (Alemania) durante las prácticas del estudiante, bajo la supervisión del PD Dr. Andreas Martin Seitz.

El trabajo se ha desarrollado principalmente en el Laboratorio de Biomecánica Clínica de Andalucía (BIOCLINA), que ha establecido un marco de colaboración entre especialistas del Servicio de Cirugía Ortopédica y Traumatología de la Clínica Espejo, el grupo del hospital Vithas y el grupo TEP-140 (Ingeniería Mecánica Málaga) del Plan Andaluz de Investigación integrado por miembros del Área de Ingeniería Mecánica de la Universidad de Málaga.

Las observaciones del Dr. Espejo sobre la incidencia de roturas de la raíz meniscal y la necesidad de mejorar la técnica quirúrgica motivaron el interés por contribuir a mejorar el conocimiento científico sobre el comportamiento mecánico del cuerno meniscal suturado sometido a cargas fisiológicas.

Los meniscos de la rodilla humana son estructuras fibrocartilaginosas, con una forma que recuerda a una media luna cuando se observan en el plano axial y una sección transversal triangular. Están ubicados entre la tibia y el fémur, en los compartimentos lateral y medial de la rodilla. El menisco desempeña un papel biomecánico crucial para el correcto funcionamiento y la conservación de la articulación de la rodilla. Su presencia reduce de manera significativa la presión de contacto sobre los cartílagos, ya que distribuye las fuerzas sobre superficies articulares más amplias, protegiendo de esta forma el cartílago articular frente a un desgaste excesivo. Al mismo tiempo, los meniscos contribuyen a mejorar la estabilidad general de la rodilla, una función clave en el movimiento diario. Además de todo lo anterior, tienen un rol importante en la absorción de impactos, lo que ayuda a proteger la articulación durante actividades de alta carga, como caminar, correr o saltar. También participan activamente en la lubricación de la articulación de la rodilla, lo que facilita el movimiento suave entre las superficies articulares, y son parte esencial en la sensibilidad propioceptiva, contribuyendo a la capacidad del cuerpo para percibir la posición de la rodilla en el espacio.

La fijación de los meniscos dentro de la articulación se lleva a cabo a través de elementos ligamentosos. Estos ligamentos mantienen los meniscos en su lugar dentro de la zona intraarticular de la rodilla. Específicamente, las terminaciones anterior y posterior de los meniscos, que se conocen como cuernos meniscales, están ancladas a la meseta tibial mediante unas estructuras ligamentosas llamadas raíces meniscales. Estas raíces están compuestas por fibras longitudinales que son una continuación directa de las fibras circunferenciales del cuerpo meniscal, lo que les otorga una gran resistencia para soportar las fuerzas de carga que atraviesan la articulación de la rodilla durante el movimiento.

Existe un amplio consenso en la literatura médica acerca de las graves consecuencias biomecánicas que tiene el desprendimiento de la raíz meniscal. Este tipo de lesión altera de manera notable la biomecánica de la rodilla. Los cambios derivados se traducen principalmente en un aumento de las presiones de contacto medias y máximas sobre las superficies articulares, así como en una disminución del área de contacto tibiofemoral. Dichos cambios son similares a los observados en pacientes que han sido sometidos a una meniscectomía total. Desde el punto de vista clínico, se ha constatado que los desprendimientos de las raíces meniscales

están estrechamente relacionados con el desarrollo precoz de enfermedades degenerativas de la rodilla, tales como la artritis y la artrosis.

En términos generales, las lesiones meniscales, que muchas veces derivan en meniscectomías parciales o totales, son responsables de más de 1,7 millones de intervenciones quirúrgicas cada año en todo el mundo. Específicamente, se ha demostrado que existe una relación directa entre la lesión de la raíz meniscal y el desarrollo progresivo de artrosis. Este proceso degenerativo a menudo conduce a la necesidad de una artroplastia de rodilla, una intervención que tiene un costo promedio anual de 3.350 euros por paciente en fases avanzadas o terminales, y representa un gasto de 8.000 millones de euros en Europa para los pacientes que requieren una artroplastia total. Se prevé que este costo aumente hasta un 525% de aquí al año 2030 en Europa.

Dada la fuerte asociación entre la avulsión de la raíz meniscal y las consecuencias negativas para la articulación de la rodilla, la preservación de su integridad ha cobrado gran importancia en la actualidad. De hecho, el paradigma médico actual se inclina claramente hacia la reparación quirúrgica de estas lesiones. Sin embargo, aunque las técnicas y los resultados clínicos son prometedores, los resultados no siempre son completamente satisfactorios.

Como ya se ha mencionado, el tratamiento quirúrgico ha pasado de la meniscectomía total o parcial a la reparación de la raíz meniscal. Actualmente, la reparación se realiza mediante diferentes técnicas que pueden clasificarse en dos enfoques principales: fijación transtibial o fijación *in situ*. Ambas técnicas implican la sutura del cuerno meniscal, lo que requiere la punción del cuerno para pasar el hilo quirúrgico. La fijación transtibial, elegida por muchos especialistas clínicos, muestra resultados clínicos moderados a medio-largo plazo en lo que respecta a los resultados de cicatrización y a la posición adecuada de inserción del hueso. La fijación *in situ* une el cuerno meniscal con la inserción nativa de la raíz meniscal en el hueso cortical de la meseta tibial mediante hilo quirúrgico y un anclaje asegurado. Existen varias modificaciones de esta técnica, basadas principalmente en el sistema de anclaje de la sutura en el hueso cortical y el sistema de bucle en el tejido meniscal. La capacidad de estas reparaciones para restablecer la biomecánica natural de la articulación de la rodilla depende de su capacidad para mantener el menisco en una posición lo más cercana posible a su ubicación anatómica durante el proceso de rehabilitación hasta que se produce la cicatrización. De este modo se evitan desplazamientos no fisiológicos que podrían dar lugar a una cicatrización incorrecta o a una posición alejada de la anatómica, imposibilitando una reconstrucción realista de la raíz meniscal en su estado intacto. Según los estudios que evalúan las presiones de contacto medias y

máximas y el área de contacto en la articulación tibiofemoral en comparación tanto con el estado intacto como con el estado de avulsión de la raíz, la biomecánica del estado de avulsión mejora parcialmente, aunque todavía no se consigue una recuperación completa.

En resumen, las técnicas actuales de reparación de la raíz meniscal comparten el requisito de perforar el cuerno meniscal para pasar la sutura quirúrgica. Tras la reparación, esta sutura se encarga de restringir el movimiento del menisco mientras está sometido a carga fisiológica, al menos hasta el final del periodo de cicatrización. En la actualidad, ninguna técnica ha demostrado la capacidad de restaurar completamente la biomecánica de la articulación de la rodilla.

La interfaz menisco-sutura se ha identificado como un factor potencialmente determinante para mejorar los resultados de la reparación quirúrgica, aunque no se conocen bien los efectos de la tracción de la sutura aplicada directamente sobre el tejido en la punción de la sutura. A pesar de esta laguna en el conocimiento, muy pocos estudios se han centrado en analizar la interacción entre el tejido meniscal y el hilo de sutura en el lugar del orificio de sutura.

Para evaluar la eficacia biomecánica de la reconstrucción de la raíz pueden utilizarse estudios in vitro o técnicas computacionales. La mayoría de los estudios in vitro comparan técnicas de reparación específicas analizando las diferencias en los desplazamientos, la distribución de la presión de contacto o el área de contacto bajo carga cíclica subcrítica tras la reparación, así como la resistencia de la construcción resultante.

Esta tesis se centra en la caracterización de las propiedades mecánicas del tejido del cuerno meniscal suturado en la zona afectada por la sutura. Comienza con una revisión de la anatomía, fisiología y mecánica de los meniscos de la rodilla humana, sus conexiones con otros elementos articulares con especial atención a las raíces meniscales, las lesiones comunes de las raíces meniscales y sus técnicas de reparación quirúrgica. También se realiza una revisión de los modelos de elementos finitos existentes de la rodilla y más especialmente del menisco, destacando diversos enfoques de modelado y las tecnologías aplicadas en los estudios experimentales utilizados para caracterizar los modelos.

El objetivo general de esta tesis es contribuir a la comprensión científica de la biomecánica del cuerno meniscal humano suturado, con el fin específico de mejorar los tratamientos quirúrgicos de las avulsiones de la raíz meniscal.

La tesis comprende objetivos específicos enmarcados en tres áreas: metodológica, proponiendo y validando métodos experimentales para cuantificar propiedades materiales de tejidos blandos y especímenes biológicos; experimental, reportando el valor de las propiedades mecánicas de especímenes y tejidos meniscales y evaluando la idoneidad de los modelos sustitutos más comúnmente utilizados para meniscos humanos de pacientes jóvenes; y computacional, evaluando el impacto en simulaciones de elementos finitos de los valores obtenidos experimentalmente en base a las metodologías propuestas.

Los objetivos específicos de esta tesis son:

1. Desarrollar una metodología, utilizando un modelo porcino, para caracterizar la resistencia y deformación de los cuernos meniscales suturados en la zona de sutura en el postoperatorio precoz cuando son sometidos a tracción inducida por sutura en la dirección de sus fibras circunferenciales.

2. Determinar las propiedades de tracción para describir el comportamiento de los cuernos meniscales suturados alrededor de la zona de sutura en el postoperatorio temprano sometidos a cargas de tracción aisladas generadas por sutura en la dirección circunferencial para tres modelos: un modelo humano que incluya únicamente meniscos de donantes dentro del rango de edad típicamente elegible para la reparación de la raíz meniscal, un modelo porcino y un modelo humano de mayor edad, ambos los sustitutos más utilizados para el primero.

3. Evaluar el impacto de la edad en la deformación y la resistencia mecánica del tejido del cuerno meniscal en el entorno de la interfaz de sutura.

4. Evaluar la idoneidad de utilizar modelos porcinos y modelos humanos de edad avanzada como sustitutos de los modelos humanos del grupo de edad habitualmente elegible para la reparación de la raíz meniscal, en el contexto de los estudios sobre técnicas quirúrgicas para la reparación de la raíz meniscal.

5. Determinar las propiedades compresivas del tejido del cuerno meniscal suturado alrededor de la zona de sutura en un modelo humano en el período postoperatorio temprano, en dos condiciones de carga: compresión axial

pura, el método de ensayo estándar, y compresión axial combinada con tracción circunferencial, que representa el estado de tensión fisiológica. Además, analizar el impacto de la tracción circunferencial en las propiedades compresivas del tejido.

6. Cuantificar, mediante un modelo de elementos finitos de un cuerno meniscal humano suturado sometido a compresión axial y tracción inducida por sutura, las ventajas de utilizar las propiedades del material en la zona de sutura derivadas de ensayos realizados en las mismas condiciones fisiológicas de carga.

La primera cuestión abordada en esta investigación es el desarrollo de una metodología robusta para caracterizar mecánicamente los cuernos meniscales suturados en la zona afectada por la sutura cuando se someten a cargas de tracción circunferenciales. La metodología está diseñada para cuantificar tanto las propiedades a nivel de tejido, como la curva de tensión-deformación en la zona del orificio y la tensión que inicia el corte, como las propiedades a nivel de espécimen, como la fuerza necesaria para iniciar el desgarro en el orificio de sutura. La metodología se aplica inicialmente a un modelo porcino con un doble propósito: validar el proceso y obtener las propiedades mecánicas de este sustituto comúnmente utilizado para los modelos de menisco humano.

Una vez que la metodología experimental está plenamente desarrollada, la tesis amplía su alcance a especímenes humanos, analizando específicamente el impacto de la edad en las propiedades mecánicas del tejido del cuerno meniscal suturado y de los especímenes meniscales suturados. Los meniscos se clasifican en función de la edad de los donantes en tres grupos: jóvenes (≤55 años), de mediana edad (entre 56 y 75 años) y mayores (75 años), y se exploran las diferencias significativas entre grupos para investigar cómo afecta la edad a la respuesta mecánica del menisco suturado, especialmente en el contexto de la reparación quirúrgica. Este análisis pretende evaluar si, desde una perspectiva biomecánica, sería aconsejable ampliar de forma rutinaria el rango de edad de los pacientes elegibles para la reparación de la raíz meniscal más allá de los 55 años. Esta decisión ha sido recomendada recientemente por investigadores clínicos para prevenir las conocidas consecuencias no deseadas de la avulsión, aunque en la actualidad no se tiene constancia de datos biomecánicos que respalden el éxito de estas intervenciones.

También se realiza una comparación entre las propiedades mecánicas en la zona afectada por la sutura de cuernos meniscales porcinos y humanos de edad avanzada frente a meniscos humanos más jóvenes. Este estudio pretende evaluar si los modelos porcinos o humanos más antiguos pueden servir como sustitutos eficaces para estudiar in vitro la reparación meniscal en pacientes más jóvenes. El uso de estos modelos sustitutos es habitual en investigación debido a su mayor disponibilidad, así como a la reducción de costes.

La segunda cuestión abordada en esta tesis se centra en la cuantificación de las propiedades de compresión axial del cuerno meniscal alrededor del orificio de sutura mediante ensayos de indentación no confinados. Las propiedades compresivas se calculan en dos disposiciones de ensayo de indentación: compresión axial pura, el método de ensayo estándar, y compresión combinada con tracción circunferencial, que representa el estado de tensión fisiológico. Se calculan las propiedades compresivas como la fuerza máxima durante la indentación, el módulo instantáneo, el módulo de relajación y el porcentaje de relajación de la tensión, y se evalúa el cambio en estas propiedades causado por la inclusión de la carga circunferencial en la prueba. Además, se investigan las posibles correlaciones entre las propiedades de tracción circunferencial y compresión axial.

Finalmente, se desarrolla un modelo computacional de elementos finitos de un cuerno meniscal suturado, incorporando las propiedades obtenidas experimentalmente. El modelo se desarrolla para estudiar la mejora en las predicciones que se puede conseguir ajustando el módulo de compresión axial al obtenido en ensayos de indentación que reproduzcan las condiciones de carga simuladas, concretamente con o sin la inclusión de tracción circunferencial combinada con cargas compresivas.

Las principales conclusiones derivadas de los trabajos experimentales realizados sometiendo a los meniscos a ensayos de carga a tracción en la dirección de sus fibras circunferenciales pueden resumirse como sigue:

- A nivel tisular, los cuernos meniscales de individuos mayores de 75 años demuestran una mayor elasticidad y una menor resistencia tisular al corte en el orificio de sutura en comparación con los de especímenes más jóvenes.

- A nivel de la muestra, el envejecimiento se asocia con un engrosamiento de los cuernos meniscales que puede influir en el rendimiento mecánico

general de los meniscos en el contexto de la reparación quirúrgica de la raíz. De hecho, los meniscos de donantes de más de 75 años muestran una resistencia comparable a la de los especímenes más jóvenes, en términos de la fuerza necesaria para iniciar el desgarro y la fuerza máxima en una prueba de carga hasta el fallo, probablemente debido a que este engrosamiento relacionado con la edad compensa la menor resistencia del tejido.

En cuanto a la idoneidad de los modelos porcinos o humanos de edad avanzada como sustitutos del menisco humano a la edad considerada habitualmente apta para la reparación quirúrgica de la raíz, esta tesis ha llegado a las siguientes conclusiones:

- Ni los meniscos porcinos ni los cadavéricos de donantes mayores de 75 años sirven como modelo global preciso para replicar el comportamiento del menisco humano adulto menor de 75 años. Las diferencias de elasticidad, grosor y resistencia limitan la capacidad de estos modelos para representar con exactitud las propiedades mecánicas de los meniscos humanos más jóvenes, y cada modelo ofrece ventajas en función de los objetivos del estudio.

- El menisco humano más viejo es un sustituto más apropiado para investigar la resistencia de la raíz meniscal suturada a nivel de espécimen, particularmente en relación con la resistencia al corte.

- El modelo porcino proporciona una representación más precisa alrededor del lugar de sutura de las propiedades relacionadas con la deformación a nivel tisular.

Tras someter muestras de menisco humano a ensayos experimentales de indentación pura no confinada y a ensayos de indentación que incluían cargas de tracción inducidas por sutura en la dirección circunferencial, puede afirmarse que:

- Las propiedades compresivas de los cuernos meniscales humanos suturados se ven significativamente afectadas por la presencia de cargas de tracción circunferenciales.

- La fuerza máxima durante la relajación, el módulo instantáneo y el módulo de relajación duplican con creces sus valores cuando en el ensayo interviene

la tracción inducida por la sutura, en comparación con la condición sin carga.

- No se observan diferencias en las propiedades de compresión cuando se aplica tracción circunferencial inducida por sutura a diferentes niveles de carga que superan los correspondientes a la región de la puntera de la curva tensión-deformación obtenida en los ensayos de carga a tracción en la dirección de sus fibras circunferenciales.

- No se encuentra correlación entre las propiedades de compresión y tracción estudiadas.

Las principales conclusiones derivadas del desarrollo y validación del modelo computacional de menisco suturado pueden resumirse como sigue:

- Las simulaciones computacionales muestran que el comportamiento compresivo del tejido alrededor del orificio de sutura bajo compresión axial combinada y tracción circunferencial generada por la sutura, se predice con mayor precisión con modelos de materiales que utilizan propiedades compresivas obtenidas a partir de ensayos de indentación que implican tracción de la sutura, en lugar de a partir de ensayos de compresión axial pura.

Contents

Acknowledgements v

Summary ix

Resumen xix

1. Introduction 1

1.1 Problem statement 1

1.2 Objectives of the Thesis 4

1.3 Structure of the Thesis 6

1.4 Development framework 8

1.5 References 9

2. Fundamentals 17

2.1 Human knee menisci 17

2.1.1 Anatomical and physiological description 19

2.1.2 Kinematic behaviour 23

2.1.3 Histological composition of meniscal tissue 25

2.2 Meniscal root lesions 27

2.2.1 Classification of meniscal root tears 27

2.2.2 Surgical repair of meniscal root tears 29

2.2.2.1 Repair techniques 30

2.2.2.2 Characteristics of suture materials for menischal root repair 31

2.2.3 The impact of meniscal root tears on knee biomechanics 32

2.3 Mechanical properties of the meniscus 34

2.3.1 Mechanical properties of meniscal tissue 36

2.3.2 Mechanical properties of meniscal roots 39

2.3.3 Mechanical properties of the repaired meniscal root 40

2.4 Computational models of human meniscus 42
2.4.1 Meniscus models in FE models of the knee joint....42
2.4.2 Inverse meniscal tissue material modelling with finite element simulations 43
2.4.3 Meniscus properties in computational models of the knee 45
2.5 Testing machines....46
2.5.1 Universal testing machines 46
2.5.1.1 Universal testing machine at BIOCLINA 46
2.5.1.1.1 General description 47
2.5.1.1.2 Characteristics of measurement systems 49
2.5.1.1.3 Characteristics of the control system 50
2.5.1.2 Universal testing machines at Institute of Orthopaedic Research and Biomechanics of the University of Ulm 50
2.5.1.2.1 Uniaxial testing machine....50
2.5.1.2.2 Indentation tests machine 52
2.6 Videogrammetric system 53
2.6.1 Image capture system....54
2.6.2 Tracking algorithm....55
2.7 References 57

3. Experimental study of circumferential tensile properties in meniscal horns around the sutured area: Application to a porcine model 77
3.1 Introduction 78
3.2 Materials and methods 79
3.2.1 Specimen preparation....80
3.2.2 Biomechanical testing....81
3.2.3 Load-to-failure analysis 84
3.3 Results....85
3.4 Discussion....87

3.5 Conclusions 92
3.6 References 92

4. Analysis of circumferential tensile properties in sutured human meniscal horns: Impact of age 99
4.1 Introduction 99
4.2 Materials and methods 100
4.2.1 Specimen preparation 100
4.2.2 Biomechanical testing 103
4.2.3 Load-to-failure analysis 106
4.2.4 Statistical analyses 107
4.3 Results 108
4.3.1 Meniscal horn thickness at the suture point, h 108
4.3.2 Meniscal cut-out force, $\boldsymbol{Fc}$ 110
4.3.3 Meniscal ultimate force, Fu 111
4.3.4 Tissue cut-out resistance, Sc 113
4.3.5 Tissue equivalent stiffness modulus, m_s 115
4.4 Discussion 117
4.5 Conclusions 122
4.6 References 123

5. Evaluating porcine and older human models as surrogates for studying resistance and deformation in young human sutured meniscal horns 127
5.1 Introduction 127
5.2 Materials and methods 129
5.2.1 Statistical analyses 130
5.3 Results 131
5.3.1 Meniscal horn thickness at the suture point, h 131
5.3.2 Meniscal cut-out force, Fc 132

5.3.3 Meniscal ultimate force, Fu 132
5.3.4 Tissue cut-out resistance, Sc 133
5.3.5 Tissue equivalent stiffness modulus, m_s 134
5.4 Discussion 136
5.5 Conclusions 139
5.6 References 139

6. Analysis of compressive properties in sutured human meniscal horn tissue using unconfined indentation: Impact of physiological loads .. 145
6.1 Introduction 146
6.2 Materials and methods 146
6.2.1 Specimen preparation 147
6.2.2 Biomechanical testing 148
6.2.2.1 Indentation test 148
6.2.2.2 Load-to-failure test 153
6.2.3 Stress-relaxation analysis 154
6.2.4 Load-to-failure analysis 156
6.2.5 Statistical analysis 157
6.3 Results 157
6.3.1 Maximum indentation force, F 158
6.3.2 Instantaneous modulus, IM 159
6.3.3 Relaxation modulus, E_{t20} 159
6.3.4 Relaxation stress percentage, $\Delta\sigma_{relax}$ 160
6.3.5 Compressive – tensile properties relationship 161
6.4 Discussion 164
6.5 Conclusions 170
6.6 References 171

7. Improved computational prediction of sutured meniscus behavior under combined axial and circumferential loading: Importance of experimental conditions in compression material properties 177

7.1 Introduction 178

7.2 Materials and methods 179

7.2.1 Development of the Finite Element models 180

7.2.2 Computational indentation test analysis 183

7.3 Results 184

7.3.1 Computational results 184

7.4 Discussion 186

7.5 Conclusions 188

7.6 References 188

8. Conclusions and Future Works 195

8.1 Conclusions of the thesis 195

8.2 Future works 197

APPENDIX A. Results of Chapter 3 203

A.1 Geometrical data of the specimens 203

A.2 Results of the load-to-failure test 204

A.3 Load-displacement curves 205

A.4 Stress-strain curves 205

APPENDIX B. Results of Chapter 4 207

B.1 Geometrical data of the specimens 207

B.2 Results of the load-to-failure test 209

B.3 Load-displacement curves 212

B.4 Stress-strain curves 213

APPENDIX C. Results of Chapter 6 215

C.1 Geometrical data of the specimens 215

C.2 Results of the indentation test 216

C.3 Results of the load-to-failure test 219

C.4 Load-displacement curves 220

C.5 Stress-strain curves 221

APPENDIX D. Results of Chapter 7 223

D.1 Results of the indentation test 223

D.2 Results of the computational modelling 223

APPENDIX E. Dissemination of the thesis results 227

E.1 Publication in Q1: Age influence on resistance and deformation of the human sutured meniscal horn in the immediate postoperative period 227

E.2 Publication in Q1: Assessment of surrogate models for research on resistance and deformation of repairs of the human meniscal roots: Porcine or older human models? 229

E.3 Contribution to an international congress: 27th Congress of the European Society of Biomechanics (ESB), 26 - 29 June 2022, Porto, Portugal. 231

E.4 Contribution to an international congress: XV Iberoamerican Congress of Mechanical Engineering (CIBIM), 22 - 24 November 2022, Madrid, Spain. . 233

E.5 Contribution to an international congress: 28th Congress of the European Society of Biomechanics (ESB), 9 - 12 July 2023, Maastricht, Netherlands. 235

E.6 Contribution to a national congress: XII Spanish Chapter of the European Society of Biomechanics (ESB), 2 - 3 November 2023, Málaga, Spain. 237

E.7 Contribution to an international congress: 29th Congress of the European Society of Biomechanics (ESB), 30 - 3 July 2024, Edinburgh, Scotland 239

E.8 Contribution to an international congress: 29th Congress of the European Society of Biomechanics (ESB), 30 - 3 July 2024, Edinburgh, Scotland 241

Figures

Chapter 2

Figure 2.1. Representation of human menisci in the human knee between the tibia and femur: a) anatomical view (L: Lateral; M: Medial; P: Posterior; A: Anterior); b) MRI view. 18

Figure 2.2. Load distribution in knee joint contact: a) with the presence of the menisci; b) without menisci.. 18

Figure 2.3. Representation of the lateral and medial meniscus on the tibial plateau with differentiation of the three zones into which it is divided. Green: anterior horn; Blue: posterior horn; Red: Central body 20

Figure 2.4. Human menisci with their meniscal roots on the tibial plate of a left knee. LMAR: Lateral Meniscus Anterior Root; LMPR: Lateral Meniscus Posterior Root; MMAR: Medial Meniscus Anterior Root; MMPR: Medial Meniscus Posterior Root; ACL: Anterior Cruciate Ligament; PCL: Posterior Cruciate Ligament; AIML: Anterior Intermeniscal Ligament 20

Figure 2.5. Representation of additional ligaments that provide stability and regulate the mobility of the meniscus. LM: Lateral Meniscus; MM: Medial Meniscus; ACL: Anterior Cruciate Ligament; PCL: Posterior Cruciate Ligament; AIM: Anterior Intermeniscal Ligament; MCL: Medial Collateral Ligament; aMFL: Anterior Menisco-Femoral Ligament; pMFL: Posterior Menisco-Femoral Ligament.....21

Figure 2.6. Representation of the insertions and junctions of the meniscotibial and meniscofemoral ligaments with the medial meniscus. MF: Meniscofemoral Ligament; MT: Meniscotibial ligament; MTP: Medial Tibial Plateau; MM: Medial Meniscus; MFC: Medial Femoral Condyle.. 22

Figure 2.7. Representation of the attachment of the Popliteofibular Ligament (PFL) to the lateral meniscus (LM). The collateral ligament (FCL) is also observed.....23

Figure 2.8. Application of axial loads on the meniscus by the femur and transformation of these into radial forces that contribute to the extrusion of the meniscus towards the outside of the joint.....24

Figure 2.9. Distribution of collagen fibers in the meniscus, representing the fibers in circumferential direction, in radial direction and the area with an irregular distribution.. 25

Figure 2.10. Distribution of collagen fibers and interaction with the rest of the elements that make up the ECM......26

Figure 2.11. Classification of meniscal root tears according to LaPrade et al. 2015 27

Figure 2.12. Representation of the types of meniscal root detachment repair by suturing. a) *In situ* fixation; b) Transtibial fixation. 30

Figure 2.13. Representation of the different test configurations, test modes and biomechanical properties obtained from each test.. 35

Figure 2.14. Finite Element Model of the knee joint including the menisci and their interaction with tibial and femoral cartilage, considering the bony elements as rigid.....42

Figure 2.15. Uniaxial testing machine designed in the Clinical Biomechanics Laboratory of Andalusia and used for the load-to-failure tests performed.....47

Figure 2.16. Lower part of the machine structure of BIOCLINA: a) CPU; b) Control panel.....48

Figure 2.17. Uniaxial testing machine available at the Institute of Orthopaedic Research and Biomechanics of the University of Ulm and used for the load-to-failure tests performed. 51

Figure 2.18. Multiaxial testing machine employed in the indentation tests.....52

Figure 2.19. Devices used in the videogrammetric system in BIOCLINA. a) Digital camera with the PENTAX lens; b) Digital camera mounted in the tripod oriented to the uniaxial testing machine.....54

Figure 2.20. Devices used in the videogrammetric system in Ulm laboratory. a) Digital camera; b) Lens used in the tests. 55

Chapter 3

Figure 3.1. Porcine lateral meniscus with a suture thread passing through its horn, simulating a root repair procedure. 81

Figure 3.2. Uniaxial testing machine and videogrammetric system, with the Z axis corresponding to the traction direction and the ZY plane parallel to the image plane.....81

Figure 3.3. a) Porcine meniscus on the testing machine with an indication of the traction direction aligned with the circunferential fibers of the specimen; b) Magnification of the suture hole area with the inked marks and the puncture point shown. 82

Figure 3.4. Testing protocol scheme. 83

Figure 3.5. Curves representing as a function of time during the load to-failure test: a) the distance between Point 1 and Point 2; b) the evolution of traction force. 86

Figure 3.6. Stress-strain curve of a representative porcine sample with a linear fit in the strain range [0-0.3] showing a high lineal behavior. 87

Chapter 4

Figure 4.1. Specimen preparation process: a) sutured meniscal horn with tapered needle; b) sutured meniscal horn placed in the uniaxial testing machine of BIOCLINA; c) placement of the inked marks on the cranial surface of the meniscal horn; d) measurement process using a manual caliper. 102

Figure 4.2. a) Lateral human meniscal horn on the testing machine with an indication of the traction direction aligned with its circunferential fibers; b) Magnification of the suture hole area with the inked marks and the puncture point shown. 105

Figure 4.3. Testing protocol scheme 105

Figure 4.4. Mean and SD of the thickness of the meniscal horns at the suture hole area for each age group. Significant difference: *Young vs. Old.....108

Figure 4.5. Mean and SD of the thickness of the meniscal horns at the suture hole area for each age group at the lateral and medial location. For the groups with significant differences, the percentage difference between means with respect to the oldest group is indicated. Significant difference: *Young vs. Old. 109

Figure 4.6. Mean and SD of the specimen cut-out force for each age group. ...110

Figure 4.7. Mean and SD of the cut-out force of the lateral and medial meniscal horns for each age group.....111

Figure 4.8. Mean and SD of the specimen ultimate force for each age group. . 112

Figure 4.9. Mean and SD of the ultimate force of the lateral and medial meniscal horns for each age group. 112

Figure 4.10. Mean and SD of tissue cut-out resistance of the meniscal horns for each age group. For the groups with significant differences, the percentage difference between means with respect to the oldest group is indicated. Significant difference: *Young vs. Old; & Middle-aged vs. Old. 113

Figure 4.11. Mean and SD of tissue cut-out resistance of the lateral and medial meniscal horns for each age group. For the groups with significant differences, the percentage difference between means with respect to the oldest group is indicated. Significant difference: *Young vs. Old; & Middle-aged vs. Old. 114

Figure 4.12. Stress-strain curves of a representative sample of each age group a linear fit in the strain range [0-0.3]. 115

Figure 4.13. Mean and SD of tissue equivalent stiffness modulus of the meniscal horns for each age group. For the groups with significant differences, the percentage difference between means with respect to the oldest group is indicated. Significant difference: *Young vs. Old; & Middle-aged vs. Old. 116

Figure 4.14. Mean and SD of tissue equivalent stiffness modulus of the lateral and medial meniscal horns for each age group. For the groups with significant differences, the percentage difference between means with respect to the oldest group is indicated. Significant difference: *Young vs. Old; & Middle-aged vs. Old. 117

Chapter 5

Figure 5.1. Mean and SD of the thickness (mm) of the meniscal horns at the suture hole area for each group. For the groups with significant differences with respect to the control group, the percentage difference between means is indicated. * Significant difference from the control group. 131

Figure 5.2. Mean and SD of cut-out force (N) of the meniscal horns. For the groups with significant differences, the percentage difference between means with respect to the control group is indicated. * Significant difference from the control group. 132

Figure 5.3. Mean and SD of ultimate force (N) of the meniscal horns. For the groups with significant differences, the percentage difference between means

with respect to the control group is indicated. * Significant difference from the control group. 133

Figure 5.4. Mean and SD of tissue cut-out resistance (MPa) of the meniscal horns at the suture insertion point area. For the groups with significant differences, the percentage difference between means with respect to the control group is indicated. * Significant difference from the control group..... 134

Figure 5.5. Curves of a representative sample of each group: a) Load-displacement curve for each group; b) Stress-strain curve for each group with a linear fit in the strain range [0-0.3]. 135

Figure 5.6. Mean and SD of tissue equivalent stiffness modulus (MPa) of the meniscal horns at the suture insertion point area. For the groups with significant differences, the percentage difference between means with respect to the control group is indicated. * Significant difference from control group. 136

Chapter 6

Figure 6.1. Sutured meniscal horn following the standard root repair procedure. 147

Figure 6.2. Multiaxial mechanical tester for indentation tests with the human samples: 1) digital camera; 2) load cell; 3) specimen container; 4) custom traction device. 149

Figure 6.3. Custom-designed traction device: 1) fastener; 2) aluminum frame; 3) load cell; 3) steel axis..... 150

Figure 6.4. Setup prepared for recording the traction force induced by the suture using the traction device while the indentation test: a) multiaxial mechanical tester with the traction device connected to the strain indicator and recorder; b) strain indicator and recorder connected to the computer. 150

Figure 6.5. STL model of the custom-designed 3D printed container. 151

Figure 6.6. Sutured meniscal horn placed in the container with the seven measurement point marked on its cranial surface. 152

Figure 6.7. a) Lateral human meniscal horn on the testing machine with an indication of the traction direction aligned with its circunferential fibers; b) Magnification of the suture hole area with the inked marks and the puncture point shown. The seven measurement points used previously in the indentations can be observed. 154

Figure 6.8. Mean and 95% confidence interval of maximum force in the indentation period of sutured meniscal horns at each suture traction level. For significantly different loading conditions, the percentage difference between means relative to the lower level is indicated. Significant difference: *Unloaded vs. 10 N; &Unloaded vs. 20 N. 158

Figure 6.9. Mean and 95% confidence interval of instantaneous modulus of sutured meniscal horns at each suture traction level. For significantly different loading conditions, the percentage difference between means relative to the lower level is indicated. Significant difference: *Unloaded vs. 10 N; & Unloaded vs. 20 N. 159

Figure 6.10. Mean and 95% confidence interval of relaxation modulus at the relaxation time of sutured meniscal horns at each suture traction level. For significantly different loading conditions, the percentage difference between means relative to the lower level is indicated. Significant difference: *Unloaded vs. 10 N; & Unloaded vs. 20 N. 160

Figure 6.11. Mean and 95% confidence interval of relaxation stress percentage of sutured meniscal horns at each suture traction level. 161

Figure 6.12. Load-strain curves of all the tested specimens with a magnification in the strain range ε = [0-0.4] showing the mean values of the forces in the toe zone and the force in $\varepsilon = 0.4$. 162

Figure 6.13. Experimental compressive properties versus the equivalent stiffness modulus : a) maximum force in the indentation period ; b) instantaneous modulus; c) relaxation modulus; d) relaxation stress percentage. 163

Figure 6.14. Variation of the experimental compressive properties from the unloaded state versus the equivalent stiffness modulus: a) maximum force ; b) instantaneous modulus; c) relaxation modulus; d) relaxation stress percentage. 164

Chapter 7

Figure 7.1. Representation of the modelled meniscal horn with the specified boundary conditions. The seven areas where distinct compression modulus were assigned are illustrated: (1) meniscal horn model incorporating the suture hole; (2) modelled indenter tip; (3) suture thread. The blue arrow indicates the direction of traction. The indentation direction matches the Z-axis of the orientation system depicted. 181

Figure 7.2. Meshes of the sutured meniscal horn and the tip of the indenter. A linear elastic axial spring modelled the suture. The blue arrow indicates the traction direction. 181

APPENDIX A

Figure A.1. Load-displacement curves until the initiation of tissue cut-out of all the sutured porcine specimens tested in the load-to-failure test under circumferential traction induced by the suture. 205

Figure A.2. Stress-strain curves with a magnification in $\varepsilon = [0\text{-}0.3]$ of all the sutured porcine specimens tested in the load-to-failure test under circumferential traction induced by the suture. 206

APPENDIX B

Figure B.1. Load-displacement curves until the initiation of tissue cut-out of all the sutured young human specimens tested in the load-to-failure test under circumferential traction induced by the suture. 212

Figure B.2. Load-displacement curves until the initiation of tissue cut-out of all the sutured middle-aged human specimens tested in the load-to-failure test under circumferential traction induced by the suture 212

Figure B.3. Load-displacement curves until the initiation of tissue cut-out of all the sutured old human specimens tested in the load-to-failure test under circumferential traction induced by the suture. 213

Figure B.4. Stress-strain curves with a magnification in $\varepsilon = [0\text{-}0.3]$ of all the sutured young human specimens tested in the load-to-failure test under circumferential traction induced by the suture. 213

Figure B.5. Stress-strain curves with a magnification in $\varepsilon = [0\text{-}0.3]$ of all the sutured middle-aged human specimens tested in the load-to-failure test under circumferential traction induced by the suture. 214

Figure B.6. Stress-strain curves with a magnification in $\varepsilon = [0\text{-}0.3]$ of all the sutured old human specimens tested in the load-to-failure test under circumferential traction induced by the suture. 214

APPENDIX C

Figure C.1. Load-displacement curves until the initiation of tissue cut-out of all the sutured human specimens tested in the load-to-failure test under circumferential traction induced by the suture. 220

Figure C.2. Stress-strain curves with a magnification in $\varepsilon = [0\text{-}0.4]$ of all the sutured human specimens tested in the load-to-failure test under circumferential traction induced by the suture. 221

Tables

Chapter 2

Table 2.1. Mean values of the mechanical properties of the human meniscal roots. 40

Table 2.2. Parameters and test results characterizing repair by different types of sutures. 41

Chapter 3

Table 3.1. Mechanical properties of the porcine meniscal horns at the suture insertion point area....86

Chapter 4

Table 4.1. Main characteristics of the three meniscus groups tested 101

Table 4.2. Main characteristics of the six meniscus groups tested 103

Table 4.3. Thickness (mm) of the meniscal horns at the suture hole area for each age group. 109

Table 4.4. Thickness (mm) of the lateral and medial meniscal horns at the suture hole area for each age group. 110

Table 4.5. Specimen cut-out force (N) for each age group. 110

Table 4.6. Specimen cut-out force (N) of the lateral and medial meniscal horns area for each age group. 111

Table 4.7. Specimen ultimate force (N) for each age group 112

Table 4.8. Specimen ultimate force (N) of the lateral and medial meniscal horns area for each age group. 113

Table 4.9. Tissue cut-out resistance (MPa) for each age group. 114

Table 4.10. Tissue cut-out resistance (MPa) of the lateral and medial meniscal horns sites for each age group. 114

Table 4.11. Tissue equivalent stiffness modulus (MPa) for each age group 116

Table 4.12. Tissue equivalent stiffness modulus (MPa) of the lateral and medial meniscal horns sites for each age group. 117

Chapter 5

Table 5.1. Main characteristics of the three meniscus groups tested. 129

Table 5.2. Meniscus thickness (mm) of the meniscal horn at the sutured area. 131

Table 5.3. Specimen cut-out force (N) of the meniscal horns. 132

Table 5.4. Specimen ultimate force (N) of the meniscal horns..... 133

Table 5.5. Tissue cut-out resistance (MPa) of the meniscal horns at the suture insertion point area..... 134

Table 5.6. Tissue equivalent stiffness modulus (MPa) of the meniscal horns at the suture insertion point area..... 136

Chapter 6

Table 6.1. Non-destructive indentation test conditions. 152

Table 6.2. Maximum indentation force (N) obtained at the three tested suture traction levels. 158

Table 6.3. Instantaneous modulus (MPa) obtained at the three tested suture traction levels. 159

Table 6.4. Relaxation modulus at the relaxation time (MPa) obtained at the three tested suture traction levels..... 160

Table 6.5. Relaxation stress percentage (%) expressed in percentage obtained at the three tested suture traction levels. 161

Chapter 7

Table 7.1. Columns 1 to 7 show IM values from the indentation test at the seven measurement points of the modelled specimen under suture traction levels 0 and 20 N. Column 8 displays mean and SD values of IM pooled for the twenty-seven specimens tested also at both traction levels..... 185

Table 7.2. Errors between experimental and simulated FT values for the four property sets considered. 185

APPENDIX A

Table A.1. Values in mm of the measurements taken for each porcine specimen tested. 203

Table A.2. Values of the specimen cut-out force, Fc; specimen ultimate force, Fu; tissue cut-out resistance, Sc; and tissue equivalent stiffness modulus, ms of all the porcine meniscal horns at the suture insertion point area. 204

APPENDIX B

Table B.1. Values in mm of the measurements taken for each young human specimen tested. 207

Table B.2. Values in mm of the measurements taken for each middle-aged human specimen tested. 208

Table B.3. Values in mm of the measurements taken for each old human specimen tested. 209

Table B.4. Values of the specimen cut-out force, Fc; specimen ultimate force, Fu; tissue cut-out resistance, Sc; and tissue equivalent stiffness modulus, ms of all the young human meniscal horns at the suture insertion point area. 209

Table B.5. Values of the specimen cut-out force, Fc; specimen ultimate force, Fu; tissue cut-out resistance, Sc; and tissue equivalent stiffness modulus, ms of all the middle-aged human meniscal horns at the suture insertion point area. 210

Table B.6. Values of the specimen cut-out force, Fc; specimen ultimate force, Fu; tissue cut-out resistance, Sc; and tissue equivalent stiffness modulus, ms of all the old human meniscal horns at the suture insertion point area. 211

APPENDIX C

Table C.1. Values in mm of the measurements taken for each human specimen tested 215

Table C.2. Values of the maximum indentation force, F; the instantaneous modulus, IM; the relaxation modulus, Et20 and the relaxation stress percentage, Δσrelax of all the human meniscal horns at the suture insertion point area in the unloaded state. 216

Table C.3. Values of the maximum indentation force, F; the instantaneous modulus, IM; the relaxation modulus, Et20 and the relaxation stress percentage,

Δσrelax of all the human meniscal horns at the suture insertion point area under 10 N in the circumferential direction. 217

Table C.4. Values of the maximum indentation force, F; the instantaneous modulus, IM; the relaxation modulus, Et20 and the relaxation stress percentage, Δσrelax of all the human meniscal horns at the suture insertion point area under 20 N in the circumferential direction. 218

Table C.5. Values of the equivalent stiffness modulus, ms; the toe force, Ftoe, and the force achieved at $\varepsilon = 0.4$, $F\varepsilon = 0.4$ of all the human meniscal horns at the suture insertion point area..... 219

APPENDIX D

Table D.1. Values of the maximum indentation force at the three circumferential tensile states of each measurement point in the suture area of the human meniscal horn used for computational modelling. 223

Table D.2. Values of the computational maximum indentation force at the three circumferential tensile states of each measurement point in the suture area of the human meniscal horn used for computational modelling incorporating specimen-specific material compression properties under 0 N of circumferential tensile loading at each indentation location..... 224

Table D.3. Values of the computational maximum indentation force at the three circumferential tensile states of each measurement point in the suture area of the human meniscal horn used for computational modelling incorporating specimen-specific material compression properties under 20 N of circumferential tensile loading at each indentation location..... 224

Table D.4. Values of the computational maximum indentation force at the three circumferential tensile states of each measurement point in the suture area of the human meniscal horn used for computational modelling incorporating the Young´s modulus in axial and radial direction in all the indentation areas as the mean IM under 0 N of circumferential tensile loading derived from the tests on the 27 specimens. 224

Table D.5. Values of the computational maximum indentation force at the three circumferential tensile states of each measurement point in the suture area of the human meniscal horn used for computational modelling incorporating the Young´s modulus in axial and radial direction in all the indentation areas as the

mean IM under 20 N of circumferential tensile loading derived from the tests on the 27 specimens. 225

1

Introduction

1.1 Problem statement

The menisci of the human knee are fibrocartilaginous structures, crescent-shaped in the axial plane with triangular cross section, that are located between the tibia and femur in the lateral and medial compartments. The meniscus plays a fundamental biomechanical role in the functioning and preservation of knee joint. Its presence reduces the contact pressure on the cartilages by distributing forces over larger contact articular surfaces, thus protecting the articular cartilage from excessive wear, and contribute to the knee stability. In addition, the menisci contribute to shock absorption, collaborate in the lubrication of the knee, and participate in its proprioceptive sensitivity (Mow et al., 1999).

The attachment of the meniscus occurs through ligamentous elements that retain it in the intraarticular area of the knee. Particularly, anterior and posterior meniscus endings, known as meniscal horns, are attached to the tibial plateau with ligamentous structures called meniscal roots compound of longitudinal fibers that continue circumferential meniscal body fibers (Johannsen et al., 2012; Villegas et al., 2008; Wang et al., 2009a).

There is a consensus that meniscal root detachment significantly alters knee biomechanics (Espejo-Reina et al., 2022; Perez-Blanca et al., 2016). These biomechanical changes mainly result in an increase in mean and maximum contact pressures and a decrease in tibiofemoral contact area, with changes in these magnitudes with respect to the healthy condition similar to those observed after total meniscectomy (Ode et al., 2012; Perez-Blanca et al., 2016). From a clinical point of view, meniscal root detachments have been found to lead to the early development of some pathologies, such as arthritis and osteoarthritis (Jones et al., 2006)(Bloecker et al., 2015; Ding et al., 2007). In general, the incidence of meniscal injuries leading to total or partial meniscectomy results in more than 1.7 million surgical interventions per year worldwide. Specifically, a direct link has

been demonstrated between root injury and the development of osteoarthritis, which lead to knee arthroplasty when it degenerates, at an annual cost of €3,350/patient in end-stage or €8 billion in Europe for patients requiring total arthroplasty. This expenditure is expected to rise by up to 525% by 2030 in Europe. Given the well-documented association between meniscal root avulsion and undesirable consequences for the knee, the importance of preserving their integrity is widely recognized. Indeed, the current paradigm shifts towards surgical repair. Although promising, the clinical results of these repairs are still not fully satisfactory (Perez-Blanca et al., 2018).

As previously mentioned, surgical treatment has changed from total or partial meniscectomy to meniscal root repair. The repair is currently performed using different techniques (Feucht et al., 2014; Laprade et al., 2015b) that can be classified into two main approaches: transtibial fixation or *in situ* fixation. Both techniques involve suturing the meniscal horn, necessitating puncture of the horn to pass the surgical thread. Transtibial fixation chosen by many clinical specialists (Ahn et al., 2007; Feucht et al., 2013; Kim et al., 2006; LaPrade et al., 2014b; Padalecki et al., 2014; Petersen and Zantop, 2006), shows moderate clinical results in the medium-long term (J. H. Kim et al., 2011; Christopher M LaPrade et al., 2015a) regarding healing outcomes and proper bone insertion position. *In situ* fixation joins the meniscal horn with the native insertion of the meniscal root in the cortical bone of the tibial plateau using surgical thread and a secured anchor (Cuéllar et al., 2017; Laprade et al., 2015b; Petersen et al., 2014). There are several modifications to this technique, mainly based on the suture anchoring system on the cortical bone and the looping system on the meniscal tissue (Balke et al., 2018; Espejo-Reina et al., 2022; Kopf et al., 2011; Zantop et al., 2004). The ability of these repairs to restore natural knee joint biomechanics depends on their capacity to maintain the meniscus in a position as close as possible to its anatomical location during the rehabilitation process until healing occurs. This avoids non-physiological displacements which could result in incorrect healing or a position far from the anatomical, making a realistic reconstruction of the meniscal root in its intact state impossible (Christopher M LaPrade et al., 2015a; Stärke et al., 2010). According to studies assessing the average and maximum contact pressures and the contact area in the tibiofemoral joint compared with both the intact state and the root avulsion state, the biomechanics of the avulsion state are partially improved, although a complete recovery is not yet achieved (Espejo-Reina et al., 2023, 2022; J. H. Kim et al., 2011; Lee et al., 2009; Moon et al., 2010; Seo et al., 2010).

In summary, current techniques for meniscal root repair share the requirement to puncture the meniscal horn to pass the surgical suture. After repair, this suture is responsible for restricting meniscal movement while being subjected to physiological loading, at least until the end of the healing period. At present, no technique has demonstrated the ability to completely restore knee joint biomechanics.

The meniscus-suture interface has been identified as a potentially determinant factor for improving the outcomes of surgical repair (Cerminara et al., 2014; Perez-Blanca et al., 2018) although the effects of suture traction directly applied to the tissue on the suture puncture are not well understood. Despite this gap in knowledge, very few studies have focused on analyzing the interaction between meniscal tissue and the suture thread at the suture hole site (Anz et al., 2014; Kopf et al., 2011; Mitchell et al., 2016; Vertullo et al., 2021).

In vitro studies or computational techniques can be used to assess the biomechanical effectiveness of root reconstruction. Most in vitro studies (Espejo-Reina et al., 2023, 2022; Nakama et al., 2019; Perez-Blanca et al., 2018, 2016; Robinson et al., 2018) compare specific repair techniques by analyzing differences in displacements, contact pressure distribution, or contact area under subcritical cyclic loading after repair , as well as the resistance of the resultant construct.

Computational analysis is a powerful tool for study. When modeling the healthy or repaired meniscus, the geometry is commonly obtained through medical image segmentation, similar to other structures of the knee. Regarding the tissue material model, it can be approached from a phenomenological point of view using energy density functions, in which the meniscus is considered at the macroscopic level. It has been experimentally observed that the meniscus exhibits anisotropic, non-linear, low compressibility and poro-visco-elastic behavior. However, the importance of considering all these effects in the material model depends on the goal of the study as well as the scenario to be studied, i.e., load intensity and dynamic characteristics. To study the joint biomechanics after meniscal root repair, the meniscus model must be integrated into a full knee model, so simpler material models are often used to reduce computational cost. These models typically simulate a homogeneous, linearly elastic and isotropic (Peña et al., 2006) or transversely isotropic (Bao et al., 2013; Zielinska and Haut Donahue, 2006) material. Another approach is the structural one, which takes into account the mechanical characteristics of the micro-constituents in the macro-mechanical response. These approaches, of higher computational cost, typically involve hyperelastic material of isotropic matrix reinforced with collagen fibres in circumferential direction (Zielinska and Haut Donahue, 2006), poro-

elastic (Freutel et al., 2015), and viscoelastic effects (Seyfi et al., 2018). However, in the published literature that assumes negligible viscoelastic effects, the constitutive model that yields the best fit for the meniscus is hyperelastic, characterized by a compressible isotropic matrix reinforced by the anisotropic properties of collagen fibers.

However, very few computational models have addressed the simulation of the biomechanics of the repaired meniscus, and even fewer have focused on sutured meniscal horns (D'lima et al., 2011; Steineman et al., 2020). Moreover, none of these studies specifically models meniscal tissue that has been perforated for suture passage and subjected to tension, either in the context of root reconstruction or repairs in other meniscal regions. The limited published researches incorporate meniscus models that do not account for the tissue-suture interface (Cardoso Gomide et al., 2019).

In conclusion, there is scientific interest in developing computational models of the biomechanical behavior of the sutured meniscal horn, with the aim of improving the effectiveness of surgical interventions for root avulsion repair, which is the recommended treatment according to the current paradigm. However, no known computational model exists for the meniscus repaired with surgical suture that addresses the mechanical characterization of the tissue affected by the suture, a factor that may be determinant for the analysis of the outcome of surgical repairs by suturing. In other words, there is a lack of knowledge about the material model needed to simulate the behavior of the sutured meniscal horn area.

1.2 Objectives of the Thesis

The overall objective of this thesis is to contribute to the scientific understanding of the biomechanics of the sutured human meniscal horn, with the specific aim of improving surgical treatments for meniscal root avulsions.

The thesis comprises specific objectives framed in three areas: methodological, proposing and validating experimental methods to quantify material properties of biological soft tissue and specimens; experimental, reporting the value of mechanical properties of meniscal specimens and tissue and evaluating the suitability of the most commonly used surrogate models for human menisci of young patients; and computational, assessing the impact on finite element

simulations of the experimentally obtained values based on the proposed methodologies.

The specific objectives of this thesis, presented in the order they appear in this document, are:

1. To develop a methodology, using a porcine model, for characterizing the resistance and deformation of sutured meniscal horns in the suture area in the early postoperative period when subjected to suture-induced traction in the direction of their circumferential fibers.

2. To compute tensile properties to describe the behavior of sutured meniscal horns around the suture area in the early postoperative period subjected to isolated suture-generated traction loads in the circumferential direction for three models: a human model including only menisci from donors within the age range typically eligible for meniscal root repair, a porcine model and an older human model, both of which are the most commonly used surrogates for the first.

3. To evaluate the impact of the age on the deformation and mechanical resistance of meniscal horn tissue in the suture-interface surroundings.

4. To assess the suitability of using porcine models and older human models as surrogates for human models of the age group routinely eligible for meniscal root repair, in the context of studies on surgical techniques for meniscal root repair.

5. To compute the compressive properties of sutured meniscal horn tissue around the suture area in a human model in the early postoperative period, under two loading conditions: pure axial compression, the standard testing method, and axial compression combined with circumferential traction, which represents the physiological stress state. Additionally, to analyze the impact of circumferential traction on the tissue's compressive properties.

6. To quantify, using a finite element model of a sutured human meniscal horn subjected to axial compression and suture-induced traction, the benefits of using material properties at the suture area derived from test conducted under the same physiological loading condition.

1.3 Structure of the Thesis

In order to achieve the objectives described in section 1.2, 5 different studies have been carried out, which are detailed in Chapters 3 to 7 of this thesis.

Chapter 2 presents information on the menisci of the human knee and their connections to other joint elements. It then describes meniscal root injuries and the current surgical repair techniques. The chapter also provides an overview of the existing knowledge on the mechanical properties of meniscal tissue and root ligaments. This is followed by a summary of the existing computational models of the meniscus, including those incorporated into models of the complete human knee and those specific to the meniscus. Finally, the equipment used in the experimental studies of this thesis is described, as well as the required technologies.

Chapter 3 focuses on developing a methodology for the characterization of the mechanical properties of the sutured meniscal horn around the suture hole under circumferential tensile loads. This methodology was validated in a porcine model. Mechanical parameters of sutured porcine menisci are studied at both the tissue and the specimen levels. At specimen level, the resistance is evaluated in terms of the force that initiates the tissue tearing and the ultimate force that the specimen is able to withstand. At the tissue level, the stress that initiates the cut-out is computed. The tissue deformation is characterized based on the linearization of the stress-strain curve of the area around the hole. This chapter fulfills specific objective 1 of those listed in section 1.2. of this thesis. In addition, it contributes to specific objectives 2 and 3. In particular, the data required for the completion of specific objective 2 regarding the porcine model are provided, as well as part of the information necessary for the completion of specific objective 4, also in relation to the porcine model.

Chapter 4 focuses on the experimental characterization of the mechanical properties of the sutured meniscal horn around the suture hole under circumferential tensile loads in human specimens. Particularly, the same parameters as in Chapter 3 are analyzed for a human model. In addition, a categorization by age of the donor is established, creating three differentiated groups: young, middle-age, and old. Significant differences between age groups for the mechanical properties calculated for the menisci are sought to assess the possible impact of age on the mechanical behavior of the meniscal suture horn. A

secondary study is conducted to examine the impact of age on the mechanical properties when the meniscal horns from the medial or lateral sites are assessed independently. In addition , the thickness of the meniscal horn in the suture zone is recorded to study its possible role in the impact of donor age on meniscal mechanical properties at specimen level, as previous publications have suggested a thickening of the meniscus with age. This chapter fulfills the specific objective 3 of those listed in section 1.2 of this thesis. The results of this work have been published in "Frontiers in Bioengineering and Biotechnology" (see Appendix E.1), a journal indexed in the 1st quartile (Q1) of the JCR ranking for the year 2023 in its corresponding category. Additionally, in conjunction with the data provided in Chapter 3, it enables the achievement of specific objective 2 and provides the complete set of data necessary to achieve specific objective 4.

Chapter 5 focuses on the comparison between the mechanical properties of the sutured meniscal horn around the suture orifice under circumferential tensile loads in older human and porcine specimens with respect to younger human menisci, in order to establish whether the use of porcine models or older human models can be considered an accurate surrogate of human meniscal horns at an age eligible for routine root repair. Both surrogate models would allow the reduction of the economic cost and facilitate the procurement of samples for testing. This chapter integrates the information provided in Chapters 3 and 4 to complete specific objective 4 listed in section 1.2 . The results of this work have been published in "Applied Sciences" (see Appendix E.2), a journal indexed in the 1st quartile of the JCR ranking for the year 2023 in its corresponding category.

Chapter 6 focuses on the determination of the axial compressive properties of the meniscal horn tissue around the suture hole in human specimens and, especially, the impact of circumferential traction on their values. Axial compression is assessed under two different loading conditions: pure axial compression, and axial compression combined with circumferential traction at two stress levels set by a traction on the suture of 10N and 20N. Compressive properties are computed from unconfined indentation tests, particularly, the maximum force reached during compression, the instantaneous modulus, the relaxation modulus and the stress relaxation percentage are computed for the three stress states. The same circumferential load-to-failure test as in chapters 3 and 4 is also carried out to calculate the equivalent stiffness modulus of the samples submitted to indentation, in order to investigate possible correlations

between tensile and compressive properties. This chapter addresses all the tasks necessary to achieve specific objective 5 listed in section 1.2.

Chapter 7 focuses on the development of a computational model of sutured meniscal horn under the loading situations studied in the previous chapters and with material properties according to the loading state at which they are found. The need to use an instantaneous modulus of compression in the axial direction that varies according to the level of circumferential load applied was also analysed, an aspect that has not been assessed so far in any computational model developed. This chapter addresses the last of the objectives outlined in section 1.2.

Chapter 8 summaries the conclusions of the work carried out and outlines potential future research works to further advance in the overall objective of this dissertation, namely, contributing to the scientific understanding of the biomechanics of the human meniscal horn.

1.4 Development framework

This thesis is developed within the PhD Program in Mechanical Engineering and Energy Efficiency, in its research line of Mechanical and Materials Engineering, and more specifically in the subline of New Surgical Methods Studies.

The development of the research has been framed within the project “Design of the fixation for meniscal transplantation without bone plugs and with natural biomechanics: NaturFix” (Grant agreement RTI2018-094339-B-IO0) funded by the Spanish State R+D+i Program Oriented to the Challenges of Society of the State Plan for Scientific and Technical Research and Innovation (PEICTI), and the project “Modeling the Sutured Meniscus Oriented to Meniscal Root Reconstruction” (Grant agreement UMA20-FEDERJA-116) funded by the Andalusian Plan for R+D+i in the Operational Programme FEDER Andalusia.

In addition, funding has been received from the Ministry of Science, Innovation and Universities of the Government of Spain through the University Teacher Training Programme (FPU) in the 2020 call for the formalization of a pre-doctoral contract (FPU20/05445) during the completion of this doctoral thesis.

The work has been mainly carried out in the Clinical Biomechanics Laboratory of Andalusia (BIOCLINA), which has established a framework of collaboration between specialists from the Orthopedic Surgery and Traumatology Service of Clinica Espejo, the Vithas hospital group and the TEP-140 group (Mechanical Engineering Malaga) of the Andalusian Research Plan composed of members of the Mechanical Engineering Area of the University of Malaga. Dr. Espejo's observations on the incidence of meniscal root tears and the need to improve the surgical technique motivated the interest in contributing to enhance the scientific knowledge on the mechanical behavior of the sutured meniscal horn subjected to physiological loads.

The research described in Chapter 6 was conducted in collaboration with the Institute of Orthopaedic Research and Biomechanics at the University of Ulm (Germany) during the student's internship, under the supervision of PD Dr. Andreas Martin Seitz.

1.5 References

Ahn, J.H., Wang, J.H., Yoo, J.C., Noh, H.K., Park, J.H., 2007. A pull out suture for transection of the posterior horn of the medial meniscus: Using a posterior trans-septal portal. Knee Surgery, Sports Traumatology, Arthroscopy 15, 1510–1513. https://doi.org/10.1007/S00167-007-0310-3/FIGURES/6

Anz, A.W., Branch, E.A., Saliman, J.D., 2014. Biomechanical Comparison of Arthroscopic Repair Constructs for Meniscal Root Tears. Am J Sports Med 42 (11), 2699–2706. https://doi.org/10.1177/0363546514549445

Balke, M., Akoto, R., Offerhaus, C., Hoeher, J., 2018. Suture Anchor Refixation of Meniscal Root Tears Without an Additional Portal. Arthrosc Tech 7, e511–e515. https://doi.org/10.1016/J.EATS.2018.01.003

Bao, H.R.C., Zhu, D., Gong, H., Gu, G.S., 2013. The effect of complete radial lateral meniscus posterior root tear on the knee contact mechanics: A finite element analysis. Journal of Orthopaedic Science 18, 256–263. https://doi.org/10.1007/S00776-012-0334-5/TABLES/3

Bloecker, K., Wirth, W., Guermazi, A., Hunter, D.J., Resch, H., Hochreiter, J., Eckstein, F., 2015. Relationship between medial meniscal extrusion and cartilage loss in specific femorotibial subregions: Data from the osteoarthritis

initiative. Arthritis Care Res (Hoboken) 67, 1545–1552. https://doi.org/10.1002/ACR.22615/ABSTRACT

Cardoso Gomide, L., De Oliveira Campos, D., Amaral Araújo, C., Lima Menegaz, G., Silva Cardoso, R., Crosara Saad, S., 2019. Mechanical study of the properties of sutures used in orthopaedics surgeries. Rev. Bras. Ortop. 54, 247–252. https://doi.org/10.1016/J.RBO.2018.02.001/ID/OR170225-10

Cerminara, A.J., LaPrade, C.M., Smith, S.D., Ellman, M.B., Wijdicks, C.A., LaPrade, R.F., 2014. Biomechanical Evaluation of a Transtibial Pull-out Meniscal Root Repair Challenging the Bungee Effect. American Journal of Sports Medicine 42, 2988–2995. https://doi.org/10.1177/0363546514549447

Cuéllar, Adrián, Cuéllar, Asier, Sánchez, A., Cuéllar, R., 2017. Posterior Lateral Meniscus Root Reattachment With Suture Anchors: An Arthroscopic Technique. Arthrosc Tech 6, e1919–e1925. https://doi.org/10.1016/J.EATS.2017.07.011

Ding, C., Martel-Pelletier, J., Pelletier, J.P., Abram, F., Raynauld, J.P., Cicuttini, F., Jones, G., 2007. Knee meniscal extrusion in a largely non-osteoarthritic cohort: Association with greater loss of cartilage volume. Arthritis Res Ther 9, 1–8. https://doi.org/10.1186/AR2132/TABLES/4

D'lima, D.D., Chen, P.C., Kessler, O., Hoenecke, H.R., Colwell, C.W., 2011. Effect of Meniscus Replacement Fixation Technique on Restoration of Knee Contact Mechanics and Stability. MCB 8, 123–134.

Espejo-Reina, A., Prado-Novoa, M., Espejo-Baena, A., Estebanez, B., Perez-Blanca, A., 2023. Improved tibiofemoral contact restoration after transtibial reinsertion of the anterior root of the lateral meniscus compared to in situ repair: a biomechanical study. Int Orthop 1, 3. https://doi.org/10.1007/s00264-023-05769-y

Espejo-Reina, A., Prado-Novoa, M., Espejo-Baena, A., Peña-Trabalon, A., Perez-Blanca, A., 2022. Biomechanical consequences of anterior root detachment of the lateral meniscus and its reinsertion. Sci Rep 12, 6182. https://doi.org/10.1038/S41598-022-10229-5

Feucht, M.J., Grande, E., Brunhuber, J., Burgkart, R., Imhoff, A.B., Md, §, Braun, S., 2013. Biomechanical Evaluation of Different Suture Techniques for Arthroscopic Transtibial Pull-out Repair of Posterior Medial Meniscus Root

Tears. Am J Sports Med 41, 2784–2790. https://doi.org/10.1177/0363546513502464

Feucht, M.J., Grande, E., Brunhuber, J., Rosenstiel, N., Burgkart, R., Imhoff, A.B., Braun, S., 2014. Biomechanical comparison between suture anchor and transtibial pull-out repair for posterior medial meniscus root tears. American Journal of Sports Medicine 42, 187–193. https://doi.org/10.1177/0363546513502946/ASSET/IMAGES/LARGE/10.1177_0363546513502946-FIG2.JPEG

Freutel, M., Galbusera, F., Ignatius, A., Dürselen, L., 2015. Material properties of individual menisci and their attachments obtained through inverse FE-analysis. J Biomech 48, 1343–1349. https://doi.org/10.1016/J.JBIOMECH.2015.03.014

Johannsen, A.M., Civitarese, D.M., Padalecki, J.R., Goldsmith, M.T., Wijdicks, C.A., LaPrade, R.F., 2012. Qualitative and Quantitative Anatomic Analysis of the Posterior Root Attachments of the Medial and Lateral Menisci. Am J Sports Med 40(10), 2342–2347. https://doi.org/10.1177/0363546512457642

Jones, A.O., Houang, M.T.W., Low, R.S., Wood, D.G., 2006. Medial meniscus posterior root attachment injury and degeneration: MRI findings. Australas Radiol 50, 306–313. https://doi.org/10.1111/J.1440-1673.2006.01586.X

Kim, J.H., Chung, J.H., Lee, D.H., Lee, Y.S., Kim, J.R., Ryu, K.J., 2011. Arthroscopic Suture Anchor Repair Versus Pullout Suture Repair in Posterior Root Tear of the Medial Meniscus: A Prospective Comparison Study. Arthroscopy: The Journal of Arthroscopic & Related Surgery 27, 1644–1653. https://doi.org/10.1016/J.ARTHRO.2011.06.033

Kim, Y.M., Rhee, K.J., Lee, J.K., Hwang, D.S., Yang, J.Y., Kim, S.J., 2006. Arthroscopic pullout repair of a complete radial tear of the tibial attachment site of the medial meniscus posterior horn. Arthroscopy 22, 795.e1-795.e4. https://doi.org/10.1016/J.ARTHRO.2005.12.040

Kohn, D., Moreno, B., 1995. Meniscus insertion anatomy as a basis for meniscus replacement: a morphological cadaveric study. Arthroscopy 11, 96–103. https://doi.org/10.1016/0749-8063(95)90095-0

Kopf, S., Colvin, A.C., Muriuki, M., Zhang, X., Harner, C.D., 2011. Meniscal root suturing techniques: Implications for root fixation. American Journal of Sports Medicine 39, 2141–2146. https://doi.org/10.1177/0363546511413250/ASSET/IMAGES/LARGE/10.1177_0363546511413250-FIG2.JPEG

LaPrade, C.M., Foad, A., Smith, S.D., Lee Turnbull, T., Dornan, G.J., Engebretsen, L., Wijdicks, C.A., LaPrade, R.F., 2015. Biomechanical Consequences of a Nonanatomic Posterior Medial Meniscal Root Repair. Am J Sports Med 43(4), 912–920. https://doi.org/10.1177/0363546514566191

LaPrade, C.M., Jansson, K.S., Dornan, G., Smith, S.D., Wijdicks, C.A., LaPrade, R.F., 2014. Altered Tibiofemoral Contact Mechanics Due to Lateral Meniscus Posterior Horn Root Avulsions and Radial Tears Can Be Restored with in Situ Pull-Out Suture Repairs. Journal of Bone and Joint Surgery 96, 471–479. https://doi.org/10.2106/JBJS.L.01252

Laprade, R.F., Laprade, C.M., James, E.W., 2015. Recent advances in posterior meniscal root repair techniques. Journal of the American Academy of Orthopaedic Surgeons 23, 71–76. https://doi.org/10.5435/JAAOS-D-14-00003

Lee, J.H., Lim, Y.J., Kim, K.B., Kim, K.H., Song, J.H., 2009. Arthroscopic Pullout Suture Repair of Posterior Root Tear of the Medial Meniscus: Radiographic and Clinical Results With a 2-Year Follow-up. Arthroscopy: The Journal of Arthroscopic & Related Surgery 25, 951–958. https://doi.org/10.1016/J.ARTHRO.2009.03.018

Mitchell, R., Pitts, R., Kim, Y.M., Matava, M.J., 2016. Medial Meniscal Root Avulsion: A Biomechanical Comparison of 4 Different Repair Constructs. Arthroscopy: The Journal of Arthroscopic & Related Surgery 32, 111–119. https://doi.org/10.1016/J.ARTHRO.2015.07.013

Moon, H.-K., Koh, Y.-G., Kim, Y.-C., Park, Y.-S., Jo, S.-B., Kwon, S.-K., 2010. Prognostic Factors of Arthroscopic Pull-out Repair for a Posterior Root Tear of the Medial Meniscus. Am J Sports Med 40(5), 1138–1143. https://doi.org/10.1177/0363546511435622

Mow, V.C., Wang, C.C., Hung, C.T., 1999. The extracellular matrix, interstitial fluid and ions as a mechanical signal transducer in articular cartilage. Osteoarthritis Cartilage 7, 41–58. https://doi.org/10.1053/JOCA.1998.0161

Nakama, G.Y., Aman, Z.S., Storaci, H.W., Kuczmarski, A.S., Krob, J.J., Strauss, M.J., 2019. Different Suture Materials for Arthroscopic Transtibial Pull-out Repair of Medial Meniscal Posterior Root Tears: A Human Biomechanical Study. Orthop J Sports Med 7. https://doi.org/10.1177/2325967119873274/ASSET/IMAGES/LARGE/10.1177_2325967119873274-FIG6.JPEG

Ode, G.E., Van Thiel, G.S., McArthur, S.A., Dishkin-Paset, J., Leurgans, S.E., Shewman, E.F., Wang, V.M., Cole, B.J., 2012. Effects of serial sectioning and repair of radial tears in the lateral meniscus. American Journal of Sports Medicine 40, 1863–1870. https://doi.org/10.1177/0363546512453291

Padalecki, J.R., Jansson, K.S., Smith, S.D., Dornan, G.J., Pierce, C.M., Wijdicks, C.A., Laprade, R.F., 2014. Biomechanical consequences of a complete radial tear adjacent to the medial meniscus posterior root attachment site: In situ pull-out repair restores derangement of joint mechanics. American Journal of Sports Medicine 42, 699–707. https://doi.org/10.1177/0363546513499314

Peña, E., Calvo, B., Martínez, M.A., Doblaré, M., 2006. A three-dimensional finite element analysis of the combined behavior of ligaments and menisci in the healthy human knee joint. J Biomech 39, 1686–1701. https://doi.org/10.1016/J.JBIOMECH.2005.04.030

Perez-Blanca, A., Espejo-Baena, A., Amat Trujillo, D., Prado Nóvoa, M., Espejo-Reina, A., Quintero López, C., Ezquerro Juanco, F., 2016. Comparative Biomechanical Study on Contact Alterations After Lateral Meniscus Posterior Root Avulsion, Transosseous Reinsertion, and Total Meniscectomy. Arthroscopy: The Journal of Arthroscopic & Related Surgery 32, 624–633. https://doi.org/10.1016/j.arthro.2015.08.040

Perez-Blanca, A., Prado Nóvoa, M., Lombardo Torre, M., Espejo-Reina, A., Ezquerro Juanco, F., Espejo-Baena, A., 2018. The role of suture cutout in the failure of meniscal root repair during the early post-operative period: a biomechanical study. Int Orthop 42, 811–818. https://doi.org/10.1007/S00264-018-3799-9/FIGURES/5

Petersen, W., Forkel, P., Feucht, M.J., Zantop, T., Imhoff, A.B., Brucker, P.U., 2014. Posterior root tear of the medial and lateral meniscus. Arch Orthop Trauma Surg 134, 237–255. https://doi.org/10.1007/S00402-013-1873-8/TABLES/3

Petersen, W., Zantop, T., 2006. Avulsionsverletzung des außenmeniskushinterhorns. Arthroskopische refixationstechnik. Unfallchirurg 109, 984–987. https://doi.org/10.1007/S00113-006-1193-3/FIGURES/4

Robinson, J.R., Frank, E.G., Hunter, A.J., Jermin, P.J., Gill, H.S., 2018. The Strength of Transosseous Medial Meniscal Root Repair Using a Simple Suture Technique Is Dependent on Suture Material and Position. American Journal of Sports Medicine 46, 924–932. https://doi.org/10.1177/0363546517749807/ASSET/IMAGES/LARGE/10.1177_0363546517749807-FIG7.JPEG

Seo, H.S., Lee, S.C., Jung, K.A., 2010. Second-Look Arthroscopic Findings After Repairs of Posterior Root Tears of the Medial Meniscus. https://doi.org/10.1177/0363546510382225 39, 99–107. https://doi.org/10.1177/0363546510382225

Seyfi, B., Fatouraee, N., Imeni, M., 2018. Mechanical modeling and characterization of meniscus tissue using flat punch indentation and inverse finite element method. J Mech Behav Biomed Mater 77, 337–346. https://doi.org/10.1016/J.JMBBM.2017.09.023

Stärke, C., Kopf, S., Gröbel, K.H., Becker, R., 2010. The Effect of a Nonanatomic Repair of the Meniscal Horn Attachment on Meniscal Tension: A Biomechanical Study. Arthroscopy: The Journal of Arthroscopic & Related Surgery 26, 358–365. https://doi.org/10.1016/J.ARTHRO.2009.08.013

Steineman, B.D., LaPrade, R.F., Haut Donahue, T.L., 2020. Nonanatomic placement of posteromedial meniscal root repairs: A finite element study. J Biomech Eng 142. https://doi.org/10.1115/1.4045893/1072350

Vertullo, C.J., Cadman, J., Dabirrahmani, D., Appleyard, R., 2021. Biomechanical Comparison of an All-Inside Meniscal Repair Device Construct Versus Pullout Sutures for Arthroscopic Transtibial Repair of Posterior Medial Meniscus Root Tears A Matched-Pair Cadaveric Study. Orthop J Sports Med 9(4), 23259671211000464. https://doi.org/10.1177/23259671211000464

Villegas, D.F., Hansen, T.A., Liu, D.F., Haut Donahue, T.L., 2008. A quantitative study of the microstructure and biochemistry of the medial meniscal horn attachments. Ann Biomed Eng 36, 123–131. https://doi.org/10.1007/s10439-007-9403-x

Wang, Y.J., Yu, J.K., Luo, H., Yu, C.L., Ao, Y.F., Xie, X., Jiang, D., Zhang, J.Y., 2009. An anatomical and histological study of human meniscal horn bony insertions and peri-meniscal attachments as a basis for meniscal transplantation. Chin Med J (Engl) 122, 536–540. https://doi.org/10.3760/CMA.J.ISSN.0366-6999.2009.05.010

Zantop, T., Eggers, A.K., Weimann, A., Hassenpflug, J., Petersen, W., 2004. Initial Fixation Strength of Flexible All-Inside Meniscus Suture Anchors in Comparison to Conventional Suture Technique and Rigid Anchors Biomechanical Evaluation of New Meniscus Refixation Systems and the. https://doi.org/10.1177/0363546503260749

Zielinska, B., Haut Donahue, T.L., 2006. 3D Finite Element Model of Meniscectomy: Changes in Joint Contact Behavior. J Biomech Eng 128, 115–123. https://doi.org/10.1115/1.2132370

2

Fundamentals

A comprehensive understanding of the anatomy and composition of the knee menisci, along with their integration with other articular structures, is crucial for elucidating their mechanical properties and their role as load distributors between the tibia and femur. The meniscal roots, which secure the menisci to the tibial plateau, are key stabilizers of knee movement. A complete rupture of these roots can significantly impair knee function, resulting in biomechanical alterations comparable to those observed following meniscectomy. Consequently, surgical repair techniques have been developed to restore the joint's natural biomechanics. Biomechanical studies have confirmed the impact of meniscal tears on joint function and have assessed the efficacy of various surgical repair methods.

2.1 Human knee menisci

Menisci are fibrocartilaginous structures found within certain synovial joints of vertebrates. In humans, they are located in the temporomandibular joint, knee, acromioclavicular joint, sternoclavicular joint, wrist, and at the junctions between the ribs and the vertebral transverse processes.

The knee menisci are two crescent-shaped, triangular cross-sectional structures that interpose between the tibial and femoral components of the tibiofemoral joint (Figure 2.1)

The incongruence between the curvatures of the femoral and tibial articular surfaces results in a limited area of direct contact. The menisci mitigate this by increasing joint congruity, thereby distributing the load transmitted through the joint more evenly across the cartilage surfaces (Figure 2.2). It is estimated that the menisci bear approximately 40-70% of the load transmitted through the knee joint (Seedhom and Hargreaves, 1979). This load distribution function reduces

the compressive stresses exerted on the articular cartilage compared to a meniscus-deficient joint.

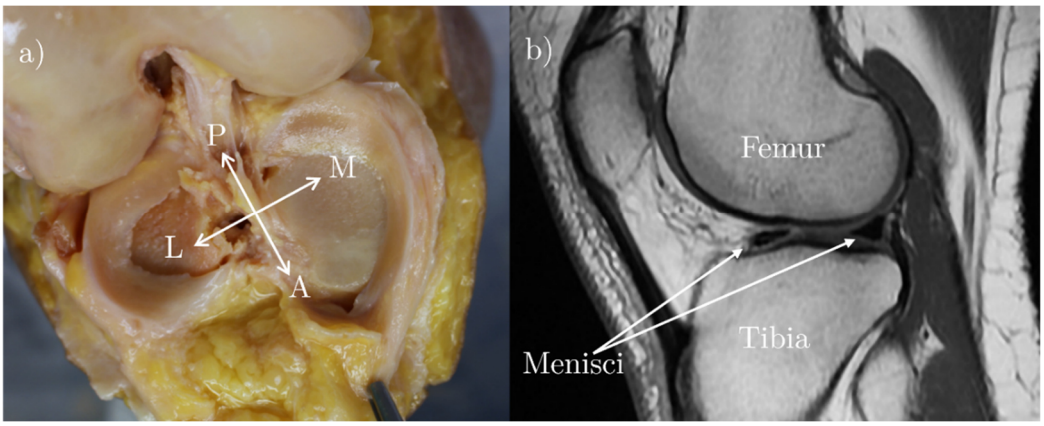

Figure 2.1. Representation of human menisci in the human knee between the tibia and femur: a) anatomical view (L: Lateral; M: Medial; P: Posterior; A: Anterior); b) MRI view.

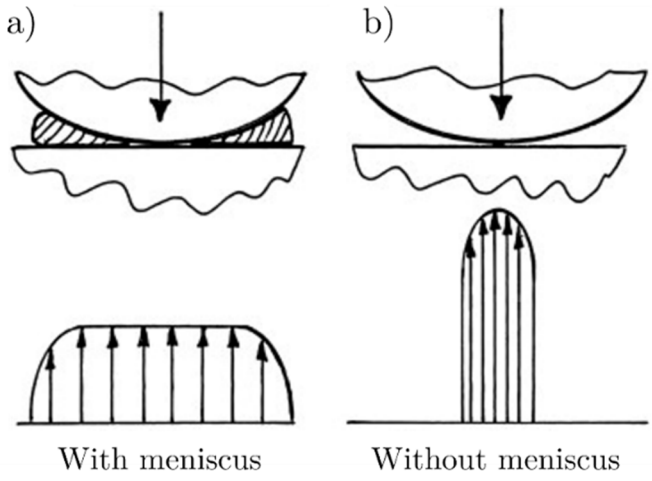

Figure 2.2. Load distribution in knee joint contact: a) with the presence of the menisci; b) without menisci. Source: (McDermott et al., 2008).

Beyond load bearing and distribution, menisci contribute to shock absorption, joint stability, lubrication, and proprioceptive feedback (Mow VC et al., 1992).

To effectively fulfill these roles, menisci are anchored to other joint components by ligaments, and their biomechanics must be understood in the context of the integrated meniscus-ligament complex.

2.1.1 Anatomical and physiological description

The human knee comprises two menisci: the lateral (outer) and medial (inner), each situated within its respective tibiofemoral compartment (Figure 2.1a). These fibrocartilaginous structures exhibit a smooth, lubricated, white, and shiny appearance. They are crescent-shaped with a roughly triangular cross-sectional profile.

Although the medial and lateral menisci share a similar overall structure, notable differences in the femorotibial compartments require specific anatomical variations in each meniscus. The lateral tibial plateau tends to be convex, whereas the medial plateau is slightly concave and larger. Consequently, the medial meniscus is approximately semicircular, with a diameter of 35 mm, and is significantly wider in the posterior horn compared to the anterior horn. It covers about 60% of the articular surface of the medial compartment. In contrast, the lateral meniscus is smaller and varies more in dimensions, shape, and thickness. It is nearly circular and more uniformly flat, covering approximately 80% of the lateral compartment's articular surface (Fox et al., 2012).

The convex outer edge of each meniscus is thicker and anchored to the joint capsule, while the thickness diminishes progressively towards the unattached inner edge. The superior surfaces of the menisci are concave, facilitating articulation with the convex femoral condyles. In contrast, the inferior surfaces are relatively flat, conforming to the geometry of the tibial plateau (Fox et al., 2012).

Each meniscus can be anatomically divided into three distinct regions: the central body and the anterior and posterior horns, which correspond to their respective positions within the joint (Figure 2.3).

The menisci are connected to other joint components by various ligamentous structures, which play a critical role in their biomechanical function. These connections, occurring at multiple levels with bones, ligaments, and the joint capsule, are essential for maintaining proper meniscal movement within the joint. Ligamentous attachments allow the menisci to move in concert with joint motions while constraining their displacement, which is vital for load distribution, shock absorption, and joint stability.

The anterior and posterior horns of each meniscus are anchored to the subchondral bone of the tibial surface by ligamentous extensions known as roots (Figure 2.4). These roots act as primary restraints against meniscal extrusion from the intra-articular space (Johannsen et al., 2012; Villegas et al., 2008; Wang et al., 2009b).

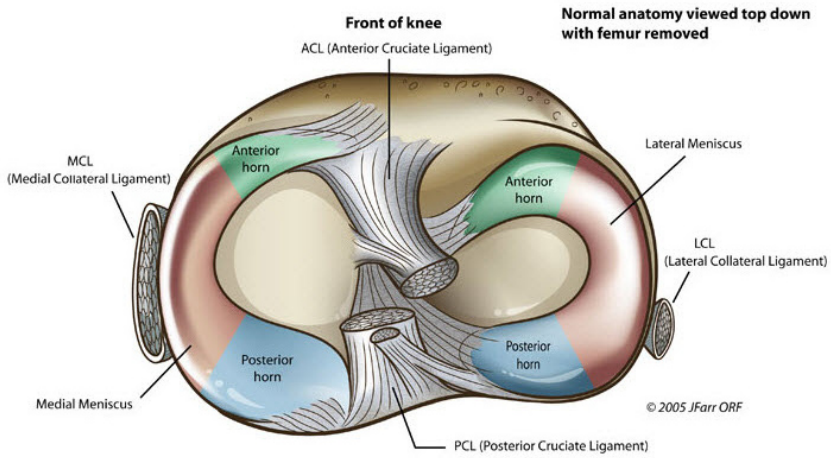

Figure 2.3. Representation of the lateral and medial meniscus on the tibial plateau with differentiation of the three zones into which it is divided. Green: anterior horn; Blue: posterior horn; Red: Central body. Source: Anatomy Note, 2005.

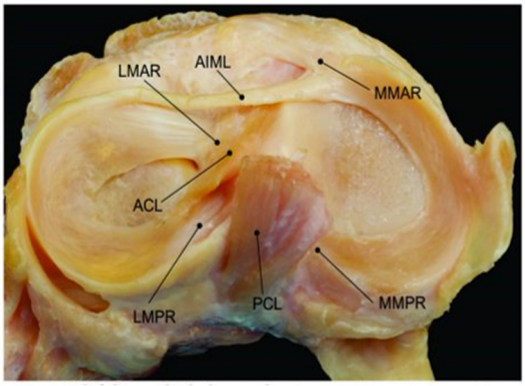

Figure 2.4. Human menisci with their meniscal roots on the tibial plate of a left knee. LMAR: Lateral Meniscus Anterior Root; LMPR: Lateral Meniscus Posterior Root; MMAR: Medial Meniscus Anterior Root; MMPR: Medial Meniscus Posterior Root; ACL: Anterior Cruciate Ligament; PCL: Posterior Cruciate Ligament; AIML: Anterior Intermeniscal Ligament. Source: Robinson et al., 2016.

Due to their relevance, several studies have investigated the geometry of meniscal roots and measured their insertion areas within the subchondral bone of the tibia. These studies generally indicate that the anterior roots are longer and possess smaller cross-sectional areas compared to the posterior roots (Hauch et al., 2010). The anterior and posterior roots of the lateral meniscus, as well as the posterior root of the medial meniscus, display an oval ligamentous morphology. In contrast, the anterior root of the medial meniscus is characterized by a flatter structure. Additionally, the insertion areas of anterior roots are larger than those of the posterior roots (Ellman et al., 2014). Furthermore, the insertion areas of

lateral meniscal roots are typically larger than those of their medial counterparts (Ellman et al., 2014; Johannsen et al., 2012; LaPrade et al., 2014a).

The anteromedial, posteromedial, and posterolateral roots exhibit a higher density of central fibers, which constitute, on average, 44.7%, 26.5%, and 25.5% of their total insertion areas, respectively. These dense central fibers are surrounded by less dense supplementary fibers, contributing to the overall structure and function of the meniscal root insertions (Ellman et al., 2014).

Additionally, the periphery of each meniscus has specific ligamentous attachments that regulate its mobility within the joint (Figure 2.5).

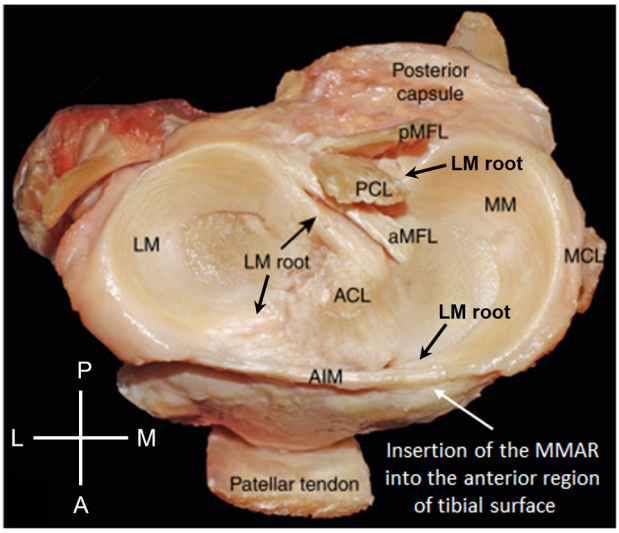

Figure 2.5. Representation of additional ligaments that provide stability and regulate the mobility of the meniscus. LM: Lateral Meniscus; MM: Medial Meniscus; ACL: Anterior Cruciate Ligament; PCL: Posterior Cruciate Ligament; AIM: Anterior Intermeniscal Ligament; MCL: Medial Collateral Ligament; aMFL: Anterior Menisco-Femoral Ligament; pMFL: Posterior Menisco-Femoral Ligament. L: Lateral; M: Medial; P: Posterior; A: Anterior Source: (Chahla et al., 2022).

In the medial meniscus, the anterior root inserts into the anterior region of the medial tibial surface, with the anterior horn also connecting posteriorly to the intermeniscal or transverse ligament (AIM) when present (Figure 2.5). This ligament links the anterior horns of both menisci. The anterior root also has connections to the patella, either directly or via an anterior capsular thickening known as the meniscopatellar ligament (Tuxøe et al., 2002). The meniscus lower periphery connects to the tibia via the meniscotibial ligament from the anterior horn to the anterior edge of the medial collateral ligament (MCL), with no other attachments to the joint capsule in this region.

However, the central area of the meniscus periphery is securely attached to both the femur and tibia through meniscofemoral and meniscotibial components,

which are part of a capsular condensation known as the deep medial ligament (LaPrade et al., 2007) (Figure 2.6).

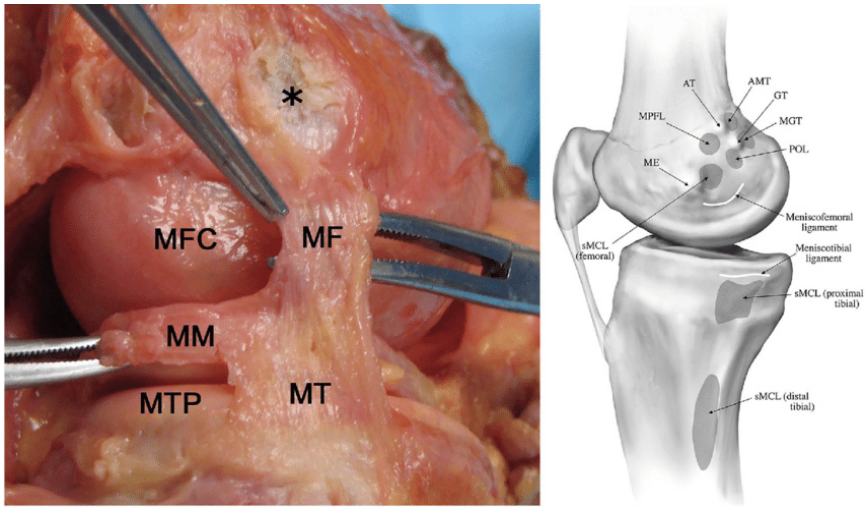

Figure 2.6. Representation of the insertions and junctions of the meniscotibial and meniscofemoral ligaments with the medial meniscus. MF: Meniscofemoral Ligament; MT: Meniscotibial ligament; MTP: Medial Tibial Plateau; MM: Medial Meniscus; MFC: Medial Femoral Condyle. Source: (Moran et al., 2021).

At the posteromedial corner, the meniscus is firmly connected to the posterior oblique ligament (LaPrade et al., 2007). The posterior horn inferior border continues its attachment to the tibia via the meniscotibial ligament, while the superior border remains unattached. The posterior root anchors the posterior horn to the tibia between the PCL insertion and the apex of the medial tibial eminence. Although there are no direct muscular attachments to the medial meniscus, indirect connections to the semimembranosus via the capsule may facilitate some retraction of the posterior root (Peterson and Renström, 2017).

In the lateral meniscus, the anterior root insertion merges with that of the ACL (Figure 2.5). The meniscotibial ligament forms a less secure connection between the meniscus and tibia in the anterior and medial body regions compared to the medial compartment, with an interruption in the area of the popliteus tendon. Additionally, there is no direct attachment between the lateral meniscus and the LCL. In the posterior body region, a firm connection exists between the meniscus and the fibula through a capsular extension called the popliteoperoneal ligament. This ligament, along with others that connect the arcuate and oblique popliteal ligaments, facilitates dynamic retraction of the posterior meniscus segment during internal tibial rotation relative to the femur during knee flexion (LaPrade et al., 2017) (Figure 2.7).

The posterior horn attaches to the tibia via the posterior root, which inserts behind the intercondylar eminence, between the ACL and the posterior root of

the medial meniscus. The posterior horn is also connected to the medial femoral condyle through the meniscofemoral ligaments (Figure 2.5): the anterior meniscofemoral ligament (aMFL) or Humphrey's ligament, which runs anterior to the PCL, and the posterior meniscofemoral ligament (pMFL) or Wrisberg's ligament, which runs posterior to the PCL (Masouros et al., 2008). These ligaments, which contribute to stabilize the posterior horn, are present together in about 50% of individuals, although at least one is present in the majority of cases (Gupte et al., 2003).

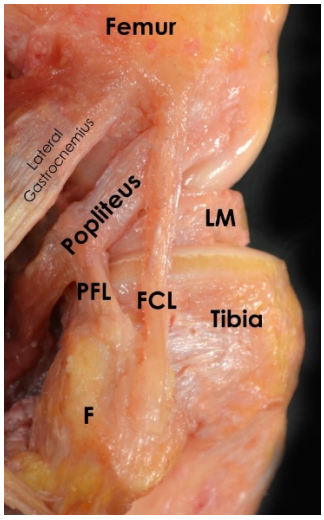

Figure 2.7. Representation of the attachment of the Popliteofibular Ligament (PFL) to the lateral meniscus (LM). The collateral ligament (FCL) is also observed. Source: (Chahla et al., 2016).

2.1.2 Kinematic behaviour

Due to the triangular cross-sectional profile of the meniscus, axial loads applied during joint articulation are transformed into radial loads (Figure 2.8). This radial load induces a tendency for the meniscus to displace outward from its position between the femoral and tibial surfaces. If this displacement is not adequately restricted, the meniscus may lose its ability to distribute loads effectively across the joint, compromising its functional role.

The restriction of meniscal displacement is primarily facilitated by the ligaments described in section 2.1.1. The peripheral edge of the meniscus is connected to the joint capsule and the deep layer of the knee's collateral ligaments, while the meniscal horns are anchored to the tibial surface through robust structures known as meniscal roots (Figure 2.4). These ligamentous attachments provide a balance between allowing necessary meniscal mobility and restricting excessive displacement. Notably, the direct insertion of the meniscal roots into the tibia serves as the primary restraint against meniscal extrusion (Kale et al., 2010; Messner Karola and Gao, 1998; Petersen and Tillmann, 1998).

This anchorage is crucial for maintaining the functional integrity of the meniscus, as it prevents uncontrolled and excesive meniscal displacement, known as meniscal extrusion. This restraint allows circumferential tensile stresses to develop within the meniscal tissue, which are absorbed by the longitudinally oriented collagen fibers and the meniscal roots.

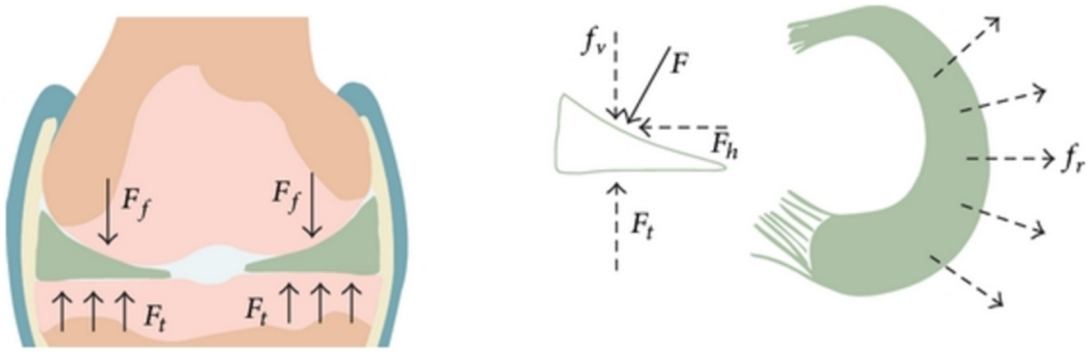

Figure 2.8. Application of axial loads on the meniscus by the femur and transformation of these into radial forces that contribute to the extrusion of the meniscus towards the outside of the joint. Source: (Guo et al., 2015).

Meniscal translation, particularly during knee flexion, is essential for the meniscus to fulfill its mechanical functions. However, the exact magnitude of meniscal translation during flexion, especially under loading conditions or in combination with tibial rotation relative to the femur, is not well-documented

The lateral meniscus exhibits greater mobility and deformability compared to the medial meniscus (Kapandji, 2012). This increased mobility is attributed to the proximity of the insertion points of the lateral meniscus's anterior and posterior roots on the tibia, as well as the absence of a posterolateral connection to the joint capsule.

During the full range of knee flexion, posterior displacement of the lateral meniscus has been measured to range between 9 and 11.2 mm, while the medial meniscus shows displacements of 2 to 5.1 mm (Brantigan and Voshell, 1941; DePalma, 1955; Thompson et al., 1991). Additionally, it has been observed that the anterior roots of both menisci exhibit greater mobility compared to the posterior roots.

In the lateral meniscus, the differences in displacement between the anterior and posterior horns are relatively small, resulting in a more cohesive movement and reduced deformability. In contrast, in the medial meniscus, the anterior horn's lateral edge displaces approximately 2.4 times more than the posterior horn, with

the posteromedial corner being the least mobile region due to its attachment to the tibial plateau via the posterior oblique ligament (Thompson et al., 1991).

2.1.3 Histological composition of meniscal tissue

The menisci are predominantly composed of a dense extracellular matrix (ECM), with water constituting approximately 72% and collagen accounting for around 22% of its composition. Embedded within this matrix are fibrochondrocytes (Fox et al., 2012; McDevitt and Webber, 1990), which are responsible for the synthesis and maintenance of the ECM (Arnoczky, 1992; Ghadially et al., 1983). Other notable components of the menisci include approximately 17% glycosaminoglycans, 2% DNA, and less than 1% each of adhesive glycoproteins and elastin (Fox et al., 2012; Makris et al., 2011; McDevitt and Webber, 1990). The relative proportions of these constituents may fluctuate depending on factors such as age, injury, or pathological conditions (McDevitt and Webber, 1990; Sweigart and Athanasiou, 2004).

Collagen serves as the primary fibrillar component of meniscal tissue, with its distribution and type varying across different regions of the meniscus (Figure 2.9).

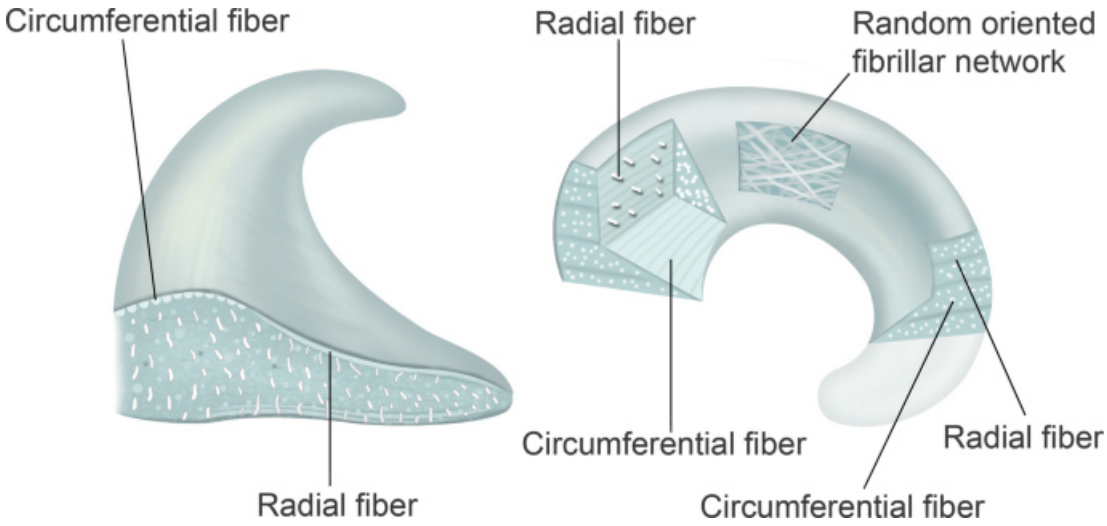

Figure 2.9. Distribution of collagen fibers in the meniscus, representing the fibers in circumferential direction, in radial direction and the area with an irregular distribution. Source: Seo et al., 2021.

In the superficial layer, collagen fibers are randomly oriented, resembling the arrangement typical of cartilage (Beaupr et al., 1986). However, in the deeper layers, fiber orientation and collagen type vary based on the specific region. In the inner third of the meniscus, collagen comprises approximately 60% type II fibers and 40% type I fibers (Cheung, 1987), with a predominant radial orientation (Pereira et al., 2013). Conversely, in the outer two-thirds, type I collagen is the

dominant form, constituting about 80% of the tissue's dry weight, with smaller quantities of other collagen types (II, III, IV, VI, and XVIII) present. In this outer zone, the deeper layers are characterized by circumferentially oriented collagen fibers, while those closer to the surface are more radially aligned. Additionally, radially oriented fibers in the deep layer intertwine with longitudinal fibers, enhancing structural integrity and preventing the propagation of longitudinal tears (Bullough et al., 1970; Ghosh and Taylor, 1987).

Glycosaminoglycans (GAGs) within the extracellular matrix (ECM) are covalently linked to core proteins, forming large proteoglycan aggregates (Figure 2.10). These complexes endow the meniscal tissue with a significant capacity to withstand compressive forces. Proteoglycans primarily function to absorb and retain water, thereby maintaining the hydration of the meniscus. Under conditions of elevated hydraulic pressure, the absorbed water can be expelled, overcoming the high frictional resistance of the dense ECM (Adams and Muir, 1981; Fox et al., 2012; Scott et al., 1997). Notably, the water content within the meniscal tissue is higher in the posterior region compared to the central or anterior regions.

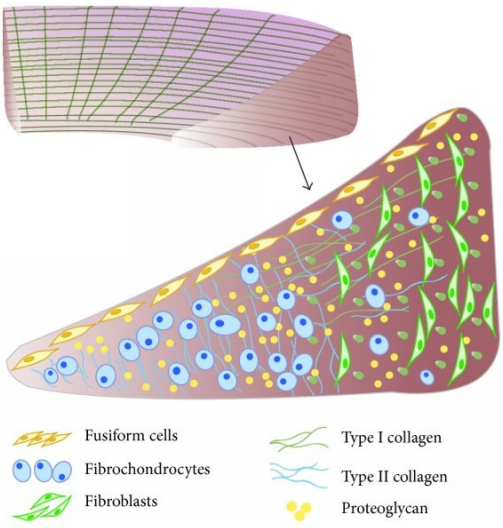

Figure 2.10. Distribution of collagen fibers and interaction with the rest of the elements that make up the ECM. Source: (Niu et al., 2016).

The meniscal body exhibits a relatively disorganized fiber pattern that transitions smoothly into a highly organized arrangement within the meniscal roots. In these roots, collagen fibers are aligned parallel to the tensile forces they are subjected to. These ligamentous tissues anchor to the tibia via fibrocartilage, forming a specialized structure known as an enthesis (Chang et al., 2014).

2.2 Meniscal root lesions

Meniscal roots, which are the only portions of the meniscus that attach directly to bone, are crucial for preventing meniscal extrusion. Their integrity is essential for maintaining proper knee biomechanics (Schillhammer et al., 2012). Damage to these roots has a significant impact on knee function and can result in consequences comparable to those observed with total meniscectomy.

The transition zone, where the meniscal root connects to the bone, is identified as the weakest area of the root structure. This zone is generally more vulnerable in the posterior roots compared to the anterior roots, which correlates with the higher incidence of injuries in this region (M. Freutel et al., 2015).

Injury to the meniscal root typically involves avulsion, where the root is pulled away from the bone, or a radial tear occurring within 1 cm of the insertion site. Such injuries are less common than those affecting the meniscal body and may often go undetected. Root injuries can be either traumatic, more frequently affecting the lateral meniscus, or degenerative, with a higher incidence in the medial meniscus. Recent literature has increasingly emphasized the critical importance of diagnosing and treating injuries to the medial meniscus due to their significant impact on joint health.

2.2.1 Classification of meniscal root tears

There are different types of meniscal root lesions depending on their morphology. LaPrade et al. (Christopher M. LaPrade et al., 2015) classified meniscal root tears into 5 types (Figure 2.11).

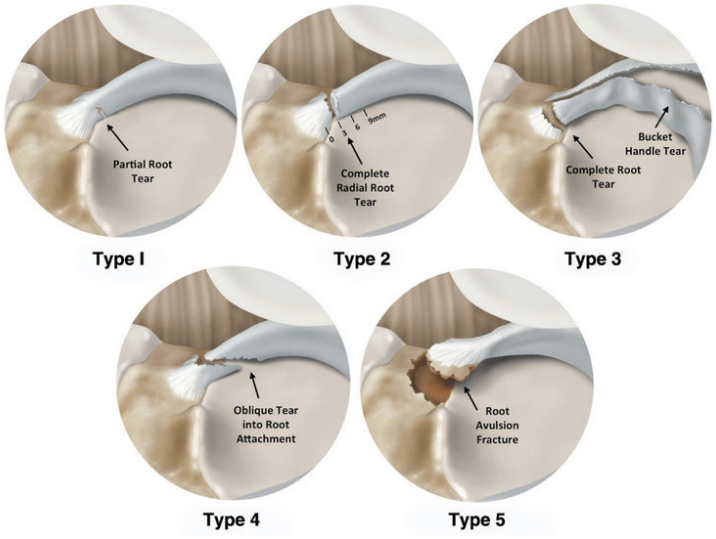

Figure 2.11. Classification of meniscal root tears according to LaPrade et al. Source: LaPrade et al., 2015

- Type 1 (7%): partial and stable posterior root rupture.

- Type 2 (67.6%): complete radial break in the 9 mm proximal to the bony insertion.
  - Type 2A (38%): less than 3 mm.
  - Type 2B (16.9%): between 3 and < 6 mm.
  - Type 2C (12.7%): 6-9 mm.

- Type 3 (5.6%): bucket loop meniscal tear with complete disinsertion of the meniscal root.

- Type 4 (9.9%): complete oblique or longitudinal tear with complete meniscal root disinsertion.

- Type 5 (9.9%): bony avulsion of the meniscal root insertion.

On the other hand, Forkel et al. (Forkel and Petersen, 2012) specifically classified injuries of the PRLM associated with ACL injury (most frequently of traumatic origin) according to the integrity of the meniscofemoral ligaments (MFL):

- Type 1: avulsion of the PRLM without involvement of the MFL.

- Type 2: Radial tear of the posterior horn of the lateral meniscus, between the PRLM and the meniscal insertion of the MFL.

- Type 3: complete tear of the meniscal root and MFL.

Bin et al. (Bin et al., 2016) classified PRMM lesions (usually of degenerative origin) according to the displacement found during arthroscopic surgery and correlated it with the extrusion previously found on MRI:

- Type I: no displacement.

- Type II: overlapping of both ends of the tear.

- Type III: extensive displacement.

In types I and II, no or minimal meniscal extrusion was found on MRI, while in type III, marked extrusion was found. Likewise, knees with type III PRMM

ruptures had a higher proportion of arthritic signs in the medial compartment (both tibia and femur) than knees with type I and II lesions.

2.2.2 Surgical repair of meniscal root tears

Treatment options for meniscal root injuries encompass a range of approaches, including non-surgical management, meniscectomy, and meniscal root repair (Berlet and Fowler, 1998). The selection of treatment is based on patient age, comorbidities, and the extent of joint degeneration:

- Non-Surgical Treatment: This approach is typically reserved for elderly patients, individuals with significant comorbidities, and those with degenerative joint changes. Symptomatic management may involve the use of analgesics and mobility aids, such as a cane, to alleviate pain and improve function.

- Meniscectomy: Often employed for symptomatic relief, meniscectomy is considered in cases where non-surgical measures have proven ineffective. It is particularly relevant for patients with degenerative joint changes. Partial meniscectomy is a viable option for patients with partial lesions where the meniscal root insertion is sufficiently preserved to maintain functional integrity.

- Meniscal Root Repair: Indications for meniscal root repair include:

  - Acute traumatic injuries in patients under 50 years of age with intact or nearly intact articular cartilage.

  - Chronic symptomatic meniscal root injuries in individuals younger than 50 years who do not exhibit significant degenerative joint changes (Bhatia et al., 2014).

Each treatment strategy is tailored to the individual patient's condition and needs, aiming to restore function and alleviate symptoms while addressing the specific nature of the meniscal root injury. While meniscectomy has traditionally been the primary surgical treatment option, as a result of research supporting meniscal preservation, there is evidence that rates of meniscal repair have increased internationally, particularly in younger populations, and rates of partial meniscectomy have decreased (Jha et al., 2024).

2.2.2.1 Repair techniques

Root repair techniques proposed so far are transtibial and *in situ* fixation:

In Situ Fixation (Figure 2.12a):

- **Technique:** This all-inside method involves suturing the meniscal hornto an implant that is anchored directly to the intra-articular surface of the tibia.

- **Advantages:** Avoids the need for tibial tunnels that might interfere with other procedures, reduces elastic elongation of sutures observed in transtibial techniques (Engelsohn et al., 2007; Feucht et al., 2014; Jung et al., 2012; J. H. Kim et al., 2011).

- **Challenges:** Anatomical placement can be difficult, particularly in the narrow joint space and in cases with associated ligament injuries (Laprade et al., 2015b).

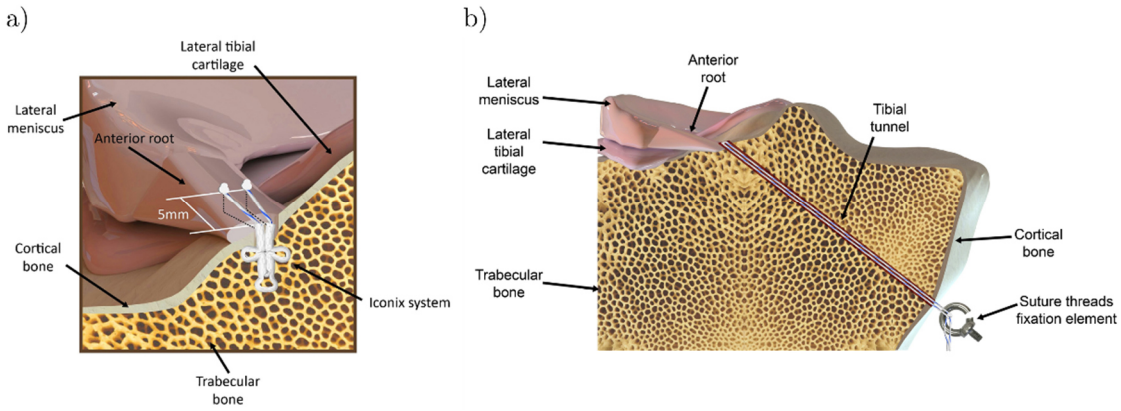

Figure 2.12. Representation of the types of meniscal root detachment repair by suturing. a) *In situ* fixation; b) Transtibial fixation. Source: (Espejo-Reina et al., 2023)

Transtibial Fixation (Figure 2.12b):

- **Technique:** This method involves suturing the meniscal horn via a tunnel drilled into the proximal tibia. These sutures are then tied off on a fixation habitually situated at the exit of the tibial tunnel.

- **Advantages:** Allows direct access to the root insertion site and can achieve secure fixation when tension is appropriately applied (Ahn et al., 2007; Kim et al., 2006; Nicholas et al., 2009; Raustol et al., 2006).

- **Considerations:** Requires precise alignment of sutures to the anatomical insertion and can be challenging if there are other existing tibial tunnels for ligament reconstructions.

2.2.2.2 Characteristics of suture materials for menischal root repair

The suture material used is critical to the success of root repair surgery. To achieve repair outcomes that closely mimic the mechanical properties of healthy meniscal roots, various suture materials and configurations have been explored.

The most commonly used suture materials are Monofilament Absorbable Polydioxanone (PDS™) threads, Non-Absorbable Polyester Fiber Braided Yarns (Ethibond™) and Ultra-High Molecular Weight Polyethylene Sutures (UHMWPE).

Monofilament Absorbable Polydioxanone (PDS™) threads has been frequently utilized in meniscal root repairs (Ahn et al., 2007; Cho, 2012; S. B. Kim et al., 2011; Lee et al., 2013; Moon et al., 2010; Seo et al., 2010). It is a biocompatible absorbable material designed to gradually degrade over time, reducing the need for a second surgery to remove sutures. However, its mechanical properties may not always match the strength and stiffness of other non-absorbable sutures, potentially leading to concerns about repair durability.

Non-absorbable Polyester Fiber Braided Yarns (Ethibond™) are commonly used due to its robust mechanical properties (Ahn et al., 2007; Forkel and Petersen, 2012; S. B. Kim et al., 2011; Kim et al., 2006; Lee et al., 2009; Rosslenbroich et al., 2013; Seo et al., 2010), which surpass those of absorbable sutures in stregth and durability. Being non-absorbable, it remains in the body indefinitely, which can be advantageous for long-term stability, although long-term biocompatibility and possible irritation may require additional consideration.

Ultra-High Molecular Weight Polyethylene Sutures (UHMWPE) have more recently emerged as an alternative of greater strength and stiffness compared to traditional sutures, and showed beneficial in biomechanical testing (Harner et al., 2009; Laprade et al., 2015a; Nicholas et al., 2009; Vyas and Harner, 2012).

Regarding the optimal number of suture threads used in the repair, Rosslenbroich et al. (Rosslenbroich et al., 2013) found that, in the repair of PRLM, the use of two threads produces mechanical properties closer to those of the healthy root than the use of a single thread, in terms of elongation and stiffness.

Regarding the size of the threads used, although some cases can be found of N.0 and N.5 threads (Lee et al., 2009) in polyester sutures, but the most commonly used is the N.2 size (Kim et al., 2006; Laprade et al., 2015b; Rosslenbroich et al., 2013). A recent study compared the biomechanical properties of the meniscal suture set with N.2 suture threads of the three types of materials mentioned: PDS™, Ethibond™ and the ultra-strong FiberWire™ (Feucht et al., 2015). None of the yarns tested showed a clear superiority in repair properties, both under cyclic loading conditions and in the failure tests. Nevertheless, the authors recommended the use of Fiberwire™ for transtibial repair of posterior meniscal roots, combining comparatively high strength and stiffness values with low cyclic displacements.

Another variant of the suture material used in tendon repairs (Gnandt et al., 2016; Ruiwen et al., 2016) is the way the material is presented. In contrast to the usual cylindrical threads, suture tapes have become available in recent years on the assumption that, by increasing the area of interaction between the tissue and the suture, the traction is spread over a larger area, reducing contact pressures (Burgess et al., 2010) and consequently reducing the damage caused to the biological tissue. On this basis, Cerminara et al. (Cerminara et al., 2014) propose the use of this alternative as a possibility for improving the mechanical properties of the repair. Subsequently, Feutch et al. (Feucht et al., 2015) included the use of 2mm ultra-strong tape material (FiberTape™) in the comparative analysis with yarns of different materials in the biomechanical study mentioned above. Under cyclic loading conditions, the displacements obtained showed no significant differences between the use of tape or yarn of the same material, and even showed a higher mean (Perez-Blanca et al., 2018). However, a significantly higher ultimate load was found with the use of tape, which may be beneficial especially for the immediate postoperative period.

2.2.3 The impact of meniscal root tears on knee biomechanics

In the last fifteen years, several biomechanical studies have analysed the influence of medial meniscal root disinsertion and subsequent reinsertion on human joint contact parameters (Allaire et al., 2008; kim et al., 2013; Christopher M LaPrade et al., 2015a; Marzo and Gurske-DePerio, 2009; Padalecki et al., 2014; Seo et al., 2009). The results have shown changes in maximum contact pressures in the medial knee compartment with this injury in cadaveric knees (kim et al., 2013; Christopher M LaPrade et al., 2015a; Marzo and Gurske-DePerio, 2009; Padalecki et al., 2014) for varying pressure angles between 0 and 90°. Pressure increases measured are in the range of 25-45% for maximum pressure. In addition, mean pressure increases of 13-126% and contact area reductions of 17-64% have been observed.

The lesion of the posterior root of the lateral meniscus has historically received less attention than that of the medial meniscus. This is probably due to the greater difficulty in diagnosing root tears in the lateral meniscus, resulting in a lower number of diagnosed cases. With the publication of data on its clinical incidence (Ahn et al., 2009; Forkel and Petersen, 2012; Lerer et al., 2004) and especially its association with of ACL rupture cases, lesions of the lateral meniscus root began to be repaired as well. However, no biomechanical studies could be found supporting this intervention before 2012, when research interest in this area increased and a number of papers have been published since then. In a study conducted by (Schillhammer et al., 2012), the pressures and contact area in the lateral compartment of the human knee were measured during a gait cycle using human cadaveric knees. The results demonstrated significant alterations in the pressure distribution of the injured compartment in the presence of external meniscal root injury. Similar outcomes were observed by (LaPrade et al., 2014b; Perez-Blanca et al., 2016) across a range of flexion angles, spanning from 0° to 90°. Conversely, the efficacy of repair at low flexion angles is inconsistent across studies, though discrepancies in experimental design and repair techniques preclude direct comparison of the findings (Christopher M LaPrade et al., 2015a) also analysed the impact of a displacement of the suture insertion point from the original attachment in the tibia, and found that a non-anatomic root repair with a posteromedially displaced insertion point of 5 mm did not restore contact parameters to the same level as an anatomic repair, with an average increase in mean pressure of 54% and peak pressure of 33%, and with a 27% reduction in contact area compared to an anatomic repair. This result underscore the significance of a precise repair procedure that maintains the native meniscus coverage of the tibial cartilage.

As for the consequences of the detachment of the anterior roots, they remain poorly understood. A recent study examined the effects of avulsion of the lateral meniscus anterior root on the tibiofemoral joint (Espejo-Reina et al., 2022). The study found knee contact alterations similar to those with detached posterior roots, whith reduced contact area and raised pressure on the injured tibiofemoral cartilage at all flexion angles. However, these changes were more pronounced at low knee flexion angles, which are the most frequent in everyday activities, the effects being similar to a total meniscectomy. Therefore, the authors concluded that accurate diagnosis and appropriate treatment are vital for detached anterior roots, as knee contact alterations may cause cartilage issues like those observed with detached posterior roots.

Other aspects of the influence of injury on knee biomechanics have also been investigated (Hein et al., 2011) analysed the extrusion resistance of the medial meniscus after posterior meniscal root disinsertion and found significantly greater medial displacements and root separations with injury compared to those

measured without injury. These findings support the theoretical relationship between posterior meniscal root tears and clinically observed extrusion of the medial meniscus. Given the well-documented association between such extrusion and the development of degenerative arthritis in the knee, the authors emphasise the importance of early clinical evaluation and surgical treatment for optimal management of this type of injury.

2.3 Mechanical properties of the meniscus

The predominant and widely accepted method for evaluating the mechanical properties of the meniscus for modeling purposes, similar to other biological tissues, involves experimentally determining the material's strength and stiffness properties through uniaxial tests. A failure criterion, along with safety factors, is then applied to account for the interactions of multiple load directions and to ensure a margin of safety in the analysis. When investigating the behavior of the meniscus, samples are subjected to quasi-static or dynamic pure tensile, compressive, or shear forces. Throughout these tests, force and deformation measurements are collected. Subsequently, by normalizing these results according to specimen dimensions, stress-strain relationships are obtained, enabling the determination of various mechanical properties independent of specimen size.

To evaluate the meniscus's resistance to circumferential tensile stresses and radial extrusion, the most common method involves gripping both ends of the test sample and pulling them apart until rupture or until a specified strain level is reached. Based on the resulting stress-strain data, tensile properties such as the elastic or Young`s modulus, ultimate tensile strength, and cut-out strain can be calculated at tissue level, or deformation at specific loads, cut-out force and maximum force at specimen level (Peña-Trabalon et al., 2024, 2023). Investigations into the tensile properties of intact (Ellman et al., 2014; Lechner et al., 2000; Tissakht and Ahmed, 1995) and sutured menisci (Anz et al., 2014; Camarda et al., 2019; Mitchell et al., 2016; Peña-Trabalon et al., 2023; Vertullo et al., 2021) have predominantly applied circumferential tensile loads, overlooking the concurrent axial compressive forces inherent in physiological conditions

Compressive properties of the meniscal tissue have been studied using different experimental methodologies (Figure 2.13). They are often assessed using either confined (Joshi et al., 1995; Martin Seitz et al., 2013; Morejon et al., 2021; Seitz et al., 2021; Warnecke et al., 2020) or unconfined (Berni et al., 2021; Chia and Hull, 2008b; Lai and Levenston, 2010; Leslie et al., 2000) compression test

setups, through creep or stress relaxation testing modes. Another equally common approach is to perform indentation tests, which can also be conducted on confined or unconfined layouts, with a small impermeable indenter to assess the surface properties of a meniscal sample or a whole meniscus in situ. Depending on the chosen compression testing method and the corresponding mathematical model used to analyze the stress-strain data, various mechanical properties can be quantified. These include the elastic modulus, equilibrium modulus, instantaneous modulus, aggregate modulus, Poisson's ratio, and hydraulic permeability. However, all these approaches obviate the simultaneous action of circumferential tensile loads.

A more complex testing methodology is to conduct multiaxial test that provide loading in the appropriate directions to simulate the actual stress state. In this sense, we are only aware of meniscal biaxial testing involving traction in two perpendicular loads on the meniscal transverse plane (Barrera et al., 2018). When comparing uniaxial and biaxial tissue responses, it has been shown to be significantly different for tissues with collagenous fibers (Eilaghi et al., 2010; Gregory and Callaghan, 2011), as well as specifically for the meniscus (Kahlon et al., 2015).

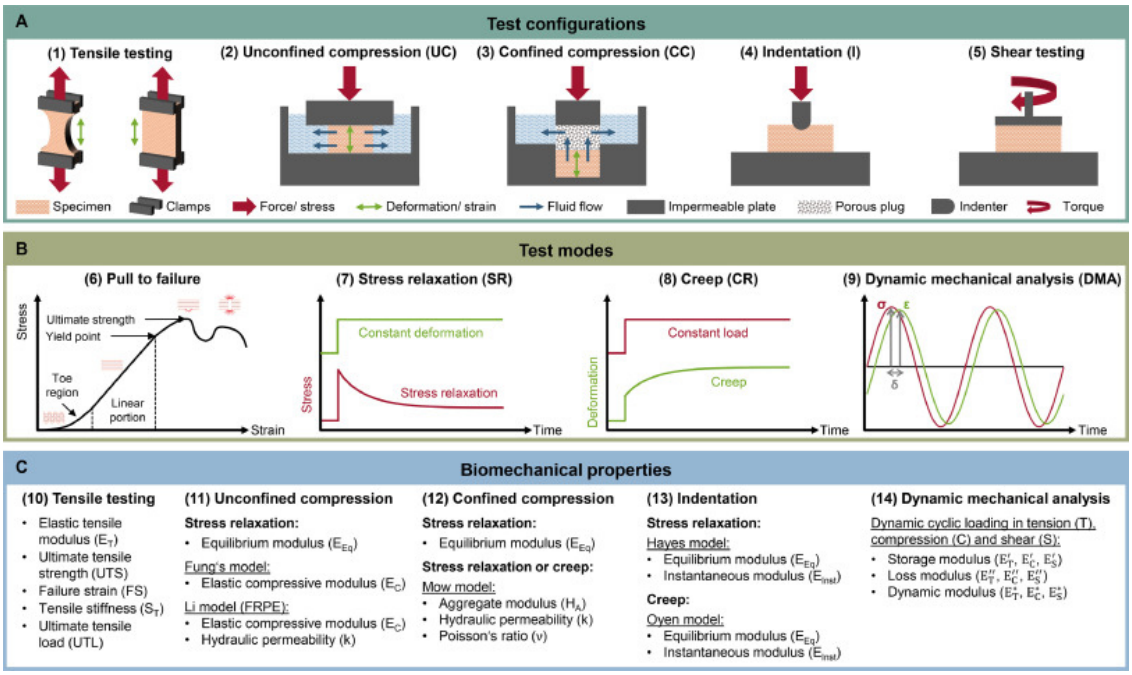

Figure 2.13. Representation of the different test configurations, test modes and biomechanical properties obtained from each test. Source: (Schwer et al., 2024).

However, if the physiological tensional state of the meniscal horn is to be reproduced, whether healthy or repaired, a testing configuration that includes traction in the direction of the circumferential fibers and compression in the axial direction should be desirable. On one hand, although the compressive properties of the healthy meniscal horn have been studied by several groups, to date, the compressive properties of the sutured meniscal horn have not yet been assessed. On the other hand, we are not aware of any studies that have addressed an approach to test any biological tissue reinforced with collagen fibers subjected to simultaneous traction and compression in different directions; obviously, not much less for the meniscus.

Experimental data obtained from mechanical tests under varying boundary and loading conditions are critical for refining analytical models that describe the mechanical behavior of meniscal tissue under combined stress states. These models, which range in complexity from basic to highly sophisticated, are frequently calibrated and validated by embedding them into FE analyses. The accuracy of these models is assessed by comparing their computational predictions with experimental results, thereby enhancing their reliability in representing the mechanical properties of the healthy or repaired menisci (Danso et al., 2015; Freutel et al., 2015; LeRoux and Setton, 2002).

2.3.1 Mechanical properties of meniscal tissue

The mechanical properties of meniscal tissue are intricately linked to its composition and structural organization, functioning as a composite material with a preferential alignment along the circumferentially oriented type I collagen fibers. In terms of stiffness, meniscal tissue exhibits significantly lower stiffness under axial compression.

Research on the tensile properties of human meniscal tissue in the circumferential direction, though limited, suggests that the tensile modulus of elasticity ranges between approximately 60 MPa and 220 MPa (Fithian and Kelly, 1990; Lechner et al., 2000; Masouros et al., 2008; Tissakht and Ahmed, 1995). However, there remains considerable debate regarding the variability of this modulus, with potential influences including the age of the specimen and the specific anatomical location within the meniscus, such as differences between the lateral and medial menisci, as well as variations across the upper, middle, or lower regions and the anterior, central, or posterior segments.

The circumferential elastic tensile modulus of the lateral meniscus demonstrates significant variation across different regions of the meniscus body. Specifically, that modulus ranges from 26.95 to 159.07 MPa in the anterior horn (AH), 27.57 to 228.79 MPa in the pars intermedia (PI), and 27.18 to 294.14 MPa in the posterior horn (PH) (Fithian and Kelly, 1990; Tissakht and Ahmed, 1995; Warnecke et al., 2020). In contrast, Yin et al. (Yin et al., 2021) reported that the circumferential elastic tensile modulus of the medial meniscus is up to 100 times lower (AH: 0.18 MPa; PI: 0.23 MPa; PH: 0.11 MPa) than values reported by other researchers (Fithian and Kelly, 1990; Lechner et al., 2000; Tissakht and Ahmed, 1995), who found modulus within a more consistent range: 72.00–159.58 MPa for the AH, 43.4–116.40 MPa for the PI, and 60.7–110.23 MPa for the PH. Additionally, studies observed a decreasing in the circumferential tensile modulus of the medial meniscus from anterior to posterior regions (AH: 159.58 MPa vs. PH: 110.23 MPa (Fithian and Kelly, 1990)) unlike the lateral meniscus, where the modulus increased posteriorly (AH: 159.07 MPa vs. PH: 294.14 MPa (Fithian and Kelly, 1990)).

Tissakht and Ahmed (Tissakht and Ahmed, 1995), and Bullough et al., (Bullough et al., 1970) studied the tensile modulus in radial direction providing values ranging from 4.07 MPa to 13.01 MPa for the AH, 4.21 MPa to 21.24 MPa for the PH, and 10.14 MPa to 14.17 MPa for the PI for the lateral meniscus (Bullough et al., 1970; Tissakht and Ahmed, 1995). Medial meniscus showed a radial elastic tensile modulus ranging from 3.59 MPa to 6.75 MPa in the AH, 2.03 MPa to 22.62 MPa for PH, and 5.60 MPa to 16.51 MPa for the PI (Bullough et al., 1970; Tissakht and Ahmed, 1995).

Research on the compressive properties in axial direction of meniscal tissue has primarily focused on several key parameters: the aggregate modulus, which measures overall tissue stiffness, the instantaneous modulus, which reflects the elastic response of the tissue without accounting for its viscoelastic properties, the relaxation modulus, which assesses the tissue's initial viscous response, and hydraulic permeability. Notably, the hydraulic permeability of meniscal tissue is reported to be an order of magnitude lower than that of articular cartilage, indicating a reduced capacity for fluid flow under pressure.

The reported compressive elastic modulus in the axial direction of both the lateral and medial meniscus varies significantly depending on the mathematical model used for evaluation, the applied load, and the strain at which it was measured. Chia and Hull (Chia and Hull, 2008a) conducted tests at a physiological strain level of 12%, evaluating the model at incremental strain levels of 3% to 12%, and found an average circumferential modulus of 0.33 MPa. In contrast, three other studies applied a destructive load of 1500 N (Leslie et al., 2000) or 100% strain (Nebelung et al., 2020; Truhn et al., 2020), resulting in a

mean circumferential modulus of 17.16 MPa at 20% strain and 329.36 MPa at 80% strain.

Berni et al. (Berni et al., 2021) performed unconfined stress relaxation tests in axial direction on cuboidal specimens from the lateral meniscus at incremental strain levels of 2%–10%, reporting an average circumferential modulus 71% higher (0.12 MPa) compared to Danso et al. (Danso et al., 2015), who used non-destructive indentation stress relaxation tests at higher strain levels (5%–20%), reporting a circumferential modulus of 0.07 MPa. Mahmood et al. (Mahmood et al., 2020) applied the poro-viscoelastic model proposed by Holmes and Mow (Holmes and Mow, 1990; Mow et al., 1980) with suitable boundary conditions for confined compression stress relaxation tests reporting a mean circumferential modulus of 0.75 MPa.

Fischenich et al. (Fischenich et al., 2015) conducted sinusoidal unconfined compression tests over 5000 cycles, evaluating the circumferential modulus based on a linear fit of the stress data from 2%–10% strain for each cycle, yielding results comparable to those of Chia and Hull (Chia and Hull, 2008a). Additionally, the circumferential modulus in the circumferential (Berni et al., 2021; Leslie et al., 2000) and radial (Berni et al., 2021; Chia and Hull, 2008a; Leslie et al., 2000) directions were found to be of similar magnitude to those measured in the axial direction (Schwer et al., 2024).

In summary, studies indicate that the mean instantaneous modulus in the axial direction ranges from approximately 0.10 MPa to 2 MPa (Danso et al., 2015; Fischenich et al., 2015; Pordzik et al., 2020a; Seitz et al., 2021), which is two orders of magnitude lower than the tensile modulus in the circumferential direction. Additionally, the axial mechanical properties are comparable to those in the radial direction. Both findings lead to the common assumption that meniscal tissue exhibits transverse isotropy in the plane perpendicular to the circumferential fibers. This pronounced deformability under axial compression enables the meniscus to conform to the changing geometry of the femur during knee flexion (Masouros et al., 2008). The reported values also underscore that meniscal tissue is highly specialized for resisting elongation forces, rather than compressive loads.

The published studies do not address the mechanical behavior of the repaired meniscal tissue in the vicinity of the suture hole when subjected to traction induced by the suture. The traction exerted on the puncture results in an alteration of the stress distribution on the affected area. The combined effect of this alteration and the compressive physiological loads is expected to generate a complex response that is challenging to predict. Given that root repair is conducted using sutures, it is essential to gain insight into the tissue's response

to this combined effect in order to adjust a material model that accurately replicates the behavior of the repair.

2.3.2 Mechanical properties of meniscal roots

Understanding the mechanical properties of meniscal root attachments is crucial for designing effective fixation systems used in both meniscal root repair and meniscal implant replacement.

Mechanical characterization of meniscal root ligaments has been achieved through various mechanical tests. These tests align the applied load with the direction of the longitudinal collagen fibres in the roots, which exhibit a specific alignment pattern that continues the circumferential orientation of the meniscal horn.

Static uniaxial tensile tests have provided data on the linear stiffness and ultimate tensile strength of complete meniscal roots (Abraham et al., 2011; Ellman et al., 2014; Hauch et al., 2010; Kopf et al., 2011) (Table 2.1). Variability in these properties has been attributed to differences in tissue quality among specimens (Ellman et al., 2014).

The contribution of less dense supplementary fibres, found in all roots except the LMAR, has been analysed. These fibres influence the mechanical properties of the roots significantly. Specifically, they account for 47.8% of the ultimate strength in the MMPR, 17.6% in the LMPR, and 28.4% in the MMAR. Their contribution to stiffness is 34.2%, 16.9%, and 8.9%, respectively. These findings highlight the importance of considering supplementary fibres in the design of meniscal attachments.

Time-dependent properties of the meniscal roots have also been evaluated through creep and stress relaxation tests (Hauch et al., 2010). The mean normalized values recorded were 0.76 for end load and -0.040 (1/ln(s)) for the relaxation ratio after 45 minutes at a constant strain of 3%. The mean normalized final displacement in the creep test was 1.036, and 0.008 for the normalized creep ratio after 45 minutes at the maximum load reached during the relaxation test. These results indicate a significant time dependence; however, as this aspect has been studied only once, further research is needed to validate these findings.

Table 2.1. Mean values of the mechanical properties of the human meniscal roots.

	Ultimate load (N)			**Stiffness (N/mm)**		**E (MPa)**
Root	Hauch et al.	Kopf et al.	Ellman et al.	Hauch et al.	Ellman et al.	Abraham et al.
MMAR	455.5	407	655.5	169.4	124.9	1.35
LMAR	652.2	692	652.8	215.8	151.1	1.21
MMPR	591.6	678	513.8	207.2	122.7	6.42
LMPR	330.3	648	509	129.5	128.7	1.21

2.3.3 Mechanical properties of the repaired meniscal root

Studies focused on investigating the mechanical properties of different suture repairs techniques for the avulsion of the meniscal root have been conducted by various researchers. The objective is to ascertain which of the proposed methodologies confers greater strength to the meniscus-suture assembly and allows the meniscus to recover greater functionality (Anz et al., 2014; Camarda et al., 2019; Kopf et al., 2011; Laprade et al., 2015b; Mitchell et al., 2016; Vertullo et al., 2021).

In order to carry out in vitro experimental investigation, the repair is simulated in the specimen to be tested and subjected to a load-to-failure test in the circumferential direction of the tissue, in order to analyse the strength and elongation of the repair. Generally, most of these studies apply preconditioning by cyclic traction (Anz et al., 2014; Camarda et al., 2019; Kopf et al., 2011; Laprade et al., 2015b; Vertullo et al., 2021), which can lead to a weakening of the meniscal tissue, and therefore, they are not comparable with studies in which the load is directly applied in tension until rupture. Other studies do not apply this type of preconditioning (Mitchell et al., 2016).

Table 2.2 shows the characteristics of each of the tests carried out by these previous studies, as well as the main relevant results obtained, and the types of specimens used.

Table 2.2. Parameters and test results characterizing repair by different types of sutures.

	Kopf et al.	**Mitchell et al.**		**Anz et al.**	**LaPrade et al.**	**Camarda et al.**		**Vertullo et al.**
	Two stitches	One stitch	Two stitches	Two stitches	Two stitches	Three stitches		Two stitches
Age	29.3±12.2 years	74 years		54±5 years	24.3 years	55.3 years	Porcine	54±4 years
n	8	12	12	10	8	12	12	10
Suture	UltraBraid No. 2	No. 0 FiberWire		No. 2 FiberWire	No. 2 FiberWire	No. 2 FiberWire		UltraBraid No. 0
Horn	Posterior	Posterior		Posterior	Posterior	Posterior		Medial posterior
Preacondi tioning	20 cycles (50N-100N) 0.5 mm/s	-		20 cycles (50N-100N) 0.5 mm/s	1000 cycles (10N-30N) 0.5 Hz	1000 cycles (10N-30N) 0.5 Hz		1000 cycles (5N-20N) 0.5 Hz
Loading velocity	0.5 mm/s	0.5 mm/s		0.5 mm/s	0.5 mm/s	0.5 mm/s		0.5 mm/s
Cut-out force (N)	-	-		137±49	-	-		82.49±14.17
Ultimate force (N)	64.1±22.5	58.2±29.6	96.2±51.4	-	192±52	161.3±25. 5	390±13.3	94.29±7.99
Stiffness (N/mm)	-	377±283	774±730	31.5±7.2	-	500 cycles 77±18 1000 cycles 79±17	500 cycles 107±45 1000 cycles 115±50	24.55±4.0

2.4 Computational models of human meniscus

2.4.1 Meniscus models in FE models of the knee joint

The majority of computational models of the meniscus described in the literature are components of a higher-level model representing the entire knee. The most prevalent methodology for developing such numerical models is the finite element (FE) method.

The purpose of these knee models is, among others, to analyse the biomechanical behavior of the knee in the event of a certain injury, to replicate surgical techniques oriented to enhancing outcomes, or to compare different repair methodologies.

Until relatively recently, meniscal pathologies were repaired by partial or total meniscectomy of the affected meniscus. Because of this, the first models created had a special interest in studying and identifying the effects of different types of meniscectomies on joint contact biomechanics (Dong et al., 2014; Mononen et al., 2013; Peña et al., 2005; Vadher et al., 2006; Zhang et al., 2021) (Figure 2.14). The continued use of partial meniscectomies in a multitude of cases nowadays evidence the continued relevance and necessity for rigorous investigations in this field.

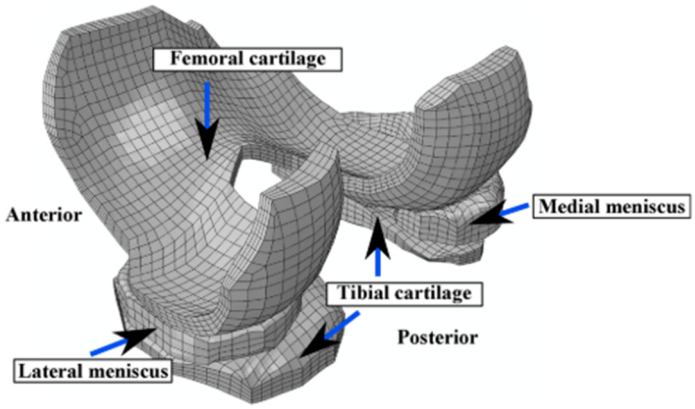

Figure 2.14. Finite Element Model of the knee joint including the menisci and their interaction with tibial and femoral cartilage, considering the bony elements as rigid. Source: Mononen et al., 2013.

Another common area of research is the contribution of soft tissues, such as menisci and the major ligaments of the knee, to knee stability. In some cases, this includes the effect of the patellar tendon and patella. (Peña et al., 2006).

The study of the effect of meniscal root avulsions and tears on joint contact biomechanics using whole knee models is more recent (Ardatov et al., 2023; Bao et al., 2013; Dong et al., 2014; Mononen et al., 2013; Steineman et al., 2020). The primary injuries examined by these models are radial tears of the posterior root of the lateral meniscus and meniscofemoral ligament tears, in comparison to total meniscectomy (Bao et al., 2013). Other, examined radial tears of the anterior and posterior root of the lateral meniscus, and of the medial meniscus body (Mononen et al., 2013). Radial tears of the medial meniscus and partial meniscectomies on it (Dong et al., 2014), as well as radial tears of the posterior root of the medial meniscus and its repair by suture (Steineman et al., 2022), have also been examined. In all cases, the results obtained were similar, indicating that the main effect of ruptures of any of the lateral or medial meniscal roots involved an increase in the mean and maximum contact pressures on the articular surface, as well as a decrease in the contact area in the compartment where the root rupture occurred. An extrusion of the meniscal body is also identified in some of the studies, with the contact area being affected (Bao et al., 2013). Because of this, the majority of medical specialists advocate for the preservation of the meniscus by repairing its root whenever feasible, and the minimisation of meniscectomy when necessary (Dong et al., 2014).

Most published works on meniscal root pathologies have focused on the posterior root of the medial meniscus. Very few studies have verified what happened when a radial rupture or an avulsion of the anterior root occurred (Mononen et al., 2013). There is limited research comparing the changes in parameters resulting from a complete radial tear of the anterior root with respect to the better-known posterior root of the lateral meniscus detachment. There is also no knowledge of any FE models that have addressed the specific simulation of the meniscal-suture interface, and the meniscal area affected by the suture in meniscal root repairs.

2.4.2 Inverse meniscal tissue material modelling with finite element simulations

FE modeling is extensively utilized in the replication and simulation of mechanical tests on biological structures. As sumarised above in Section 2.4, a substantial number of FE models are dedicated to studying the human meniscus and its role in the biomechanics of knee joint contact.

A primary challenge in developing FE models of human menisci lies in applying material models that can accurately and realistically replicate the mechanical behavior of meniscal tissue. Consequently, inverse FE analysis has gained widespread use in this field, as it provides an effective method for predicting material behavior, assessing mechanical properties, and examining variations in the function of biological tissues (Wheatley et al., 2015).

This method involves conducting experimental tests on the structure whose material is to be mechanically characterized. A FE model is then developed to replicate the experimental test, and using the experimental results along with an optimization algorithm, the coefficients of the selected material model are determined. This process allows for the accurate characterization of the structure's behavior. While this approach has been applied in various engineering fields, there has been growing interest in recent years in using it to characterize the mechanical behavior of meniscal tissue.

Recent research on the characterization of meniscal tissue using FE models has concentrated on developing methods to accurately determine the material properties of the meniscus from in vitro MRI data of intact knee joints, utilizing data from prior trials with porcine specimens (Freutel et al., 2015).

The development and application of a FE model of the meniscus, which incorporates a novel constitutive approach treating the meniscus as a hyper-poro-viscoelastic structure, was used to predict the tissue's behavior under non-destructive indentation relaxation testing (Wheatley et al., 2015). This model also includes a hyperelastic and transversely isotropic transverse deformation energy density function based on the Holzapfel model, enabling a more accurate simulation of the meniscal tissue's mechanical response.

Seyfi et al. (Seyfi et al., 2018) developed a new constitutive model that accounts for the local collagen network and created a fiber-reinforced poro-viscoelastic FE analysis to derive the constitutive parameters of the meniscus.

The latest work by De Rosa et al. (De Rosa et al., 2022a) focuses on a constitutive model that represents collagen fibers embedded within the extracellular matrix of the meniscus. This model aims to characterize the tissue's mechanical properties, with a particular emphasis on the circumferential fibers.

As has been observed, a common factor in these studies is that the FE method enables the characterization of meniscal tissue behavior through complex constitutive models. These models allow for a more accurate replication of meniscal tissue behavior by incorporating elements such as collagen fibers (Seyfi et al., 2018) or viscoelastic considerations (De Rosa et al., 2022a; Seyfi et al., 2018; Wheatley et al., 2015), whose effects on the material properties would otherwise be difficult to account for.

Currently, the use of inverse finite element models in the characterization of meniscal tissue is primarily focused on healthy menisci, with limited development in modeling menisci with sutured roots.

2.4.3 Meniscus properties in computational models of the knee

The human meniscus exhibits anisotropic, nonlinear, low compressibility and poro-viscoelastic behavior, although the necessity for considering all these effects depends on the load intensity and variation characteristics.

Meniscus modeling can be approached from a phenomenological point of view using energy density functions, where the meniscus is considered at the macroscopic level, with simple models of homogeneous, linearly elastic and isotropic $(E = 59\,MPa, \upsilon = 0.49)$ (Peña et al., 2006), or transversely isotropic material $(E_\theta = 120\,MPa;\ E_{r,z} = 20\,MPa; \upsilon_{\theta,r} = 0.20;\ \upsilon_z = 0.30)$ (Bao et al., 2013; Zielinska and Haut Donahue, 2006). Another approach is the structural one, which considers the characteristics of micro-constituents in the macro-mechanical response, with hyperelastic material models of isotropic matrix $(E_\theta = 150\,MPa;\ E_{r,z} = 20\,MPa; \upsilon_{\theta,r} = 0.20;\ \upsilon_z = 0.30; G = 57.70\,MPa)$ reinforced with collagen fibers in circumferential direction (Zielinska and Haut Donahue, 2006) as well as poro-elastic (Freutel et al., 2015), and even extended to include viscoelastic effects (Seyfi et al., 2018). In the published works, with the assumption of negligible viscoelastic effects, the constitutive model that produces the best fit for the meniscus, is the hyperelastic one with a compressible isotropic matrix and reinforced by the anisotropic effect of collagen fibers.

As for meniscal roots, they are usually modelled as a set ten linear springs with stiffness values of 200 N/mm, resulting in a value of 2000 N/mm for each horn (Donahue et al., 2002) or modelled as an isotropic, homogeneous material

with Young´s modulus between 111 MPa (Kiapour et al., 2014) and 120 MPa (Wang et al., 2021).

Regarding the suture-repaired meniscus root, very few computational models simulate the behavior of the sutures that replace the ligaments. These sutures are typically included as linear elastic elements with the stiffness of the suture thread, without consideration of the specific suturing technique or the complex behavior at the suture-tissue interface, as observed in experimental in-vitro studies (Perez-Blanca et al., 2018). These findings suggest the necessity for a more sophisticated modelling approach, encompassing both the suture and its interaction with the meniscus.

2.5 Testing machines

In this thesis, two different types of testing machines were used depending on the characteristics of tests conducted. The first group of test benches was used for tests involving traction, specifically traction load-to-failure tests, while the second type of tester was used for indentation tests.

2.5.1 Universal testing machines

Two universal testing machines were used in this thesis: one was located at the BIOCLINA laboratory of the University of Malaga in Spain, used for the experimental test described in Chapter 3 and Chapter 4, and the other one at the Institute of Orthopaedic Research and Biomechanics of the University of Ulm in Germany, used for the experimental tests described in Chapter 6.

2.5.1.1 Universal testing machine at BIOCLINA

The uniaxial traction/compression testing machine used for the tests described in Chapter 3 and Chapter 4 (Figure 2.15) was designed and built by the BIOCLINA research group for its specific use in the testing of biological tissues (Prado et al., 2013). It is a compact electromechanical single-column testing machine, with the load applied in vertical direction, and installed on a mobile platform. It was designed with a versatile configuration to allow for testing a wide range of biological tissues, which do not demand high loads nor high frequencies in the test protocols, and to perform tests in tension, compression, bending, tearing or peeling. The machine is equipped with a user-friendly interface for both control and the output of the test results.

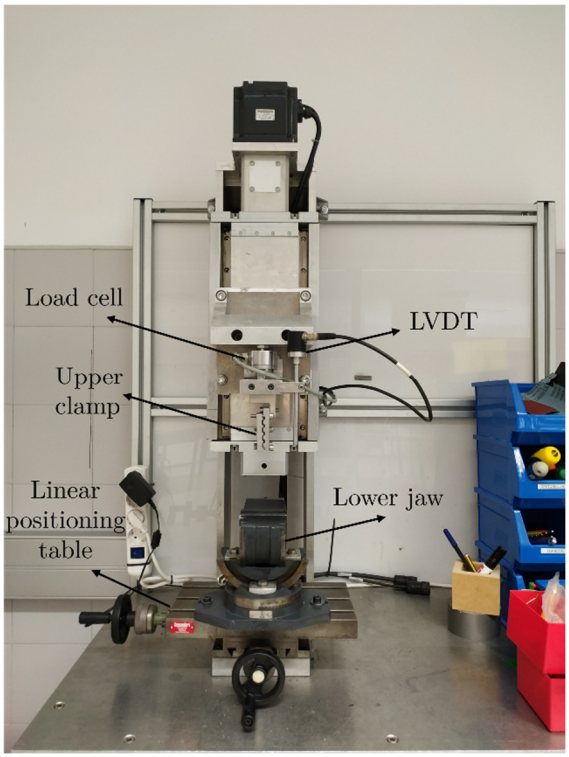

Figure 2.15. Uniaxial testing machine designed in the Clinical Biomechanics Laboratory of Andalusia and used for the load-to-failure tests performed.

2.5.1.1.1 General description

The machine features an electromechanical loading system that includes a vertical spindle with a recirculating ball screw (Accuslide 2HBE20, Tecnopower, Spain) driven by an electrical servosystem (Sigma II Servo System, Omron Electronics Iberia, S.A.U., Spain). The servomotor is fixed and mounted at the upper end of the column of the machine. The motion is transmitted directly through a coupling mechanism, without any reduction or amplification, to the recirculating ball screw. This direct coupling ensures efficient and accurate transfer of motion from the motor to the vertical spindle. The ball screw converts the rotary motion of the motor into linear displacement, with a pitch of 10 mm, and a maximum stroke of 500 mm.

The electrical system comprises a 1.5 kW servomotor with an encoder (SGMPH-15A1A61D-OY) and a servo drive (SGDH-15AE-S-OY). This setup enables precise control of the motor's speed and position, tailored to the needs of the application. The motor is relatively compact, making them well-suited for applications that require optimal load matching.

For gripping and correct positioning of the specimens to be tested a versatile solution was adopted, which includes:

- A flat plate that constitutes the moving head of the testing machine. The plate includes a screwed housing for the positioning of a load cell as detailed in section 5.2.1.1.2: Various fixtures are available for attachment to the lower end of the load cell to secure the testing samples: mechanical clamps, punch, compression contact plane, fix pin...

- The fixture at the base of the testing machine provides up to 5 degrees of freedom for the correct positioning of the samples. Specifically, a three rotatory degrees of freedom jaw (TLT/SP-75, Wilton Tools, USA) is used to mechanically clamp the samples. This jaw is mounted on a two-axis linear positioning table (FB-H milling table, Demanders®, Sweden), allowing for two additional linear degrees of freedom, i.e., movement in two directions perpendicular to the loading direction.

All the mechanical systems mentioned above are placed on top of a structure made of aluminum profiles and iron plates (Figure 2.15), which provides sufficient rigidity for the applied loads while maintaining a moderate weight. The lower part of the structure houses the electrical and control components, which includes the CPU and the control panel (Figure 2.16). The structure incorporates four wheels to facilitate its mobility.

Figure 2.16. Lower part of the machine structure of BIOCLINA: a) CPU; b) Control panel.

2.5.1.1.2 Characteristics of measurement systems

The system is equipped with both force and displacement measurement systems to gather the necessary signals for controlling the machine and to acquire testing variables.

To measure the vertical force exerted on the specimen, the machine built-in a measurement system comprising a load cell, which is easily interchangeable, and an amplifier (Clip AE101, HBM, Darmstadt, Germany). For this thesis a uniaxial load cell with a maximum measurement range of 2 kN and an accuracy class of 0.1 (U2B, HBM, Darmstadt, Germany) was mounted with the measurement axis aligned with the loading direction. The amplifier enables adjustment of the working range to match the expected maximum forces, with the accuracy of the system being ±0.1% of the nominal force, depending on the set maximum value. For the purposes of this thesis, the measurement range was customized to meet the specific requirements of each test, as described in the respective sections.

There are three measurement sensors integrated into the machine's control, two displacement sensors and the load cell mentioned in previous paragraph. The signals from the three sensors can be used to control the servo system's output during displacement-controlled or force-controlled tests.

Both displacement sensors are inductive sensors, although with very different measuring ranges:

- A 16-bit encoder that records the displacement of the servomotor spindle, with a resolution of 65536 pulses/motor revolution.

- A linear variation differential transformer (LVDT) model LVP-100-ZA-2.5 SR7-I (Micro-Epsilon, Ortenburg, Germany). Its measuring range is 100 mm and its resolution is 0.03 mm according to the manufacturer. The sensor body can be fixed to any points of the machine or specimen and its core can also be rested or fixed on any surface, thus enabling direct measurement of any local displacement in any direction depending on the planned test.

Signals can also be recorded to obtain the absolute displacement of the head with respect to the base of the testing machine and relative displacements between the points monitored by the LVDT.

2.5.1.1.3 Characteristics of the control system

The testing machine operates under the control of a servo system and signals from the load or position sensors. As previously explained, the stepper motor's control signal or the LVDT signal can be used for displacement-controlled tests, while the load cell signal is employed for force-controlled tests.

All sensor signals are captured by a data acquisition card integrated into a CPU, which controls the machine, manages the tests, and records data. The control program designed using LabVIEW® (LabVIEW 2018, National Instruments, United States), features a clear and user-friendly interface. This interface includes tools for operating the machine, visualizing data graphs, providing usage instructions, and setting the necessary test parameters.

Data collected during the tests include signals from the load cell, the LVDT, and the position of the servomotor (translate to linear displacement of the machine head). The interface allows users to define the sampling frequency for data storage. The software provides real-time graphical displays of the sensor signals, enabling continuous monitoring of the test's progress.

Additionally, a 5V signal can be activated at the start of the tensile test to synchronize the acquired data with other systems. This signal was used in the tests described in chapters 3 to 6 to synchronize image capture with load and displacement data.

The control software supports manual operation for positioning the specimen and offers various test configurations used for analysing the mechanical behaviour of soft tissues, such as preconditioning, cyclic load testing, and rupture testing.

2.5.1.2 Universal testing machines at Institute of Orthopaedic Research and Biomechanics of the University of Ulm

2.5.1.2.1 Uniaxial testing machine

The uniaxial traction/compression testing machine used for the tests described in Chapter 6 (Figure 2.17) is the Zwick Z010 universal testing machine (ZwickRoell, Germany). It is a customizable and highly versatile testing machine, well-suited for applications across various fields. The machine can be used to perform tests in tension, compression and bending. The machine is equipped with an interface for both control and the output of the test results.

The machine is capable of operating at a maximum test force of 10 kN, with a crosshead speed ranging from 0.0005 mm/min to 2000 mm/min. The maximum return speed of the crosshead is 3000 mm/min, and the machine requires a drive power of 500 W.

Its mechanical modularity allows for easy expansion of the testing system through a wide range of interchangeable specimen grips. This flexibility enables a broad variety of tests to be conducted using the same machine and allows for quick adaptation to different testing requirements.

Figure 2.17. Uniaxial testing machine available at the Institute of Orthopaedic Research and Biomechanics of the University of Ulm and used for the load-to-failure tests performed.

For gripping and correct positioning of the specimens to be tested, there is:

- A head which is directly driven by the upper crosshead of the machine. An indenter, a clamp and a punch can be attached to this head.

- A lower area which is fixed to the base of the machine, where testing chambers, clamps and contact planes can be attached.

The machine is also equipped with the testControl II measuring and control electronics (ZwickRoell, Germany), mounted vertically on the side of the loading frame. This design protects the electronics from exposure to liquids and conductive particles, ensuring reliable performance during testing.

2.5.1.2.2 Indentation tests machine

In the development of this the Biomomentum indenter (MACH-1 v500css, Biomomentum Inc., Laval, QC, Canada) available at the Institute of Orthopaedic Research and Biomechanics of the University of Ulm in Germany was used (Figure 2.18). It is a compact, mobile and versatile multiaxial loading machine.

The Mach-1™ Micromechanical System is comprised of several key components, including the tester frame, one to three motorized stages, manual stages, a motion controller, one or more load cells, a load cell amplifier, a computer, and various accessories such as testing chambers, grips, and fixtures, depending on the specific configuration purchased.

During operation, the motorized stages are programmed to compress, stretch, or bend the test sample, while the load cell measures the force generated by the sample in response to this deformation. The load cell amplifier supplies power to the load cell and converts the analog force measurement into a digital signal, which is subsequently transmitted to the computer. The motion controller directs the movement of the stages, which are controlled by the Mach-1 software.

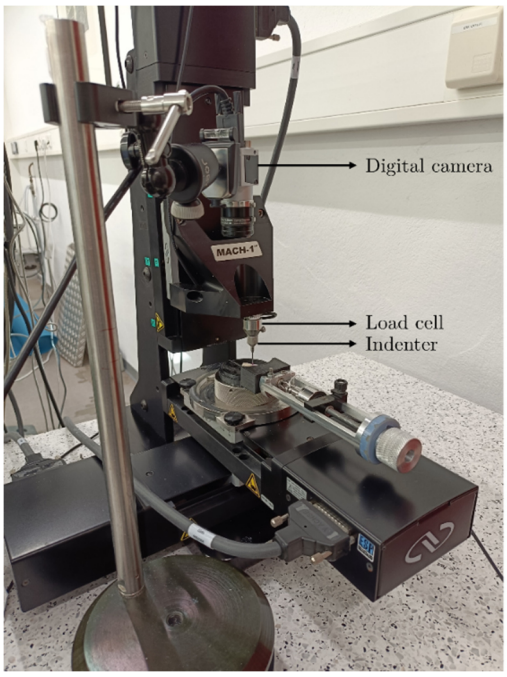

Figure 2.18. Multiaxial testing machine employed in the indentation tests.

The Mach-1 software enables control of stage displacement, with motion options that can be manually operated or automatically programmed according to user-defined protocols. Examples of controlled motion routines include "Stress Relaxation," "Sinusoid," and "Ramp-Release." For the stress relaxation tests described in Chapter 6 of this thesis, a deformation or strain is applied to the sample, and the resulting response is monitored over a specified period.

For gripping and correct positioning of the specimens to be tested, there is:

- A head which is directly driven by the machine body. An indenter, a clamp and a punch can be attached to this head.
- A lower area where testing chambers, clamps and contact planes can be attached to this region.

- A multiaxial linear positioning system that allows movement in three directions (x, y, z).

The system is equipped with both force and displacement measurement systems for controlling the machine and obtaining the output parameters during testing. These measurement systems capture the necessary signals to regulate the machine's operations and provide data on the force applied and the resulting displacement.

To measure the vertical force exerted on the specimen, the machine uses a load cell with an amplification module (FTIFPS1, ATI, Michigan, USA). The load cell has a maximum measurement range of 250 N and a resolution of 12.5 mN. The displacement is recorded by the machine servo-controller (Biomomentum Inc., Laval, QC, Canada).

A digital camera (MA732, Biomomentum Inc., Laval, QC, Canada) is integrated with the system to capture images during testing. The camera is equipped with a CMOS sensor providing a resolution of 1280x1024 pixels, a focal length of 12.5 mm, and a minimum field of view of 7.1 mm (HF12.5HA-1B, Fujifilm, Tokyo, Japan).

2.6 Videogrammetric system

The videogrammetric system used in this thesis consists of an image capture system, and a post-processing algorithm for the images captured during the experimental test. The algorithm was designed as part of this thesis to compute the strain between dots of interest marked on the tissue surface, with the aim of

obtaining stress-strain curves when combined with the force obtained from the universal testing machines described in Sections 2.5.1.1 and 2.5.1.2.1.

2.6.1 Image capture system

Two image capture systems were used in this thesis: one for the experimental test described in Chapter 3 and Chapter 4 conducted at the BIOCLINA laboratory of the University of Malaga in Spain, and the other one for the experimental tests described in Chapter 6 conducted at the Institute of Orthopaedic Research and Biomechanics of the University of Ulm in Germany.

For the experimental tests conducted in the BIOCLINA laboratory, the images were recorded with a Baumer Digital color camera, model VCXU-124C (Baumer, Frauenfeld, Switzerland). It is characterized by CMOS sensors with a resolution of 4096x3000 pixels and a maximum frame rate of 29 frames per second. The camera incorporates a PENTAX C7528 lens (Pentax Ricoh Imaging Company Ltd, Japan), with a focal length of 75mm ± 5%, a maximum aperture range of 1:2.8 and a focal ratio (f) 2.8 to 32. To ensure stability, the camera was mounted on a tripod, fixing all its displacements and rotations in space (Figure 2.19).

Figure 2.19. Devices used in the videogrammetric system in BIOCLINA. a) Digital camera with the PENTAX lens; b) Digital camera mounted in the tripod oriented to the uniaxial testing machine.

The images were acquired using a software previously developed at the BIOCLINA laboratory in the LabVIEW® (LabVIEW 2018, National Instruments, United States) environment. The software facilitates the adjustment of various acquisition parameters such as exposure time, number of images to capture, capture frequency, and total recording time. The activation of the acquisition is controlled by this software, which responds to the signal sent by the control system to the traction testing machine to ensure synchronization between the captured images and the variables acquired by the testing machine.

For the experimental tests conducted in the University of Ulm the images were recorded with a JAI Digital color camera, model GO-5100C-USB (JAI

Cameras, Valby, Denmark). It is characterized by a Sony Pregius IMx250CMOS imager and a maximum frame rate of 74 frames per second. The camera incorporates a Computar V1624-MPZ lens (Computar, Japan), with a focal length of 16mm, a maximum aperture range of 1:2.4 and a focal ratio (f) 2.4 to 16 (Figure 2.20).

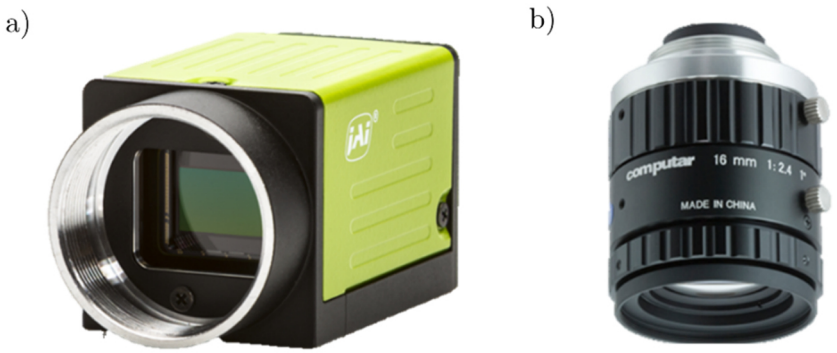

Figure 2.20. Devices used in the videogrammetric system in Ulm laboratory. a) Digital camera; b) Lens used in the tests.

2.6.2 Tracking algorithm

The videogrammetric software, developed in MATLAB® (MATLAB 2018b, MathWorks, USA), was designed to track marks on the image planes, wich correspond to dots marked on tissues, specifically in this thesis on the meniscus surface. The software first tracks the marks throughout the recorded test and computes the coordinates of these marks in each calibrated frame, storing them in a vector referenced to the same time frame as the testing machine. Thus, the videogrammetric outputs are synchronized with the outputs of the testing machine. Next, vectors with the distance between each two selected marks are computed.

This algorithm comprises the four following phases:

Calibration

Before the test begins, the user is required to capture an image for calibration. This image must include a measurement pattern that is visible within the same image plane as the marks to be tracked during the test. The algorithm performs the calibration process on this image, that allows to translate the coordinates of the image plane collected in pixels into coordinates expressed in units of length.

This transformation is retained and used for the computation of the coordinates of the marks during the test expressed in units of length

Image processing

Firstly, the number of marks to be tracked is selected. For the applications in this thesis, the number is set to 2 marks. Additionally, the approximate diameter of these marks in pixels must be indicated. To assist with this task, the software allows to measure the diameter of any mark on the initial image captured for calibration using the screen ruler tool.

Next, a colour filtering threshold must be selected. This filter is applied to the captured images using the HSV (Hue, Saturation, Value) color model. The software executes a thresholding process with specific ranges: a hue range between 0 and 0.20, a saturation range between 0 and 0.60, and a value range between 0 and 0.05, all normalized to a maximum of 1. Pixels that do not meet the threshold criteria are assigned a value of 0, while those that do are assigned a value between 1 and 255, with 255 being the maximum. After applying the thresholding process, binarization is performed on each frame using an 8-bit format.

Subsequently, a morphological closing operation is conducted using a disk-shaped structuring element with a radius of 4 pixels. This step helps smooth the borders of identified regions and fills any small holes. To exclude irrelevant data, a minimum area filter of 50 pixels^2 is applied, which removes small isolated pixels that are not part of any significant mark. To further refine the results, the software applies an intensity grayscale threshold of 50, which eliminates areas that meet the colour threshold but have an intensity lower than the specified value. Only areas with pixel values exceeding 50 are retained in the frame.

This entire process is uniformly applied to all frames acquired by the cameras during the load-to-failure test, ensuring consistent and accurate identification of the marks throughout the test.

Computation of the coordinates of each mark

In the first frame, the initial position of each mark to be tracked is manually identified. These initial positions serve as reference points for the algorithm, which then confines its search area to a 10x10 pixel region around these marks in subsequent frames. By focusing the search within this confined area, the algorithm

streamlines the process of identifying the circular regions corresponding to the marks, significantly reducing the time required for processing each frame.

This iterative procedure is consistently applied across all the captured frames, ensuring that the tracking remains accurate and efficient throughout the entire test. The algorithm updates the coordinates of the marks in each frame based on their positions in the previous frame, allowing it to maintain continuity in tracking.

Once all frames have been processed, the software generates a matrix containing the 2D coordinates of the centroids of the marks in each frame. These coordinates initially expressed in pixels, are then converted to units in length (milometers by default) at this point by using the transformation computed in the calibration phase.

Calculation of the distances between marks

Distances between the marks are computed across all frames, providing a detailed record of the displacement evolution between the marks throughout the test.

The vector data (2D coordinates of the marks and distances between marks) are saved into the MATLAB® workspace, ensuring that they are preserved for further analysis and review.

2.7 References

Abraham, A.C., Moyer, J.T., Villegas, D.F., Odegard, G.M., Haut Donahue, T.L., 2011. Hyperelastic properties of human meniscal attachments. J Biomech 44, 413–418. https://doi.org/10.1016/j.jbiomech.2010.10.001

Adams, M.E., Muir, H., 1981. The glycosaminoglycans of canine menisci. Biochemical Journal 197, 385–389. https://doi.org/10.1042/BJ1970385

Ahn, J.H., Lee, Y.S., Chang, J.Y., Chang, M.J., Eun, S.S., Kim, S.M., 2009. Arthroscopic all inside repair of the lateral meniscus root tear. Knee 16, 77–80. https://doi.org/10.1016/J.KNEE.2008.07.008

Ahn, J.H., Wang, J.H., Yoo, J.C., Noh, H.K., Park, J.H., 2007. A pull out suture for transection of the posterior horn of the medial meniscus: Using a

posterior trans-septal portal. Knee Surgery, Sports Traumatology, Arthroscopy 15, 1510–1513. https://doi.org/10.1007/S00167-007-0310-3/FIGURES/6

Allaire, R., Muriuki, M., Gilbertson, L., Harner, C.D., 2008. Biomechanical consequences of a tear of the posterior root of the medial meniscus: Similar to total meniscectomy. Journal of Bone and Joint Surgery 90, 1922–1931. https://doi.org/10.2106/JBJS.G.00748

Anz, A.W., Branch, E.A., Saliman, J.D., 2014. Biomechanical Comparison of Arthroscopic Repair Constructs for Meniscal Root Tears. Am J Sports Med 42 (11), 2699–2706. https://doi.org/10.1177/0363546514549445

Ardatov, O., Aleksiuk, V., Maknickas, A., Stonkus, R., Uzieliene, I., Vaiciuleviciute, R., Pachaleva, J., Kvederas, G., Bernotiene, E., 2023. Modeling the Impact of Meniscal Tears on von Mises Stress of Knee Cartilage Tissue. Bioengineering 2023, Vol. 10, Page 314 10, 314. https://doi.org/10.3390/BIOENGINEERING10030314

Arnoczky, S., 1992. Gross and vascular anatomy of the meniscus and its role in meniscal healing, regeneration, and remodeling. Knee meniscus: basic and clinical foundations 1–14.

Bao, H.R.C., Zhu, D., Gong, H., Gu, G.S., 2013. The effect of complete radial lateral meniscus posterior root tear on the knee contact mechanics: A finite element analysis. Journal of Orthopaedic Science 18, 256–263. https://doi.org/10.1007/S00776-012-0334-5/TABLES/3

Barrera, O., Bologna, E., Zingales, M., Alotta, G., 2018. Experimental Characterization of the Human Meniscal Tissue. IEEE 4th International Forum on Research and Technologies for Society and Industry, RTSI 2018 - Proceedings. https://doi.org/10.1109/RTSI.2018.8548369

Beaupr, A., Choukroun, R., … R.G.-C.O., 1986, undefined, 1986. Knee menisci: correlation between microstructure and biomechanics. Clin Orthop Relat Res 72–75.

Berlet, G.C., Fowler, P.J., 1998. The anterior horn of the medical meniscus. An anatomic study of its insertion. Am J Sports Med 26, 540–543. https://doi.org/10.1177/03635465980260041201

Berni, M., Marchiori, G., Cassiolas, G., Grassi, A., Zaffagnini, S., Fini, M., Lopomo, N.F., Maglio, M., 2021. Anisotropy and inhomogeneity of permeability and fibrous network response in the pars intermedia of the human lateral meniscus. Acta Biomater 135, 393–402. https://doi.org/10.1016/J.ACTBIO.2021.08.020

Bhatia, S., Laprade, C.M., Ellman, M.B., Laprade, R.F., 2014. Meniscal root tears: Significance, diagnosis, and treatment. American Journal of Sports Medicine 42, 3016–3030. https://doi.org/10.1177/0363546514524162/ASSET/IMAGES/LARGE/10.1177_0363546514524162-FIG7.JPEG

Bin, S. Il, Jeong, T.W., Kim, S.J., Lee, D.H., 2016. A new arthroscopic classification of degenerative medial meniscus root tear that correlates with meniscus extrusion on magnetic resonance imaging. Knee 23, 246–250. https://doi.org/10.1016/J.KNEE.2015.07.003

Brantigan, O., Voshell, A.F., 1941. THE MECHANICS OF THE LIGAMENTS AND MENISCI OF THE KNEE JOINT. Journal of Bone and Joint Surgery, American Volume.

Bullough, P.G., Munuera, L., Murphy, J., Weinstein, A.M., 1970. The strength of the menisci of the knee as it relates to their fine structure. J Bone Joint Surg Br 52, 564–567. https://doi.org/10.1302/0301-620X.52B3.564/LETTERTOEDITOR

Burgess, R., Elder, S., Mclaughlin, R., Constable, P., 2010. In Vitro Biomechanical Evaluation and Comparison of FiberWire, FiberTape, OrthoFiber, and Nylon Leader Line for Potential Use During Extraarticular Stabilization Of Canine Cruciate Deficient Stifles. Veterinary Surgery 39, 208–215. https://doi.org/10.1111/J.1532-950X.2009.00637.X

Camarda, L., Bologna, E., Pavan, D., Morello, F., Monachino, F., Giacco, F., Zingales, M., 2019. Posterior meniscal root repair: a biomechanical comparison between human and porcine menisci. Muscle Ligaments and Tendons Journal 9, 76–81. https://doi.org/10.32098/MLTJ.01.2019.03

Cerminara, A.J., LaPrade, C.M., Smith, S.D., Ellman, M.B., Wijdicks, C.A., LaPrade, R.F., 2014. Biomechanical Evaluation of a Transtibial Pull-out

Meniscal Root Repair Challenging the Bungee Effect. American Journal of Sports Medicine 42, 2988–2995. https://doi.org/10.1177/0363546514549447

Chahla, J., Beletsky, A., Smigielski, R., Brown, C.H., 2022. Meniscal Pathology: Meniscus Anatomy. Evidence-Based Management of Complex Knee Injuries: Restoring the Anatomy to Achieve Best Outcomes 157–175. https://doi.org/10.1016/B978-0-323-71310-8.00013-X

Chahla, J., Moatshe, G., Dean, C.S., LaPrade, R.F., 2016. Posterolateral Corner of the Knee: Current Concepts. Archives of Bone and Joint Surgery 4, 97.

Cheung, H.S., 1987. Distribution of Type I, II, III and V in the Pepsin Solubilized Collagens in Bovine Menisci. Connect Tissue Res 16, 343–356. https://doi.org/10.3109/03008208709005619

Chia, H.N., Hull, M.L., 2008a. Compressive moduli of the human medial meniscus in the axial and radial directions at equilibrium and at a physiological strain rate. Journal of Orthopaedic Research 26, 951–956. https://doi.org/10.1002/JOR.20573

Chia, H.N., Hull, M.L., 2008b. Compressive moduli of the human medial meniscus in the axial and radial directions at equilibrium and at a physiological strain rate. Journal of Orthopaedic Research 26, 951–956. https://doi.org/10.1002/JOR.20573

Cho, J.H., 2012. Modified Pull-out Suture in Posterior Root Tear of the Medial Meniscus: Using a Posteromedial Portal. Knee Surg Relat Res 24, 124. https://doi.org/10.5792/KSRR.2012.24.2.124

Danso, E.K., Mäkelä, J.T.A., Tanska, P., Mononen, M.E., Honkanen, J.T.J., Jurvelin, J.S., Töyräs, J., Julkunen, P., Korhonen, R.K., 2015. Characterization of site-specific biomechanical properties of human meniscus—Importance of collagen and fluid on mechanical nonlinearities. J Biomech 48, 1499–1507. https://doi.org/10.1016/J.JBIOMECH.2015.01.048

De Rosa, M., Filippone, G., Best, T.M., Jackson, A.R., Travascio, F., 2022. Mechanical properties of meniscal circumferential fibers using an inverse finite element analysis approach. J Mech Behav Biomed Mater 126, 105073. https://doi.org/10.1016/J.JMBBM.2022.105073

DePalma, A., 1955. Diseases of the Knee: Management in Medicine and Surgery. Phys Ther 35, 158–159. https://doi.org/10.1093/PTJ/35.3.158B

D'lima, D.D., Chen, P.C., Kessler, O., Hoenecke, H.R., Colwell, C.W., 2011. Effect of Meniscus Replacement Fixation Technique on Restoration of Knee Contact Mechanics and Stability. MCB 8, 123–134.

Donahue, T.L.H., Hull, M.L., Rashid, M.M., Jacobs, C.R., 2002. A Finite Element Model of the Human Knee Joint for the Study of Tibio-Femoral Contact. J Biomech Eng 124, 273–280. https://doi.org/10.1115/1.1470171

Dong, Yuefu, Hu, G., Dong, Yinghai, Hu, Y., Xu, Q., 2014. The effect of meniscal tears and resultant partial meniscectomies on the knee contact stresses: a finite element analysis. http://dx.doi.org/10.1080/10255842.2012.753063 17, 1452–1463. https://doi.org/10.1080/10255842.2012.753063

Eilaghi, A., Flanagan, J.G., Tertinegg, I., Simmons, C.A., Wayne Brodland, G., Ross Ethier, C., 2010. Biaxial mechanical testing of human sclera. J Biomech 43, 1696–1701. https://doi.org/10.1016/J.JBIOMECH.2010.02.031

Ellman, M.B., Laprade, C.M., Smith, S.D., Rasmussen, M.T., Engebretsen, L., Wijdicks, C.A., Laprade, R.F., 2014. Structural properties of the meniscal roots. American Journal of Sports Medicine 42, 1881–1887. https://doi.org/10.1177/0363546514531730

Engelsohn, E., Umans, H., DiFelice, G.S., 2007. Marginal fractures of the medial tibial plateau: Possible association with medial meniscal root tear. Skeletal Radiol 36, 73–76. https://doi.org/10.1007/S00256-006-0089-1/FIGURES/3

Espejo-Reina, A., Prado-Novoa, M., Espejo-Baena, A., Estebanez, B., Perez-Blanca, A., 2023. Improved tibiofemoral contact restoration after transtibial reinsertion of the anterior root of the lateral meniscus compared to in situ repair: a biomechanical study. Int Orthop 1, 3. https://doi.org/10.1007/s00264-023-05769-y

Espejo-Reina, A., Prado-Novoa, M., Espejo-Baena, A., Peña-Trabalon, A., Perez-Blanca, A., 2022. Biomechanical consequences of anterior root detachment of the lateral meniscus and its reinsertion. Sci Rep 12, 6182. https://doi.org/10.1038/S41598-022-10229-5

Feucht, M.J., Grande, E., Brunhuber, J., Rosenstiel, N., Burgkart, R., Imhoff, A.B., Braun, S., 2015. Biomechanical evaluation of different suture materials for arthroscopic transtibial pull-out repair of posterior meniscus root tears. Knee Surg Sports Traumatol Arthrosc 23, 132–139. https://doi.org/10.1007/S00167-013-2656-Z

Feucht, M.J., Grande, E., Brunhuber, J., Rosenstiel, N., Burgkart, R., Imhoff, A.B., Braun, S., 2014. Biomechanical comparison between suture anchor and transtibial pull-out repair for posterior medial meniscus root tears. American Journal of Sports Medicine 42, 187–193. https://doi.org/10.1177/0363546513502946/ASSET/IMAGES/LARGE/10.1177_0363546513502946-FIG2.JPEG

Fischenich, K.M., Lewis, J., Kindsfater, K.A., Bailey, T.S., Haut Donahue, T.L., 2015. Effects of degeneration on the compressive and tensile properties of human meniscus. J Biomech 48, 1407–1411. https://doi.org/10.1016/J.JBIOMECH.2015.02.042

Fithian, D.C., Kelly, M.A., 1990. Material Properties and Structure-Function Relationships in the Menisci. Clin Orthop Relat Res.

Forkel, P., Petersen, W., 2012. Posterior root tear fixation of the lateral meniscus combined with arthroscopic ACL double-bundle reconstruction: Technical note of a transosseous fixation using the tibial PL tunnel. Arch Orthop Trauma Surg 132, 387–391. https://doi.org/10.1007/S00402-011-1429-8/FIGURES/6

Fox, A.J.S., Bedi, A., Rodeo, S.A., 2012. The Basic Science of Human Knee Menisci: Structure, Composition, and Function. Sports Health 4, 340. https://doi.org/10.1177/1941738111429419

Freutel, M., Galbusera, F., Ignatius, A., Dürselen, L., 2015. Material properties of individual menisci and their attachments obtained through inverse FE-analysis. J Biomech 48, 1343–1349. https://doi.org/10.1016/J.JBIOMECH.2015.03.014

Ghadially, F.N., Lalonde, J.-M.A., Wedge, J.H., 1983. Ultrastructure of normal and torn menisci of the human knee joint. J Anat 136, 773.

Ghosh, P., Taylor, T.K.F., 1987. The knee joint meniscus. A fibrocartilage of some distinction. Clin Orthop Relat Res 52–63.

Gnandt, R.J., Smith, J.L., Nguyen-Ta, K., McDonald, L., Leclere, L.E., 2016. High-Tensile Strength Tape Versus High-Tensile Strength Suture: A Biomechanical Study. Arthroscopy: The Journal of Arthroscopic & Related Surgery 32, 356–363. https://doi.org/10.1016/J.ARTHRO.2015.08.013

Gregory, D.E., Callaghan, J.P., 2011. A comparison of uniaxial and biaxial mechanical properties of the annulus fibrosus: A porcine model. J Biomech Eng 133. https://doi.org/10.1115/1.4003327/383547

Guo, W., Liu, S., Zhu, Y., Yu, C., Lu, S., Yuan, M., Gao, Y., Huang, J., Yuan, Z., Peng, J., Wang, A., Wang, Y., Chen, J., Zhang, L., Sui, X., Xu, W., Guo, Q., 2015. Advances and Prospects in Tissue-Engineered Meniscal Scaffolds for Meniscus Regeneration. Stem Cells Int 2015, 517520. https://doi.org/10.1155/2015/517520

Gupte, C.M., Bull, A.M.J., Thomas, R.D., Amis, A.A., 2003. The meniscofemoral ligaments: secondary restraints to the posterior drawer. Analysis of anteroposterior and rotary laxity in the intact and posterior-cruciate-deficient knee. J Bone Joint Surg Br 85, 765–773. https://doi.org/10.1302/0301-620x.85b5.13771

Harner, C.D., Mauro, C.S., Lesniak, B.P., Romanowski, J.R., 2009. Biomechanical Consequences of a Tear of the Posterior Root of the Medial Meniscus. Journal of Bone and Joint Surgery 91, 257–270. https://doi.org/10.2106/JBJS.I.00500

Hauch, K.N., Villegas, D.F., Haut Donahue, T.L., 2010. Geometry, time-dependent and failure properties of human meniscal attachments. J Biomech 43, 463–468. https://doi.org/10.1016/J.JBIOMECH.2009.09.043

Hein, C.N., Deperio, J.G., Ehrensberger, M.T., Marzo, J.M., 2011. Effects of medial meniscal posterior horn avulsion and repair on meniscal displacement. Knee 18, 189–192. https://doi.org/10.1016/J.KNEE.2010.04.006

Holmes, M.H., Mow, V.C., 1990. The nonlinear characteristics of soft gels and hydrated connective tissues in ultrafiltration. J Biomech 23, 1145–1156. https://doi.org/10.1016/0021-9290(90)90007-P

Jha, V., Professor, A., of Orthopaedics, D., 2024. Rate of meniscal repair versus meniscectomy has improved, and should continue to improve. Arthroscopy 0. https://doi.org/10.1016/J.ARTHRO.2024.10.006

Johannsen, A.M., Civitarese, D.M., Padalecki, J.R., Goldsmith, M.T., Wijdicks, C.A., LaPrade, R.F., 2012. Qualitative and Quantitative Anatomic Analysis of the Posterior Root Attachments of the Medial and Lateral Menisci. Am J Sports Med 40(10), 2342–2347. https://doi.org/10.1177/0363546512457642

Joshi, M.D., Suh, J. -K, Marui, T., Woo, S.L. -Y, 1995. Interspecies variation of compressive biomechanical properties of the meniscus. J Biomed Mater Res 29, 823–828. https://doi.org/10.1002/JBM.820290706

Jung, Y.H., Choi, N.H., Oh, J.S., Victoroff, B.N., 2012. All-inside repair for a root tear of the medial meniscus using a suture anchor. American Journal of Sports Medicine 40, 1406–1411. https://doi.org/10.1177/0363546512439181/ASSET/IMAGES/LARGE/10.1177_0363546512439181-FIG8.JPEG

Kahlon, A., Hurtig, M.B., Gordon, K.D., 2015. Regional and depth variability of porcine meniscal mechanical properties through biaxial testing. J Mech Behav Biomed Mater 41, 108–114. https://doi.org/10.1016/J.JMBBM.2014.10.008

Kale, A., Kopuz, C., Dikici, F., Demir, M.T., Çorumlu, U., Ince, Y., 2010. Anatomic and arthroscopic study of the medial meniscal horns' insertions. Knee Surgery, Sports Traumatology, Arthroscopy 18, 754–759. https://doi.org/10.1007/S00167-009-0907-9/FIGURES/6

Kiapour, A., Kiapour, A.M., Kaul, V., Quatman, C.E., Wordeman, S.C., Hewett, T.E., 2014. Finite element model of the knee for investigation of injury mechanisms: Development and validation. J Biomech Eng 136. https://doi.org/10.1115/1.4025692/370070

kim, J.G., Lee, Y.S., Bae, T.S., Ha, J.K., Lee, D.H., Kim, Y.J., Ra, H.J., 2013. Tibiofemoral contact mechanics following posterior root of medial meniscus tear, repair, meniscectomy, and allograft transplantation. Knee

Surgery, Sports Traumatology, Arthroscopy 21, 2121–2125. https://doi.org/10.1007/s00167-012-2182-4

Kim, J.H., Chung, J.H., Lee, D.H., Lee, Y.S., Kim, J.R., Ryu, K.J., 2011. Arthroscopic Suture Anchor Repair Versus Pullout Suture Repair in Posterior Root Tear of the Medial Meniscus: A Prospective Comparison Study. Arthroscopy: The Journal of Arthroscopic & Related Surgery 27, 1644–1653. https://doi.org/10.1016/J.ARTHRO.2011.06.033

Kim, S.B., Ha, J.K., Lee, S.W., Kim, D.W., Shim, J.C., Kim, J.G., Lee, M.Y., 2011. Medial Meniscus Root Tear Refixation: Comparison of Clinical, Radiologic, and Arthroscopic Findings With Medial Meniscectomy. Arthroscopy: The Journal of Arthroscopic & Related Surgery 27, 346–354. https://doi.org/10.1016/J.ARTHRO.2010.08.005

Kim, Y.M., Rhee, K.J., Lee, J.K., Hwang, D.S., Yang, J.Y., Kim, S.J., 2006. Arthroscopic pullout repair of a complete radial tear of the tibial attachment site of the medial meniscus posterior horn. Arthroscopy 22, 795.e1-795.e4. https://doi.org/10.1016/J.ARTHRO.2005.12.040

Kopf, S., Colvin, A.C., Muriuki, M., Zhang, X., Harner, C.D., 2011. Meniscal root suturing techniques: Implications for root fixation. American Journal of Sports Medicine 39, 2141–2146. https://doi.org/10.1177/0363546511413250/ASSET/IMAGES/LARGE/10.1177_0363546511413250-FIG2.JPEG

Lai, J.H., Levenston, M.E., 2010. Meniscus and cartilage exhibit distinct intra-tissue strain distributions under unconfined compression. Osteoarthritis Cartilage 18, 1291–1299. https://doi.org/10.1016/J.JOCA.2010.05.020

LaPrade, C.M., Ellman, M.B., Rasmussen, M.T., James, E.W., Wijdicks, C.A., Engebretsen, L., Laprade, R.F., 2014a. Anatomy of the anterior root attachments of the medial and lateral menisci: A quantitative analysis. American Journal of Sports Medicine 42, 2386–2392. https://doi.org/10.1177/0363546514544678/ASSET/IMAGES/LARGE/10.1177_0363546514544678-FIG4.JPEG

LaPrade, Christopher M, Foad, A., Smith, S.D., Lee Turnbull, T., Dornan, G.J., Engebretsen, L., Wijdicks, C.A., LaPrade, R.F., 2015. Biomechanical

Consequences of a Nonanatomic Posterior Medial Meniscal Root Repair. Am J Sports Med 43(4), 912–920. https://doi.org/10.1177/0363546514566191

LaPrade, Christopher M., James, E.W., Cram, T.R., Feagin, J.A., Engebretsen, L., Laprade, R.F., 2015. Meniscal Root Tears: A Classification System Based on Tear Morphology. Am J Sports Med 43, 363–369. https://doi.org/10.1177/0363546514559684/ASSET/IMAGES/LARGE/10.1177_0363546514559684-FIG3.JPEG

LaPrade, C.M., Jansson, K.S., Dornan, G., Smith, S.D., Wijdicks, C.A., LaPrade, R.F., 2014b. Altered Tibiofemoral Contact Mechanics Due to Lateral Meniscus Posterior Horn Root Avulsions and Radial Tears Can Be Restored with in Situ Pull-Out Suture Repairs. Journal of Bone and Joint Surgery 96, 471–479. https://doi.org/10.2106/JBJS.L.01252

LaPrade, R.F., Arendt, E.A., Getgood, A., Faucett, S., 2017. The menisci: A comprehensive review of their anatomy, biomechanical function and surgical treatment. The Menisci: A Comprehensive Review of their Anatomy, Biomechanical Function and Surgical Treatment 1–198. https://doi.org/10.1007/978-3-662-53792-3/COVER

LaPrade, R.F., Engebretsen, A.H., Ly, T. V., Johansen, S., Wentorf, F.A., Engebretsen, L., 2007. The anatomy of the medial part of the knee. Journal of Bone and Joint Surgery - Series A 89, 2000–2010. https://doi.org/10.2106/JBJS.F.01176

Laprade, R.F., Laprade, C.M., Ellman, M.B., Turnbull, T.L., Cerminara, A.J., Wijdicks, C.A., 2015a. Cyclic displacement after meniscal root repair fixation: A human biomechanical evaluation. American Journal of Sports Medicine 43, 892–898. https://doi.org/10.1177/0363546514562554/ASSET/IMAGES/LARGE/10.1177_0363546514562554-FIG4.JPEG

Laprade, R.F., Laprade, C.M., James, E.W., 2015b. Recent advances in posterior meniscal root repair techniques. Journal of the American Academy of Orthopaedic Surgeons 23, 71–76. https://doi.org/10.5435/JAAOS-D-14-00003

Lechner, K., Hull, M.L., Howell, S.M., 2000. Is the circumferential tensile modulus within a human medial meniscus affected by the test sample location

and cross-sectional area? Journal of Orthopaedic Research 18, 945–951. https://doi.org/10.1002/JOR.1100180614

Lee, D.W., Jang, S.H., Ha, J.K., Kim, J.G., Ahn, J.H., 2013. Meniscus root refixation technique using a modified Mason-Allen stitch. Knee Surgery, Sports Traumatology, Arthroscopy 21, 654–657. https://doi.org/10.1007/S00167-012-1992-8/FIGURES/6

Lee, J.H., Lim, Y.J., Kim, K.B., Kim, K.H., Song, J.H., 2009. Arthroscopic Pullout Suture Repair of Posterior Root Tear of the Medial Meniscus: Radiographic and Clinical Results With a 2-Year Follow-up. Arthroscopy: The Journal of Arthroscopic & Related Surgery 25, 951–958. https://doi.org/10.1016/J.ARTHRO.2009.03.018

Lerer, D.B., Umans, H.R., Xu, M.X., Jones, M.H., 2004. The role of meniscal root pathology and radial meniscal tear in medial meniscal extrusion. Skeletal Radiol 33, 569–574. https://doi.org/10.1007/S00256-004-0761-2/FIGURES/5

LeRoux, M.A., Setton, L.A., 2002. Experimental and Biphasic FEM Determinations of the Material Properties and Hydraulic Permeability of the Meniscus in Tension. J Biomech Eng 124, 315–321. https://doi.org/10.1115/1.1468868

Leslie, B.W., Gardner, D.L., McGeough, J.A., Moran, R.S., 2000. Anisotropic response of the human knee joint meniscus to unconfined compression. http://dx.doi.org/10.1243/0954411001535651 214, 631–635. https://doi.org/10.1243/0954411001535651

Mahmood, M.F., Clarke, M.J., Riches, D.P., 2020. Proteoglycans exert a significant effect on human meniscal stiffness through ionic effects. Clinical Biomechanics 77, 105028. https://doi.org/10.1016/J.CLINBIOMECH.2020.105028

Makris, E.A., Hadidi, P., Athanasiou, K.A., 2011. The knee meniscus: Structure–function, pathophysiology, current repair techniques, and prospects for regeneration. Biomaterials 32, 7411–7431. https://doi.org/10.1016/J.BIOMATERIALS.2011.06.037

Martin Seitz, A., Galbusera, F., Krais, C., Ignatius, A., Dürselen, L., 2013. Stress-relaxation response of human menisci under confined compression conditions. J Mech Behav Biomed Mater 26, 68–80. https://doi.org/10.1016/J.JMBBM.2013.05.027

Marzo, J.M., Gurske-DePerio, J., 2009. Effects of medial meniscus posterior horn avulsion and repair on tibiofemoral contact area and peak contact pressure with clinical implications. Am J Sports Med 37, 124–129. https://doi.org/10.1177/0363546508323254

Masouros, S.D., McDermott, I.D., Amis, A.A., Bull, A.M.J., 2008. Biomechanics of the meniscus-meniscal ligament construct of the knee. Knee Surgery, Sports Traumatology, Arthroscopy 16, 1121–1132. https://doi.org/10.1007/S00167-008-0616-9/FIGURES/8

McDermott, I.D., Masouros, S.D., Amis, A.A., 2008. Biomechanics of the menisci of the knee. Curr Orthop 22, 193–201. https://doi.org/10.1016/J.CUOR.2008.04.005

McDevitt, C.A., Webber, R.J., 1990. The ultrastructure and biochemistry of meniscal cartilage. Clin Orthop Relat Res 252, 8–18. https://doi.org/10.1097/00003086-199003000-00003

Messner Karola, Gao, J., 1998. The menisci of the knee joint. Anatomical and functional characteristics, and a rationale for clinical treatment. J Anat 193, 161–178. https://doi.org/10.1046/J.1469-7580.1998.19320161.X

Mitchell, R., Pitts, R., Kim, Y.M., Matava, M.J., 2016. Medial Meniscal Root Avulsion: A Biomechanical Comparison of 4 Different Repair Constructs. Arthroscopy: The Journal of Arthroscopic & Related Surgery 32, 111–119. https://doi.org/10.1016/J.ARTHRO.2015.07.013

Mononen, M.E., Jurvelin, J.S., Korhonen, R.K., 2013. Effects of radial tears and partial meniscectomy of lateral meniscus on the knee joint mechanics during the stance phase of the gait cycle - A 3D finite element study. Journal of Orthopaedic Research 31, 1208–1217. https://doi.org/10.1002/JOR.22358

Moon, H.-K., Koh, Y.-G., Kim, Y.-C., Park, Y.-S., Jo, S.-B., Kwon, S.-K., 2010. Prognostic Factors of Arthroscopic Pull-out Repair for a Posterior Root

Tear of the Medial Meniscus. Am J Sports Med 40(5), 1138–1143. https://doi.org/10.1177/0363546511435622

Moran, J., Katz, L.D., Schneble, C.A., Li, D., Kahan, J.B., Wang, A., Porrino, J., Jokl, P., Hewett, T.E., Medvecky, M.J., 2021. Injury to the Meniscofemoral Portion of the Deep MCL Is Associated with Medial Femoral Condyle Bone Marrow Edema in ACL Ruptures. JBJS Open Access 6. https://doi.org/10.2106/JBJS.OA.21.00069

Morejon, A., Norberg, C.D., De Rosa, M., Best, T.M., Jackson, A.R., Travascio, F., 2021. Compressive Properties and Hydraulic Permeability of Human Meniscus: Relationships With Tissue Structure and Composition. Front Bioeng Biotechnol 8, 622552. https://doi.org/10.3389/FBIOE.2020.622552/BIBTEX

Mow, V.C., Kuei, S.C., Lai, W.M., Armstrong, C.G., 1980. Biphasic Creep and Stress Relaxation of Articular Cartilage in Compression: Theory and Experiments. J Biomech Eng 102, 73–84. https://doi.org/10.1115/1.3138202

Mow VC, Ratcliffe A, Chern KY, 1992. Structure and function relationships of the menisci of the knee. Knee meniscus : basic and clinical foundations.

Nebelung, S., Dötsch, L., Shah, D., Abrar, D.B., Linka, K., Knobe, M., Sewerin, P., Thüring, J., Kuhl, C., Truhn, D., 2020. Functional MRI Mapping of Human Meniscus Functionality and its Relation to Degeneration. Scientific Reports 2020 10:1 10, 1–14. https://doi.org/10.1038/s41598-020-59573-4

Nicholas, S.J., Golant, A., Schachter, A.K., Lee, S.J., 2009. A new surgical technique for arthroscopic repair of the meniscus root tear. Knee Surgery, Sports Traumatology, Arthroscopy 17, 1433–1436. https://doi.org/10.1007/S00167-009-0874-1/FIGURES/6

Niu, W., Guo, W., Han, S., Zhu, Y., Liu, S., Guo, Q., 2016. Cell-Based Strategies for Meniscus Tissue Engineering. Stem Cells Int 2016, 4717184. https://doi.org/10.1155/2016/4717184

Padalecki, J.R., Jansson, K.S., Smith, S.D., Dornan, G.J., Pierce, C.M., Wijdicks, C.A., Laprade, R.F., 2014. Biomechanical consequences of a complete radial tear adjacent to the medial meniscus posterior root attachment site: In

situ pull-out repair restores derangement of joint mechanics. American Journal of Sports Medicine 42, 699–707. https://doi.org/10.1177/0363546513499314

Peña, E., Calvo, B., Martínez, M.A., Doblaré, M., 2006. A three-dimensional finite element analysis of the combined behavior of ligaments and menisci in the healthy human knee joint. J Biomech 39, 1686–1701. https://doi.org/10.1016/J.JBIOMECH.2005.04.030

Peña, E., Calvo, B., Martínez, M.A., Palanca, D., Doblaré, M., 2005. Finite element analysis of the effect of meniscal tears and meniscectomies on human knee biomechanics. Clinical Biomechanics 20, 498–507. https://doi.org/10.1016/J.CLINBIOMECH.2005.01.009

Peña-Trabalon, A., Perez-Blanca, A., Moreno-Vegas, S., Belen Estebanez-Campos, M., Prado-Novoa, M., 2024. Assessment of Surrogate Models for Research on Resistance and Deformation of Repairs of the Human Meniscal Roots: Porcine or Older Human Models? Applied Sciences 2024, Vol. 14, Page 670 14, 670. https://doi.org/10.3390/APP14020670

Peña-Trabalon, A., Perez-Blanca, A., Moreno-Vegas, S., Estebanez Campos, M.B., Prado-Novoa, M., 2023. Age influence on resistance and deformation of the human sutured meniscal horn in the immediate postoperative period. Front Bioeng Biotechnol 11. https://doi.org/10.3389/FBIOE.2023.1249982/FULL

Pereira, H., Silva-Correia, J., Oliveira, J.M., Reis, R.L., Espregueira-Mendes, J., 2013. The Meniscus: Basic Science. Meniscal Transplantation 7–14. https://doi.org/10.1007/978-3-642-38106-5_2

Perez-Blanca, A., Espejo-Baena, A., Amat Trujillo, D., Prado Nóvoa, M., Espejo-Reina, A., Quintero López, C., Ezquerro Juanco, F., 2016. Comparative Biomechanical Study on Contact Alterations After Lateral Meniscus Posterior Root Avulsion, Transosseous Reinsertion, and Total Meniscectomy. Arthroscopy: The Journal of Arthroscopic & Related Surgery 32, 624–633. https://doi.org/10.1016/j.arthro.2015.08.040

Perez-Blanca, A., Prado Nóvoa, M., Lombardo Torre, M., Espejo-Reina, A., Ezquerro Juanco, F., Espejo-Baena, A., 2018. The role of suture cutout in the failure of meniscal root repair during the early post-operative period: a

biomechanical study. Int Orthop 42, 811–818. https://doi.org/10.1007/S00264-018-3799-9/FIGURES/5

Petersen, W., Tillmann, B., 1998. Collagenous fibril texture of the human knee joint menisci. Anat Embryol (Berl) 197, 317–324. https://doi.org/10.1007/S004290050141/METRICS

Peterson, Lars., Renström, Per., 2017. Sports injuries : prevention, treatment and rehabilitation 619.

Pordzik, J., Bernstein, A., Mayr, H.O., Latorre, S.H., Maks, A., Schmal, H., Seidenstuecker, M., 2020. Analysis of Proteoglycan Content and Biomechanical Properties in Arthritic and Arthritis-Free Menisci. Applied Sciences 2020, Vol. 10, Page 9012 10, 9012. https://doi.org/10.3390/APP10249012

Prado, M., Martín-Castilla, B., Espejo-Reina, A., Serrano-Fernández, J.M., Pérez-Blanca, A., Ezquerro, F., 2013. Close-looped graft suturing improves mechanical properties of interference screw fixation in ACL reconstruction. Knee Surgery, Sports Traumatology, Arthroscopy 21, 476–484. https://doi.org/10.1007/S00167-012-1975-9/TABLES/3

Raustol, O.A., Poelstra, K.A., Chhabra, A., Diduch, D.R., 2006. The Meniscal Ossicle Revisited: Etiology and an Arthroscopic Technique for Treatment. Arthroscopy: The Journal of Arthroscopic & Related Surgery 22, 687.e1-687.e3. https://doi.org/10.1016/J.ARTHRO.2005.12.022

Rosslenbroich, S.B., Borgmann, J., Herbort, M., Raschke, M.J., Petersen, W., Zantop, T., 2013. Root tear of the meniscus: Biomechanical evaluation of an arthroscopic refixation technique. Arch Orthop Trauma Surg 133, 111–115. https://doi.org/10.1007/S00402-012-1625-1

Ruiwen, L., Lam, P.H., Shepherd, H., Murrell, G.A., 2016. Tape versus Suture - A Biomechanical and Clinical Analysis in Arthroscopic Rotator Cuff Repair of Large Tears. https://doi.org/10.1177/2325967116S00078 4, 2325967116S0007. https://doi.org/10.1177/2325967116S00078

Schillhammer, C.K., Werner, F.W., Scuderi, M.G., Cannizzaro, J.P., 2012. Repair of lateral meniscus posterior horn detachment lesions: A biomechanical evaluation. American Journal of Sports Medicine 40, 2604–2609. https://doi.org/10.1177/0363546512458574

Schwer, J., Ignatius, A., Seitz, A.M., 2024. The biomechanical properties of human menisci: A systematic review. Acta Biomater 175, 1–26. https://doi.org/10.1016/J.ACTBIO.2023.12.010

Scott, P.G., Nakano, T., Dodd, C.M., 1997. Isolation and characterization of small proteoglycans from different zones of the porcine knee meniscus. Biochimica et Biophysica Acta (BBA) - General Subjects 1336, 254–262. https://doi.org/10.1016/S0304-4165(97)00040-8

Scotti, C., Hirschmann, M.T., Antinolfi, P., Martin, I., Peretti, G.M., 2014. Meniscus repair and regeneration : review on current methods and research potential. Eur Cell Mater 26, 150–170. https://doi.org/10.22203/eCM.v026a11

Seedhom, B.B., Hargreaves, D.J., 1979. Transmission of the Load in the Knee Joint with Special Reference to the Role of the Menisci. http://dx.doi.org/10.1243/EMED_JOUR_1979_008_051_02 8, 220–228. https://doi.org/10.1243/EMED_JOUR_1979_008_051_02

Seitz, A.M., Osthaus, F., Schwer, J., Warnecke, D., Faschingbauer, M., Sgroi, M., Ignatius, A., Dürselen, L., 2021. Osteoarthritis-Related Degeneration Alters the Biomechanical Properties of Human Menisci Before the Articular Cartilage. Front Bioeng Biotechnol 9. https://doi.org/10.3389/FBIOE.2021.659989/FULL

Seo, H.S., Lee, S.C., Jung, K.A., 2010. Second-Look Arthroscopic Findings After Repairs of Posterior Root Tears of the Medial Meniscus. https://doi.org/10.1177/0363546510382225 39, 99–107. https://doi.org/10.1177/0363546510382225

Seo, J.H., Li, G., Shetty, G.M., Kim, J.H., Bae, J.H., Jo, M.L., Kim, J.S., Lee, S.J., Nha, K.W., 2009. Effect of Repair of Radial Tears at the Root of the Posterior Horn of the Medial Meniscus With the Pullout Suture Technique: A Biomechanical Study Using Porcine Knees. Arthroscopy: The Journal of Arthroscopic & Related Surgery 25, 1281–1287. https://doi.org/10.1016/J.ARTHRO.2009.05.014

Seyfi, B., Fatouraee, N., Imeni, M., 2018. Mechanical modeling and characterization of meniscus tissue using flat punch indentation and inverse

finite element method. J Mech Behav Biomed Mater 77, 337–346. https://doi.org/10.1016/J.JMBBM.2017.09.023

Steineman, B.D., Laprade, R.F., Haut Donahue, T.L., 2022. Loosening of Posteromedial Meniscal Root Repairs Affects Knee Mechanics: A Finite Element Study. J Biomech Eng 144. https://doi.org/10.1115/1.4053100/1128894

Steineman, B.D., LaPrade, R.F., Haut Donahue, T.L., 2020. Nonanatomic placement of posteromedial meniscal root repairs: A finite element study. J Biomech Eng 142. https://doi.org/10.1115/1.4045893/1072350

Sweigart, M.A., Athanasiou, K.A., 2004. Toward Tissue Engineering of the Knee Meniscus. https://home.liebertpub.com/ten 7, 111–129. https://doi.org/10.1089/107632701300062697

Thompson, W.O., Thaete, F.L., Fu, F.H., Dye, S.F., 1991. Tibial meniscal dynamics using three-dimensional reconstruction of magnetic resonance images. https://doi.org/10.1177/036354659101900302 19, 210–216. https://doi.org/10.1177/036354659101900302

Tissakht, M., Ahmed, A.M., 1995. Tensile stress-strain characteristics of the human meniscal material. J Biomech 28, 411–422. https://doi.org/10.1016/0021-9290(94)00081-E

Truhn, D., Brill, N., Braun, B., Merhof, D., Kuhl, C., Knobe, M., Thüring, J., Nebelung, S., 2020. A multi-purpose force-controlled loading device for cartilage and meniscus functionality assessment using advanced MRI techniques. J Mech Behav Biomed Mater 101, 103428. https://doi.org/10.1016/J.JMBBM.2019.103428

Tuxøe, J.I., Teir, M., Winge, S., Nielsen, P.L., 2002. The medial patellofemoral ligament: A dissection study. Knee Surgery, Sports Traumatology, Arthroscopy 10, 138–140. https://doi.org/10.1007/S00167-001-0261-Z/METRICS

Vadher, S.P., Nayeb-Hashemi, H., Canavan, P.K., Warner, G.M., 2006. Finite element modeling following partial meniscectomy: Effect of various size of resection. Annual International Conference of the IEEE Engineering in Medicine and Biology - Proceedings 2098–2101. https://doi.org/10.1109/IEMBS.2006.259378

Vertullo, C.J., Cadman, J., Dabirrahmani, D., Appleyard, R., 2021. Biomechanical Comparison of an All-Inside Meniscal Repair Device Construct Versus Pullout Sutures for Arthroscopic Transtibial Repair of Posterior Medial Meniscus Root Tears A Matched-Pair Cadaveric Study. Orthop J Sports Med 9(4), 23259671211000464. https://doi.org/10.1177/23259671211000464

Villegas, D.F., Hansen, T.A., Liu, D.F., Haut Donahue, T.L., 2008. A quantitative study of the microstructure and biochemistry of the medial meniscal horn attachments. Ann Biomed Eng 36, 123–131. https://doi.org/10.1007/s10439-007-9403-x

Vyas, D., Harner, C.D., 2012. Meniscus root repair. Sports Med Arthrosc Rev 20, 86–94. https://doi.org/10.1097/JSA.0B013E31825186CA

Wang, J.Y., Qi, Y.S., Bao, H.R.C., Xu, Y.S., Wei, B.G., Wang, Y.X., Ma, B.X., Zhou, H.W., Lv, F., 2021. The effects of different repair methods for a posterior root tear of the lateral meniscus on the biomechanics of the knee: a finite element analysis. J Orthop Surg Res 16, 1–8. https://doi.org/10.1186/S13018-021-02435-0/FIGURES/4

Wang, Y.J., Yu, J.K., Luo, H., Yu, C.L., Ao, Y.F., Xie, X., Jiang, D., Zhang, J.Y., 2009. An anatomical and histological study of human meniscal horn bony insertions and peri-meniscal attachments as a basis for meniscal transplantation. Chin Med J (Engl) 122, 536–540. https://doi.org/10.3760/CMA.J.ISSN.0366-6999.2009.05.010

Warnecke, D., Balko, J., Haas, J., Bieger, R., Leucht, F., Wolf, N., Schild, N.B., Stein, S.E.C., Seitz, A.M., Ignatius, A., Reichel, H., Mizaikoff, B., Dürselen, L., 2020. Degeneration alters the biomechanical properties and structural composition of lateral human menisci. Osteoarthritis Cartilage 28, 1482–1491. https://doi.org/10.1016/J.JOCA.2020.07.004

Wheatley, B.B., Fischenich, K.M., Button, K.D., Haut, R.C., Haut Donahue, T.L., 2015. An optimized transversely isotropic, hyper-poro-viscoelastic finite element model of the meniscus to evaluate mechanical degradation following traumatic loading. J Biomech 48, 1454–1460. https://doi.org/10.1016/J.JBIOMECH.2015.02.028

Yin, X.Y., Chung, J.Y., Park, D.Y., Song, H.K., Kim, B.K., Bae, H.W., Park, K.H., Min, B.H., 2021. The Perimensical Capsule: Potential Supporting Structure Surrounding Meniscus. Cartilage 13, 208S-215S. https://doi.org/10.1177/1947603519892316

Zhang, X., Yuan, S., Wang, J., Liao, B., Liang, D., 2021. Biomechanical characteristics of tibio-femoral joint after partial medial meniscectomy in different flexion angles: a finite element analysis. BMC Musculoskelet Disord 22, 1–8. https://doi.org/10.1186/S12891-021-04187-8/FIGURES/3

Zielinska, B., Haut Donahue, T.L., 2006. 3D Finite Element Model of Meniscectomy: Changes in Joint Contact Behavior. J Biomech Eng 128, 115–123. https://doi.org/10.1115/1.2132370

3

Experimental study of circumferential tensile properties in meniscal horns around the sutured area: Application to a porcine model

This chapter is framed within a set of four chapters included in this document, focused on the experimental characterization of the mechanical properties of the sutured meniscal horn around the suture hole. The main objective of this initial chapter is to develop, using a porcine model, the methodology for characterising the mechanical properties of sutured meniscal horns in the suture area when subjected to suture-induced traction in the direction of their circumferential fibres. The mechanical properties are studied at two different levels, namely, tissue level and specimen level. At the specimen level, resistance is assessed by identifying the force required to initiate tearing and the ultimate force the specimen is able to withstand. At the tissue level, resistance is studied by calculating the stress that initiates the tissue cut out, and the deformation is studied by characterizing the linear zone of the stress-strain curve around the suture hole, and determining the boundaries of this linear behaviour. The methodology established in this chapter will be applied to human models in subsequent chapters. Additionally, the experimental outcomes of this chapter will be confronted in a later chapter with cadaveric models in order to evaluate the suitability of the porcine model as a surrogate for human models for in vitro studies of surgical repair of meniscal roots. The chapter addresses the first specific objective stated in Section 1.2 by developing a methodology for in-vitro characterization of the resistance and deformation around the suture area of sutured meniscal horns subjected to circumferential traction. It also partially addresses the second specific objective, directed to the computation of the tensile properties around the suture area which is restricted to a porcine model in this chapter.

3.1 Introduction

As explained in the previous chapter, the menisci of the knee are anchored by ligamentous attachments that secure them within the intra-articular zone while allowing for necessary mobility, up to 10 mm (Fox et al., 2012), to accommodate the shifting contact area between the tibia and femur during flexion-extension. Among these attachments, the meniscal roots are the only ones with direct insertion into the bone, making them vital to the overall function of the meniscus. Complete avulsion of a meniscal root leads to significant alterations in knee biomechanics, notably increasing pressure and reducing the contact area on the cartilage of the affected compartment. These changes can be of similar magnitude to those reported after a total meniscectomy (Allaire et al., 2008; Espejo-Reina et al., 2022; Perez-Blanca et al., 2016). Additionally, biomechanical research underscores the importance of meniscal roots as secondary stabilizers of knee kinematics, contributing to the control of antero-posterior translation and internal-external rotation (Musahl et al., 2010; Shiwaku et al., 2022; Shoemaker and Markolf, 1986). Clinically, detachment of a meniscal root can precipitate rapid joint degeneration, potentially leading to arthritis (Krych et al., 2017) or osteonecrosis (Hussain et al., 2019) due to the altered biomechanical environment.

For all the reasons aforementioned, the surgical approach to treating meniscal root avulsions has evolved from partial meniscectomy to procedures aimed at reinserting the meniscal root (Pache et al., 2018). These surgical repairs are typically carried out using one of two techniques: transtibial fixation (Ahn et al., 2007; Feucht et al., 2013) or *in-situ* fixation (Balke et al., 2018; Espejo-Reina et al., 2022), both of which involve passing sutures through the injured meniscal horn to secure it back into place.

Several research studies have subjected sutured meniscal horn specimens to in-vitro tests to assess the performance of various surgical suture materials (Espejo-Reina et al., 2019; Feucht et al., 2015; Robinson et al., 2018; Wu et al., 2018), the effectiveness of different suture techniques (Chung et al., 2018; Feucht et al., 2013; Fujii et al., 2017; Okimura et al., 2019; Rosslenbroich et al., 2013), the validity of suturing or fixation devices (Forkel et al., 2017; Okimura et al., 2019; Prado-Novoa et al., 2020; Wu et al., 2020), and the suitability of surgical approaches (Chung et al., 2018; Feucht et al., 2014; Kim et al., 2016; Seo et al., 2009). These investigations typically focus on two key aspects: the resistance of the meniscal horn to suture traction without initiating tears, and the deformation that occurs at the suture site.

Knowing the resistance of the repaired meniscus, specifically the resistance to suture-induced traction, is critical for preventing the failure of surgical interventions. If the meniscal horn cannot withstand the forces applied by the

sutures, the repair will fail, leading to poor clinical outcomes or even requiring revision surgery. Knowledge of the maximum forces that can be tolerated postoperatively without damaging the tissue is also key in defining rehabilitation strategies. The movements and loads that are allowed or recommended to the patient before complete healing will depend on the forces that the repaired area can withstand. Additionally, it is essential to control the displacements generated by suture traction after repair to ensure that these movements remain within clinically acceptable limits (Stärke et al., 2010). Excessive displacement at the repair site can compromise the stability and function of the meniscus, leading to incomplete healing or healing in a non-anatomic position, a situation expected to alter biomechanics of joint contact (Christopher M LaPrade et al., 2015b; Stärke et al., 2010) and potentially lead to further clinical complications.

Porcine models are commonly used in in-vitro experimental meniscal studies (Chung et al., 2018; Feucht et al., 2015, 2013; Fujii et al., 2017; Kim et al., 2016; Okimura et al., 2019; Perez-Blanca et al., 2018; Robinson et al., 2018; Seo et al., 2009; Stärke et al., 2010; Wu et al., 2018, 2020) due to their low anatomical, histological, and structural variability and their close resemblance to human menisci in terms of anatomical structure, vascularity, volume, and weight, though porcine menisci are generally wider (Takroni et al., 2016). The kinematics of the porcine knee also mirrors that of the human knee to a significant degree, making it a practical and cost-effective option for biomechanical testing of meniscal repair and replacement techniques. This similarity allows researchers to translate findings from porcine models to human clinical applications with a reasonable degree of confidence (Deponti et al., 2015; Kyle Martin et al., 2016; Polito et al., 2020; Sweigart et al., 2004). Therefore, further knowledge of the biomechanical properties of porcine meniscal horns commonly used in experimental biomechanical studies as surrogates for human models is of scientific interest in itself.

The objective of this study is to characterize the mechanical properties of porcine meniscal horns that have undergone root repair under tensile forces applied in the circumferential direction. Unlike the conventional approach that typically focuses on the ultimate resistance of the meniscus-suture construct, this study emphasizes the initiation of tissue cut-out at the suture-meniscus interface. Additionally, a key objective is to establish a consistent and robust methodology for assessing the mechanical properties of sutured meniscus samples, which will be used in the subsequent chapters of this thesis.

3.2 Materials and methods

To focus the study on the behavior of the tissue-suture interface isolated meniscus-suture constructs were used for the experiments. Menisci were extracted

from 22 stifle joints of adult porcine specimens, which were donated by a local Spanish slaughterhouse. The animals were skeletally mature, slaughtered at 6 months of age for the food market, weighing approximately 100 kg.

All procedures adhered to legal and ethical standards.

3.2.1 Specimen preparation

Porcine stifle joints were individually stored at a temperature of -20°C in sealed plastic bags. The day prior to testing, the joints were allowed to thaw at room temperature, wrapped in dampened gauze. Once thawed, the joints were dissected to extract the menisci, which were then visually inspected for any damage or pathology, particularly at the roots and horns. The eligibility criteria required the absence of macroscopic changes and traumatic damage. Menisci meeting these criteria were randomly assigned to undergo either anterior or posterior surgery. Each meniscus was then wrapped in dampened gauze and individually sealed in a plastic bag to maintain hydration in a cooler until testing. A total of 22 porcine menisci were included in the study, resulting in 11 medial and 11 lateral menisci, 10 for anterior and 12 for posterior surgery.

At the time of testing, the meniscus was retrieved from the cooler and removed from the plastic bag. A surgical suture of the horn was simulated by inserting a No. 2 non-absorbable, high-resistance, 100% UHMWPE, braided fiber thread (Force Fiber® No. 2, Stryker Iberia, Madrid, Spain) using the attached ½ circle tapered needle. A single simple suture was chosen for the surgical simulation. The puncture was made 5 mm from the internal meniscal edge and from the end of its root to ensure consistency with the typical surgical hole location during the procedure carried out in humans (Kim et al., 2006; Menge TJ et al., 2016; Perez-Blanca et al., 2018) (Figure 3.1). Although a single simple stitch is neither the most resistant nor the most commonly applied method for repairing a complete meniscal horn tear, it was selected to avoid the uncertainties in load distribution introduced by multiple threads, which complicate accurate load determination at the meniscus-suture interface. The use of a single suture provided a straightforward tissue-suture interface, facilitating the quantification of the tissue resistant area.

Following suturing, the meniscus thickness was measured at the needle insertion point using a manual caliper (model 500-182-30, Mitutoyo, Japan). The suture-meniscus set was then rewrapped in dampened gauze to maintain hydration.

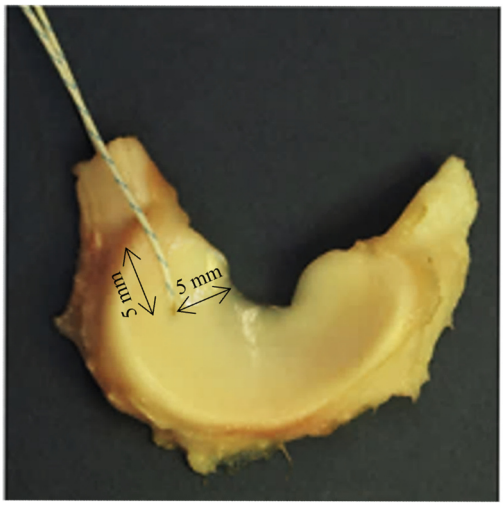

Figure 3.1. Porcine lateral meniscus with a suture thread passing through its horn, simulating a root repair procedure.

3.2.2 Biomechanical testing

The single-axis testing machine previously described in Section 2.5.1 was employed to conduct a load-to-failure test on the sutured meniscus. This testing machine defines three orthogonal axes, with the z-axis aligned with the servomotor screw, which establishes the direction of traction (Figure 3.2). The process of placing the suture-meniscus set in the testing machine involved two main phases.

Figure 3.2. Uniaxial testing machine and videogrammetric system, with the Z axis corresponding to the traction direction and the ZY plane parallel to the image plane.

In the first phase, the meniscus was secured with a clamp approximately 8 mm from the suture point. Sandpaper was used around the clamping area to increase friction. The meniscus was oriented with its cranial surface facing outward in the testing machine, ensuring the longitudinal fibers of the horn were aligned with the loading direction, and the suture hole was centered with the actuator head along the loading direction.

In the second phase, the free ends of the suture were wrapped in sandpaper and attached to a mechanical clamp on the machine head, maintaining a 55 mm distance between the puncture point and the clamp limit when the suture was manually pulled just enough to keep it vertical. This 55 mm distance was chosen to represent the typical suture length in transtibial meniscal horn repair (Cerminara et al., 2014; Espejo-Reina et al., 2019).

An electronic inclinometer (Bubble Level 3D, v. 2.2.4, Maleirbag, 2022, Puebla, Mexico, installed on the smartphone M2002F4LG, Xiaomi, Beijing, China) was used to ensure the meniscus was oriented such that its cranial and caudal surfaces were within the plane containing the z-axis (traction direction) and the y-axis (transverse direction) of the testing machine.

After positioning the meniscus-suture construct in the testing machine, two ink marks were made on its cranial side using a surgical pen. Guided by the inclinometer to identify the direction of traction on the meniscal surface, the marks were placed along a line passing through the suture hole (Figure 3.3):

- Point 1 on the suture limb at the meniscus-suture interface.
- Point 2 on the opposite side of the hole in its immediate vicinity.

These marks were used for videogrammetric analysis to monitor the displacements around the hole in the direction of traction using the videogrametric software explained in the previous Section 2.6.2.

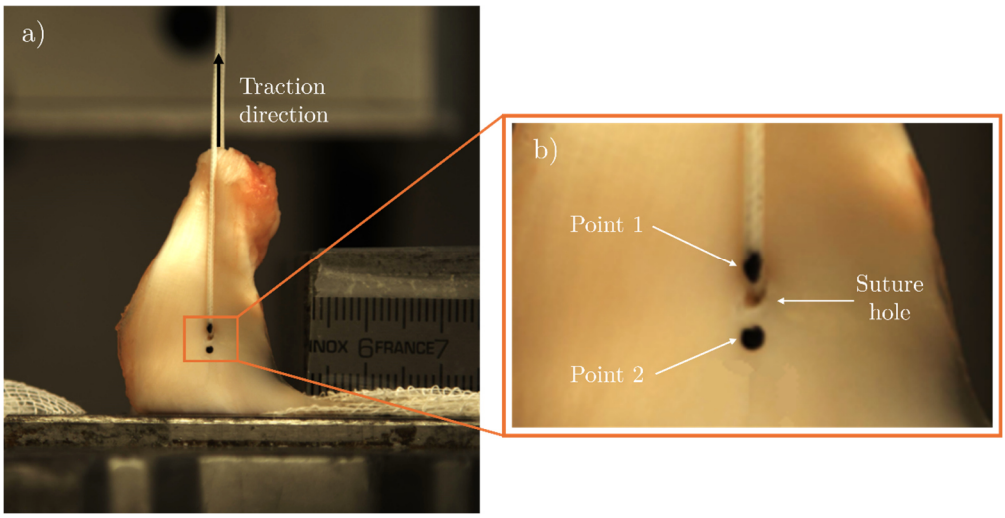

Figure 3.3. a) Porcine meniscus on the testing machine with an indication of the traction direction aligned with the circunferential fibers of the specimen; b) Magnification of the suture hole area with the inked marks and the puncture point shown.

The actuator displacement in the pulling direction was recorded by the servo-controller of the testing machine (SGDH-15AE-S-OY, Yaskawa Electric, Japan), while a 2000 N load cell of class 0.1 (U2B, HBM, Darmstadt, Germany) measured the applied traction force. Both data were sampled at a frequency of 1000 Hz. For the videogrammetric analysis, a digital camera (VCXU-124C, Baumer, Switzerland) (Figure 3.2) was synchronized with the testing machine sensors and positioned to capture the cranial surface of the meniscus. This camera was mounted on a tripod (808RC4, Manfrotto, Cassola, Italy) equipped with three orthogonal rotational mechanisms, and its alignment was ensured using an electronic inclinometer. The camera image plane was aligned with the z-y plane of the testing machine, i.e., parallel to the meniscus mid-transverse plane. The camera was fitted with a 2.8/75mm lens (C7528-M, Pentax, Japan), and images were captured at a sampling period of 250 ms.

Initially, the suture-meniscus construct was subjected to a preload protocol, illustrated in Figure 3.4, consisting of pulling the suture up to 1 N at a velocity of 0.05 mm/s and maintained at this load for 5 seconds to ensure stabilization. Subsequently, a displacement-controlled load-to-failure test was performed at a rate of 0.1 mm/s until reaching a displacement of 20 mm of the head of the testing machine.

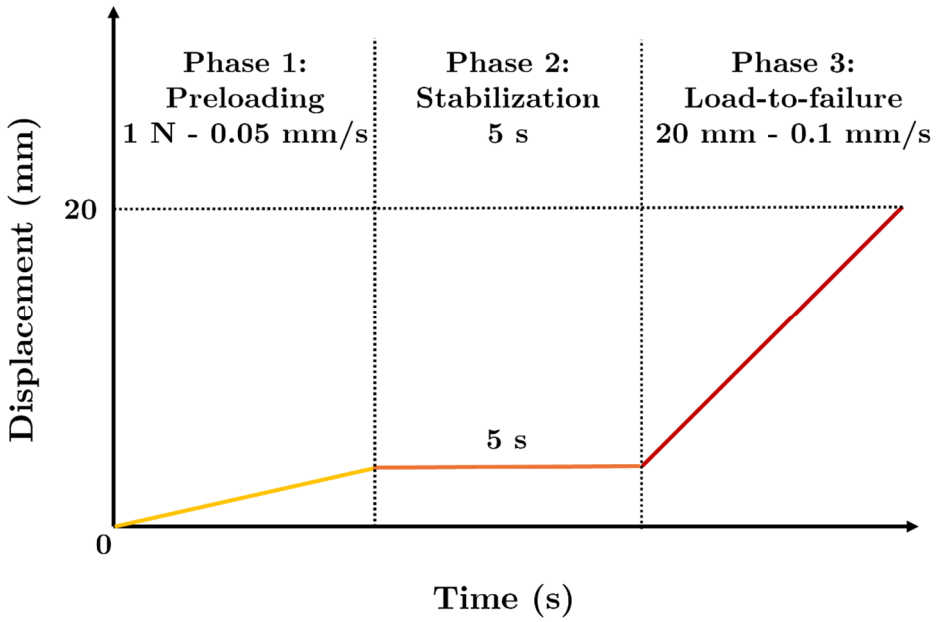

Figure 3.4. Testing protocol scheme.

Before starting the tests, a calibration image was taken with the digital camera. This image featured a precise measurement pattern on the image plane to ensure accurate measurements of displacements in units of lengths during testing (as explained in depth in section 2.6 of Chapter 2). During the load-to-failure phase, the testing machine's load cell recorded the tensile force (traction)

at a sampling frequency of 1,000 Hz. Synchronization between the camera images and the force data from the testing machine was accomplished using an internal trigger.

3.2.3 Load-to-failure analysis

The parameters described in this section will be also studied and analyzed in the following Chapters 4, 5 and 6.

To measure resistance at the specimen level, the force that initiated the meniscal tear, meniscal cut-out force, $\boldsymbol{F_c}$, was computed for each sample. The tear initiation was identified by detecting a change in the slope of the curve $\boldsymbol{D-t}$ (Perez-Blanca, 2019), where:

- $\boldsymbol{D}$ is the displacement of Point 1 relative to Point 2, i.e., the elongation at the suture area.

- $\boldsymbol{t}$ is the time axis of the displacement-controlled load-to-failure test conducted at a constant rate, which is directly proportional to the displacement of the actuator.

To identify the change of slope on the $\boldsymbol{D-t}$ curve (Figure 3.5) a bilinear fitting was conducted. The fitting process searched for the optimal transition point that minimizes the root mean square error between the experimental data and the bilinear fit. The time coordinate of this point was then used to determine the traction borne by the specimen at that moment. Additionally, the tearing starting point was visually identified from the images in a cumbersome and subjective task and the load withstood by the specimen at that instant computed, to verify the concordance between the change of slope point and the force at the cut-out initiation visually found, as proposed by Perez-Blanca et al. (Perez-Blanca, 2019).

Additionally, the highest force the specimen withstood during the load-to-failure test, ultimate force, $\boldsymbol{F_u}$, was also recorded.

At the tissue level, the tissue cut-out resistance of the meniscal horn, S_c, was calculated as the engineering stress at the suture-meniscal interface at the onset of tearing. The expression used for this calculation was Equation 3.1.

$$S_c = \frac{F_C}{\phi \cdot h} \tag{3.1}$$

where ϕ represents the nominal diameter of the suture and h denotes the thickness of the meniscus at the suture hole. The denominator in Equation 3.1 is the projected area at the meniscus-suture interface. Equation 3.1 may initially underestimate the contact surface area, as the suture may not be perfectly orthogonal to the meniscal surfaces under the initial 1 N tensile force. However, the suture will align correctly as the test proceeds.

To evaluate tissue deformation around the suture site, an equivalent stiffness modulus in the direction of suture traction, m_s, was calculated. This modulus was set to the slope of the linear fit of the stress-strain curve, $\sigma - \varepsilon$, within the strain range of $\varepsilon = [0 - 0.3]$.

The engineering stress in the traction direction at the meniscus-suture interface during the test was computed using an expression analogous to Equation 3.1, expressed in Equation 3.2.

$$\sigma = \frac{F}{\phi \cdot h} \tag{3.2}$$

where F represents the traction force recorded by the load cell during the test. The strain was calculated using the Equation 3.3.

$$\varepsilon = \frac{D}{D_0} - 1 \tag{3.3}$$

where D_0 is the relative distance between Point 1 and Point 2 in the initial frame of the load-to-failure test after the stabilization phase, i.e., the value of D at the beginning of the load-to-failure test.

Descriptive statistics of the experimental data sets were computed using the software Excel® (Excel 2019, Microsoft, United States).

3.3 Results

Checking of the videogrammetric recorders revealed that the marks on the meniscal surfaces were inscribed within circles, with a mean radius of 0.40 mm (SD = 0.07) and ranging from 0.25 mm to 0.48 mm, ensuring high uniformity.

The results shown in this chapter correspond to mean and SD values of the experimental data sets. For the complete data set, see Appendix A.

Porcine meniscus showed a mean value of the thickness of 4.98 mm with a standard deviation of 1.13 mm (Table 3.1 row 1).

Following the load-to-failure test, porcine samples showed a mean value of the force needed to start the tissue cut-out, F_c, of 168.86 N with a standard deviation of 50.43 N (Table 3.1 row 2).

Analysis of the captured images confirmed that the tearing initiate at the point of change in the slope of the curve $D - t$ (Figure 3.5).

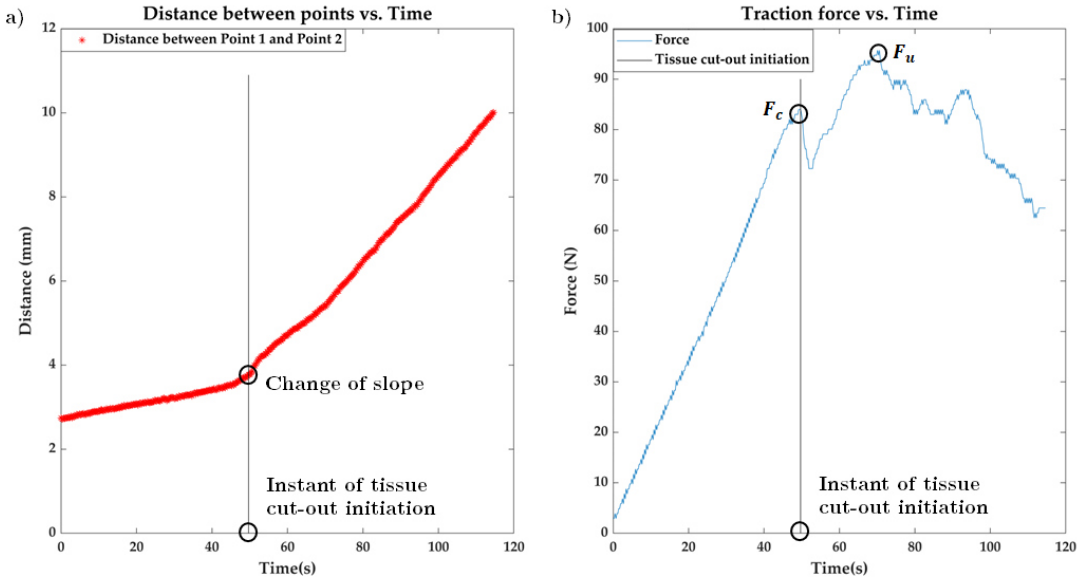

Figure 3.5. Curves representing as a function of time during the load to-failure test: a) the distance between Point 1 and Point 2; b) the evolution of traction force.

Table 3.1. Mechanical properties of the porcine meniscal horns at the suture insertion point area.

	Mean	**SD**
$\boldsymbol{h}$ **(mm)**	4.98	1.13
$\boldsymbol{F_c}$ **(N)**	168.86	50.43
$\boldsymbol{F_u}$ **(N)**	205.79	74.31
$\boldsymbol{S_c}$ **(MPa)**	74.49	27.54
$\boldsymbol{m_s}$ **(MPa)**	111.34	52.09

The load-to-failure test evidenced that the porcine specimens are characterized by a mean value of the ultimate force, F_u, of 205.79 N with a standard deviation of 74.31 N (Table 3.1 row 3). In comparison with the values of the force needed to start the cut-out, F_c, the ultimate force, F_u, resulted 21.9% higher than F_c.

At the tissue level, tissue cut-out initiation a mean value of the stress, S_c, was 74.49 MPa with a standard deviation of 27.54 MPa (Table 3.1 row 4)

All porcine meniscal horns showed highly linear behavior in the strain range [0-0.3] (Figure 3.6), where the equivalent stiffness modulus, m_s, was computed. The adjusted R-square of the linear fit always fell in the range [0.93, 0.99] for the complete set of tested specimens. The tissue equivalent stiffness modulus, m_s, computed from the linear fits was 111.34 MPa with a SD of 52.09 MPa, (Table 3.1 row 5).

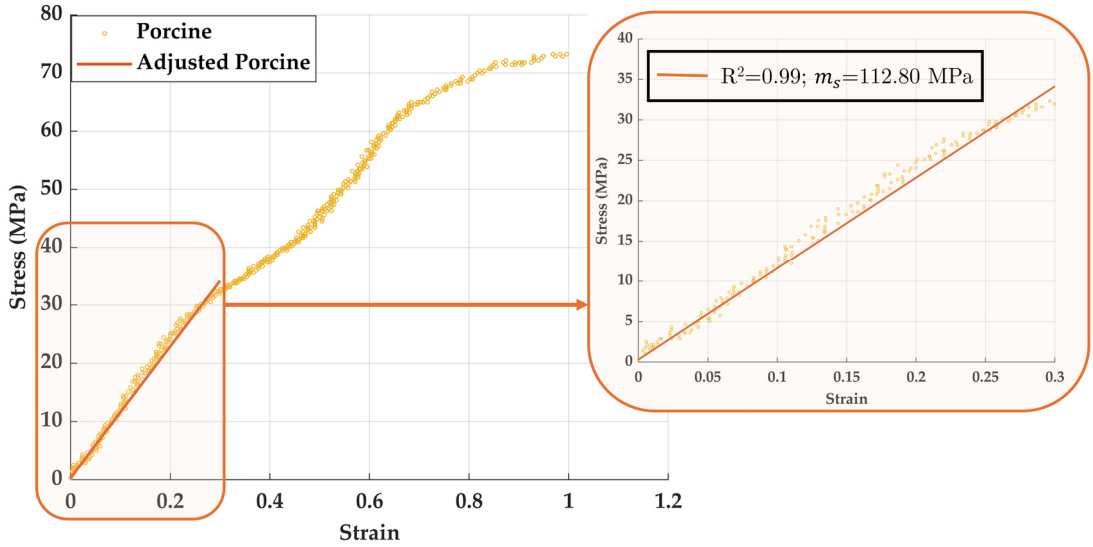

Figure 3.6. Stress-strain curve of a representative porcine sample with a linear fit in the strain range [0-0.3] showing a high lineal behavior.

3.4 Discussion

This chapter focuses on quantifying the mechanical properties of porcine meniscal horns following root repair when subjected to tensile forces in the circumferential direction. The study characterizes these properties at both the specimen and tissue levels. Resistance is assessed by identifying the cut-out initiation and the maximum load in a load-to failure test; deformation is studied at the tissue level by characterizing the linear region of the stress-strain curve, where the physiological loads occur in human specimens (as verified later in this thesis) However, fundamentally, this chapter aims to develop a consistent and robust experimental methodology for the evaluation of the mechanical properties at the suture area, allowing for the characterization of the behavior of repaired meniscal horn subjected to physiologically occurring circumferential loads. The methodology validated herein in a porcine model is applied to human models in subsequent chapters of this thesis.

Regarding the resistance at specimen level, the tissue cut-out was initiated in the porcine sutured specimens under a mean traction force in the circumferential direction induced by the suture, F_c, of 168.86 N. This value was 17.9% lower with respect to the mean maximum traction force that specimens could bear, F_u, which had a mean value of 205.79 N. In scientific literature, the maximum force withstood by the specimen in load-to-failure tests, F_u, is the property typically used to characterize the failure of repaired menisci. However, this thesis focuses on the initiation point of cut-out, F_c, at the specimen level and the stress to cut-out, S_c, at the tissue level, considering them more relevant for evaluating meniscal repair. This is because a meniscal horn tear, even if it does not progress to final failure, implies damage to the meniscus. The damage, on the one hand, can hinder healing and, on the other hand, can result in displacements leading to repair in non-anatomical positions that have been shown to be unfavorable from a clinical point of view (Espejo-Reina et al., 2019). Additionally, this tear is an initiation point of failure that weakens the specimen in the suture area computed from a load-to-failure test. If the area is subsequently subjected to cyclic loading, as is to be expected in accelerated rehabilitation processes that allow for mobilization of the joint, it is expected that the weakened meniscal horn will be able to withstand lower loads than if the tear had not been initiated. Further research is needed to corroborate this hypothesis, which has not been addressed in any article published in the scientific literature to our knowledge. After the initiation of cut-out, the tear can propagate along various and unpredictable paths within the meniscus, which has variable thickness. Consequently, the load-deformation curve exhibited significant heterogeneity from the point of cut-out initiation to the absolute maximum force. This variability observed under laboratory conditions is expected to be even more pronounced in a repaired knee subjected to physiological loads. Therefore, the cut-out initiation point provides a more consistent basis for characterizing and comparing results across different groups. It marks the onset of structural integrity loss and is less affected by the subsequent tear progression.

At the tissue level, resistance was quantified in terms of tissue cut-out stress at the meniscus-suture interface, S_c, with porcine specimens showing a value of 74.49 MPa. S_c translates at the tissue level the results provided by F_c at the specimen level, disaggregating them from the morphology of the porcine meniscus (sutured porcine meniscal horns showed a thickness at the puncture point of 4.98 mm). This aspect is especially important in this animal model, given that porcine menisci are considerably thicker than human menisci (as verified in a later chapter of this thesis). On the other hand, both levels of study are of scientific interest: quantification of strength at the specimen level relevant for assessing the suitability of porcine models for in vitro meniscus testing, while at the tissue level, it is fundamental for studies that seek to characterize material properties and provide data for computational models.

To study deformation at the tissue level, the equivalent stiffness modulus, m_s, was defined as a parameter describing the relationship between stress and strain in the suture hole area when the experimental results are linearly fit in the strain range between 0 and 30%. m_s showed a mean value of 111.34 MPa. This approach disregards the presence of the toe zone, a region observed in the human meniscus and other soft tissues with collagen fibers (Bruce et al., 2015; Tissakht and Ahmed, 1995). The toe zone is considered a phase of the stress-strain curve where the collagen fibers of the tissue undergo straightening and alignment, which occurs just prior to the onset of elongation. Although no initial region of the curve, where the toe zone would typically occur, was excluded from the fitting process, the linear fit effectively describes the porcine tissue in the strain range of [0, 0.3], as the adjusted R-square values were higher than 0.93 for all specimens even reaching up to 0.99 in some cases.

Large animal models serve as invaluable tools in biomechanical engineering, facilitating both preliminary in-vitro and in-vivo testing. Species such as dogs, rabbits, cows, sheep, and pigs have been extensively employed to investigate the natural meniscus, its kinematic behavior, knee joint biomechanics, and the efficacy of engineered tissues for meniscal replacement, as well as to assess surgical meniscal repair techniques. Historically, canine models were widely used; however, their prevalence has diminished, likely due to increased scrutiny from animal advocacy organizations. Furthermore, most surgical procedures on the canine meniscus necessitate arthrotomy, often involving the rupture of the medial collateral ligament, which differs significantly from the arthroscopic procedures typically performed on humans.

The rabbit model exhibits distinct differences from human menisci in terms of vascularity, collagen orientation, and glycosaminoglycan content. Additionally, the kinematics of the rabbit femorotibial joint diverge markedly from those of the human knee (Bansal et al., 2017; Deponti et al., 2015; Polito et al., 2020). The bovine model, although significantly larger than the human meniscus, has limited applicability in biomechanical studies due to its size disparity (Bansal et al., 2017; Polito et al., 2020). Similarly, while the ovine meniscus is anatomically comparable to the human meniscus, differences in kinematics and contact force distribution render it unsuitable for non-isolated studies of meniscal repairs (Deponti et al., 2015; Polito et al., 2020; Takroni et al., 2016).

In contrast, the porcine model closely mirrors the human meniscus in anatomical structure, vascularity, volume, and weight (Deponti et al., 2015; Polito et al., 2020; Takroni et al., 2016), despite having a wider meniscus. The kinematics of the porcine knee also approximate those of the human knee more closely. Consequently, the porcine model has become the preferred surrogate for in-vitro testing of the human meniscus (Chung et al., 2018; Feucht et al., 2015,

2013; Fujii et al., 2017; Kim et al., 2016; Okimura et al., 2019; Perez-Blanca et al., 2018; Robinson et al., 2018; Seo et al., 2009; Stärke et al., 2010; Wu et al., 2018, 2020), widely used in biomechanical studies of meniscal repair and replacement techniques, thereby facilitating effective translation to clinical applications. Additionally, all porcine specimens used in this study were obtained from a single local slaughterhouse, raising the question of whether different origins of porcine models might yield varying results (De Roy et al., 2023).

To focus the study on the meniscus-suture interface, the experimental design involved testing isolated meniscus-suture constructs restricted to the suture area, rather than complete menisci attached to tibial bones. This approach concentrates the examination on the tissue-suture interface, free from the variables introduced by tibial fixation. A similar experimental layout was followed in previous studies investigating meniscal repairs (Anz et al., 2014; Mitchell et al., 2016; Perez-Blanca et al., 2018; Vertullo et al., 2021). The suture was positioned parallel to the loading direction to minimize shear friction, again with the aim of focusing the tensile forces on the meniscus-suture interface, which was the primary interest of this study. This solution can be found in other biomechanical studies (Anz et al., 2014; Mitchell et al., 2016; Perez-Blanca et al., 2018; Vertullo et al., 2021). The orientation of the meniscal horn, with the circumferential fibers parallel to the loading direction, was chosen to induce maximal tissue damage, providing a conservative estimate of the maximum load that the meniscal repair could endure.

A single simple suture was employed at the meniscal horn, which deviates from the more commonly used surgical methods. This choice was made to facilitate the accurate computation of forces acting on the individual tissue-suture interface. When multiple stitches are used, the pulling load is distributed among them, making it challenging to achieve uniform load distribution even under laboratory conditions. Although a single simple stitch is neither the strongest nor the most commonly used clinical technique for meniscal root repair, it simplifies the quantification of the meniscus-thread contact area, which is crucial for calculating stress at the suture-meniscus interface. This straightforward approach also reduces the influence of variations in meniscal anatomy and surgeon skill, compared to more complex suture techniques.

To accurately detect the initiation of cut-out, an automatic detection method, previously proposed (Perez-Blanca, 2019), was employed. To reinforce the validity of the procedure, a meticulous and labor-intensive task was carried out, reviewing the images recorded in the load-to-failure test of the 22 samples to verify that the change of slope in the curve representing the elongation between the marks at the suture area as a function of the displacement of the testing machine head corresponds to the instant at which the onset of tissue cutting is visually detected.

Cryo-protectant solutions are often proposed to prevent freezing damage in biological tissues; however, their use was excluded in this study for two primary reasons. First, they are not typically employed for the preservation of meniscus specimens, which are the focus of this research. Second, there is insufficient data demonstrating that cryo-protectants better preserve the mechanical properties of the sutured meniscal horn, especially regarding elasticity and resistance, compared to the preservation methods employed in this work.

The results for the porcine model in this study fall within the previously published range of failure loads, although it is important to note that the range of published data is quite broad. For instance, a study that utilized a single simple stitch with a UHMWPE No.2 suture (Feucht et al., 2015) reported an ultimate load of 169 ± 73.4 N. This result is comparable to our finding of 206.79 ± 74.31 N, especially considering that the specimens in that study were pre-weakened with 1,000 cycles of loading between 5 and 20 N. In contrast, other studies using porcine models have reported results for two sutures ranging from 129.8 ± 14.6 N (Fujii et al., 2017) to 221.67 ± 43 N (Perez-Blanca et al., 2018), albeit with different suturing techniques and suture materials. These discrepancies in failure loads can be attributed not only to variations in testing protocols but also to the diverse origins of the animals used. While using animal surrogate models ensures uniformity among donors, differences in breed, diet, stabling conditions, and other factors can introduce significant variability, even within the same species. This issue has been highlighted in previous research and, in our view, warrants further investigation (De Roy et al., 2023). Other properties of porcine menisci, such as force or stress at tissue cut-out and equivalent stiffness modulus, have not been previously reported in the literature to our knowledge

This study faces limitations inherent to in-vitro testing, primarily the absence of the natural healing process over time. As previously discussed, utilizing an isolated meniscal setup intentionally excludes the effects of surrounding soft tissues, ligaments, cartilage, and bones. A single simple suture was used, contrary to typical clinical practice, for reasons already discussed. Consequently, the cut-out and ultimate forces reported in this chapter do not quantitatively represent the maximum traction forces that a clinically repaired meniscus with other, more common suturing techniques might withstand, especially since the forces were computed from a porcine model. The load-to-failure test was conducted at a displacement velocity of 0.1 mm/s, representing a quasi-static condition that is slower than the velocities expected during knee movement in daily activities (Prado-Novoa et al., 2022). This approach reduces the potential impact of viscous effects on the test, which was not the focus of this study.

3.5 Conclusions

At the specimen level, porcine sutured meniscal horns showed a resistance to tensile forces in the circumferential direction of 168.86 N. This resistance was 17.9% lower compared to the ultimate load, which had a value of 205.79 N. At the tissue level, the tissue cut-out stress at the meniscus-suture interface was 74.49 MPa. In terms of deformation, the equivalent stiffness modulus of the porcine specimens was 111.34 MPa, computed after linear fits of the stress-strain curves with adjusted R-squared values ranging from 0.93 to 0.99. Morphologically, the sutured porcine meniscal horns exhibited an average thickness at the puncture point of 4.98 mm.

A methodology for in-vitro testing was developed to obtain the biomechanical properties mentioned in the previous paragraph for meniscal horns subjected to suture-induced traction in the circumferential direction around the suture area during a load-to-failure test. This methodology was validated in a porcine model.

3.6 References

Ahn, J.H., Wang, J.H., Yoo, J.C., Noh, H.K., Park, J.H., 2007. A pull out suture for transection of the posterior horn of the medial meniscus: Using a posterior trans-septal portal. Knee Surgery, Sports Traumatology, Arthroscopy 15, 1510–1513. https://doi.org/10.1007/S00167-007-0310-3/FIGURES/6

Allaire, R., Muriuki, M., Gilbertson, L., Harner, C.D., 2008. Biomechanical consequences of a tear of the posterior root of the medial meniscus: Similar to total meniscectomy. Journal of Bone and Joint Surgery 90, 1922–1931. https://doi.org/10.2106/JBJS.G.00748

Anz, A.W., Branch, E.A., Saliman, J.D., 2014. Biomechanical Comparison of Arthroscopic Repair Constructs for Meniscal Root Tears. Am J Sports Med 42 (11), 2699–2706. https://doi.org/10.1177/0363546514549445

Balke, M., Akoto, R., Offerhaus, C., Hoeher, J., 2018. Suture Anchor Refixation of Meniscal Root Tears Without an Additional Portal. Arthrosc Tech 7, e511–e515. https://doi.org/10.1016/J.EATS.2018.01.003

Bansal, S., Keah, N.M., Neuwirth, A.L., O'Reilly, O., Qu, F., Seiber, B.N., Mandalapu, S., Mauck, R.L., Zgonis, M.H., 2017. Large Animal Models of Meniscus Repair and Regeneration: A Systematic Review of the State of the

Field. Tissue Eng Part C Methods 23, 661. https://doi.org/10.1089/TEN.TEC.2017.0080

Bruce, R., David, M., Burr, B., Sharkey, N.A., Fyhrie, D.P., 2015. Skeletal Tissue Mechanics, Second. ed. Springer, New York. https://doi.org/10.1007/978-1-4939-3002-9

Cerminara, A.J., LaPrade, C.M., Smith, S.D., Ellman, M.B., Wijdicks, C.A., LaPrade, R.F., 2014. Biomechanical Evaluation of a Transtibial Pull-out Meniscal Root Repair Challenging the Bungee Effect. American Journal of Sports Medicine 42, 2988–2995. https://doi.org/10.1177/0363546514549447

Chung, K.S., Choi, C.H., Bae, T.S., Ha, J.K., Jun, D.J., Wang, J.H., Kim, J.G., 2018. Comparison of Tibiofemoral Contact Mechanics After Various Transtibial and All-Inside Fixation Techniques for Medial Meniscus Posterior Root Radial Tears in a Porcine Model. Arthroscopy - Journal of Arthroscopic and Related Surgery 34, 1060–1068. https://doi.org/10.1016/J.ARTHRO.2017.09.041

De Roy, L., Morejon, A., Jackson, A.R., Travascio, F., Seitz, A.M., 2023. A COMPARATIVE STUDY ON THE BIOMECHANICAL PROPERTIES OF PORCINE MENISCUS IN CONFINED COMPRESSION, in: 28th Congress of the European Society of Biomechanics. Maastricht, the Netherlands.

Deponti, D., Giancamillo, A. Di, Scotti, C., Peretti, G.M., Martin, I., 2015. Animal models for meniscus repair and regeneration. J Tissue Eng Regen Med 9, 512–527. https://doi.org/10.1002/TERM.1760

Espejo-Reina, A., Prado-Novoa, M., Espejo-Baena, A., Peña-Trabalon, A., Perez-Blanca, A., 2022. Biomechanical consequences of anterior root detachment of the lateral meniscus and its reinsertion. Sci Rep 12, 6182. https://doi.org/10.1038/S41598-022-10229-5

Espejo-Reina, A., Prado-Novoa, M., Espejo-Reina, M.J., Gómez-Cáceres, A., Dalla Rosa-Nogales, J., Espejo-Baena, A., 2019. Non anatomic reinsertion after amputation of the anterior horn of the lateral meniscus. Orthop Traumatol Surg Res 105, 1115–1118. https://doi.org/10.1016/J.OTSR.2019.04.007

Feucht, M.J., Grande, E., Brunhuber, J., Burgkart, R., Imhoff, A.B., Md, §, Braun, S., 2013. Biomechanical Evaluation of Different Suture Techniques for Arthroscopic Transtibial Pull-out Repair of Posterior Medial Meniscus Root

Tears. Am J Sports Med 41, 2784–2790. https://doi.org/10.1177/0363546513502464

Feucht, M.J., Grande, E., Brunhuber, J., Rosenstiel, N., Burgkart, R., Imhoff, A.B., Braun, S., 2015. Biomechanical evaluation of different suture materials for arthroscopic transtibial pull-out repair of posterior meniscus root tears. Knee Surg Sports Traumatol Arthrosc 23, 132–139. https://doi.org/10.1007/S00167-013-2656-Z

Feucht, M.J., Grande, E., Brunhuber, J., Rosenstiel, N., Burgkart, R., Imhoff, A.B., Braun, S., 2014. Biomechanical comparison between suture anchor and transtibial pull-out repair for posterior medial meniscus root tears. American Journal of Sports Medicine 42, 187–193. https://doi.org/10.1177/0363546513502946/ASSET/IMAGES/LARGE/10.1177_0363546513502946-FIG2.JPEG

Forkel, P., Foehr, P., Meyer, J.C., Herbst, E., Petersen, W., Brucker, P.U., Burgkart, R., Imhoff, A.B., 2017. Biomechanical and viscoelastic properties of different posterior meniscal root fixation techniques. Knee Surgery, Sports Traumatology, Arthroscopy 25, 403–410. https://doi.org/10.1007/S00167-016-4237-4/METRICS

Fox, A.J.S., Bedi, A., Rodeo, S.A., 2012. The Basic Science of Human Knee Menisci: Structure, Composition, and Function. Sports Health 4, 340. https://doi.org/10.1177/1941738111429419

Fujii, M., Furumatsu, T., Xue, H., Miyazawa, S., Kodama, Y., Hino, T., Kamatsuki, Y., Ozaki, T., 2017. Tensile strength of the pullout repair technique for the medial meniscus posterior root tear: a porcine study. Int Orthop 41, 2113–2118. https://doi.org/10.1007/S00264-017-3561-8

Hussain, Z.B., Chahla, J., Mandelbaum, B.R., Gomoll, A.H., LaPrade, R.F., 2019. The Role of Meniscal Tears in Spontaneous Osteonecrosis of the Knee: A Systematic Review of Suspected Etiology and a Call to Revisit Nomenclature. American Journal of Sports Medicine 47, 501–507. https://doi.org/10.1177/0363546517743734

Kim, Y.M., Joo, Y.B., Noh, C.K., Park, I.Y., 2016. The optimal suture site for the repair of posterior horn root tears: Biomechanical evaluation of pullout strength in porcine menisci. Knee Surg Relat Res 28, 147–152. https://doi.org/10.5792/KSRR.2016.28.2.147

Kim, Y.M., Rhee, K.J., Lee, J.K., Hwang, D.S., Yang, J.Y., Kim, S.J., 2006. Arthroscopic pullout repair of a complete radial tear of the tibial attachment site of the medial meniscus posterior horn. Arthroscopy 22, 795.e1-795.e4. https://doi.org/10.1016/J.ARTHRO.2005.12.040

Krych, A., Reardon, P., Johnson, N., Mohan, R., Peter, L., Levy, B., Stuart, M.J., 2017. Non-operative management of medial meniscus posterior horn root tears is associated with worsening arthritis and poor clinical outcome at 5-year follow-up. Knee Surgery, Sports Traumatology, Arthroscopy 25, 383–389.

Kyle Martin, R., Gillis, D., Leiter, J., Shantz, J.S., MacDonald, P., 2016. A Porcine Knee Model Is Valid for Use in the Evaluation of Arthroscopic Skills: A Pilot Study. Clin Orthop Relat Res 474, 965–970. https://doi.org/10.1007/S11999-015-4498-0

LaPrade, C.M., Foad, A., Smith, S.D., Lee Turnbull, T., Dornan, G.J., Engebretsen, L., Wijdicks, C.A., LaPrade, R.F., 2015. Biomechanical Consequences of a Nonanatomic Posterior Medial Meniscal Root Repair. Am J Sports Med 43(4), 912–920. https://doi.org/10.1177/0363546514566191

Menge TJ, J, C., CS, D., JJ, M., G, M., RF, L., 2016. Anterior Meniscal Root Repair Using a Transtibial Double-Tunnel Pullout Technique. Arthroscopic Techniques 5, e679–e684.

Mitchell, R., Pitts, R., Kim, Y.M., Matava, M.J., 2016. Medial Meniscal Root Avulsion: A Biomechanical Comparison of 4 Different Repair Constructs. Arthroscopy: The Journal of Arthroscopic & Related Surgery 32, 111–119. https://doi.org/10.1016/J.ARTHRO.2015.07.013

Musahl, V., Citak, M., O'Loughlin, P., Choi, D., Bedi, A., Pearle, A., 2010. The effect of medial versus lateral meniscectomy on the stability of the anterior cruciate ligament-deficient knee. Am J Sports Med 38, 1591–1597.

Okimura, S., Mae, T., Tachibana, Y., Iuchi, R., Nakata, K., Yamashita, T., Shino, K., 2019. Biomechanical comparison of meniscus-suture constructs for pullout repair of medial meniscus posterior root tears. J Exp Orthop 6, 1–6. https://doi.org/10.1186/S40634-019-0186-4/TABLES/2

Pache, S., Aman, Z.S., Kennedy, M., Nakama, G.Y., Moatshe, G., Ziegler, C., LaPrade, R.F., 2018. Meniscal Root Tears: Current Concepts Review. Archives of Bone and Joint Surgery 6, 250.

Perez-Blanca, A., 2019. Biomecánica de la Reinserción Transtibial de la raíz Posterior del Menisco Lateral de la Rodilla: Avances en la Técnica de Reparación No Title (PhD Thesis,). University of Malaga.

Perez-Blanca, A., Espejo-Baena, A., Amat Trujillo, D., Prado Nóvoa, M., Espejo-Reina, A., Quintero López, C., Ezquerro Juanco, F., 2016. Comparative Biomechanical Study on Contact Alterations After Lateral Meniscus Posterior Root Avulsion, Transosseous Reinsertion, and Total Meniscectomy. Arthroscopy: The Journal of Arthroscopic & Related Surgery 32, 624–633. https://doi.org/10.1016/j.arthro.2015.08.040

Perez-Blanca, A., Prado Nóvoa, M., Lombardo Torre, M., Espejo-Reina, A., Ezquerro Juanco, F., Espejo-Baena, A., 2018. The role of suture cutout in the failure of meniscal root repair during the early post-operative period: a biomechanical study. Int Orthop 42, 811–818. https://doi.org/10.1007/S00264-018-3799-9/FIGURES/5

Polito, U., Andreis, M., Di Giancamillo, A., Modina, S., Scurati, R., Marmotti, A., Michielon, G., Domenicucci, M., Lombardo, M., Di Giancamillo, M., Herrera, V., Mangiavini, L., Agnoletto, M., Brambilla, L., Peretti, G.M., 2020. Clinical anatomy of the meniscus in animal models: pros and cons. J Biol Regul Homeost Agents 34.

Prado-Novoa, M., Perez-Blanca, A., Espejo-Reina, A., Espejo-Reina, M.J., Espejo-Baena, A., 2020. Initial Biomechanical Properties of Transtibial Meniscal Root Repair are Improved By Using a Knotless Anchor as a Post-Insertion Tensioning Device. Sci. Rep. 10. https://doi.org/10.1038/S41598-020-58656-6

Prado-Novoa, M., Perez-Sanchez, L., Estebanez, B., Moreno-Vegas, S., Perez-Blanca, A., 2022. Influence of Loading Conditions on the Mechanical Performance of Multifilament Coreless UHMWPE Sutures Used in Orthopaedic Surgery. Materials 2022, Vol. 15, Page 2573 15, 2573. https://doi.org/10.3390/MA15072573

Robinson, J.R., Frank, E.G., Hunter, A.J., Jermin, P.J., Gill, H.S., 2018. The Strength of Transosseous Medial Meniscal Root Repair Using a Simple Suture Technique Is Dependent on Suture Material and Position. American Journal of Sports Medicine 46, 924–932. https://doi.org/10.1177/0363546517749807/ASSET/IMAGES/LARGE/10.1177_0363546517749807-FIG7.JPEG

Rosslenbroich, S.B., Borgmann, J., Herbort, M., Raschke, M.J., Petersen, W., Zantop, T., 2013. Root tear of the meniscus: Biomechanical evaluation of an arthroscopic refixation technique. Arch Orthop Trauma Surg 133, 111–115. https://doi.org/10.1007/S00402-012-1625-1

Seo, J.H., Li, G., Shetty, G.M., Kim, J.H., Bae, J.H., Jo, M.L., Kim, J.S., Lee, S.J., Nha, K.W., 2009. Effect of Repair of Radial Tears at the Root of the Posterior Horn of the Medial Meniscus With the Pullout Suture Technique: A Biomechanical Study Using Porcine Knees. Arthroscopy: The Journal of Arthroscopic & Related Surgery 25, 1281–1287. https://doi.org/10.1016/J.ARTHRO.2009.05.014

Shiwaku, K., Kamiya, T., Suzuki, D., Yamakawa, S., Otsubo, H., Suzuki, T., Takahashi, K., Okada, Y., Teramoto, A., Ohnishi, H., Fujie, H., Yamashita, T., 2022. The Role of the Medial Meniscus in Anterior Knee Stability. Orthop J Sports Med 10. https://doi.org/10.1177/23259671221132845

Shoemaker, S., Markolf, K., 1986. The role of the meniscus in the anterior-posterior stability of the loaded anterior cruciate-deficient knee. Effects of partial versus total excision. J Bone Joint Surg 68, 71–79.

Stärke, C., Kopf, S., Gröbel, K.H., Becker, R., 2010. The Effect of a Nonanatomic Repair of the Meniscal Horn Attachment on Meniscal Tension: A Biomechanical Study. Arthroscopy: The Journal of Arthroscopic & Related Surgery 26, 358–365. https://doi.org/10.1016/J.ARTHRO.2009.08.013

Sweigart, M.A., Zhu, C.F., Burt, D.M., Deholl, P.D., Agrawal, C.M., Clanton, T.O., Athanasiou, K.A., 2004. Intraspecies and interspecies comparison of the compressive properties of the medial meniscus. Ann Biomed Eng 32, 1569–1579. https://doi.org/10.1114/B:ABME.0000049040.70767.5C/METRICS

Takroni, T., Laouar, L., Adesida, A., Elliott, J.A.W., Jomha, N.M., 2016. Anatomical study: comparing the human, sheep and pig knee meniscus. J Exp Orthop 3, 1–13. https://doi.org/10.1186/S40634-016-0071-3/TABLES/4

Tissakht, M., Ahmed, A.M., 1995. Tensile stress-strain characteristics of the human meniscal material. J Biomech 28, 411–422. https://doi.org/10.1016/0021-9290(94)00081-E

Vertullo, C.J., Cadman, J., Dabirrahmani, D., Appleyard, R., 2021. Biomechanical Comparison of an All-Inside Meniscal Repair Device Construct Versus Pullout Sutures for Arthroscopic Transtibial Repair of Posterior Medial

Meniscus Root Tears A Matched-Pair Cadaveric Study. Orthop J Sports Med 9(4), 23259671211000464. https://doi.org/10.1177/23259671211000464

Wu, J.L., Lee, C.H., Yang, C.T., Chang, C.M., Li, G., Cheng, C.K., Chen, C.H., Huang, H.S., Lai, Y.S., 2018. Novel technique for repairing posterior medial meniscus root tears using porcine knees and biomechanical study. PLoS One 13, e0192027. https://doi.org/10.1371/JOURNAL.PONE.0192027

Wu, S.H., Yeh, T. Te, Hsu, W.C., Wu, A.T.H., Li, G., Chen, C.H., Lee, C.H., Wu, J.L., 2020. Biomechanical comparison of four tibial fixation techniques for meniscal root sutures in posterior medial meniscus root repair: A porcine study. J Orthop Translat 24, 144–149. https://doi.org/10.1016/J.JOT.2020.01.006

4

Analysis of circumferential tensile properties in sutured human meniscal horns: Impact of age

This chapter follows the methodology described in Chapter 3, where the circumferential tensile mechanical properties of the sutured meniscal horn around the puncture were experimentally characterized in a porcine model. In this chapter, the same methodology is applied to a human model, focusing mainly on determining the stress at the initiation of cut-out, the force required to achieve the cut-out, the ultimate force that the specimen is able to withstand, and the equivalent stiffness modulus, as defined in Chapter 3. Additionally, the influence of donor age on mechanical parameters at both the tissue and specimen levels is examined.

This chapter, along with Chapter 3, fulfils the second specific objective in Section 1.2 of Chapter 1, by completing the data set on circumferential tensile properties for the various meniscal models assessed in this thesis. Additionally, by analysing the experimental results for the human models of different age ranges obtained in this chapter, the fourth objective is also fulfilled. The main findings presented in this chapter were published in "Frontiers in Bioengineering and Biotechnology" (see Appendix E.1), a journal indexed in the 1st quartile (Q1) of the JCR ranking for the year 2023 in its corresponding category.

4.1 Introduction

As discussed in Chapters 1, 2, and 3, numerous biomechanical studies have demonstrated that detaching the meniscal roots significantly impacts knee joint kinematics and contact mechanics. These changes resemble those seen following meniscectomy (Ode et al., 2012; Perez-Blanca et al., 2016). Clinically, such alterations are linked to early cartilage degeneration, which speeds up the

progression of degenerative joint conditions such as arthritis and osteoarthritis (Jones et al., 2006). Consequently, treatment has changed to meniscal root surgical reinsertion.

Previous biomechanical research has highlighted the tissue-suture interface as a potentially critical factor in improving the outcomes of the repair of meniscal roots (Cerminara et al., 2014; Steineman et al., 2020). Gaining a deeper understanding of the mechanical properties of the meniscal horn tissue, particularly in regions affected by suture, could lead to enhancements in surgical procedures. Moreover, assessing the age-dependent mechanical response of meniscal tissue around the suture site is crucial, as it may affect surgical decision-making. As already discussed in Chapter 3, while various experimental studies have examined the mechanical properties of human meniscal tissue under diverse conditions, such as uniaxial tensile testing (Yan et al., 2016) and compression testing at physiological strain rates (Chia and Hull, 2008b), these studies have primarily focused on intact meniscus and their native attachments.

This chapter aims to investigate the mechanical properties of meniscal horn tissue in the region influenced by suture passage in human specimens across various age groups during the early post-operative phase, before tissue healing occurs. The main hypothesis is that the deformation characteristics and mechanical resistance of the meniscal horn tissue near the suture interface are age-dependent.

4.2 Materials and methods

Following approval from the Ethical Committee of Experimentation at the University of Malaga (CEUMA), cryopreserved human knees, extending from the mid-femur to the mid-tibia, were obtained from a specialized supplier and utilized for the study in compliance with all legal and ethical standards.

4.2.1 Specimen preparation

To concentrate the study on the tissue-suture interface, isolated cadaveric meniscus-suture constructs were examined. Knees were categorized into three age groups:

- **Young:** under 55 years old.
- **Middle-aged:** from 56 to 75 years old.
- **Old:** over 75 years old.

Following the same procedure described in Section 3.2.1, human knees were stored frozen individually in sealed plastic bags at -20°C. One day prior to testing, each knee was thawed at room temperature and wrapped in damp gauze. Following thawing, the knee was dissected, and the menisci were extracted and inspected visually to ensure integrity and absence of pathologies, with particular attention to the horns and roots. The inclusion criterion required a macroscopic quality grade of 3 or higher, based on the scale by Pauli et al. (Pauli et al., 2011). Menisci meeting this criterion were randomly assigned for either anterior or posterior horn repair. Each meniscus was then wrapped in damp gauze, placed in a sealed plastic bag, and stored in a cooler until testing.

A total of 66 menisci met the inclusion criteria and were divided into three age groups of 22 specimens each with the characteristics shown in Table 4.1.

Table 4.1. Main characteristics of the three meniscus groups tested

	Young	**Middle-aged**	**Old**
Sample number (N)	22	22	22
Number of donates	12	12	14
Medial menisci	11	11	11
Lateral menisci	11	11	11
Anterior horn	11	11	10
Posterior horn	11	11	12
Men	18	8	10
Women	4	14	12
Age: mean (SD)	37.87 years (6.25)	62.96 years (3.97)	85.63 years (4.51)
Age : median	41 years	64 years	83 years
Age: Range	28 to 47 years	57 to 67 years	82 to 95 years
Number of exclusions and reason	1 meniscus: failure to meet the inclusion criteria 1 meniscus: omitted to adhere to the group size limit	2 menisci: failure to meet the inclusion criteria	6 menisci: failure to meet the inclusion criteria

Previous testing, a No. 2 non-absorbable, high-resistance, 100% UHMWPE braided fiber thread (FiberForce® No. 2, Stryker Endoscopy, San José, CA) was inserted into the meniscal horn 5 mm from both its internal edge and its root junction (Figure 4.1a), using the attached ½ circle tapered needle. This puncture point was selected to replicate the typical location of surgical holes (Kim et al., 2006; Moon et al., 2010). The thickness of the meniscus at the insertion point was measured with a manual caliper (caliper 500-182-30, Mitutoyo, Japan) (Figure 4.1d).

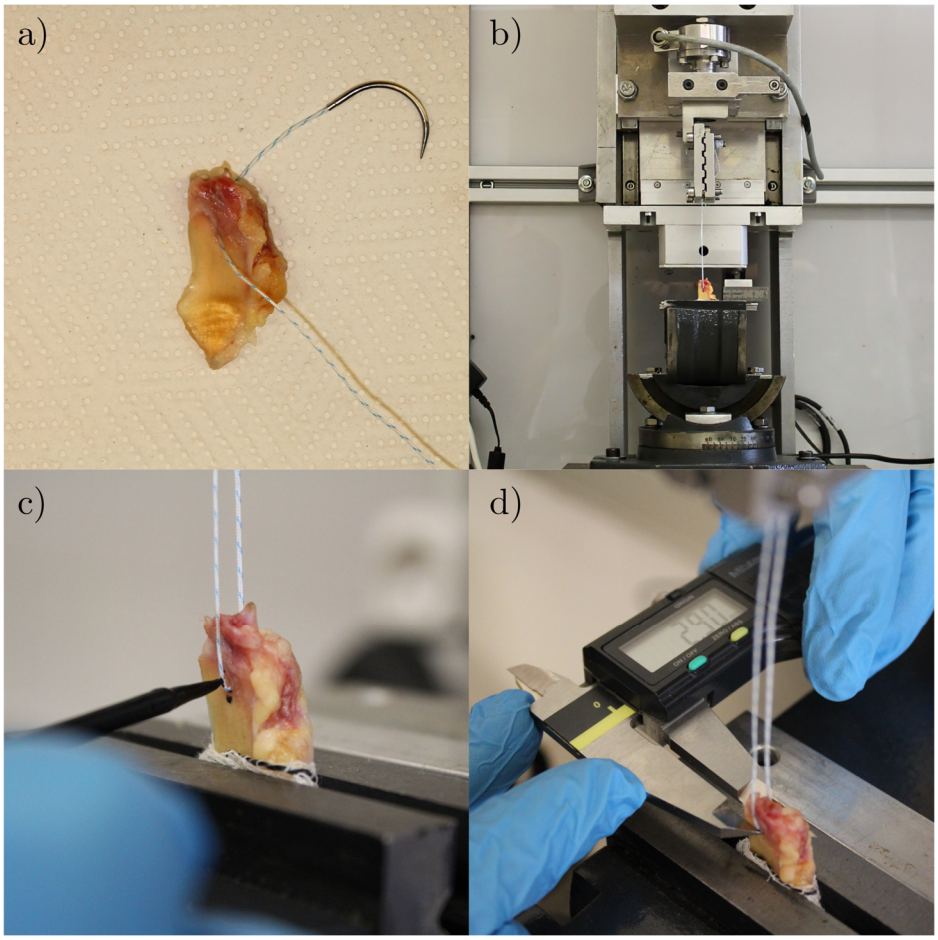

Figure 4.1. Specimen preparation process: a) sutured meniscal horn with tapered needle; b) sutured meniscal horn placed in the uniaxial testing machine of BIOCLINA; c) placement of the inked marks on the cranial surface of the meniscal horn; d) measurement process using a manual caliper.

To assess whether the impact of age was comparably significant between the lateral and medial sites, the three age groups were stratified into two subgroups of 11 specimens each, categorized according to their respective anatomical locations and shown in Table 4.2.

Table 4.2. Main characteristics of the six meniscus groups tested

	Young		Middle-aged		Old	
	Medial	**Lateral**	**Medial**	**Lateral**	**Medial**	**Lateral**
Sample number (N)	11	11	11	11	11	11
Number of donates	12		12		14	
Anterior horn	4	7	5	6	5	5
Posterior horn	7	4	6	5	6	6
Men	9	9	4	4	5	5
Women	2	2	7	7	6	6
Age: mean (SD)	38.90 years (6.15)	37.83 years (6.39)	61.89 years (4.37)	63.36 years (4.13)	84.36 years (3.26)	85.40 years (4.50)
Age : median	41 years	39 years	60 years	64 years	83 years	83 years
Age: Range	28 to 47 years	28 to 47 years	57 to 67 years	57 to 67 years	82 to 91 years	82 to 95 years
Number of exclusions and reason	1 meniscus: failure to meet the inclusion criteria	1 meniscus: omitted to adhere to the group size limit	1 meniscus: failure to meet the inclusion criteria	1 meniscus: failure to meet the inclusion criteria	2 menisci: failure to meet the inclusion criteria	4 menisci: failure to meet the inclusion criteria

4.2.2 Biomechanical testing

The custom-designed, single-column uniaxial testing machine (Perez-Blanca, 2019) detailed in Section 2.5.1.1 of Chapter 2 was also employed for these experiments (Figure 4.1b). The same procedure described in Section 3.2.2 of Chapter 3 was followed in this chapter, specifically:

1. Meniscus-suture construct was partially wrapped between sandpaper strips up to approximately 8 mm from the suture insertion point

2. Specimen area wrapped in sandpaper was clamped to the testing machine using a multi-degree-of-freedom clamp (TLT/SP-75, Wilton Tools, La Vergne, TN, USA). Meniscus horn was positioned vertically, with its cranial surface facing outward, the longitudinal fibers aligned with the direction of the applied load and ensuring the suture hole was centered along the pull line directed at the machine actuator head.

3. Free ends of the suture were also wrapped in sandpaper.

4. Suture free ends were attached to the machine head using a mechanical clamp, maintaining a 55 mm distance from the puncture point to the clamp while manually applying just enough tension to keep the suture vertical.

5. Reference lines were drawn on the meniscus and suture at the points of contact with the jaw and clamp.

6. Two reference points were marked on the cranial side of the meniscal horn in alignment with the pulling direction (Figure 4.2):

    - Point1: on the suture limb coinciding with the meniscus-suture interface
    - Point2: just beyond the hole.

7. The digital camera described in Section 2.6 of Chapter 2 was mounted directly in front of the testing machine meticulously aligned so that its image plane was parallel to the medial transversal plane of the meniscus.

The meniscus-suture construct underwent the testing protocol illustrated in Figure 4.3. Initially, a tensile force of 1 N was applied at a displacement rate of 0.05 mm/s. This load was maintained for 5 seconds, to allow for stabilization of the construct. After this stabilization phase, a load-to-failure test also controlled in displacement was performed at a rate of 0.1 mm/s. The displacement was maintained until reaching a maximum stroke of 20 mm.

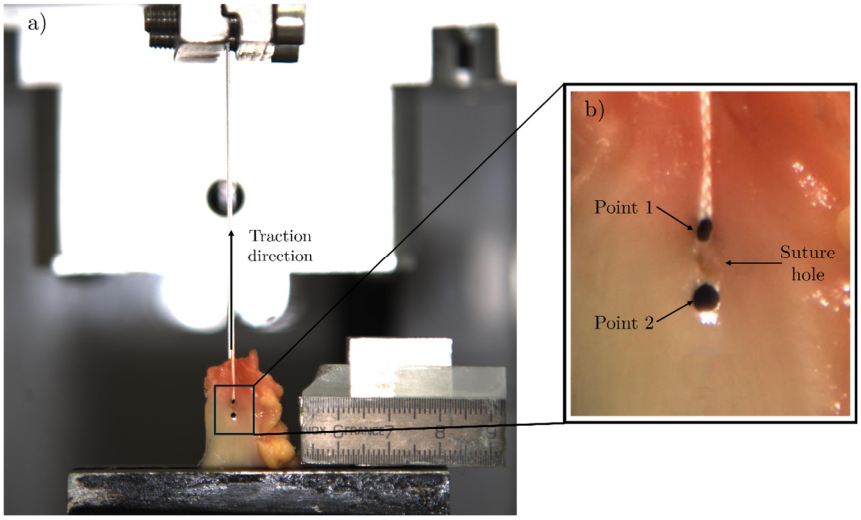

Figure 4.2. a) Lateral human meniscal horn on the testing machine with an indication of the traction direction aligned with its circunferential fibers; b) Magnification of the suture hole area with the inked marks and the puncture point shown.

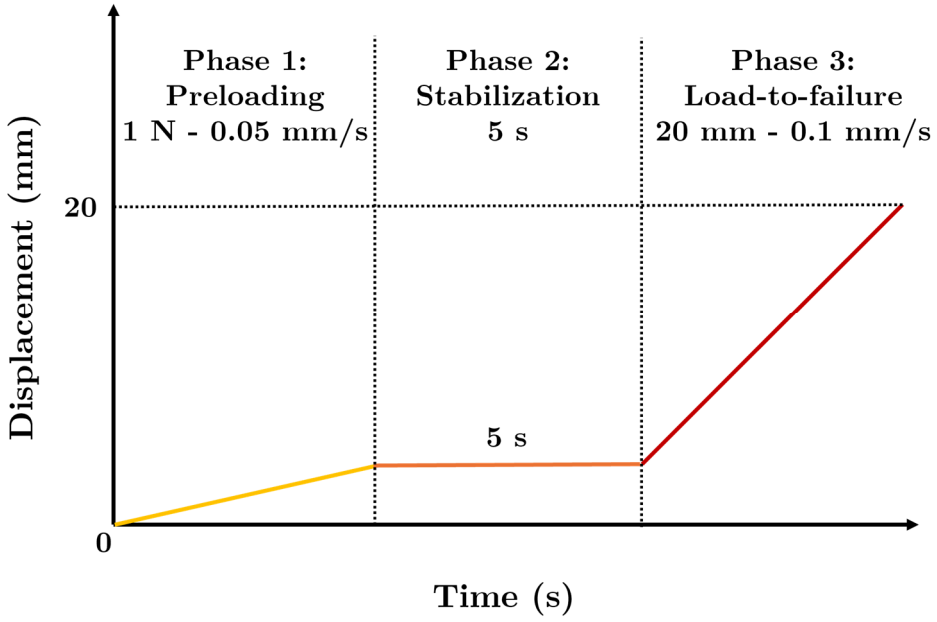

Figure ¡Error! No hay texto con el estilo especificado en el documento.**4.3.** Testing protocol scheme

Prior to commencing the tests, a calibration image was captured by the digital camera. This calibration image included a precise measurement pattern into the image plane to ensure accuracy in tracking displacements during the test. During the load-to-failure phase, the camera recorded images at regular intervals of 250 ms with an exposure time of 50 ms. Simultaneously, the testing machine's load cell monitored the tensile force (traction) at a frequency of 1,000Hz.

Synchronization between the camera images and the force data from the testing machine was achieved using an internal trigger.

4.2.3 Load-to-failure analysis

The custom videogrammetric software explained in Section 2.6 of Chapter 2 was employed to facilitate the automatic identification of the two marks on the meniscus, obtain their coordinates in each calibrated frame, and compute the distance between them. The same mechanical parameters at specimen and tissue level as exposed in Chapter 3 will be computed in these experimental tests.

- Meniscal cut-out force, F_c: the corresponding force in the instant of change of slope of the displacement-force curve (Perez-Blanca, 2019), where the displacement between the marks, D, was plotted as a function of the applied traction force, F.

- Ultimate force, F_u: the maximum force withstand by the specimen during the load-to-failure test.

- Tissue cut-out resistance of the meniscal horn , S_c: calculated as the stress at the tearing initiation as:

$$S_c = \frac{F_C}{\phi \cdot h} \tag{4.1}$$

where ϕ represents the nominal diameter of the suture and h denotes the thickness of the meniscus at the suture hole.

- Equivalent stiffness modulus of the meniscal tissue in the direction of traction at the suture site, m_s: the slope of the linear segment of the stress-strain curve. Tissue strain, ε, in the direction of traction at the hole area was calculated for each frame of the test as:

$$\varepsilon = \frac{D}{D_0} - 1 \tag{4.2}$$

and the tissue engineering stress, σ, in the same direction was computed at each frame of the test following:

$$\sigma = \frac{F}{\phi \cdot h} \tag{4.3}$$

As in previous chapter, this analysis was confined to the strain range $\varepsilon = [0 - 0.3]$.

4.2.4 Statistical analyses

The sample size determination was computed from S_c measurements from the first five specimens in each age category, which yielded mean values of 42.20 MPa for young, 38.60 MPa for middle-aged, and 31.50 MPa for elderly samples, with a maximum standard deviation of 10.50 MPa. Using G*Power 3.1.9.2 software (Faul et al., 2007), a large effect size (f = 0.44) was calculated for a one-way ANOVA test. To detect a smaller effect size of 0.42 with $\alpha = 0.05$ and a power of $(1 - \beta) = 0.80$, a minimum sample size of $n = 20$ was deemed necessary. To account for a potential dropout rate of 10%, a final conservative sample size of $n = 22$ per group was adopted.

Other statistical analysis were carried out using SPSS Statistics (v.20, IBM Corp). To investigate how age affects the mechanical properties of sutured meniscal horns, we compared the ultimate force, F_u, the cut-out force, F_c, the tissue cut-out stress, S_c, and equivalent stiffness modulus, m. Firstly, comparations were made without distinguishing between lateral and medial menisci. A one-way ANOVA test was performed to assess overall differences among the three age groups for each mechanical property at $\alpha = 0.05$. When a significant global difference was revealed by the ANOVA test, Student's t-tests with Bonferroni corrections for multiple comparisons were carried out. In all cases, statistical significance was set to $p \leq 0.05$. With $n = 22$, a minimum detectable difference of 10 MPa (representing 25% of the resistance observed in the young group) was computed for S_c.

As an additional analysis, age effects were studied separately for the medial and lateral meniscal sides within each age group. Due to smaller subgroup sizes, the Shapiro-Wilk test was used to check for normality. Because the data did not meet normality assumptions, it was employed the Kruskal-Wallis test for non-parametric analysis of variance. When significant global differences were found, further examined using Mann-Whitney U tests with Bonferroni adjustments were conducted to account for multiple comparisons. Again, statistical significance was set to $p \leq 0.05$.

If difference between groups were detected, the percentage differences between their means were computed always relative to the oldest age group, to quantify the level of the difference.

4.3 Results

This section presents the results of the four parameters described in Section 4.2.2. In each subsection, the results are first presented for the three age groups without distinguishing between lateral and medial location of the meniscus and secondly, for the six groups formed by splitting each age group of meniscal horns according to whether they are from the medial or lateral meniscus.

The results shown in this chapter include only the main statistics of the measurements, specifically mean and SD. For the complete dataset see Appendix B.

4.3.1 Meniscal horn thickness at the suture point, *h*

Mean and SD found for meniscus thickness at the suture are shown in Table 4.3 for the three age groups and represented in a bar diagram in Figure 4.4 A significant overall variation in meniscus thickness at the suture area was observed ($p < 0.001$). As it is depicted in Figure 4.4 and indicated at the foot note of Table 4.3, pairwise comparisons revealed that the menisci from the young group were 26.0% thinner than those from the old group ($p < 0.001$). It is worth noting that a near-significant difference ($p = 0.075$) was revealed between the middle-aged and old groups, with the middle-aged menisci being 13.6% thinner. However, it difference was not enough and no statistically significant difference was found between the groups more proximal in age, i.e., young vs. middle-aged group ($p = 0.086$) and middle-aged vs. old group ($p = 0.075$) .

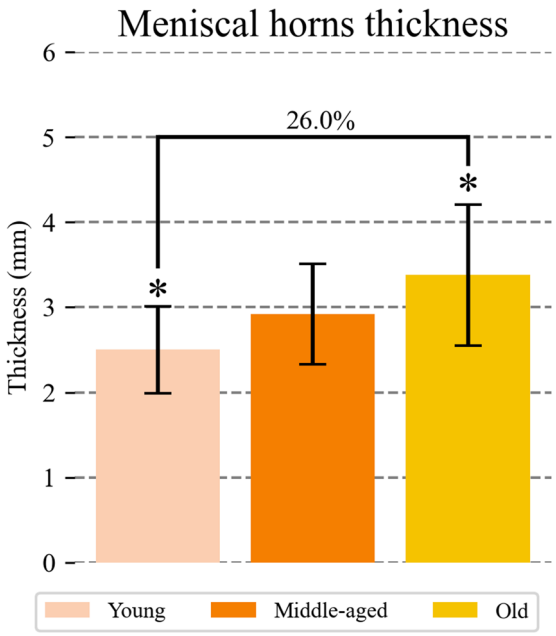

Figure 4.4. Mean and SD of the thickness of the meniscal horns at the suture hole area for each age group. Significant difference: *Young vs. Old.

Table 4.3. Thickness (mm) of the meniscal horns at the suture hole area for each age group.

	Young	Middle-aged	Old
Mean	2.50*	2.92	3.38*
SD	0.51	0.59	0.83

Significant difference: *Young vs. Old.

Figure 4.5 and Table 4.4 present the values found for the meniscus thickness at the suture site on the lateral and medial regions independently. When studying the influence of age on the disaggregated group, significant overall variability with age was observed only in the lateral meniscus ($p = 0.005$). Pairwise analysis for these lateral menisci revealed a behavior similar to that found for the gathered groups. Particularly, the older specimens were 34.9% thicker than those from the younger group ($p < 0.001$) with no detectable differences between groups more similar in age.

In contrast, the thickness of medial menisci did not show significant differences across age groups.

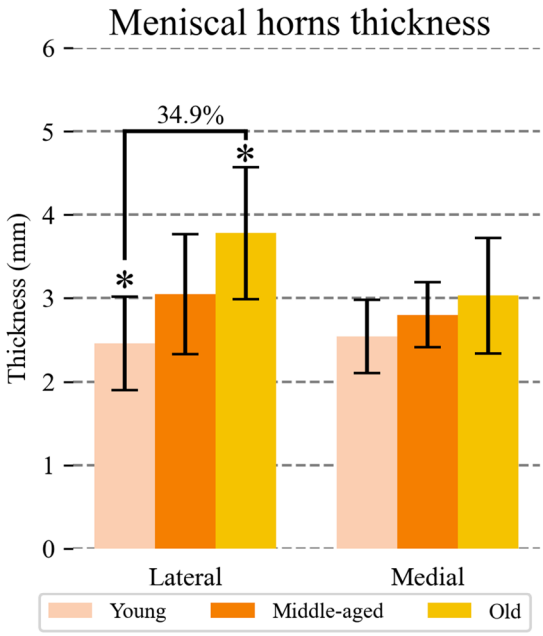

Figure 4.5. Mean and SD of the thickness of the meniscal horns at the suture hole area for each age group at the lateral and medial location. For the groups with significant differences, the percentage difference between means with respect to the oldest group is indicated. Significant difference: *Young vs. Old.

Table 4.4. Thickness (mm) of the lateral and medial meniscal horns at the suture hole area for each age group.

	Lateral meniscus			Medial meniscus		
	Young	**Middle-aged**	**Old**	**Young**	**Middle-aged**	**Old**
Mean	2.46*	3.05	3.78*	2.54	2.80	3.03
SD	0.56	0.72	0.79	0.44	0.39	0.69

Significant difference: *Young vs. Old.

4.3.2 Meniscal cut-out force, Fc

Figure 4.6 depict mean and SD of the resistance to suture traction at the specimen level, F_c, for the three global age groups. These values are also listed in Table 4.5. statistical comparisons did not reveal significant differences in suture resistance across different age categories. The average resistance values varied by only 7.2% between the young and middle-aged groups, 6.1% between the young and old groups, and 14.4% between the middle-aged and old groups.

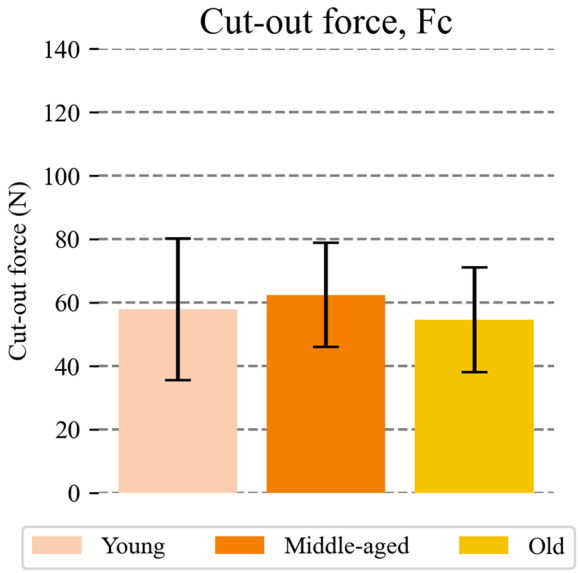

Figure 4.6. Mean and SD of the specimen cut-out force for each age group.

Table 4.5. Specimen cut-out force (N) for each age group.

	Young	**Middle-aged**	**Old**
Mean	57.84	62.33	54.50
SD	22.39	16.40	16.51

Figure 4.7 and Table 4.6 display the mean and standard deviation of suture traction resistance at the specimen level, F_c, when distinguishing between the

lateral and medial meniscus within each age group. After this division, the data neither reveal significant differences between the age groups at either location.

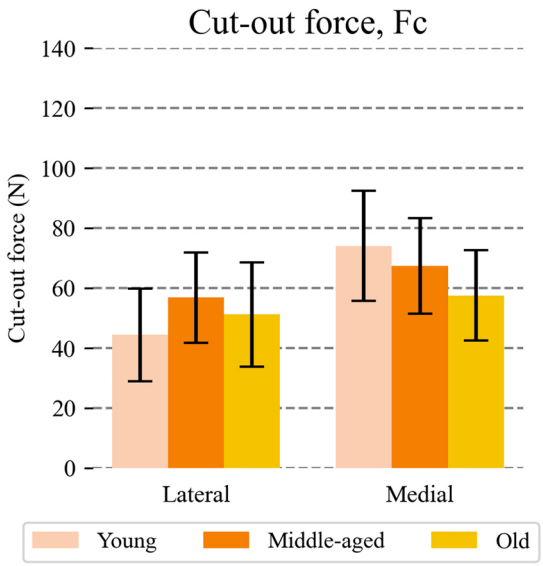

Figure 4.7. Mean and SD of the cut-out force of the lateral and medial meniscal horns for each age group.

Table 4.6. Specimen cut-out force (N) of the lateral and medial meniscal horns area for each age group.

	Lateral meniscus			**Medial meniscus**		
	Young	**Middle-aged**	**Old**	**Young**	**Middle-aged**	**Old**
Mean	57.86	61.88	67.29	101.55	82.36	73.40
SD	22.93	16.12	16.77	29.40	25.28	24.39

4.3.3 Meniscal ultimate force, F_u

Figure 4.8 illustrates the ultimate load, F_u, computed for the three global age groups, with the mean and SD values listed in Table 4.7 The statistical analysis indicated that F_u was of comparable magnitude among the age groups, as no statistical differences were detected and means differed by only 7.1% between the young and middle-aged groups, 10.3% between the young and old groups, and 2.9% between the middle-aged and old groups.

As expected, F_u exceeded F_c in all age groups. Specifically, F_u was 34.4% lower than F_c in the young group, 16.4% in the middle-aged group and 29.3% in the old group, resulting in an overall increase of 26.4% of F_u with respect F_c when all data were gathered.

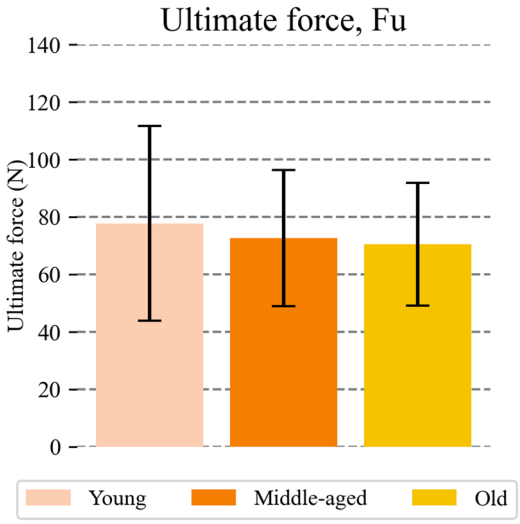

Figure 4.8. Mean and SD of the specimen ultimate force for each age group.

Table 4.7. Specimen ultimate force (N) for each age group**.**

	Young	**Middle-aged**	**Old**
Mean	77.72	72.56	70.49
SD	33.95	23.72	21.33

Figure 4.9 and Table 4.8 further differentiate the ultimate load by anatomical site. Similar results to those found in the study without distinguishing between anatomical sites were observed: no significant differences between age groups at either the lateral or medial locations were detected, and F_u exceeded F_c in all age groups.

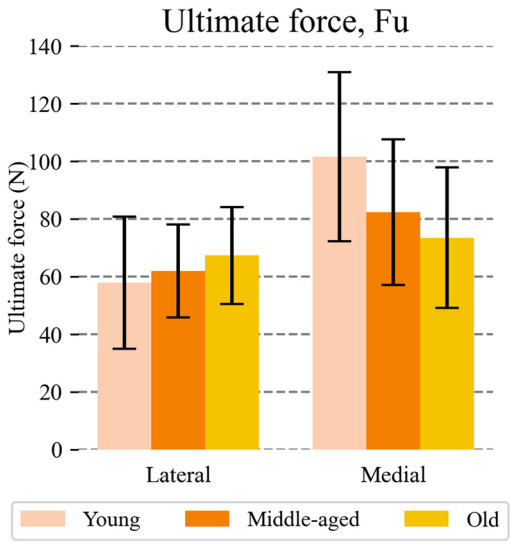

Figure 4.9. Mean and SD of the ultimate force of the lateral and medial meniscal horns for each age group.

Table 4.8. Specimen ultimate force (N) of the lateral and medial meniscal horns area for each age group.

	Lateral meniscus			Medial meniscus		
	Young	**Middle-aged**	**Old**	**Young**	**Middle-aged**	**Old**
Mean	57.86	61.88	67.29	101.55	82.36	73.40
SD	22.93	16.12	16.77	29.40	25.28	24.39

4.3.4 Tissue cut-out resistance, Sc

Figure 4.10 and Table 4.9 depict the mean and standard deviation of tissue cut-out resistance, S_c, across the different age groups. Statistical analysis indicated a significant overall difference between groups ($p = 0.012$). Notably, the resistance in the older cohort was significantly lower compared to the younger cohort ($p = 0.015$), with S_c in the younger group being 39.6% higher. A trend towards significant differences was also observed between the middle-aged and older groups ($p = 0.061$) with S_c in the middle-aged group being 32.2% higher than in the older group. There were no significant differences between the younger and middle-aged groups.

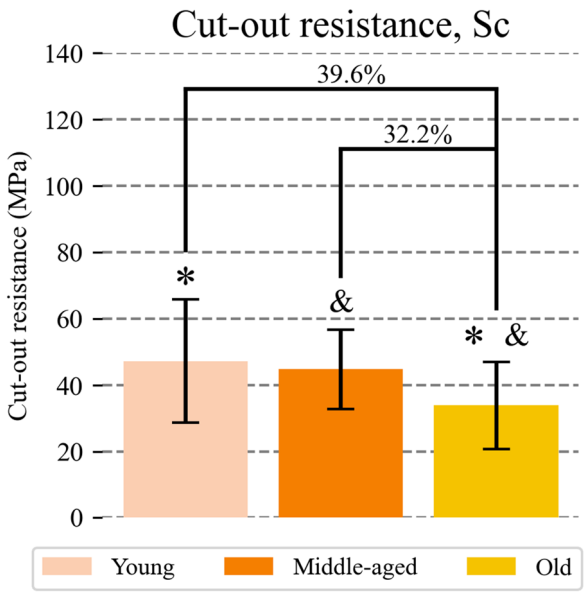

Figure 4.10. Mean and SD of tissue cut-out resistance of the meniscal horns for each age group. For the groups with significant differences, the percentage difference between means with respect to the oldest group is indicated. Significant difference: *Young vs. Old; & Middle-aged vs. Old.

Table 4.9. Tissue cut-out resistance (MPa) for each age group.

	Young	Middle-aged	Old
Mean	47.20*	44.68[&]	33.81*[&]
SD	18.49	11.91	13.09

Significant difference: *Young vs. Old; [&] Middle-aged vs. Old

In Figure 4.11 and Table 4.10, S_c values are compared between age groups for the lateral and medial meniscal horns independently. For the lateral meniscus, no significant differences between age groups were detected. However, for the medial meniscus, an overall significant difference was observed ($p = 0.008$). When comparing between groups, tissue from the older group demonstrated significantly lower resistance with respect to both the younger group ($p = 0.03$) and the middle-aged group ($p = 0.03$), with reductions of 53.6% and 27.4%, respectively

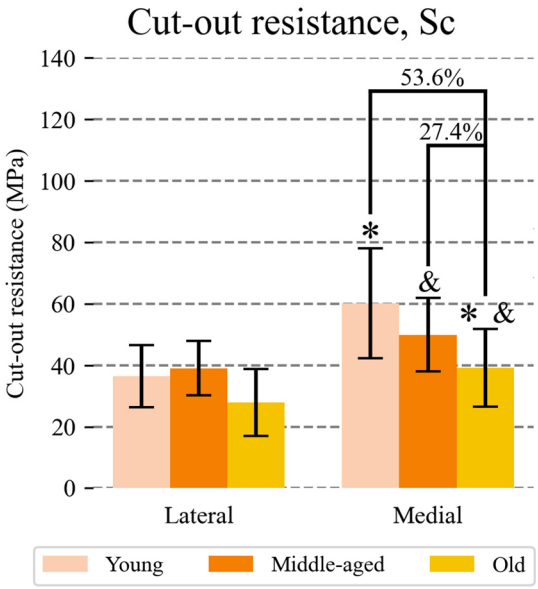

Figure 4.11. Mean and SD of tissue cut-out resistance of the lateral and medial meniscal horns for each age group. For the groups with significant differences, the percentage difference between means with respect to the oldest group is indicated. Significant difference: *Young vs. Old; [&] Middle-aged vs. Old.

Table 4.10. Tissue cut-out resistance (MPa) of the lateral and medial meniscal horns sites for each age group.

	Lateral meniscus			Medial meniscus		
	Young	**Middle-aged**	**Old**	**Young**	**Middle-aged**	**Old**
Mean	36.41	39.01	27.94	60.15*	49.88[&]	39.15*[&]
SD	10.10	8.87	10.88	17.94	11.96	12.63

Significant difference: *Young vs. Old; [&] Middle-aged vs. Old.

4.3.5 Tissue equivalent stiffness modulus, m_s

All meniscal horns demonstrated a highly linear response in the strain range of [0-0.3]. As an example, Figure 4.12 shows the results of such linear fits in the strain zone below 30%, superimposed on the complete set of experimental data obtained for a specimen from each age group. It can be observed that in the zone where the fit is performed, the correspondence between the experimental values and the linear model is very strong. In contrast, for higher strains, the linearity vanishes, and the experimental data exhibit a behavior that is more difficult to model. Similar results were observed for all the specimens with the linear regression fits consistently achieved an adjusted R-squared value greater than 0.91, indicating robust model accuracy.

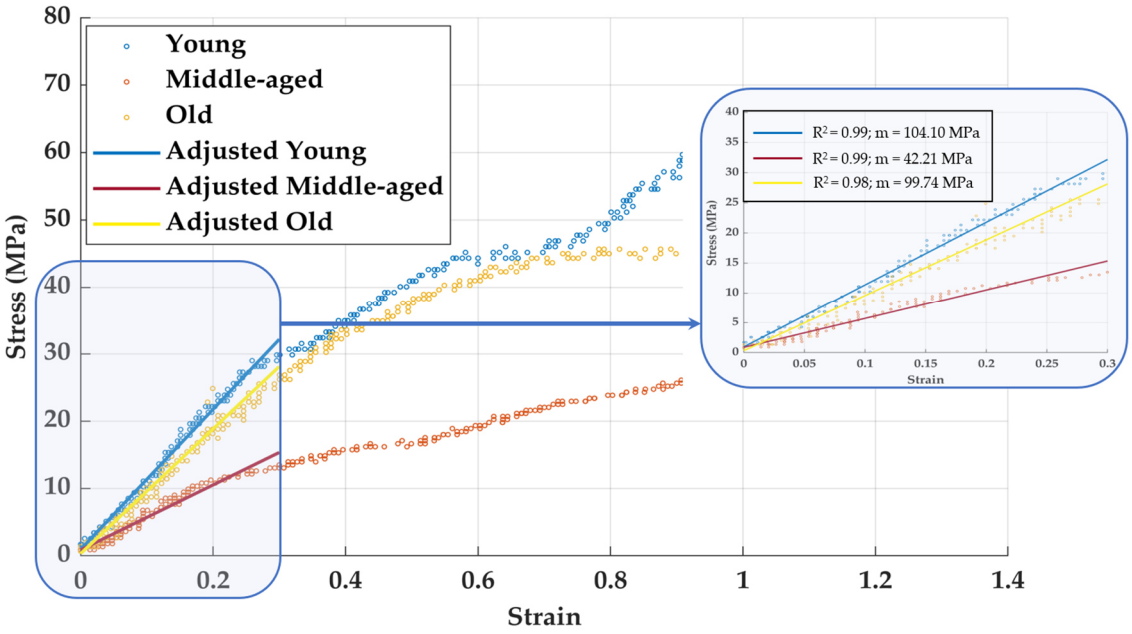

Figure 4.12. Stress-strain curves of a representative sample of each age group a linear fit in the strain range [0-0.3].

Therefore, the equivalent stiffness modulus of the tissue at the suture site, m_s, was calculated based on this linearity in the range ε=[0-0.3]. Figure 4.13 and Table 4.11 depict the mean and standard deviation of m for the three global age groups. In terms of age-related variations, an overall significant difference was observed among groups ($p<0.001$). Pairwise comparisons showed that the meniscal tissue from the elderly cohort exhibited greater elasticity compared to both the younger group ($p = 0.002$) and middle-aged group ($p = 0.004$.) For the younger cohort it was 97.5% greater, and for the middle-aged cohort, it was 87.9% greater. No significant differences were found between the younger and middle-aged groups.

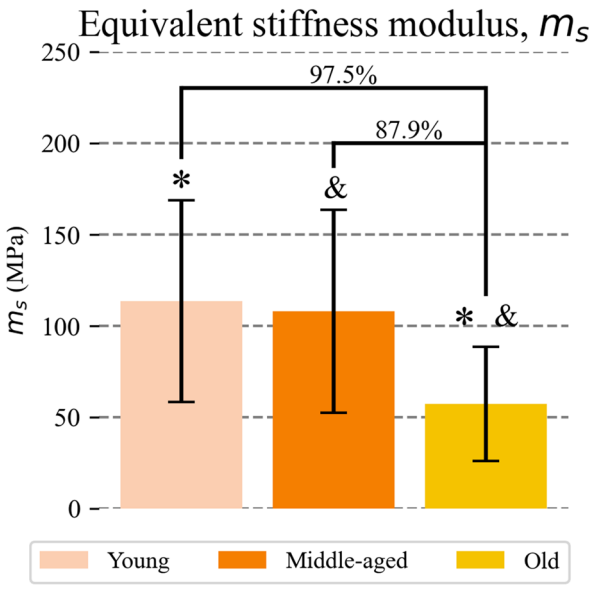

Figure 4.13. Mean and SD of tissue equivalent stiffness modulus of the meniscal horns for each age group. For the groups with significant differences, the percentage difference between means with respect to the oldest group is indicated. Significant difference: *Young vs. Old; & Middle-aged vs. Old.

Table 4.11. Tissue equivalent stiffness modulus (MPa) for each age group

	Young	**Middle-aged**	**Old**
Mean	113.56*	108.01&	57.48*&
SD	55.04	55.56	31.27

Significant difference: *Young vs. Old; & Middle-aged vs. Old

Figure 4.14 and Table 4.12 list the mean and SD values of m for the groups formed by splitting lateral and medial menisci. When examining the effects of age independently for both location similar trends as for the global groups emerged, especially at the lateral compartment. For these lateral groups, a significant overall difference was found ($p = 0.005$). Subsequently, m for the older group was 104.6% lower compared to the younger group ($p = 0.009$) and 122.2% lower compared to the middle-aged group ($p = 0.012$). There were no significant differences between the younger and middle-aged groups.

For medial menisci, an overall significant difference was also observed ($p = 0.008$). The older group equivalent stiffness modulus was 101.4% lower than that of the younger group ($p = 0.012$) and 66.8% lower than that of the middle-aged group but only a trend towards significance could be detected ($p = 0.060$). As for the gathered groups and for the groups of the lateral menisci, no significant differences were noted between the younger and middle-aged groups.

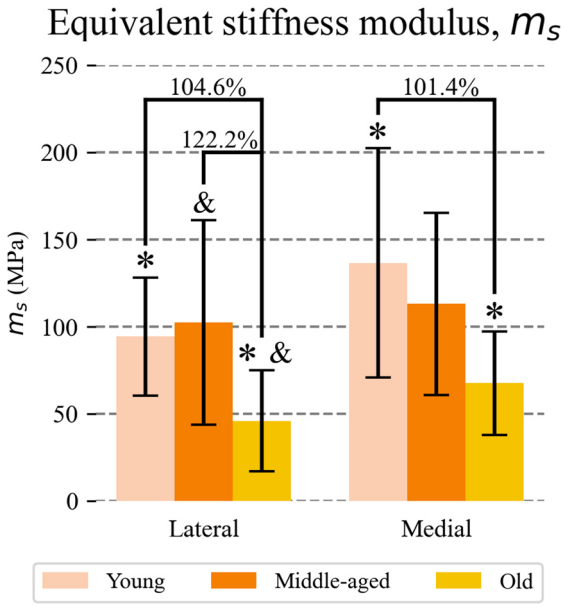

Figure 4.14. Mean and SD of tissue equivalent stiffness modulus of the lateral and medial meniscal horns for each age group. For the groups with significant differences, the percentage difference between means with respect to the oldest group is indicated. Significant difference: *Young vs. Old; & Middle-aged vs. Old.

Table 4.12. Tissue equivalent stiffness modulus (MPa) of the lateral and medial meniscal horns sites for each age group.

	Lateral meniscus			**Medial meniscus**		
	Young	**Middle-aged**	**Old**	**Young**	**Middle-aged**	**Old**
Mean	94.38*	102.47&	46.12*&	136.58*	113.09	67.80*
SD	33.70	58.59	28.98	65.80	52.11	29.66

Significant difference: *Young vs. Old; & Middle-aged vs. Old.

4.4 Discussion

The mechanical properties of sutured human meniscal horn subjected to traction from the suture in the immediate postoperative period and the impact of the age of the donor on these properties were investigated in this chapter. To analyze age-impact, the meniscal specimens were classified into three age groups: young (under 55 years old), middle-aged (55 to 75 years old), and old (over 75 years old). The in vitro experiments revealed that meniscal tissue from individuals over 75 years old exhibited greater elasticity and reduced resistance to cut-out at the suture site compared to younger specimens. Despite this, an age-related increase in meniscal thickness was observed, which mitigated differences in the maximum load the meniscal horn could withstand under suture traction.

The deformation behavior of meniscal tissue around the suture hole was effectively represented by a linear model within the strain range of [0-0.3], which was located prior to cut-out initiation. Therefore, the slope of this linear fit of the traction-strain curve, the tissue equivalent stiffness modulus, resulted in a suitable parameter to characterized linear deformation. The analysis of the value of m for the age groups revealed that meniscal tissue from individuals over 75 years old was significantly more elastic compared to that from younger individuals. The difference in elasticity was pronounced between the oldest group and the younger groups, with elasticity being 87.9% in the group under 55 years old and 97.5% higher in the group between 55 and 75 years old. However, no significant differences in elasticity were observed between the two younger age groups.

Regarding the meniscal horn capacity to withstand suture traction at tissue level, older meniscal tissue exhibited reduced cut-out resistance, measured as the stress needed to initiate tearing. This decrease was evident when comparing the oldest group to the younger groups. Despite this reduction in tissue resistance, there was no corresponding decrease in cut-out resistance at specimen level, as assessed by the maximum force the meniscal horn could withstand in the load-to-failure test. This lack of difference in maximum force can be attributed to the observed thickening of the meniscal horns with age, which results in an increased resistant area. Although the tissue itself becomes less resistant with age (Figure 4.10, Table 4.9), the increased thickness, i.e. the increased resistant area, compensates for this decline, leading to no detectable difference in resistance at the specimen level, as represented by the maximum pulling force before tearing occurred (Figure 4.6, Table 4.5) and the ultimate force (Figure 4.8, Table 4.7).

When examining the lateral and medial menisci separately, the results were less conclusive, likely due to reduced statistical power, as the sample sizes were originally statistical estimated without considering these anatomical distinctions.

Regarding deformation at the suture site, the older age group exhibited greater elasticity at both anatomical sites, aligning with the trends observed in the study without discerning between anatomical sites.

Regarding resistance at tissue and specimen levels, outcomes were ambiguous, preventing us from drawing solid conclusions. On one hand, for the lateral menisci, no age-related effects were observed in terms of tissue resistance, ultimate force, or cut-out force. However, a notable thickening in the old group compared to the young group was identified. On the other hand, for the medial menisci, a decline in tissue cut-out resistance was evident in the older group compared to the younger groups. Additionally, age did not appear to influence thickening.

Despite both observations, no significant differences could be detected across age groups at specimen level, i.e., for the meniscal cut-out force or ultimate force.

The alterations in biomechanical properties of the meniscal tissue with age are likely due to a combination of histological and biochemical changes. Our study provides an initial insight into how aging impacts the performance of sutured menisci. Once significant differences in tissue resistance and elasticity have been identified, subsequent research should focus on uncovering the specific factors driving these changes. This deeper understanding will help elucidate the mechanisms behind the age-related variations observed in meniscal function.

In biomechanical studies, sutured meniscal models are often employed to evaluate the effectiveness of surgical repair techniques and devices under laboratory conditions. These studies typically assess the repair ability to withstand loads induced by suture traction (Anz et al., 2014; Mitchell et al., 2016) and the displacements caused by such loads (Vertullo et al., 2021). These analyses are essential to ensure that repairs remain within clinically acceptable limits and to identify the methods that best replicate the natural biomechanics of the meniscus. The results of this study suggest establishing recommendations to limit the acceptable age for in-vitro meniscal assays, as those mentioned above. Specifically, it is suggested to restrict the age of donors to below 75 years for in vitro tests if the results are meant to apply to patients younger than 75. Similarly, if the study's results are to be relevant for patients older than 75 years, the menisci should come from donors in that age group.

The results of this study lead us to expect a notable increase in displacements before the onset of tearing for patients over 75 years old, which may jeopardize the success of surgical repairs. Displacements exceeding 5 mm following meniscal root reinsertion can adversely affect knee biomechanics (Prado-Novoa et al., 2020; Sekaran et al., 2002). However, our findings did not indicate a reduction in the traction resistance of the sutured meniscal horns for this age group. The diminished strength of the tissue in older menisci seems to be balanced by an increase in the thickness of the meniscal horns

This shift in meniscal anatomy has been indirectly suggested in earlier studies (Seitz et al., 2021), where researchers differentiated between mildly and severely degenerated menisci, conditions that the study also correlated with the donor's age.

From a clinical perspective, the outcomes presented in this chapter indicate that there is no contraindication for extending meniscal repairs with sutures to patients up to 75 years old. However, it is important to note that this conclusion

is based solely on mechanical properties observed in vitro and does not consider biological factors that could enhance the healing process in younger patients or other clinical variables not addressed herein.

The study also assessed whether aging affects the mechanical properties of the lateral or medial meniscus differently. The results indicated that age-related increased elasticity at the sutured area was consistent across both compartments, with significant percentage differences between the age groups. A decrease in tissue resistance was noted, but it was only statistically significant in the medial meniscus. No other significant differences were observed, likely due to the study's limited power for this specific analysis. These findings suggest that further research focusing on the impact of age on each meniscal root would be valuable.

Previous studies have looked at the cut-out resistance to suture traction of meniscal horns, but they mainly focused on comparing different suturing techniques or devices for root reattachment, without considering the impact of aging. Anz et al. (Anz et al., 2014) conducted a load-to-failure test on human menisci from donors aged 46-64 years, pulling from the sutured posterior horn with two simple stitches using a No. 2 surgical suture of UHMWPE. They identified the initial peak on the load-displacement curve as the point of structural integrity loss or cut-out initiation. Although testing protocols differed, their reported mean initial peak force of 137±49 N for two stitches is consistent with our findings for the middle-aged group, where we observed a mean F_c of 62.3±16 N with a single stitch. Vertullo et al. (Vertullo et al., 2021) reported an ultimate load of 94.29±7.99 N for posterior medial menisci from donors with a mean age of 54±4 years, using two simple No. 2 sutures. This result aligns with our findings, especially considering that their samples were subjected to 1,000 cycles of loading between 5 N and 20 N before the ultimate load test, and the use of two stitches, which often introduces asymmetries in traction distribution, complicating predictions of ultimate load. Mitchell et al. (Mitchell et al., 2016) found a mean ultimate force of 58.2±29.6 N when testing posterior horns of human medial menisci from donors aged 48 to 88 years, sutured with one simple stitch. Their values are lower than our F_u results, likely because they used a No. 0 surgical suture of UHMWPE, which has a smaller diameter that results in a 42.9% thinner nominal resistant area than the sutures used in our study.

The statement that meniscal stiffness increases with age has been suggested by some authors (Sarbacher and Halper, 2019; Tsujii et al., 2017) based on research on other soft tissues. Specifically, it was reported that advanced glycation end-products (AGEs) can make tendons stiffer with age. Since AGEs accumulate in the meniscus as well, it was hypothesized that meniscal stiffness might also rise

with age (Sarbacher and Halper, 2019; Tsujii et al., 2017). However, the findings of our study, conducted specifically on meniscal tissues contradict the hypothesis. We are not aware of any other studies that have calculated the equivalent stiffness modulus of sutured meniscus tissue under traction, or a similar parameter. Most biomechanical works have focused on the stiffness of the suture-meniscus construct rather than the meniscal tissue itself and therefore are strongly influenced by the rigidity of the sutures. Moreover, significant variability can be observed between published studies that reported the elasticity of the meniscus-suture set, even when examining the same repair technique (Mitchell et al., 2016; Vertullo et al., 2021), which complicates direct comparisons with our results. The wide dispersion in these studies can be attributed to factors unrelated to the meniscal tissue, such as the free lengths of suture threads, which are not always reported, and the different history of cyclic loading prior to load-to-failure tests. The later would influence the elasticity of surgical sutures if the resting period is insufficient (Prado-Novoa et al., 2022). Thus, our study provides a unique perspective on the elasticity of meniscal tissue itself, isolated from these confounding factors.

In this in vitro investigation, it was chosen to use manually operated mechanical grippers for securing the meniscus and suture to the testing machine, aligning with practices observed in previous studies (Anz et al., 2014; Cerminara et al., 2014; Feucht et al., 2013; Mitchell et al., 2016; Perez-Blanca et al., 2018; Prado-Novoa et al., 2020; Vertullo et al., 2021; Zantop et al., 2004). This method was preferred over pneumatic clamps (Massey et al., 2019) due to its ability to easily apply gradual and controlled gripping forces, which minimizes the risk of damage to the meniscal tissue during clamping. To verify the effectiveness of the clamping and to ensure that no slippage occurred, we placed marks along the meniscus and suture at their points of contact with the grippers. These marks were monitored through our videogrammetric system, as described in Sections 4.2.2 and 4.2.3, to detect any displacement or inaccuracies.

Similar limitations as expressed in Chapter 3 are inherent to this type of in vitro studies and are relevant to this research. The study lacks the absence of natural healing effects over time, therefore only the immediate postoperative period can be examined. While the primary focus of this study was to assess the impact of age on the effectiveness of meniscal root repairs and the suitability of different age models for in vitro evaluations, we only tested isolated meniscus-suture constructs. This approach excluded the influence of surrounding tissues such as ligaments, cartilage, and bone, which play crucial roles in the meniscus biomechanical performance. This isolated setup was chosen to concentrate on the tissue-suture interface, an approach commonly followed in similar studies (Anz et

al., 2014; Mitchell et al., 2016; Perez-Blanca et al., 2018; Vertullo et al., 2021), deliberately excluding tibial fixation factors.

In alignment with previous studies, we oriented the suture in the loading direction to eliminate shear friction and focus solely on the tensile forces at the meniscus-suture interface. This alignment, while not reflecting any specific anatomical scenario, allowed us to concentrate on the interface behavior, which was the primary aim of our investigation.

We used a single simple suture for its advantages in force calculation. Although not the most common surgical choice (Anz et al., 2014; Mitchell et al., 2016; Perez-Blanca et al., 2018; Vertullo et al., 2021), a single suture facilitates force measurement and stress calculation at the meniscus-suture interface, avoiding complications from multiple sutures that could affect uniform load distribution.

The load-to-failure test was conducted at a rate of 0.1 mm/s, representing a quasi-static displacement, which is slower than typical knee movement speeds (Prado-Novoa et al., 2022). This choice was made to minimize the influence of potential viscous effects, although the viscoelastic behavior of the meniscus in compression (De Rosa et al., 2022b; Morejon et al., 2022; Norberg et al., 2021) suggests that further research is needed to fully understand the dynamic response of sutured meniscal tissue.

To accurately identify cut-out initiation, we employed two methods: an automated detection method validated by Perez-Blanca et al. (Perez-Blanca, 2019) and subsequent verification through video analysis. Our findings confirmed that tear initiation occurred at a load slightly below the first local peak of the load-deformation curve, consistent with previous reports (Perez-Blanca, 2019).

4.5 Conclusions

In this in vitro study, the mechanical properties of the human sutured meniscal horn subjected to traction in the fiber direction and the impact of age on these properties were assessed. From the study findings it can be concluded that:

- Mechanical properties related to deformation and resistance at tissue and specimen levels of repaired human meniscal horns subjected to suture traction, are computed and categorized into three donor age groups: young (under 55 years), middle-aged (55 to 77 years), and older (over 75 years)

- At tissue level, meniscal horns from individuals over 75 years old exhibited greater elasticity and lower tissue resistance to cut-out at the suture hole compared to younger specimens.

- Aging also leads to a thickening of the meniscal horns.

- The increase in thickness mitigates the differences in resistance at specimen level, which vanish for specimens older than 75 years of age when the specimen resistance is evaluated in terms of force required to initiate a tear or the maximum force withstood by the specimen during a load-to-failure test.

4.6 References

Anz, A.W., Branch, E.A., Saliman, J.D., 2014. Biomechanical Comparison of Arthroscopic Repair Constructs for Meniscal Root Tears. Am J Sports Med 42 (11), 2699–2706. https://doi.org/10.1177/0363546514549445

Cerminara, A.J., LaPrade, C.M., Smith, S.D., Ellman, M.B., Wijdicks, C.A., LaPrade, R.F., 2014. Biomechanical Evaluation of a Transtibial Pull-out Meniscal Root Repair Challenging the Bungee Effect. American Journal of Sports Medicine 42, 2988–2995. https://doi.org/10.1177/0363546514549447

Chia, H.N., Hull, M.L., 2008. Compressive moduli of the human medial meniscus in the axial and radial directions at equilibrium and at a physiological strain rate. Journal of Orthopaedic Research 26, 951–956. https://doi.org/10.1002/JOR.20573

De Rosa, M., Filippone, G., Best, T.M., Jackson, A.R., Travascio, F., 2022. Mechanical properties of meniscal circumferential fibers using an inverse finite element analysis approach. J Mech Behav Biomed Mater 126, 105073. https://doi.org/10.1016/J.JMBBM.2022.105073

Faul, F., Erdfelder, E., Lang, A.G., Buchner, A., 2007. G*Power 3: a flexible statistical power analysis program for the social, behavioral, and biomedical sciences. Behav Res Methods 39, 175–191. https://doi.org/10.3758/BF03193146

Feucht, M.J., Grande, E., Brunhuber, J., Burgkart, R., Imhoff, A.B., Md, §, Braun, S., 2013. Biomechanical Evaluation of Different Suture Techniques for Arthroscopic Transtibial Pull-out Repair of Posterior Medial Meniscus Root Tears. Am J Sports Med 41, 2784–2790. https://doi.org/10.1177/0363546513502464

Jones, A.O., Houang, M.T.W., Low, R.S., Wood, D.G., 2006. Medial meniscus posterior root attachment injury and degeneration: MRI findings. Australas Radiol 50, 306–313. https://doi.org/10.1111/J.1440-1673.2006.01586.X

Kim, Y.M., Rhee, K.J., Lee, J.K., Hwang, D.S., Yang, J.Y., Kim, S.J., 2006. Arthroscopic pullout repair of a complete radial tear of the tibial attachment site of the medial meniscus posterior horn. Arthroscopy 22, 795.e1-795.e4. https://doi.org/10.1016/J.ARTHRO.2005.12.040

Massey, P., McClary, K., Parker, D., Barton, R.S., Solitro, G., 2019. The rebar repair for radial meniscus tears: a biomechanical comparison of a reinforced suture repair versus parallel and cross-stitch techniques. J Exp Orthop 6. https://doi.org/10.1186/S40634-019-0206-4

Mitchell, R., Pitts, R., Kim, Y.M., Matava, M.J., 2016. Medial Meniscal Root Avulsion: A Biomechanical Comparison of 4 Different Repair Constructs. Arthroscopy: The Journal of Arthroscopic & Related Surgery 32, 111–119. https://doi.org/10.1016/J.ARTHRO.2015.07.013

Moon, H.-K., Koh, Y.-G., Kim, Y.-C., Park, Y.-S., Jo, S.-B., Kwon, S.-K., 2010. Prognostic Factors of Arthroscopic Pull-out Repair for a Posterior Root Tear of the Medial Meniscus. Am J Sports Med 40(5), 1138–1143. https://doi.org/10.1177/0363546511435622

Morejon, A., Mantero, A.M.A., Best, T.M., Jackson, A.R., Travascio, F., 2022. Mechanisms of energy dissipation and relationship with tissue composition in human meniscus. Osteoarthritis Cartilage 30, 605–612. https://doi.org/10.1016/J.JOCA.2022.01.001

Norberg, C., Filippone, G., Andreopoulos, F., Best, T.M., Baraga, M., Jackson, A.R., Travascio, F., 2021. Viscoelastic and equilibrium shear properties of human meniscus: Relationships with tissue structure and composition. J Biomech 120. https://doi.org/10.1016/J.JBIOMECH.2021.110343

Ode, G.E., Van Thiel, G.S., McArthur, S.A., Dishkin-Paset, J., Leurgans, S.E., Shewman, E.F., Wang, V.M., Cole, B.J., 2012. Effects of serial sectioning and repair of radial tears in the lateral meniscus. American Journal of Sports Medicine 40, 1863–1870. https://doi.org/10.1177/0363546512453291

Pauli, C., Grogan, S., Patil, S., Otsuki, S., Hasegawa, A., Koziol, J., Lotz, M., D'Lima, D.D., 2011. Macroscopic and histopathologic analysis of human knee menisci in aging and osteoarthritis. Osteoarthritis Cartilage 19, 1132–1141.

Perez-Blanca, A., 2019. Biomecánica de la Reinserción Transtibial de la raíz Posterior del Menisco Lateral de la Rodilla: Avances en la Técnica de Reparación No Title (PhD Thesis,). University of Malaga.

Perez-Blanca, A., Espejo-Baena, A., Amat Trujillo, D., Prado Nóvoa, M., Espejo-Reina, A., Quintero López, C., Ezquerro Juanco, F., 2016. Comparative Biomechanical Study on Contact Alterations After Lateral Meniscus Posterior Root Avulsion, Transosseous Reinsertion, and Total Meniscectomy. Arthroscopy: The Journal of Arthroscopic & Related Surgery 32, 624–633. https://doi.org/10.1016/j.arthro.2015.08.040

Perez-Blanca, A., Prado Nóvoa, M., Lombardo Torre, M., Espejo-Reina, A., Ezquerro Juanco, F., Espejo-Baena, A., 2018. The role of suture cutout in the failure of meniscal root repair during the early post-operative period: a biomechanical study. Int Orthop 42, 811–818. https://doi.org/10.1007/S00264-018-3799-9/FIGURES/5

Prado-Novoa, M., Perez-Blanca, A., Espejo-Reina, A., Espejo-Reina, M.J., Espejo-Baena, A., 2020. Initial Biomechanical Properties of Transtibial Meniscal Root Repair are Improved By Using a Knotless Anchor as a Post-Insertion Tensioning Device. Sci. Rep. 10. https://doi.org/10.1038/S41598-020-58656-6

Prado-Novoa, M., Perez-Sanchez, L., Estebanez, B., Moreno-Vegas, S., Perez-Blanca, A., 2022. Influence of Loading Conditions on the Mechanical Performance of Multifilament Coreless UHMWPE Sutures Used in Orthopaedic Surgery. Materials 2022, Vol. 15, Page 2573 15, 2573. https://doi.org/10.3390/MA15072573

Sarbacher, C.A., Halper, J.T., 2019. Connective tissue and age-related diseases. Subcell Biochem 91, 281–310. https://doi.org/10.1007/978-981-13-3681-2_11/COVER

Seitz, A.M., Osthaus, F., Schwer, J., Warnecke, D., Faschingbauer, M., Sgroi, M., Ignatius, A., Dürselen, L., 2021. Osteoarthritis-Related Degeneration Alters the Biomechanical Properties of Human Menisci Before the Articular Cartilage. Front Bioeng Biotechnol 9. https://doi.org/10.3389/FBIOE.2021.659989/FULL

Sekaran, S.V., Hull, M.L., Howell, S.M., 2002. Nonanatomic location of the posterior horn of a medial meniscal autograft implanted in a cadaveric knee adversely affects the pressure distribution on the tibial plateau. American Journal of Sports Medicine 30, 74–82. https://doi.org/10.1177/03635465020300012601/ASSET/IMAGES/LARGE/10.1177_03635465020300012601-FIG4.JPEG

Steineman, B.D., LaPrade, R.F., Haut Donahue, T.L., 2020. Nonanatomic placement of posteromedial meniscal root repairs: A finite element study. J Biomech Eng 142. https://doi.org/10.1115/1.4045893/1072350

Tsujii, A., Nakamura, N., Horibe, S., 2017. Age-related changes in the knee meniscus. Knee 24, 1262–1270. https://doi.org/10.1016/J.KNEE.2017.08.001

Vertullo, C.J., Cadman, J., Dabirrahmani, D., Appleyard, R., 2021. Biomechanical Comparison of an All-Inside Meniscal Repair Device Construct Versus Pullout Sutures for Arthroscopic Transtibial Repair of Posterior Medial Meniscus Root Tears A Matched-Pair Cadaveric Study. Orthop J Sports Med 9(4), 23259671211000464. https://doi.org/10.1177/23259671211000464

Yan, S.H., Ou-Yang, H.K., Shan, Y.L., Luo, D.Z., Wang, H., Zhang, K., 2016. Tensile biomechanical characteristics of human meniscus. Emerging Materials Research 5, 44–49. https://doi.org/10.1680/jemmr.15.00031

Zantop, T., Eggers, A.K., Weimann, A., Hassenpflug, J., Petersen, W., 2004. Initial Fixation Strength of Flexible All-Inside Meniscus Suture Anchors in Comparison to Conventional Suture Technique and Rigid Anchors Biomechanical Evaluation of New Meniscus Refixation Systems and the. https://doi.org/10.1177/0363546503260749

5

Evaluating porcine and older human models as surrogates for studying resistance and deformation in young human sutured meniscal horns

This chapter is the culmination of Chapters 3 and 4, completing the fourth specific objective stated in Section 1.2. The mechanical properties of the sutured meniscal horn around the suture hole under circumferential tensile loads in aged human models, obtained in Chapter 4, and porcine models, obtained in Chapter 3, are compared with the results for young human models, also obtained in Chapter 4. The comparisons aim to analyse whether porcine models or older human models provide a better approximation to the mechanical behaviour of young human meniscal horns when assessing the deformation and strength at the suture hole area. Both surrogate models would allow the reduction of the economic cost and facilitate the procurement of specimens. The results of this work have been published in "Applied Sciences" (see Appendix E.2), a journal indexed in the 1st quartile of the JCR ranking for the year 2023 in its corresponding category.

5.1 Introduction

As discussed in Chapter 3, porcine models are commonly used in experimental research on menisci (Chung et al., 2018; Feucht et al., 2015, 2013; Fujii et al., 2017; Kim et al., 2016; Okimura et al., 2019; Perez-Blanca et al., 2018; Robinson et al., 2018; Seo et al., 2009; Stärke et al., 2010; Wu et al., 2018, 2020) due to their anatomical and physiological similarities to human menisci. These similarities include comparable structural characteristics, vascular patterns, volume, and weight, although porcine menisci have a greater width (Takroni et al., 2016). The kinematics of the porcine knee also closely mimics that of the human knee. Thus, porcine models are a cost-effective and practical option for biomechanical testing of human meniscal repair and replacement techniques, with

findings often being translatable to clinical settings (Deponti et al., 2015; Kyle Martin et al., 2016; Polito et al., 2020; Sweigart et al., 2004). Despite the broad use of porcine meniscal models, it is not fully established that all the biomechanical properties of porcine menisci match those of human menisci accurately enough (Camarda et al., 2019; Polito et al., 2020; Sweigart et al., 2004), prompting concerns about their use as human surrogate models and emphasizing the necessity of evaluating their applicability for each specific biomechanical parameters intended to be studied.

Other in-vitro studies opt for menisci from human donors (Anz et al., 2014; Espejo-Reina et al., 2023, 2022; Krych et al., 2018; Mitchell et al., 2016), even though the samples present higher variability due to differences among donors. A significant concern arises because meniscal root repair is primarily indicated for younger patients, although age thresholds increasing in most recent treatment guidelines (Kopf et al., 2020; Poland et al., 2019; Ventura et al., 2023). However, many in-vitro biomechanical studies do not restrict donor age, often including tissues from elderly donors, which are more readily available, particularly in developed countries where most research is concentrated. This mismatch may lead to results that do not accurately reflect the target population for these surgical interventions.

Computational modeling of meniscal tissue frequently employs data obtained from in-vitro testing of samples from various sources, including both animal models and human models which include samples from elderly donors. In particular, computational models have been used for refining and optimizing different suturing techniques for meniscal root repair, which demand a material model of the sutured meniscal horn. To achieve a proper tissue model, that accurately simulates the effects of suture thread traction at the repair site, extensive experimentation is required. However, the availability of suitable tissue samples remains a significant constraint, impacting the development and validation of these computational models.

The effectiveness of using porcine or aged cadaveric tissue for studying the repaired meniscal roots in adults within the recommended age range for repair is currently unverified. There is a lack of comparative research evaluating whether these models accurately replicate the behavior of young human meniscal tissue. This chapter aims to determine the appropriateness of the porcine and aged human models for in-vitro evaluation of meniscal root repairs, focusing on suture pull-out resistance and suture-induced displacements at the repair site.

We propose the following hypotheses regarding the mechanical performance of sutured meniscal horns in adults:

- Meniscal tissue from donors aged 75 years or older does not accurately reflect the biomechanical characteristics of younger meniscus.

- The porcine meniscus is a suitable surrogate for the human meniscus in patients at an age that is typically considered eligible for meniscal repair.

5.2 Materials and methods

The mechanical properties assessed in this chapter come from Chapter 3 for the porcine models. Regarding the mechanical properties of human menisci, and after verifying in Chapter 4 that no significant differences were found between the young (≤ 55 years) and middle-aged (56-75 years) groups in tissue resistance and deformation, and that clearly significant differences were found between these younger groups and the older group≥ (75 years), a new division has been made into two age groups: Human $<$ 75 years and Human ≥ 75 years.

Consequently, in this chapter, three distinct groups of isolated sutured menisci are studied: Human $<$ 75 years, Human ≥ 75 years, and Porcine. The group of Human $<$ 75 years served as the control, while the Human ≥ 75 years and Porcine groups were analyzed as possible surrogates for the control.

The characteristics of the three groups of study are summarized in Table 5.1.

Table 5.1. Main characteristics of the three meniscus groups tested.

	Human $<$ 75 Years	**Human ≥ 75 Years**	**Porcine**
Number of meniscal horn samples	44	22	22
Number of donors	24 knees 24 donors (4 menisci excluded)	14 knees 14 donors(6 menisci excluded)	11 knees 11 donors
Age: mean (SD)	51.00 (13.56) years	85.63 (4.51) years	6-month
Age: range	28- 67 years	82-95 years	6-month
Male/female	26/18	10/12	22/0
Medial/Lateral site	22/22	11/11	11/11
Anterior/posterior horn	22/22	10/12	10/12

The parameters described in Section 3.2.3 of Chapter 3 and Section 4.2.3 of Chapter 4 are the interest measures considered in this study. Specifically, this chapter focuses on two parameters at specimen level and two properties at tissue

level calculated from a load-to-failure test performed in pulling in the direction of the circumferential fibers of the horn, namely:

- The meniscal thickness, h, as the measurement obtained by a digital caliper (model 500-182-30, Mitutoyo, Japan) in the direction normal to the meniscal axial plane at the position of the suture hole.

- The meniscal cut-out force, F_c, as the force that initiated this meniscal tear for each specimen.

- The ultimate force, F_u, as the maximum force borne by the specimen in the load-to-failure test.

- The tissue cut-out resistance of the meniscal horn, S_c, computed with Equation 3.1.

- The equivalent stiffness modulus in the traction direction of the suture, m_s, as the slope of the linear approximation of the stress-strain curve, $\sigma - \varepsilon$, in the range of $\varepsilon = [0 - 0.3]$, where the engineering stress in the traction direction at the meniscus-suture interface was computed using Equation 3.2 and the strain was calculated with Equation 3.3.

5.2.1 Statistical analyses

Sample size calculations for this study were conducted using G*Power 3.1.9.7 software (Faul et al., 2007). The goal was to detect a minimum difference of 15 N between the older human group and the younger human control group, employing a t-test with a significance level, α, of 0.05 and a desired power of 0.80, with an allocation ratio of $N/Nc = 0.5$. This calculation determined that at least 41 specimens were needed for the control group. The 15 N difference represents 25% of the estimated 60 N cut-out force, F_c, for the younger human group, based on the research done in Chapters 3 and 4. This threshold was deemed sufficiently large to assess whether the experimental models, Human $\geq$ 75 years and Porcine groups, were adequately representative compared to the control group, Human $<$ 75 years. To accommodate potential specimen exclusions and maintain statistical robustness, the final sample sizes were set at 44 for the control group and 22 for each experimental group.

Statistical analyses were performed using IBM® SPSS® Statistics v.23 (IBM, Chicago, IL, USA). To evaluate variations in the mechanical properties at the suture site between the younger human control group and each experimental model group, non-parametric Kruskal-Wallis omnibus tests for independent samples were employed. Upon identifying significant differences, post hoc analyses

were conducted using pre-planned pairwise comparisons between each experimental model and the control group via Dunn-Bonferroni tests, with corrections made for multiple comparisons. The selection of non-parametric methods was necessitated by the failure of all samples to meet the assumptions of normality tests or homogeneity of variance tests. Statistical significance was set at $p \leq 0.05$.

5.3 Results

In this section, specimen and tissue level properties listed in section 5.2. are compared between the human control group (< 75 years) and each of the two possible surrogate models: aged human (≥ 75 years) and porcine.

5.3.1 Meniscal horn thickness at the suture point, *h*

At the suture site, menisci from older humans were significantly thicker than those from younger humans, showing an average increase of 24.7% ($p = 0.012$). In comparison, the porcine menisci were even thicker, with a mean increase of 83.8% relative to the control human menisci ($p < 0.001$) (Figure 5.1 and Table 5.2).

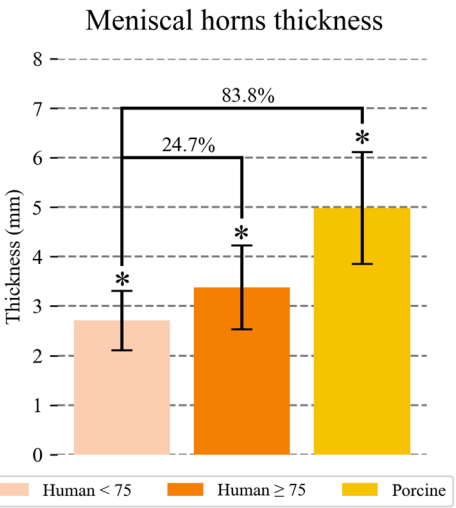

Figure 5.1. Mean and SD of the thickness (mm) of the meniscal horns at the suture hole area for each group. For the groups with significant differences with respect to the control group, the percentage difference between means is indicated. * Significant difference from the control group.

Table 5.2. Meniscus thickness (mm) of the meniscal horn at the sutured area.

	Human < 75 years	**Human ≥ 75 years**	**Porcine**
Mean	2.71	3.38*	4.98*
SD	0.60	0.83	1.13

* Significant difference from control group.

5.3.2 Meniscal cut-out force, F_c

When comparing to the younger human group, the resistance to cut-out initiation from suture traction, F_c, was significantly greater in the porcine group, with an increase of 172.1% respect to the control group ($p < 0.001$) (Figure 5.2 and Table 5.3). In contrast, no significant differences were observed between the younger and older human groups.

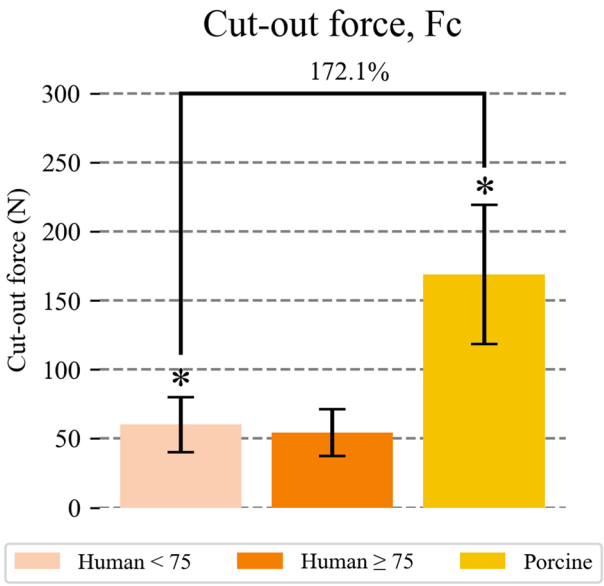

Figure 5.2. Mean and SD of cut-out force (N) of the meniscal horns. For the groups with significant differences, the percentage difference between means with respect to the control group is indicated. * Significant difference from the control group.

Table 5.3. Specimen cut-out force (N) of the meniscal horns.

	Human < 75 years	**Human ≥ 75 years**	**Porcine**
Mean	60.13	54.50	168.86*
SD	19.91	16.51	50.43

* Significant difference from the control group.

5.3.3 Meniscal ultimate force, F_u

The findings for the ultimate meniscal force mirrored those observed for the cut-out resistance, F_c (Figure 5.3 and Table 5.4). Specifically, the ultimate force in the older human group was no different to that of the younger group, with only a 6.1% difference in mean values. In contrast, the porcine model demonstrated a significantly greater ultimate force, showing a 174.1% increase compared to the younger human group ($p < 0.001$).

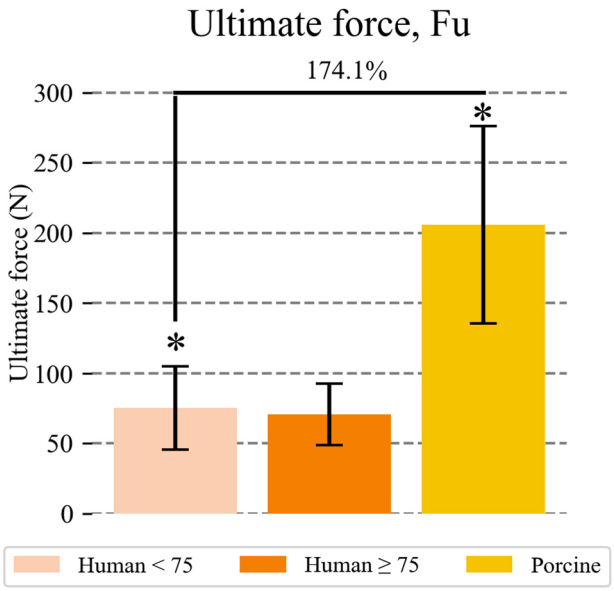

Figure 5.3. Mean and SD of ultimate force (N) of the meniscal horns. For the groups with significant differences, the percentage difference between means with respect to the control group is indicated. * Significant difference from the control group.

Table 5.4. Specimen ultimate force (N) of the meniscal horns.

	Human < 75 years	**Human ≥ 75 years**	**Porcine**
Mean	75.08	70.49	205.79*
SD	29.62	21.33	74.31

* Significant difference from control group.

For every group, the ultimate force, F_u, was consistently higher than the cut-out force, F_c. In the younger human group, F_u was 24.9% greater than F_c; in the older human group, it was 29.3% greater; and in the porcine model, it was 21.9% higher.

5.3.4 Tissue cut-out resistance, S_c

When comparing the human meniscus groups at the tissue level, the older human specimens exhibited lower tissue resistance to cut-out, with an S_c value that was 28.7% lower than that of the younger human group ($p = 0.012$). Conversely, the porcine meniscus tissue demonstrated significantly higher resistance, requiring a mean stress value that was 57.2% greater to initiate tearing compared to the younger human tissue ($p < 0.001$) (Figure 5.4 and Table 5.5).

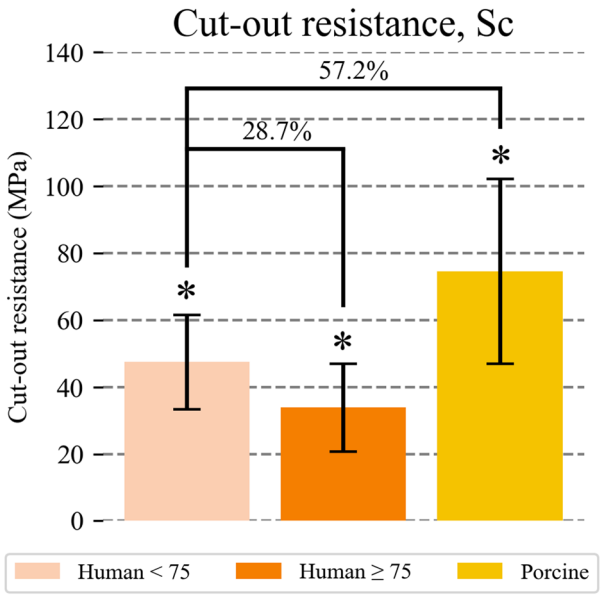

Figure 5.4. Mean and SD of tissue cut-out resistance (MPa) of the meniscal horns at the suture insertion point area. For the groups with significant differences, the percentage difference between means with respect to the control group is indicated. * Significant difference from the control group.

Table 5.5. Tissue cut-out resistance (MPa) of the meniscal horns at the suture insertion point area.

	Human < 75 years	**Human ≥ 75 years**	**Porcine**
Mean	47.40	33.81*	74.49*
SD	14.11	13.09	27.54

* Significant difference from control group.

5.3.5 Tissue equivalent stiffness modulus, m_s

All meniscal horns displayed highly linear behavior within the strain range [0-0.3], allowing for proper calculation of the equivalent stiffness modulus, m. The adjusted R-squared values for the linear fit consistently exceeded 0.91. Specifically, the R-squared values , fell between 0.91 and 0.99 for the human group younger than 75 years, between 0.92 and 0.99 In the older human group (≥75 years), and between 0.93 and 0.99 for the porcine model. Figure 5.5 presents a representative load-displacement and stress-strain curves for each group, along with the linear fits of the strain-stress curves for the strain interval [0, 0.3] and corresponding R-squared values

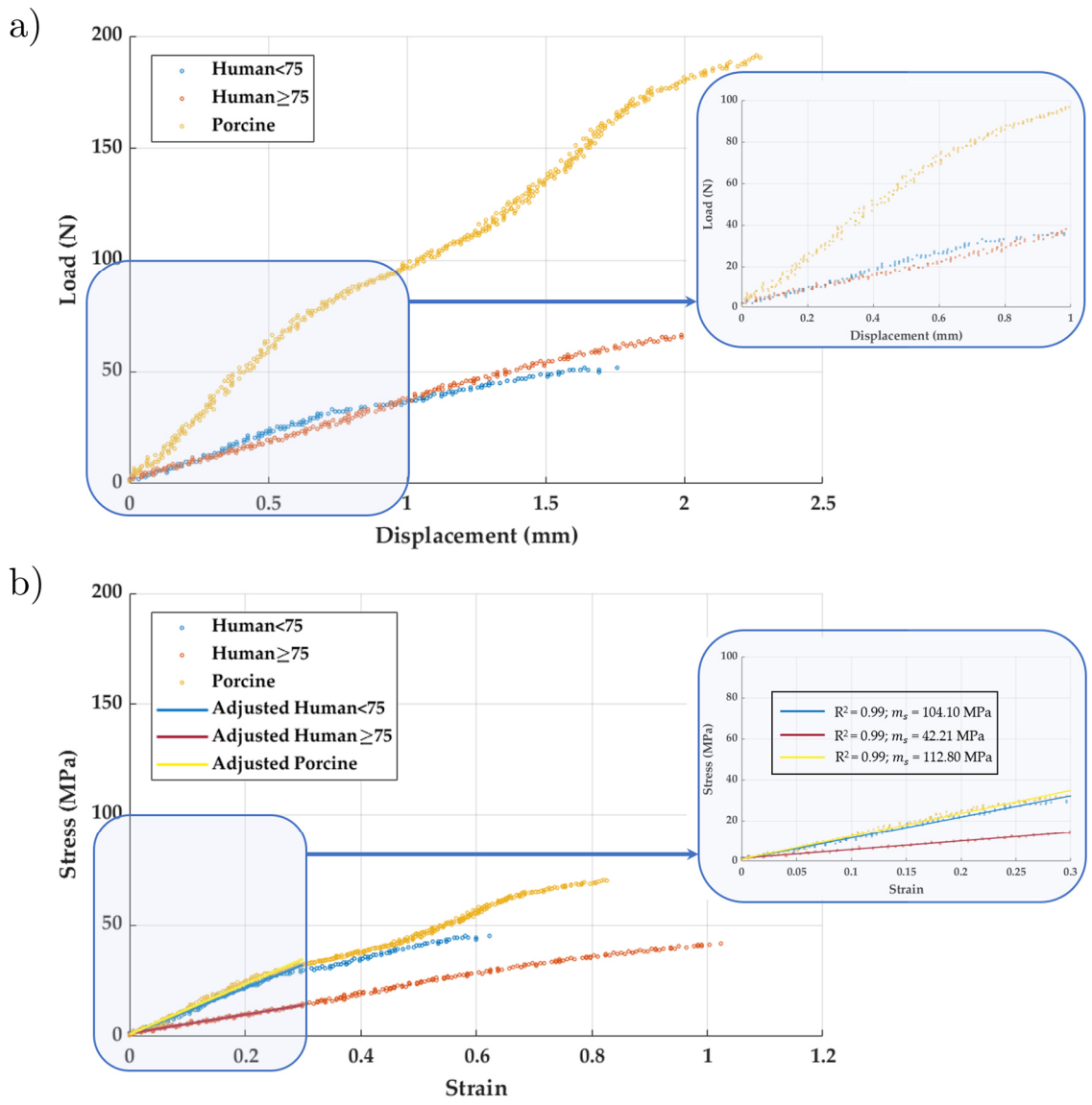

Figure 5.5. Curves of a representative sample of each group: a) Load-displacement curve for each group; b) Stress-strain curve for each group with a linear fit in the strain range [0-0.3].

Meniscal tissue from the older human group was significantly more elastic compared to the younger group, with a 48.1% higher mean stiffness modulus ($p < 0.001$). The elasticity of the porcine menisci was comparable to that of the younger human menisci, with a difference in stiffness modulus of less than 0.6% (Figure 5.6 and Table 5.6).

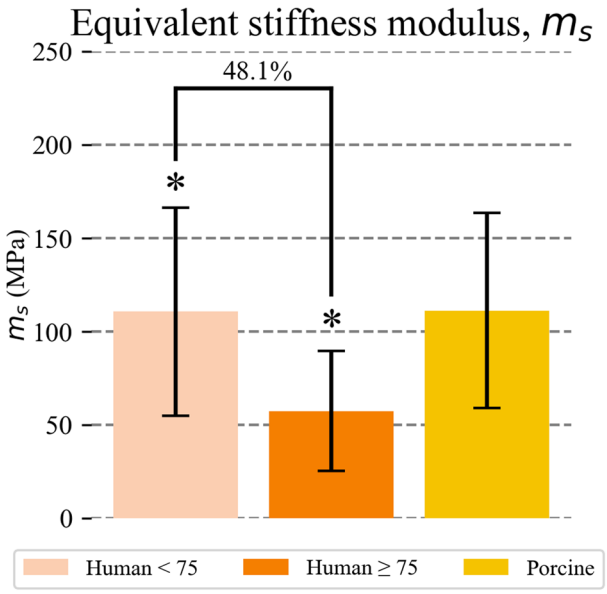

Figure 5.6. Mean and SD of tissue equivalent stiffness modulus (MPa) of the meniscal horns at the suture insertion point area. For the groups with significant differences, the percentage difference between means with respect to the control group is indicated. * Significant difference from control group.

Table 5.6. Tissue equivalent stiffness modulus (MPa) of the meniscal horns at the suture insertion point area.

	Human < 75 years	**Human ≥ 75 years**	**Porcine**
Mean	110.72	57.48*	111.34
SD	55.60	31.27	52.09

* Significant difference from control group.

5.4 Discussion

The main finding of this study is that neither the porcine model nor the human cadaveric tissue from donors older than 75 years accurately replicates all the mechanical properties of meniscal specimens from adults under 75 years. Although neither model provides a clear representation for general use in biomechanical in-vitro testing, each model has its strengths for examining specific aspects of the sutured meniscal horn.

In terms of resistance to suture-induced traction at the specimen level, no significant difference was observed between the older and younger human menisci, which partially contradicts our hypothesis that meniscal tissue from older donors (≥ 75 years) would not be representative of younger tissue. On the other hand, the porcine model showed significantly greater resistance at the specimen level

than the younger human model, with increases of 172.1% in cut-out force, F_c, and 174.1% in ultimate force, F_u, which is contrary to our second hypothesis.

Regarding tissue-level analysis, specifically concerning tissue cut-out resistance, S_c, at the meniscus-suture interface, both models differed notably from the younger human group. The porcine model exhibited a 57.2% higher cut-out stress compared to younger human menisci, while the older human menisci ($\geq$ 75 years) had a 28.7% lower resistance. This shows that porcine specimens are more resistant to suture-induced tearing, while menisci from older human donors are less resistant compared to their younger counterparts.

As for tissue deformation at the suture area, assessed in terms of the equivalent stiffness modulus, m_s, the porcine model was comparable to the younger human group as no significant difference could be detected despite a high number of samples in both groups (44 for human group and 22 for the more homogenous porcine group) exhibiting only a 5.1% difference between means. In contrast, the older human menisci ($\geq$ 75 years) demonstrated a 48.1% decrease in stiffness compared to the younger human group, indicating that older meniscal tissue is more elastic.

Consequently, the suitability of a meniscal model in an in-vitro biomechanical study depends on the specific focus of the study, partially contradicting our initial hypotheses that meniscal tissue from older donors ($\geq$ 75 years) does not adequately represent younger tissue ($<$ 75 years)and that the porcine meniscus is a good surrogate for the human meniscus typically eligible for repair.

For research on mechanical properties at the specimen level, particularly in analyzing the resistance of sutured meniscal roots, the older human meniscus model proved to be a preferable surrogate compared to the porcine model. Conversely, if the focus is on deformation issues before cut-out initiation in the sutured area, the porcine model offers a more accurate representation.

At the tissue level, neither model reliably represented the resistance properties of younger human menisci. However, for studies where only tissue deformation prior to cut-out initiation is of interest, the porcine model may be preferable. Nevertheless, caution is advised, as this model would not adequately characterize tissue stresses.

In summary, while neither model perfectly replicates the mechanical properties of younger human menisci, each has its strengths depending on the specific mechanical property under investigation. Researchers should choose the

model that best aligns with their study objectives, keeping in mind the limitations of each.

The differences found in the suitability of the surrogate models for studies evaluating meniscal root resistance at the specimen or tissue level may be partially attributed to the observed variations in thickness among the groups. The porcine model offers a surrogate for the human meniscus under 75 years old with a more resistant tissue, characterized by a higher cut-out stress, S_c, of 57.2%. This increased tissue resistance is further amplified at the specimen level due to the thicker roots of the porcine meniscus, leading to a significantly higher cut-out force, F_c, by 172.1% and ultimate force, F_u, by 174.1%. Conversely, for the older human meniscus, despite the tissue being less resistant than the younger human meniscus, with a 28.7% lower S_c, this reduction is offset at the specimen level. This offset is likely because the meniscal root of the older group was thicker than that of the younger group, vanishing the differences at the specimen level.

In summary, the thicker meniscal roots in both surrogate models lead to greater specimen level resistance, despite differing tissue level properties. This highlights the importance of considering both tissue and specimen-level characteristics when selecting surrogate models for biomechanical studies.

Historically, surgical repair of meniscal root avulsions has predominantly been performed in patients younger than 35–40 years of age. However, there has been a paradigm shift towards preserving the meniscus through repair techniques whenever possible. According to the 2019 consensus statement by the European Society for Sports Traumatology, Knee Surgery, and Arthroscopy (ESSKA) (Kopf et al., 2020), which reviewed data from studies on patients aged 9 to 58 years, it is now recommended that many meniscal tears previously deemed irreparable should be repaired, including those of older onset. This shift is further supported by recent follow-up studies demonstrating the positive outcomes of extending surgical interventions to patients over 60 years old (Husen et al., 2022; Ventura et al., 2023).

On the other hand, in Chapter 4 of this document no significant differences could be found between sutured human meniscal horns from donors younger than 55 years and meniscal horns from donors aged between 56 and 75 years in tissue resistance and deformation, while clear significant differences were found between these younger groups and sutured meniscal horns from donors over 75 years.

Given the evolution of clinical practice and the biomechanical findings of this thesis, the study on a proper surrogate model for in-vitro testing of meniscal horns at an age eligible for root repair, expanded the age range of the control group to

include patients up to 75 years old. This decision, from a clinical standpoint, is aligned with the criteria set by the orthopedic surgeons of the BIOCLINA group. It is considered that menisci from donors older than 75 years are representative of a group of patients generally deemed too advanced in age to be routinely considered for meniscal root repair surgery. This decision reflects the growing recognition of the benefits of meniscal repair in older populations and the practical considerations of current surgical practices.

5.5 Conclusions

The main findings of this study are:

- Neither porcine nor human menisci from donors over 75 years old serve as an accurate model for replicating the behavior of adult human meniscus under 75 years old in in-vitro biomechanical testing, representative of an age eligible for routine root repair.

- Each model offers advantages depending on the focus of the study: the older human meniscus is a more suitable surrogate for investigating the resistance of sutured meniscal root at specimen level, while the porcine model provides a more accurate representation of deformation-related properties around the suture site at the tissue level.

5.6 References

Anz, A.W., Branch, E.A., Saliman, J.D., 2014. Biomechanical Comparison of Arthroscopic Repair Constructs for Meniscal Root Tears. Am J Sports Med 42 (11), 2699–2706. https://doi.org/10.1177/0363546514549445

Camarda, L., Bologna, E., Pavan, D., Morello, F., Monachino, F., Giacco, F., Zingales, M., 2019. Posterior meniscal root repair: a biomechanical comparison between human and porcine menisci. Muscle Ligaments and Tendons Journal 9, 76–81. https://doi.org/10.32098/MLTJ.01.2019.03

Chung, K.S., Choi, C.H., Bae, T.S., Ha, J.K., Jun, D.J., Wang, J.H., Kim, J.G., 2018. Comparison of Tibiofemoral Contact Mechanics After Various Transtibial and All-Inside Fixation Techniques for Medial Meniscus Posterior Root Radial Tears in a Porcine Model. Arthroscopy - Journal of Arthroscopic and Related Surgery 34, 1060–1068. https://doi.org/10.1016/J.ARTHRO.2017.09.041

Deponti, D., Giancamillo, A. Di, Scotti, C., Peretti, G.M., Martin, I., 2015. Animal models for meniscus repair and regeneration. J Tissue Eng Regen Med 9, 512–527. https://doi.org/10.1002/TERM.1760

Espejo-Reina, A., Prado-Novoa, M., Espejo-Baena, A., Estebanez, B., Perez-Blanca, A., 2023. Improved tibiofemoral contact restoration after transtibial reinsertion of the anterior root of the lateral meniscus compared to in situ repair: a biomechanical study. Int Orthop 1, 3. https://doi.org/10.1007/s00264-023-05769-y

Espejo-Reina, A., Prado-Novoa, M., Espejo-Baena, A., Peña-Trabalon, A., Perez-Blanca, A., 2022. Biomechanical consequences of anterior root detachment of the lateral meniscus and its reinsertion. Sci Rep 12, 6182. https://doi.org/10.1038/S41598-022-10229-5

Faul, F., Erdfelder, E., Lang, A.G., Buchner, A., 2007. G*Power 3: a flexible statistical power analysis program for the social, behavioral, and biomedical sciences. Behav Res Methods 39, 175–191. https://doi.org/10.3758/BF03193146

Feucht, M.J., Grande, E., Brunhuber, J., Burgkart, R., Imhoff, A.B., Md, §, Braun, S., 2013. Biomechanical Evaluation of Different Suture Techniques for Arthroscopic Transtibial Pull-out Repair of Posterior Medial Meniscus Root Tears. Am J Sports Med 41, 2784–2790. https://doi.org/10.1177/0363546513502464

Feucht, M.J., Grande, E., Brunhuber, J., Rosenstiel, N., Burgkart, R., Imhoff, A.B., Braun, S., 2015. Biomechanical evaluation of different suture materials for arthroscopic transtibial pull-out repair of posterior meniscus root tears. Knee Surg Sports Traumatol Arthrosc 23, 132–139. https://doi.org/10.1007/S00167-013-2656-Z

Fujii, M., Furumatsu, T., Xue, H., Miyazawa, S., Kodama, Y., Hino, T., Kamatsuki, Y., Ozaki, T., 2017. Tensile strength of the pullout repair technique for the medial meniscus posterior root tear: a porcine study. Int Orthop 41, 2113–2118. https://doi.org/10.1007/S00264-017-3561-8

Husen, M., Kennedy, N.I., Till, S., Reinholz, A., Stuart, M.J., Krych, A.J., Saris, D.B., 2022. Benefits of Meniscal Repair in Selected Patients Aged 60 Years and Older. Orthop J Sports Med 10, 23259671221117492. https://doi.org/10.1177/23259671221117491

Kim, Y.M., Joo, Y.B., Noh, C.K., Park, I.Y., 2016. The optimal suture site for the repair of posterior horn root tears: Biomechanical evaluation of pullout strength in porcine menisci. Knee Surg Relat Res 28, 147–152. https://doi.org/10.5792/KSRR.2016.28.2.147

Kopf, S., Beaufils, P., Hirschmann, M.T., Rotigliano, N., Ollivier, M., Pereira, H., Verdonk, R., Darabos, N., Ntagiopoulos, P., Dejour, D., Seil, R., Becker, R., 2020. Management of traumatic meniscus tears: the 2019 ESSKA meniscus consensus. Knee Surg Sports Traumatol Arthrosc 28, 1177–1194. https://doi.org/10.1007/S00167-020-05847-3

Krych, A.J., Johnson, N.R., Wu, I.T., Smith, P.A., Stuart, M.J., 2018. A simple cinch is superior to a locking loop for meniscus root repair: a human biomechanical comparison of suture constructs in a transtibial pull-out model. Knee Surgery, Sports Traumatology, Arthroscopy 26, 2239–2244. https://doi.org/10.1007/S00167-017-4652-1

Kyle Martin, R., Gillis, D., Leiter, J., Shantz, J.S., MacDonald, P., 2016. A Porcine Knee Model Is Valid for Use in the Evaluation of Arthroscopic Skills: A Pilot Study. Clin Orthop Relat Res 474, 965–970. https://doi.org/10.1007/S11999-015-4498-0

Mitchell, R., Pitts, R., Kim, Y.M., Matava, M.J., 2016. Medial Meniscal Root Avulsion: A Biomechanical Comparison of 4 Different Repair Constructs. Arthroscopy: The Journal of Arthroscopic & Related Surgery 32, 111–119. https://doi.org/10.1016/J.ARTHRO.2015.07.013

Okimura, S., Mae, T., Tachibana, Y., Iuchi, R., Nakata, K., Yamashita, T., Shino, K., 2019. Biomechanical comparison of meniscus-suture constructs for pullout repair of medial meniscus posterior root tears. J Exp Orthop 6, 1–6. https://doi.org/10.1186/S40634-019-0186-4/TABLES/2

Perez-Blanca, A., Prado Nóvoa, M., Lombardo Torre, M., Espejo-Reina, A., Ezquerro Juanco, F., Espejo-Baena, A., 2018. The role of suture cutout in the failure of meniscal root repair during the early post-operative period: a biomechanical study. Int Orthop 42, 811–818. https://doi.org/10.1007/S00264-018-3799-9/FIGURES/5

Poland, S., Everhart, J.S., Kim, W., Axcell, K., Magnussen, R.A., Flanigan, D.C., 2019. Age of 40 Years or Older Does Not Affect Meniscal Repair Failure Risk at 5 Years. Arthroscopy: The Journal of Arthroscopic & Related Surgery 35, 1527–1532. https://doi.org/10.1016/J.ARTHRO.2018.11.061

Polito, U., Andreis, M., Di Giancamillo, A., Modina, S., Scurati, R., Marmotti, A., Michielon, G., Domenicucci, M., Lombardo, M., Di Giancamillo, M., Herrera, V., Mangiavini, L., Agnoletto, M., Brambilla, L., Peretti, G.M., 2020. Clinical anatomy of the meniscus in animal models: pros and cons. J Biol Regul Homeost Agents 34.

Robinson, J.R., Frank, E.G., Hunter, A.J., Jermin, P.J., Gill, H.S., 2018. The Strength of Transosseous Medial Meniscal Root Repair Using a Simple Suture Technique Is Dependent on Suture Material and Position. American Journal of Sports Medicine 46, 924–932. https://doi.org/10.1177/0363546517749807/ASSET/IMAGES/LARGE/10.1177_0363546517749807-FIG7.JPEG

Seo, J.H., Li, G., Shetty, G.M., Kim, J.H., Bae, J.H., Jo, M.L., Kim, J.S., Lee, S.J., Nha, K.W., 2009. Effect of Repair of Radial Tears at the Root of the Posterior Horn of the Medial Meniscus With the Pullout Suture Technique: A Biomechanical Study Using Porcine Knees. Arthroscopy: The Journal of Arthroscopic & Related Surgery 25, 1281–1287. https://doi.org/10.1016/J.ARTHRO.2009.05.014

Stärke, C., Kopf, S., Gröbel, K.H., Becker, R., 2010. The Effect of a Nonanatomic Repair of the Meniscal Horn Attachment on Meniscal Tension: A Biomechanical Study. Arthroscopy: The Journal of Arthroscopic & Related Surgery 26, 358–365. https://doi.org/10.1016/J.ARTHRO.2009.08.013

Sweigart, M.A., Zhu, C.F., Burt, D.M., Deholl, P.D., Agrawal, C.M., Clanton, T.O., Athanasiou, K.A., 2004. Intraspecies and interspecies comparison of the compressive properties of the medial meniscus. Ann Biomed Eng 32, 1569–1579. https://doi.org/10.1114/B:ABME.0000049040.70767.5C/METRICS

Takroni, T., Laouar, L., Adesida, A., Elliott, J.A.W., Jomha, N.M., 2016. Anatomical study: comparing the human, sheep and pig knee meniscus. J Exp Orthop 3, 1–13. https://doi.org/10.1186/S40634-016-0071-3/TABLES/4

Ventura, M., Seabra, P., Oliveira, J., Sousa, P., Quesado, M., Sousa, H., Pereira, R., Costa, A., Carvalho, P., 2023. Meniscal Injuries in Patients Aged 40 Years or Older: A Comparative Study Between Meniscal Repair and Partial Meniscectomy. Cureus 15. https://doi.org/10.7759/CUREUS.33270

Wu, J.L., Lee, C.H., Yang, C.T., Chang, C.M., Li, G., Cheng, C.K., Chen, C.H., Huang, H.S., Lai, Y.S., 2018. Novel technique for repairing posterior

medial meniscus root tears using porcine knees and biomechanical study. PLoS One 13, e0192027. https://doi.org/10.1371/JOURNAL.PONE.0192027

Wu, S.H., Yeh, T. Te, Hsu, W.C., Wu, A.T.H., Li, G., Chen, C.H., Lee, C.H., Wu, J.L., 2020. Biomechanical comparison of four tibial fixation techniques for meniscal root sutures in posterior medial meniscus root repair: A porcine study. J Orthop Translat 24, 144–149. https://doi.org/10.1016/J.JOT.2020.01.006

6

Analysis of compressive properties in sutured human meniscal horn tissue using unconfined indentation: Impact of physiological loads

At this point of this thesis, the properties that mechanically characterize the meniscal tissue around the suture hole of repaired human and porcine menisci subjected to tensile loads in the circumferential direction have been studied. However, physiologically the meniscal horn is subjected to a combination of tensile loads in the circumferential direction and compression in the axial direction. Therefore, this chapter focuses on the experimental characterization of the mechanical behavior of sutured human meniscal horns through indentation tests under two loading conditions: pure axial compression, and axial compression combined with circumferential traction loads. This chapter addresses the fifth specific objective declared in Section 1.2 with a twofold approach:

- To compute the compressive properties of sutured meniscal horn tissue around the suture area in a human model in the early postoperative period, under two loading conditions: pure axial compression, the standard testing method, and axial compression combined with circumferential traction, which represents the physiological stress state.

- To analyze the impact of the traction circumferential traction on the compressive properties of the tissue.

6.1 Introduction

As detailed described in Chapter 2, the menisci are firmly anchored to the tibial plateau via their anterior and posterior root attachments. In this way, axial compressive joint loads are transformed into circumferential tensile strains while radial extrusion of the meniscus is limited. Specifically, the meniscal horns are physiologically subjected to a combination of forces including axial compressive forces and circumferential tensile loads from the meniscal root attachments (Messner Karola and Gao, 1998). This biaxial loading state is characteristic of the meniscal horn area.

Following the description about menisci and testing methods detailed in Chapter 2, this chapter aims to address the twofold objectives:

- To investigate whether incorporating fiber-directional traction in indentations tests impacts on the compressive properties computed from the tests.

- To explore possible correlations between tensile and compressive properties of the meniscal horn.

The primary hypotheses of this chapter are that the compressive properties of the sutured meniscal horn computed from indentation tests are affected by the presence of circumferential tensile loading. Significant correlation exists between its tensile and compressive properties is proposed as a secondary hypothesis.

Experimental work in this chapter has been carried out at the Institute of Orthopaedic Research and Biomechanics of the University of Ulm in Germany under the direction of Dr. Andreas Martin Seitz. This work used its facilities and fresh human meniscus specimens, which were ethically sourced from patients undergoing total knee replacement surgery, adhering to all legal and ethical guidelines after receiving IRB approval (Ulm University No. 101/24).

6.2 Materials and methods

A non-destructive indentation tests at seven different points were conducted on sutured meniscal horn specimens, applying different levels of circumferential traction induced by the surgical suture. The tensile conditions included no load,

10 N, and 20 N. After these tests, a load-to-failure test was performed to establish the load-deformation curve of the sutured meniscus in the direction of the traction and assess correlation between the tensile and compressive properties.

6.2.1 Specimen preparation

To concentrate on the behavior of the meniscal tissue, as in the previous chapters, isolated cadaveric meniscus-suture constructs were tested. The study utilized 16 menisci from donors (mean age 65 ± 6 years; 10 women, 6 men) who had undergone total knee replacement. From these, 27 meniscal horns were selected based on the absence of significant macroscopic degeneration or injury. Immediately after extraction, the menisci were cryopreserved at -20ºC in sealed plastic bags submerged in saline solution. The day before testing, the specimens were thawed to room temperature while still in the saline solution.

During experimentation, each meniscus was cut into two halves to create two test samples. As in the Chapter 3 and 4, a No. 2 non-absorbable, braided, high-strength UHMWPE suture (Force Fiber® No. 2, Stryker Iberia, Madrid, Spain) was then inserted into the meniscal horn to simulate a meniscal root repair. This suture was positioned 5 mm from both the inner edge and the root junction of the meniscus (Figure 6.1), using a half circle tapered needle. As already justified in this document, this placement aimed to replicate the typical location of the surgical perforation during standard root repair procedures (Kim et al., 2006; Moon et al., 2010).

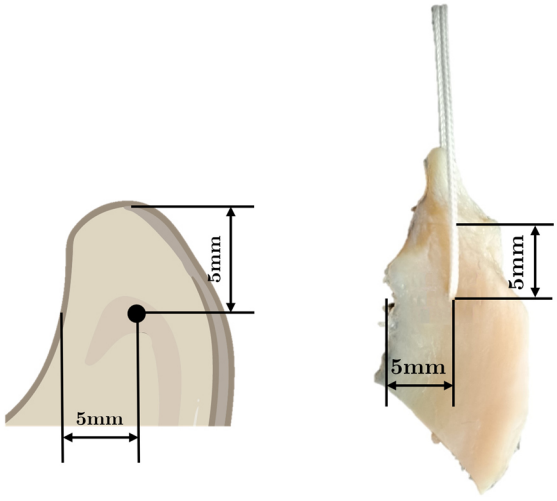

Figure 6.1. Sutured meniscal horn following the standard root repair procedure.

The following measures of the specimen were registered using an electronic caliper (model 500-182-30, Mitutoyo, Japan):

- The thickness at the puncture point, the inner edge, and the outer edge in a radial plane 1 mm from the orifice edge closest to the root and extending towards the cutting plane.

- The radial distance from the outer edge to the orifice and between both edges in the same plane.

- The distance between Point 1 and Point 2 marked on the cranial surface of the meniscal horn.

- The distance between Point 1 and the tip of the meniscal horn.

- The length of the sample in the circumferential direction.

The measures of all tested specimens are included in Appendix C.

6.2.2 Biomechanical testing

This section explains the two experimental tests conducted to determine the compressive and tensile properties of sutured human menisci.

6.2.2.1 Indentation test

The multiaxial mechanical tester (MACH-1 v500css, Biomomentum Inc., Laval, QC, Canada) exposed in Section 2.5 of Chapter 2 was equipped with a 2 mm diameter spherical indenter and was used to perform the non-destructive indentation tests of this chapter (Figure 6.2). Compressive forces were measured with a 70 N load cell (FTIFPS1, ATI, Michigan, USA), while the displacement was recorded by the machine servo-controller. A digital camera (MA732, Biomomentum Inc., Laval, QC, Canada) was positioned parallel to the base of the tester, where the specimen was mounted, to capture images. The camera was equipped with a CMOS sensor offering a resolution of 1280x1024 pixels, a focal length of 12.5 mm, and a minimum field of view of 7.1 mm (HF12.5HA-1B, Fujifilm, Tokyo, Japan).

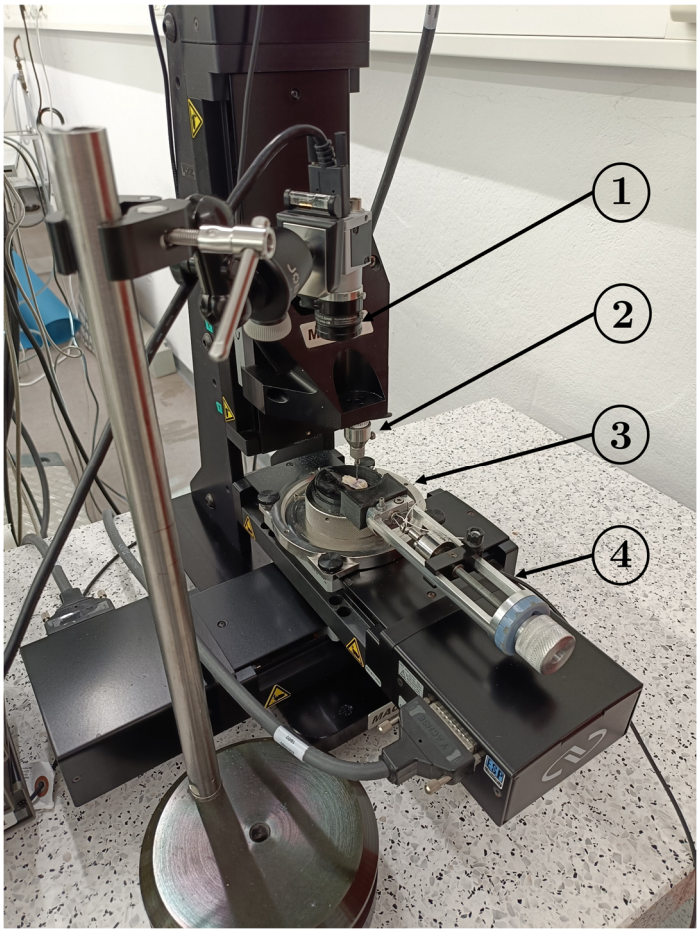

Figure 6.2. Multiaxial mechanical tester for indentation tests with the human samples: 1) digital camera; 2) load cell; 3) specimen container; 4) custom traction device.

A custom device (Figure 6.3) was designed and built to apply traction to the suture thread that was puncturing the meniscal horn and to record the tension applied. This device comprised an aluminum frame supporting a steel axis with a welded fastener at its tip. The surgical thread, after passing through the meniscal horn and the hole in the 3D printed container where the sample rests (described later in this section), was attached to the fastener tip, whose position could be manually adjusted along the steel axis, generating a tensile force in the suture that induces tensile stress in the meniscal horn puncture area. A 200 N load cell (U9C, HBM Spain, Madrid, Spain) installed in the steel axis measured the suture traction force. The main advantage of this traction device over other procedures is that the traction load applied to the suture is completely supported between the meniscal-suture construct and the custom device ,thus avoiding overloading the indentation machine, which has a very low capacity to support loads and moments on its axes.

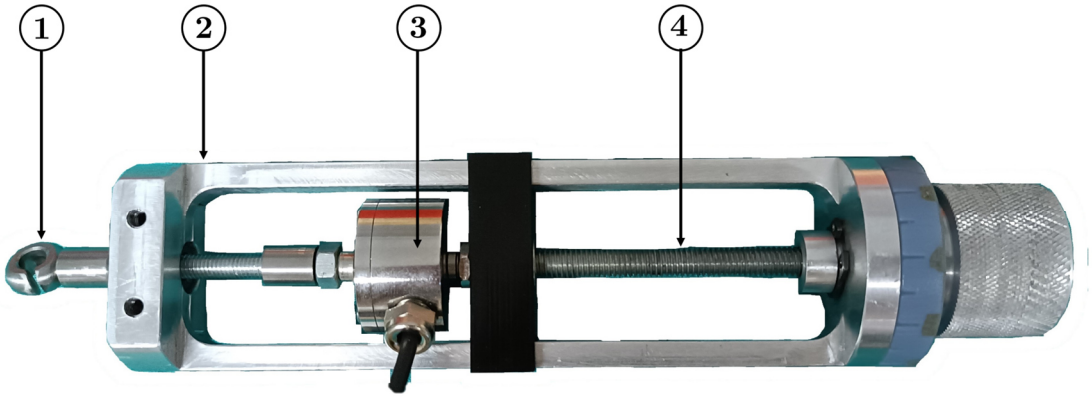

Figure 6.3. Custom-designed traction device: 1) fastener; 2) aluminum frame; 3) load cell; 3) steel axis.

The load cell was connected to a strain indicator and recorder (Model P3, MicroMeasurements, Wendell, North Carolina), which is a portable, battery-operated instrument with a wide variety of measurement applications as amplifier, strain indicator and digital data logger, capable of acquiring the output from the load cell and displaying the force value on an LCD screen (Figure 6.4). This device is comprised of four channels for reading values; however, only one channel was utilized in this instance, to which the load cell was connected. The strain recorder can be also interfaced with a computer, allowing for the direct saving and reading of force values on the computer via the software provided by MicroMeasurements (Model P3 Software, MicroMeasurements, Wendell, North Carolina).

Figure 6.4. Setup prepared for recording the traction force induced by the suture using the traction device while the indentation test: a) multiaxial mechanical tester with the traction device connected to the strain indicator and recorder; b) strain indicator and recorder connected to the computer.

A custom-designed 3D printed container (Figure 6.5) was utilized to position the sutured meniscal horn on the multiaxial tester. The container featured a ring mounted on a flat base, with the ring designed to hold the caudal surface of the meniscus at a 30º angle relative to the horizontal plane. This inclination was intended to counteract the natural slope of the meniscus, thereby achieving a more horizontal alignment of the cranial surface, which is optimal for indentation testing. The ring incorporated a through-hole aligned with the expected height of the meniscal root, facilitating the passage of the suture thread. Additionally, the traction device was affixed to the outer surface of the ring, ensuring that the metal shaft of the device, which houses the load cell, was precisely aligned with the ring bore. This setup ensured proper alignment and effective application of tensile forces during the testing process.

Each meniscal half was placed with its caudal surface resting on the base of the container, with the suture thread passing through the hole designed for this purpose. After manually tensioning the suture, the position of the meniscus was readjusted to correctly align its circumferential fibers in the direction in which the traction will be applied. Next, to securely fix the meniscus, adhesive was applied along the meniscal cutting plane and caudal surface, extending up to approximately 1 cm from the hole.

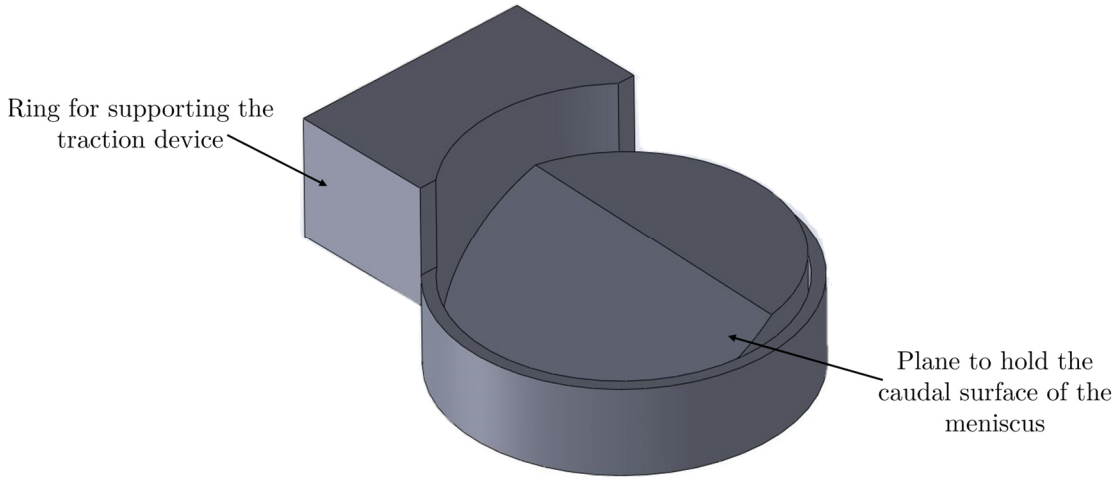

Figure 6.5. STL model of the custom-designed 3D printed container.

On the cranial surface of the meniscus, seven measurement points were marked around the suture hole using a tissue marker. Points were arranged in a 3x3 grid with 2 mm spacing (Figure 6.6). Subsequently, the suture ends were tied to the fastener of the traction device, and its position was adjusted to achieve the desired tension. During the indentation testing, the suture was held in place under three different traction conditions: unloaded, 10 N, and 20 N.

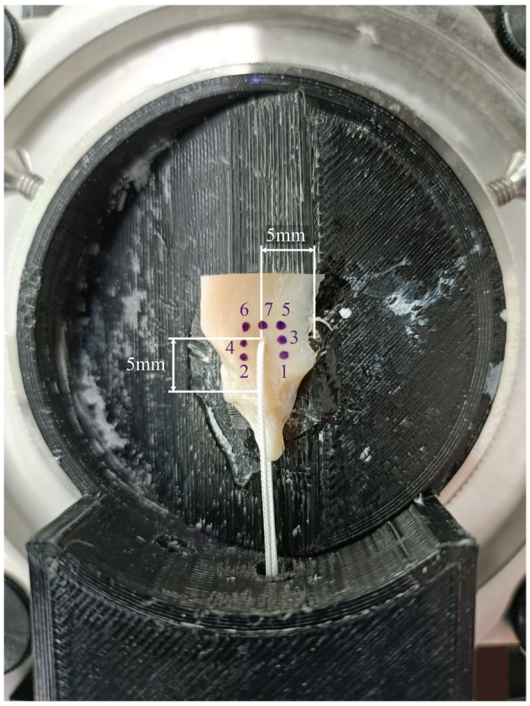

Figure 6.6. Sutured meniscal horn placed in the container with the seven measurement point marked on its cranial surface.

At the beginning of the indentation procedure, a reference image was taken to align the marked coordinates on the cranial surface of the meniscus with the internal coordinate system of the multiaxial testing machine. The indentation tests were conducted at seven predefined measurement points under the following conditions (Seitz et al., 2021) specified in Table 6.1.

Table 6.1. Non-destructive indentation test conditions.

Parameter	Value
Contact velocity	0.5 mm/s
Contact force threshold	0.049 N
Scanning grid resolution	0.05 mm,
Indentation amplitude	0.5 mm
Indentation speed	0.25 mm/s
Relaxation time	20 seconds
Force sampling rate	100 Hz

After completing the indentation tests, the procedure was repeated to measure meniscus thickness. For this purpose, the process was conducted with and without the meniscus in place, with the conditions listed in Table 6.1, but a contact criterion of 0.10 N.

6.2.2.2 Load-to-failure test

Once the non-destructive test was completed, to maintain hydration, the meniscus-suture construct was wrapped in a damp gauze without covering the ink dots marked on the horn until the time of the test. A load-to-failure test was conducted using the testing machine (Zwick Z010, ZwickRoell, Ulm, Germany) described in Section 2.5.1.2.1 of Chapter 2, equipped with a 500 N load cell (KAF-W, AST, Germany), and the digital camera (GO-5100C-USB, Jai, Denmark) described in Section 2.6.1 of the same chapter, equipped with a CMOS sensor with a resolution of 2464x2056 pixels and a 2.4/16 mm lens (V1624-MPZ, Computar, Japan).

The test followed the procedure detailed in Section 3.2.2 of Chapter 3. Briefly:

1. Meniscus-suture construct was fixed to the base of the testing machine at approximately 8 mm from the suture hole using a mechanical/pneumatic clamp (Figure 6.7a) with sandpaper interposed between the tissue and the clamp to enhance friction. The horn was positioned with its cranial surface oriented towards the outer side of the testing machine, the longitudinal fibers aligned parallel to the loading direction, and the suture hole situated along a pull line passing through the center of the machine actuator head.

2. The two free ends of the suture were also enveloped in sandpaper and fastened to the machine head using a mechanical clamp. To simulate a representative suture length for a transtibial repair, and in line with previous studies (Cerminara et al., 2014; Perez-Blanca et al., 2018), a length of 55 mm was set between the puncture point on the meniscus and the clamp limit during manual suture traction, ensuring only sufficient force for vertical orientation.

3. After positioning the specimen, two lines were delineated using a surgical pen on both the meniscus and the suture, demarcating their respective boundaries with both mechanical clamps to assess the potential occurrence of slippage.
4. For videogrammetric analysis, two dots were marked on the horn, aligned with the pulling direction (Figure 6.7b):

    - Point 1 on the suture limb at the cranial side of the meniscus, precisely coinciding with the meniscus-suture interface.

- Point 2, on the same meniscal surface and positioned on the opposite side of the hole in the loading direction, as close to the hole as feasible.

5. The digital camera was mounted directly in front of the testing machine, meticulously aligned so that its image plane was parallel to the medial transverse plane of the meniscus.

6. A traction force of 1 N was maintained for 5 seconds as a stabilization phase.

7. Next, a displacement-controlled load to failure test at 0.1 mm/s was conducted. During the test force was recorded by the load cell of the testing machine at 10 Hz, and images were captured by the videogrammetric system.

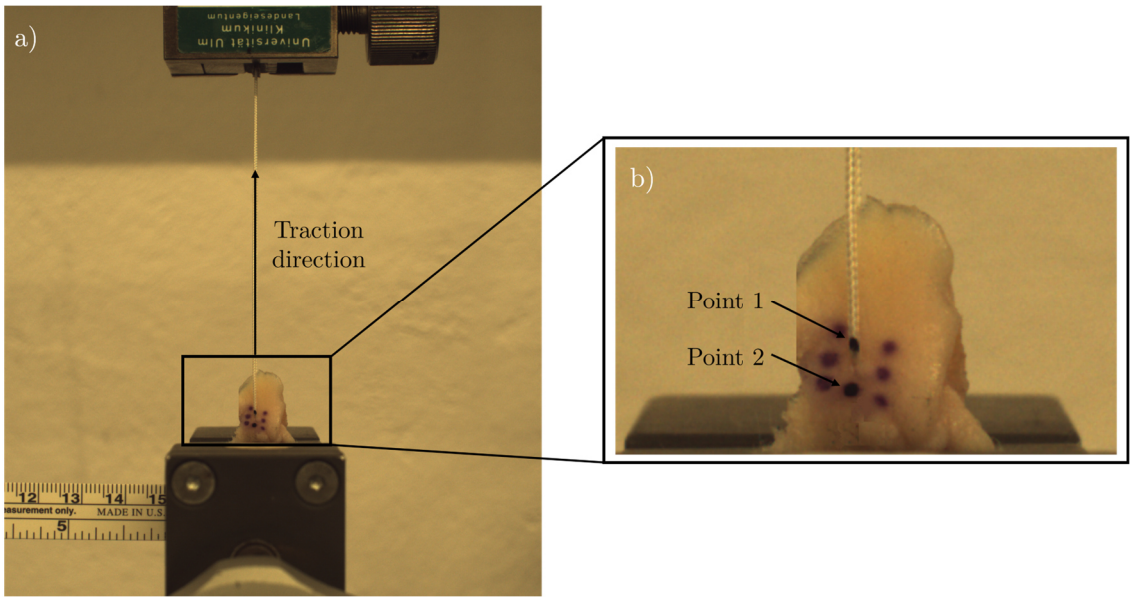

Figure 6.7. a) Lateral human meniscal horn on the testing machine with an indication of the traction direction aligned with its circunferential fibers; b) Magnification of the suture hole area with the inked marks and the puncture point shown. The seven measurement points used previously in the indentations can be observed.

6.2.3 Stress-relaxation analysis

From the indentation test, for each traction condition T (unloaded, 10 N, or 20 N in the suture), the maximum indentation force at each measurement point i, denoted as $F^{i,T}$, was recorded. This force occurs just before the onset of

relaxation. The thickness of the meniscus at the point i, h^i, was determined by calculating the difference in indenter displacement with and without the meniscus present, using a contact criterion of 0.10 N, as detailed in section 2.1.2 (Jurvelin et al., 1995).

The instantaneous modulus, $IM^{i,T}$, reflects the initial elastic response of the meniscal tissue before relaxation. It was calculated with Equation 6.1.

$$IM^{i,T} = \frac{F^{i,T}}{\Delta L} \cdot \frac{1-\upsilon^2}{2a\kappa^i} \tag{6.1}$$

where:

- ΔL is the indentation amplitude, set to 0.5 mm.
- υ is the Poisson´s ratio of the tissue, set to 0.32 (Morejon et al., 2021).
- a is the radius of the contact area.
- κ^i is the correction factor computed based on the model proposed by Hayes et al. (Hayes et al., 1972), which is a function of a and h^i.

The relaxation modulus, $E_{t20}^{i,T}$, at the point i after the 20 seconds of relaxation period was computed with Equation 6.2.

$$E_{t20}^{i,T} = \frac{F_{t20}^{i,T}/A}{\Delta L/h^i} \tag{6.2}$$

where:

- $F_{t20}^{i,T}$ is the force recorded at this point i after the relaxation time of 20 seconds.
- A is the meniscus-indenter contact area (Seitz et al., 2021).

The stress during the indentation process was computed dividing the recorded force by the meniscus-indenter contact area, A, using Equation 6.3.

$$\sigma_t^{i,T} = \frac{F_t^{i,T}/A}{\Delta L/h^i} \tag{6.3}$$

where $F_t^{i,T}$ is the force recorded for the point i and traction condition T at the time t of the indentation test.:

The relaxation stress percentage (Coluccino et al., 2017), at the measurement point i for the traction state T was calculated with Equation 6.4.

$$\Delta\sigma_{relax}^{i,T}(\%) = \frac{\sigma_{t20}^{i,T}}{\sigma_{max}^{i,T}} \cdot 100 \tag{6.4}$$

where:

- $\sigma_{t20}^{i,T}$ is the relaxation stress modulus at the relaxation time of 20 s.

- $\sigma_{max}^{i,T}$ is the maximum stress in the relaxation period, i.e., the maximum of the values computed by Equation 6.3 that must occurs at the initiation of relaxation, as for $F^{i,T}$.

6.2.4 Load-to-failure analysis

As in Chapter 3, the equivalent stiffness modulus in the traction direction, m, was determined by calculating the slope of the linear segment of the stress-strain curve of the load-to-failure test within the strain range of $\varepsilon = [0 - 0.4]$. The , $\sigma - \varepsilon$, curve is the plot of the strain computed with Equation 6.5.

$$\sigma = \frac{F}{\phi \cdot h} \tag{6.5}$$

where F is the traction force recorded by the load cell of the testing machine during the test, ϕ is the nominal diameter of the suture and h denotes the thickness of the meniscus at the suture hole, as a function of the strain calculated with Equation 6.6.

$$\varepsilon = \frac{D}{D_0} - 1 \tag{6.6}$$

where D is the distance between Point 1 and Point 2 calculated by the videogrammetric software described in Section 2.6 during the test, and D_0 is this distance in the initial frame of the test between the two points

The linear region of the force-strain curve, $F - \varepsilon$, of the sutured meniscal horn was identified by calculating the toe force, F_{toe}, which is defined as the force at which the behavior transitions from non-linear to linear. This transition point, as detailed in Chapter 4 of Bruce et al. (Bruce et al., 2015), is crucial because it marks the onset of a consistent elastic response of the meniscal tissue.

Additionally, the force corresponding to 40% strain, $F_{\varepsilon 40}$, was measured.

6.2.5 Statistical analysis

The sample size for the experimental setup was determined based on the maximum indentation force, $F^{i,T}$, recorded during the stress-relaxation phase across different loading conditions in the initial five specimens. The mean values were:

- 0.34 N for the unloaded condition.
- 1.04 N for 10 N of suture traction.
- 1.08 N for 20 N of suture traction.

The highest standard deviation among groups was 0.51 N. Using G*Power 3.1.9.2 software (Faul et al., 2007), a minimum group size of $n = 24$ was calculated to detect a small effect size of 0.70 at a significance level of $\alpha = 0.05$, with a statistical power of $(1 - \beta) = 0.951$. To mitigate the impact of potential sample loss, a conservative group size of $n = 27$ was selected.

A one-way ANOVA was conducted to assess the effect of circumferential traction induced by the suture on the compressive properties of the sutured human meniscal horn. This statistical analysis compared the compressive properties outlined in section 6.2.4 across three traction conditions: unloaded, 10 N, and 20 N. Upon detecting significant differences among the groups, pairwise comparisons were performed using Student's t-tests with Bonferroni correction to identify specific differences between the loading conditions.

To identify correlations between the compressive and tensile properties of the sutured meniscal horn, a Pearson bivariate correlation test was performed between the equivalent stiffness modulus, m, and the compressive properties computed in each traction condition. Significant correlations were considered at $p < 0.05$.

The later statistical analyses were carried out using SPSS Statistics (v.20, IBM Corp).

6.3 Results

In this section, the compressive and tensile properties described in Sections 6.2.4 and 6.2.5 for the indentation and load-to-failure tests are presented. For the

indentation tests, the results are compared between the three circumferential tensile load levels.

The results shown in the figures of this chapter correspond to the mean and 95% confidence interval of the 9 samples tested in each group, and the seven indentation points for the properties obtained from indentation tests in sections 6.3.1 to 6.3.4. The results listed in the tables of this chapter correspond to the mean and SD of the same properties. For the complete set of experimental data, refer to Appendix C.

6.3.1 Maximum indentation force, $F^{i,T}$

The maximum force in the indentation test, $F^{i,T}$, for each traction condition is shown in Figure 6.8 and Table 6.2. With respect to the unloaded condition, specimens under 10 N of circumferential tensile load showed a maximum force that was 101.6% higher ($p = 0.02$), while those under 20 N exhibited a maximum force that was 114.1% higher ($p = 0.007$). No significant differences between the two conditions under suture traction, 10 N and 20 N, were found.

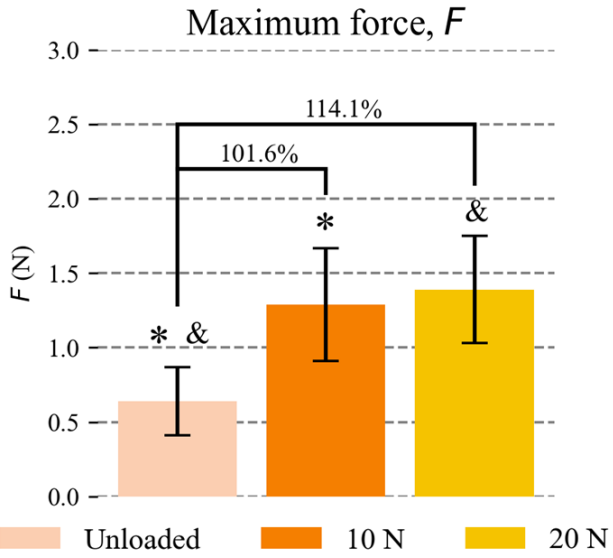

Figure 6.8. Mean and 95% confidence interval of maximum force in the indentation period of sutured meniscal horns at each suture traction level. For significantly different loading conditions, the percentage difference between means relative to the lower level is indicated. Significant difference: *Unloaded vs. 10 N; &Unloaded vs. 20 N.

Table 6.2. Maximum indentation force (N) obtained at the three tested suture traction levels.

	Unloaded	**10 N**	**20 N**
Mean	0.64*&	1.29*	.39&
95% confidence interval	0.23	0.38	0.36

Significant difference: *Unloaded vs. 10 N; &Unloaded vs. 20 N.

6.3.2 Instantaneous modulus, $IM^{i,T}$

The mean and 95% confidence interval of the instantaneous modulus, $IM^{i,T}$, for each traction condition are shown in Figure 6.9 and Table 6.3. Specimens under 10 N and 20 N tensile load showed IM that were significantly higher than in the unloaded condition, by 104.6% ($p = 0.002$) and 123.1% ($p < 0.001$) respectively. No differences were found between the values in the two loaded conditions.

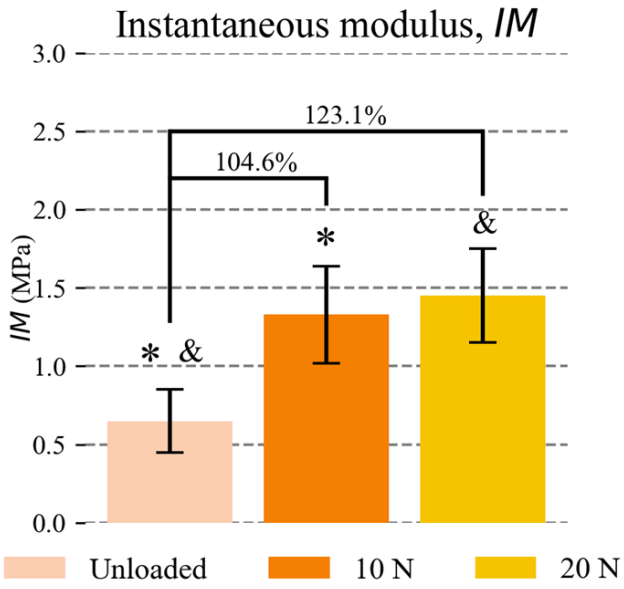

Figure 6.9. Mean and 95% confidence interval of instantaneous modulus of sutured meniscal horns at each suture traction level. For significantly different loading conditions, the percentage difference between means relative to the lower level is indicated. Significant difference: *Unloaded vs. 10 N; & Unloaded vs. 20 N.

Table 6.3. Instantaneous modulus (MPa) obtained at the three tested suture traction levels.

	Unloaded	**10 N**	**20 N**
Mean	0.65*&	1.33*	1.45&
95% confidence interval	0.20	0.31	0.30

Significant difference: *Unloaded vs. 10 N; &Unloaded vs. 20 N.

6.3.3 Relaxation modulus, $E_{t20}^{i,T}$

Figure 6.10 and Table 6.4 show the mean and 95% confidence interval of the relaxation modulus at the relaxation time, $E_{t20}^{i,T}$, for each loading condition. Similar to the behavior observed for previous compressive properties, specimens under 10 N tensile load exhibited a relaxation modulus that was 120% higher than in the unloaded condition ($p < 0.001$), and specimens under 20 N tensile load showed a

relaxation modulus that was 151.4% higher than in the unloaded state ($p < 0.001$). Again, no differences were found between the two loading conditions.

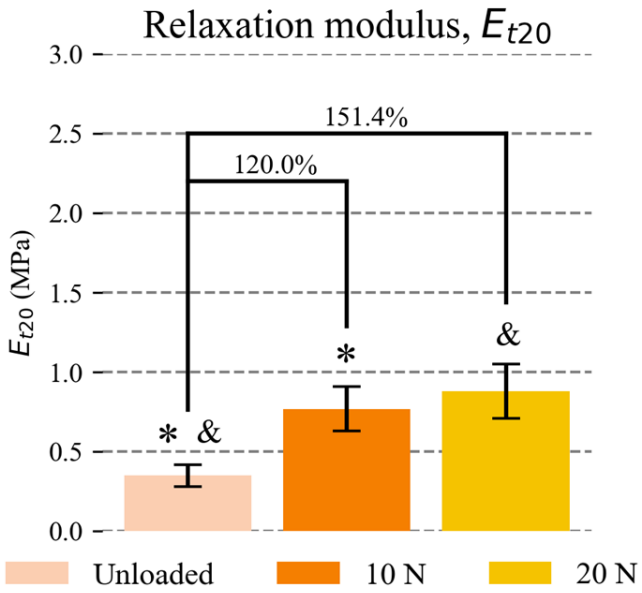

Figure 6.10. Mean and 95% confidence interval of relaxation modulus at the relaxation time of sutured meniscal horns at each suture traction level. For significantly different loading conditions, the percentage difference between means relative to the lower level is indicated. Significant difference: *Unloaded vs. 10 N; & Unloaded vs. 20 N.

Table 6.4. Relaxation modulus at the relaxation time (MPa) obtained at the three tested suture traction levels.

	Unloaded	**10 N**	**20 N**
Mean	0.35*&	0.77*	0.88&
95% confidence interval	0.07	0.14	0.17

Significant difference: *Unloaded vs. 10 N; &Unloaded vs. 20 N.

6.3.4 Relaxation stress percentage, $\Delta\sigma_{relax}^{i,T}(\%)$

The results for the relaxation stress percentage, $\Delta\sigma_{relax}^{i,T}(\%)$, for each loading condition are shown in Figure 6.11 and Table 6.5. No significant overall differences were found between the three tensile loading conditions tested; therefore, no differences could be detected for this property between the unloaded condition and any of the loaded conditions. The mean $\Delta\sigma_{relax}^{i,10}$was 6.2% and mean $\Delta\sigma_{relax}^{i,20}$ 6.6% lower than the unloaded condition, while mean $\Delta\sigma_{relax}^{i,10}$was 0.4% lower than mean $\Delta\sigma_{relax}^{i,20}$. It can also be observed that the deviations of the data within each group were small.

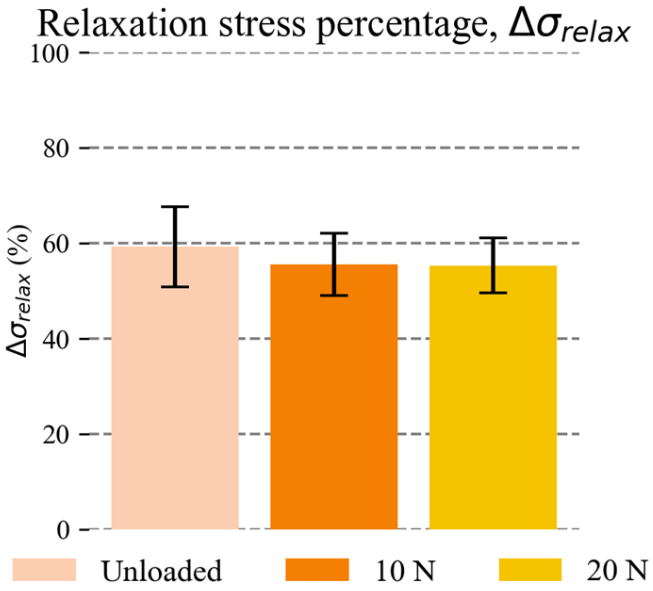

Figure 6.11. Mean and 95% confidence interval of relaxation stress percentage of sutured meniscal horns at each suture traction level.

Table 6.5. Relaxation stress percentage (%) expressed in percentage obtained at the three tested suture traction levels.

	Unloaded	**10 N**	**20 N**
Mean	59.29	55.60	55.15
95% confidence interval	3.31	2.60	2.26

6.3.5 Compressive – tensile properties relationship

The mean and SD of the equivalent stiffness modulus in the traction direction, m_s, was 47.25 MPa $\pm$ 31.69 MPa. The adjusted R-squared value of the linear fitting of all the tested specimens range from 0.91 to 0.96.

The mean and SD value of the toe force, F_{toe}, that identifies the transition from non-linear to linear behavior of the $\sigma - \varepsilon$, curve was 8.17 N $\pm$ 2.64 N. The force corresponding to a strain of 40%, $F_{\varepsilon 40}$, was 31.34 N $\pm$ 12.00 N. $F_{\varepsilon 40}$ can be assumed to represent the upper threshold for the traction force exerted on the meniscal suture under physiological conditions. The maximum force at the meniscal root has been estimated to be approximately 50 N (Stärke et al., 2013). Given that repairs are typically performed using two stitches in clinical practice, each suture would be expected to bear half of this total force. If an additional 25% increase is considered to account for potential non-uniform load distribution

between the suture limbs, this results in an estimated upper limit of 31.25 N per suture.

Figure 6.12 shows the suture load-strain curves of all the tested specimens with indicators showing the limit of the toe zone and the zone of 40% strain. It can be observed that the two traction loads to which the horns were subjected in the indentation tests described in section 6.2.3.1 (10N and 20N) fell in the linear region of the curve, i.e., between F_{toe} and $F_{\varepsilon 40}$. Clearly, the state with no suture traction was out of this region.

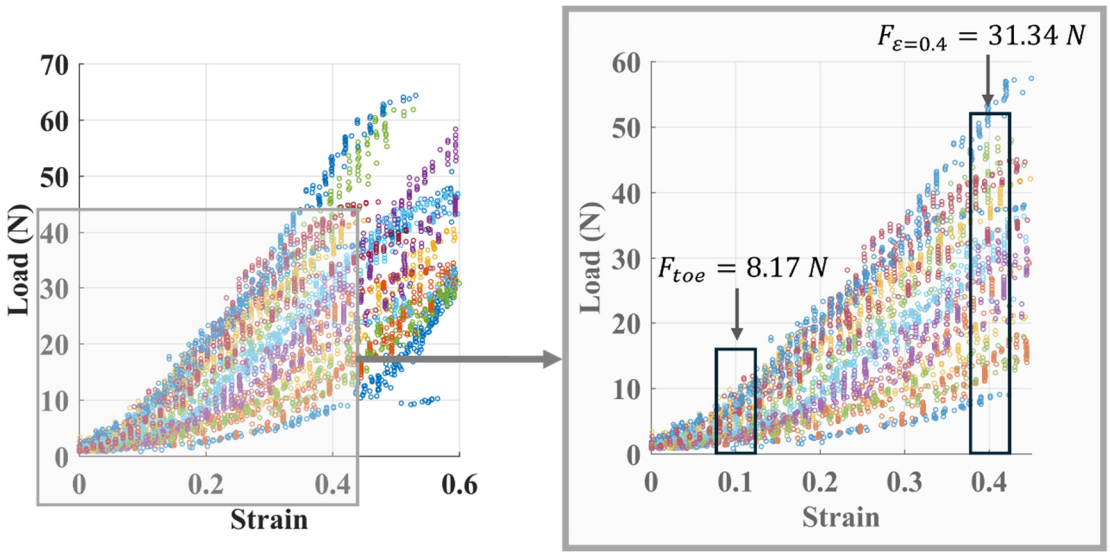

Figure 6.12. Load-strain curves of all the tested specimens with a magnification in the strain range $\boldsymbol{\varepsilon} = [0\text{-}0.4]$ showing the mean values of the forces in the toe zone and the force in $\varepsilon = 0.4$.

Following the procedure described in section 6.2.6 of this chapter, no correlations were found between the equivalent stiffness modulus and any of the computed compressive properties under any suture traction condition. Figure 6.13 plots the compressive properties as a function of the equivalent stiffness modulus with a different color for each suture traction condition. The influence of suture traction on the compressive properties can be foreseen in the plots corresponding to F, IM, E_{t20} and $\Delta\sigma_{relax}$. This conclusion was already statistically confirmed in sections 6.3.1 to 6.3.4.

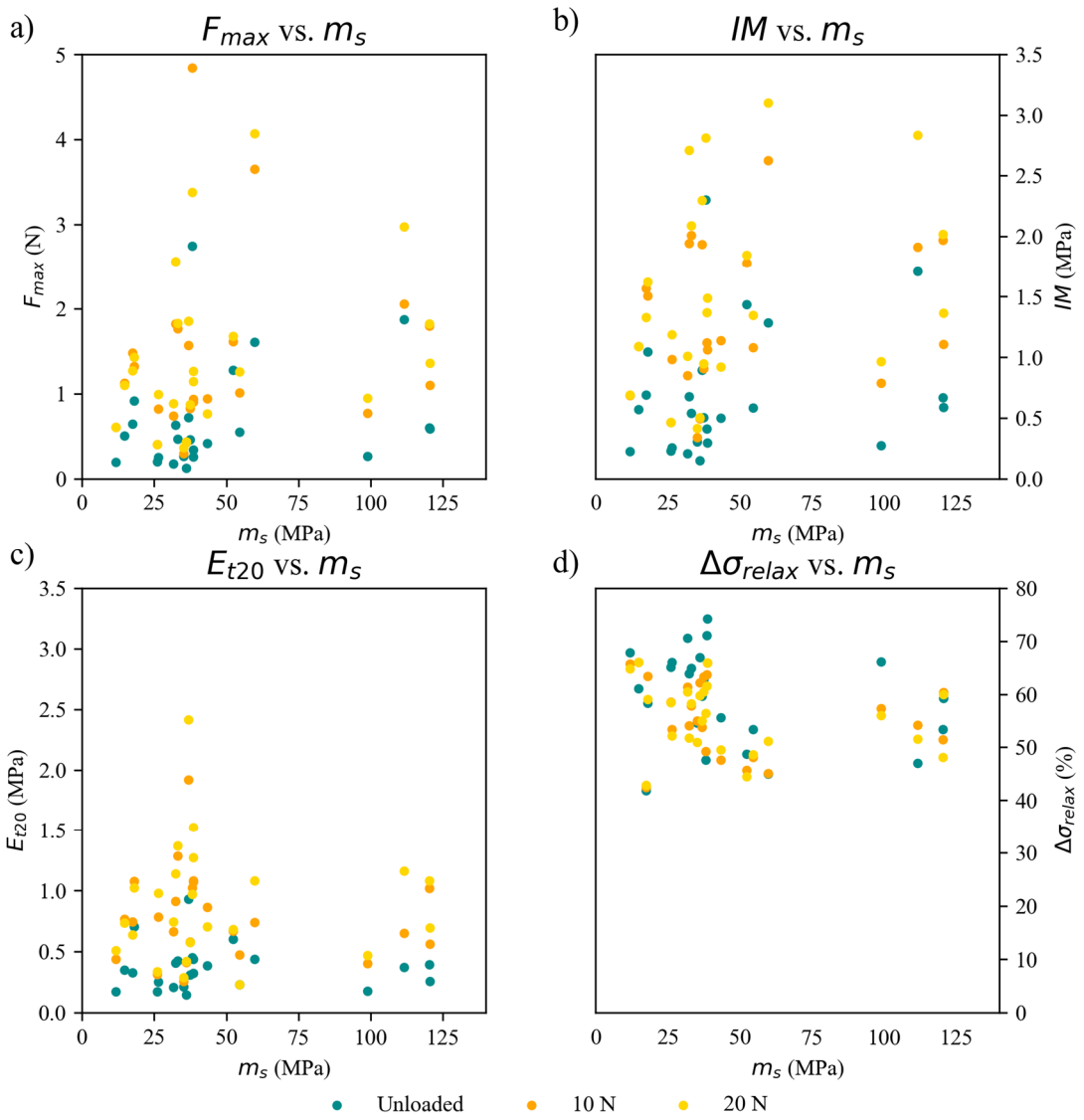

Figure 6.13. Experimental compressive properties versus the equivalent stiffness modulus : a) maximum force in the indentation period ; b) instantaneous modulus; c) relaxation modulus; d) relaxation stress percentage.

Figure 6.14 plots the variation in compressive properties, as a function of m_s , due to the applied tension in the suture relative to its value in the same specimen without tension. Each traction state is distinguished by a different color. The figure does not suggest any noticeable difference between the variations induced by the two suture traction, 10 N or 20 N. This observation is consistent with the outcomes in sections 6.3.1 to 6.3.4, where it was stated that no statistical differences were found between the compressive properties under the two suture traction states.

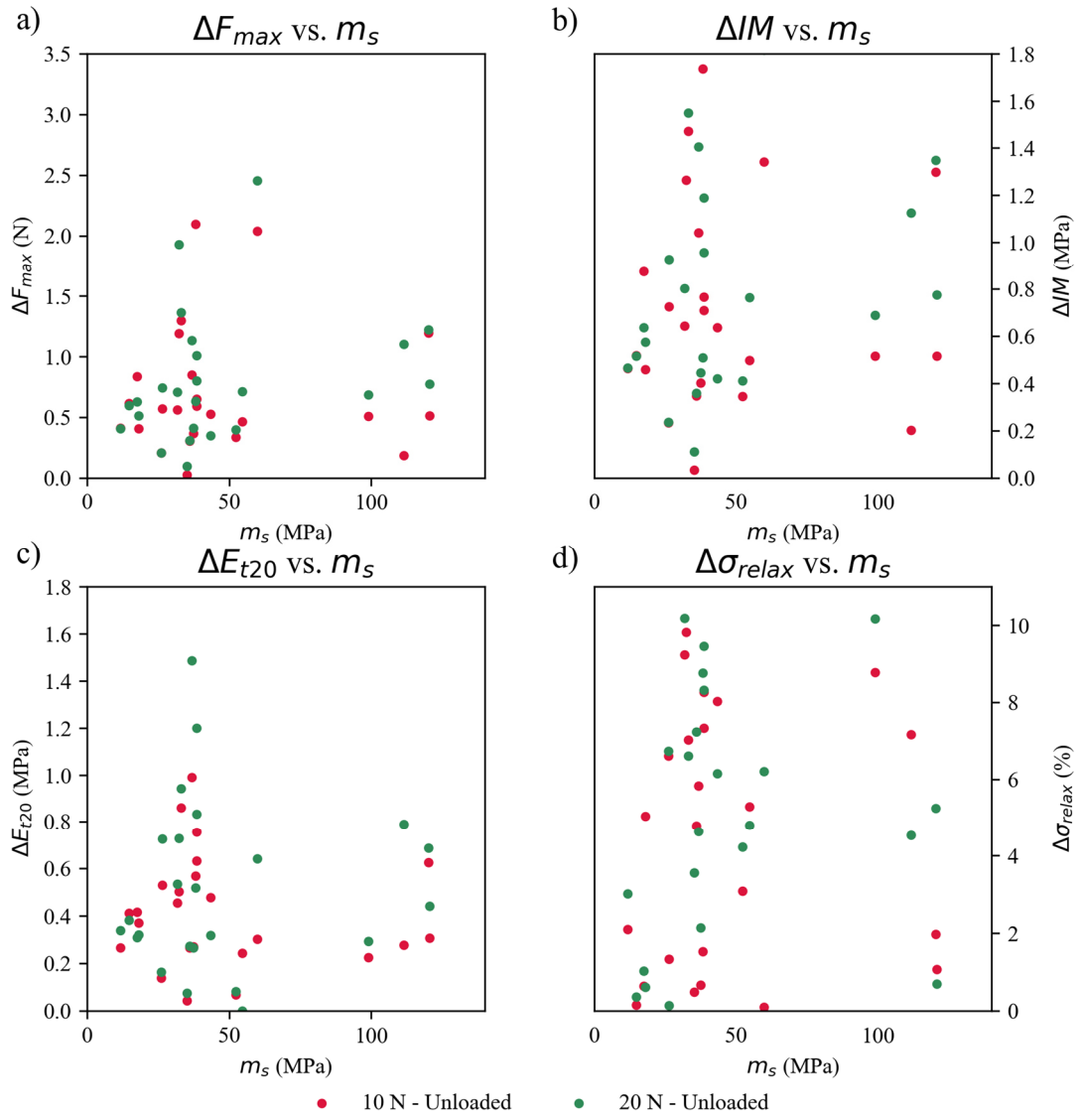

Figure 6.14. Variation of the experimental compressive properties from the unloaded state versus the equivalent stiffness modulus: a) maximum force ; b) instantaneous modulus; c) relaxation modulus; d) relaxation stress percentage.

6.4 Discussion

The main finding of this chapter was that the material properties obtained in unconfined indentation tests of sutured human meniscal horns in the suture area, to characterize the tissue axial compression, are influenced by the presence of suture-generated traction in the direction of its circumferential fibers. Despite the influence detected, it was not possible to establish a correlation between the axial compression properties calculated and the equivalent modulus of stiffness used to characterize the tissue circumferential traction, i.e., the secondary hypothesis initially proposed could not be corroborated.

The results of the *in vitro* indentation tests revealed an important variation in the maximum force during the indentation, the instantaneous modulus and the relaxation modulus when circumferential traction is involved in the indentation test. Specifically, their values were more than doubled those without suture traction. This finding is consistent with expectations based on general mechanical properties of most tissues and considering that the collagen fibers of the meniscal horn are oriented parallel to the traction direction. Since these properties are primarily related to the elasticity of the tissue, when the suture pulling exerts traction on the circumferentially oriented meniscal fibers a significant impact on the compressive elastic behavior of the meniscus is revealed. However, the very large difference in their values raises concerns about the potential errors introduced when modeling the meniscal horn using compressive axial properties obtained from pure indentation tests. This issue is further addressed in the following chapter of this thesis.

Regarding the relaxation stress percentage, it was not affected by circumferential stress in the horn. This property reflects the variation in stress under constant deformation, a phenomenon related to the dynamic effects involved in the stress relaxation that occurs after reaching the maximum indentation force. Because stress relaxation is more closely related to fluid motion, it is not surprising to be less impacted by the existence of traction on the circumferential collagen fibers, which is likely the primary cause of the changes observed in the other three axial compressive properties

Variations in compressive properties related to the elasticity of the tissue were observed between conditions with and without suture-induced traction, whereas no significant differences were found between the two loaded states. This outcome is likely attributable to both suture traction values falling within the linear portion of the stress-strain curve obtained from the loaded -to-failure test conducted pulling in the fiber direction, i.e., between the forces that define the upper limit of the toe region, F_{toe}, and the strain of 40%, $F_{\varepsilon=0.4}$. In contrast, the unloaded condition clearly falls within the toe zone. It is hypothesized that the influence of suture-induced traction on the axial compressive properties of the meniscal horn may be restricted to the phase where meniscal fibers undergo straightening and alignment, occurring just prior to the onset of elongation. This region has been identified as the toe region, upper bounded by F_{toe} (Bruce et al., 2015; Tissakht and Ahmed, 1995). Further studies are required to validate this hypothesis.

The correlation between the axial compressive properties and the circumferential equivalent stiffness modulus was subject of the study, which required the undertaking of a load-to-failure test on the same sutured meniscal horn that was previously submitted to the indentation test. For that reason, to avoid damage to the meniscal tissue, the maximum tensile load chosen in the indentation test was 20 N.

The equivalent stiffness modulus computed in the stress-strain curve of the load-to-failure test showed a value of 47.25 MPa $\pm$ 31.69 MPa, with adjusted R-squared values for the linear fitting ranging from 0.91 to 0.96 for all the tested specimens. The high correlation coefficient found suggests that this property as a suitable parameter for the characterization of the linear zone of the curve. However, a high degree of deviation was observed in the results, which prevents drawing the conclusion that it is a generically applicable value for modelling of human meniscal horn in the suture zone. Further research is needed to propose a valid model of circumferential tensile behavior in the suture zone. One proposal would be to differentiate between the different anatomical zones: medial and lateral meniscus, and anterior and posterior horn. However, the number of specimens involved in this study limits such an investigation with sufficient statistical power. The force in the toe zone, F_{toe}, was 8.17 N $\pm$ 2.64 N and the force achieved at $\varepsilon = 0.4$, $F_{\varepsilon=0.4}$, was 31.34 N $\pm$ 12.00 N. As far as it is known, this property has not been previously studied by other researchers for repaired meniscal horns, this work is the first to address this analysis.

Regarding the correlation between the compressive properties considered in this study and the equivalent stiffness modulus in the strain range of $\varepsilon = [0 - 0.4]$, a clear non-correlation between them was exhibited.

To the best of our knowledge, this study presents two novel methodologies. Firstly, it is the first to analyze indentation data of the meniscus under unconfined compression in conjunction with circumferential traction loads, thereby simulating physiological conditions. As a result, comparisons with previous research on the impact of circumferential stress traction on meniscal compressive properties are not feasible. Secondly, this study pioneers the assessment of the compressive behavior of a sutured meniscal horn specifically within the suture region, a critical area of interest following meniscal root repair surgery.

Previous research has primarily focused on assessing the axial compressive properties of the untreated meniscus under isolated compression conditions. The study described in this chapter involves loading in directions that simulate a stress state closer to the physiological situation by including circumferential traction. The properties investigated in previous indentation test of the meniscus with pure compression (Berni et al., 2021; Chia and Hull, 2008b; Danso et al., 2015; Fischenich et al., 2015; Joshi et al., 1995; Lai and Levenston, 2010; Leslie et al., 2000; Martin Seitz et al., 2013; Morejon et al., 2021; Pordzik et al., 2020b; Seitz et al., 2021; Warnecke et al., 2020). include the maximum force observed during the relaxation phase, as well as various moduli such as the relaxation modulus, aggregate modulus, instantaneous modulus, and equilibrium modulus.

Seitz et al. (Seitz et al., 2021) previously studied the maximum force in the anterior and posterior horn and in the meniscal body, differentiating between lateral and medial, and mild and severe degenerated under confined pure axial compression. The forces values range between 0.01 N and 1.12 N, which are in line with the values obtained in this chapter for the unloaded condition, where the values ranged between 0.12 N and 2.74 N. The differences between both studies could be due to variations in the setup of the indentation test as the different confinement condition. Pordzik et al. (Pordzik et al., 2020b, 2020a) studied the maximum force in arthritic and arthritic-free menisci. The study reported force values of the arthritic-free menisci of 0.01 $\pm$ 0.01 N, which are lower than the values obtained in the present work and by Setiz et al. (Seitz et al., 2021). It could be due to Pordzik et al. used an indenter whose diameter was 1 mm while the diameter of the indenter in this study was 2 mm. Moreover, the contact criteria considered by Pordzik et al. was 0.1 N while in this study was 0.049 N, and their indentation amplitude was 0.2 mm compared to the 0.5 mm used in this study.

Coluccino et al. (Coluccino et al., 2017) analyzed the stress-relaxation response of bovine menisci, evaluating the compressive stiffness and the stress-relaxation properties under unconfined compression held constant during 1800 s. The study showed relaxation stress percentages between t79% and 88% depending on the direction of the fibers assessed. The results of the work in this chapter exhibited a mean value of 59.3% in the same unloaded condition as in the Coluccino et al. study, a percentage lower than their findings. Considering the relaxation time of 20 s used in the present work against the 1800 s used by Coluccino et al., and the morphological and structural differences between bovine

and human menisci (Joshi et al., 1995; Proffen et al., 2012), the reduced value obtained by our work is understandable. Likewise, Seitz et al. (Seitz et al., 2021) analyzed the relaxation stress percentage using severely and mildly degenerated human meniscus, obtaining values between 50% and 65% after 20 s of relaxation time, a range within which the value obtained in the current work using human meniscus also falls.

The equilibrium properties has not been assessed in this study, due to the necessity of perform the stress-relaxation test until the meniscus reach its equilibrium, which normally takes between 30 min and 60 min (Chia and Hull, 2008b; Martin Seitz et al., 2013; Warnecke et al., 2020). Instead, in the current study, where it was not possible to meet with the equilibrium time due to the high time consumption of the stress-relaxation test and the necessity of maintain the tissue without time damage, the same procedure as other works (Pordzik et al., 2020b; Seitz et al., 2021) was employed, using a reduced relaxation time of 20 s to compute the relaxation modulus at 20 s. This point is one of the main limitations of the current work, due to the impossibility of computing the equilibrium modulus, which is widely studied in the literature (Boschetti and Peretti, 2008; Chia and Hull, 2008b; Coluccino et al., 2017; Fischenich et al., 2015; Morejon et al., 2021; Warnecke et al., 2020) and representative of the compressive properties of the meniscus. Regarding the values of the relaxation modulus at relaxation time of 20 s, Seitz et al. (Seitz et al., 2021), who differentiated between human menisci in function of their degeneration state, obtained values ranged from 0.01 MPa to 0.55 MPa for mildly degenerated human menisci and between 0.04 MPa and 0.73 MPa for severely degenerated human menisci. Their results are in line with those obtained in this chapter, where no degeneration differentiation was made, and all the samples compounded a common group. The relaxation modulus in the current work showed a mean value of 0.35 MPa with an indentation test setup similar to the one conducted by as Seitz et al. (Seitz et al., 2021), result within the range provided by their study for human menisci (0.01 – 0.55 MPa).

The instantaneous modulus provides information about the initial elastic response of the meniscal tissue when a load is not sustained over time and the viscous properties of the tissue are not involved. The instantaneous modulus is an extensively studied parameter when the compressive properties of the human meniscus want to be assessed (Danso et al., 2015; Fischenich et al., 2015; Moyer et al., 2012; Pordzik et al., 2020b; Seitz et al., 2021). Moyer et al. (Moyer et al.,

2012) submitted human menisci to a nanoindentation test with a nanoindenter of 300 μm of diameter with a spherical tip and computed the instantaneous modulus, obtaining values ranging from 3.56 ± 0.19 MPa to 3.86 ± 0.30 MPa in the central and anterior part of the menisci respectively. These values are between 598.0% and 656.9% higher than the instantaneous modulus of 0.65 ± 0.50 MPa obtained in the unloaded state in the current work. These differences may be due to the variation in the type of indentation test and the reduction in the diameter of the tip of the indenter, it is known that very different values are be obtained from nanoindentation test depending on the specific indented point. Danso et al. (Danso et al., 2015) performed a stress-relaxation test in the anterior, middle, and posterior sites of the human meniscus to determine the elastic, viscoeslastic and poroelastic properties in healthy menisci. The study does not provide the numerical values of the instantaneous modulus, but the data showed are approximately between 0.5 MPa and 1.7 MPa, a range in line with the results of the current study in the same unloaded condition. In this case, the type of indentation is the same as that performed in the present work and the only differences were the diameter of the indenter (Danso et al.: 1.19 mm vs. Present study: 2 mm) and the relaxation time (Danso et al.: 15 min vs. Present study: 20 s). Fischenich et al. (Fischenich et al., 2015) focused their work on studying the effect of the degeneration on the compressive and tensile properties of human meniscus. Following their objective, a stress-relaxation test was performed during 1200 s achieving equilibrium conditions and obtaining values for the instantaneous modulus ranging approximately between 0.25 MPa until 2 MPa, which aligns with the results of the present study. Pordzik et al. (Pordzik et al., 2020b) performed a similar stress-relaxation test than in the current study, but the relaxation time was 10 s instead of 20 s, the diameter of the indenter was 1 mm instead of 2 mm and the indentation amplitude was 0.2 mm instead of 0.5 mm. The value of 0.13 ± 0.07 MPa for the instantaneous modulus of healthy posterior horn of human menisci provided by Pordzik et al. is lower than our result of 0.51 ± 0.41 MPa in the same unloaded condition, which is understandable considering all the mentioned differences mainly the reduction in the indentation depth. As Fischenich et al., the study carried out by Seitz et al. (Seitz et al., 2021) performed a stress-relaxation test to assess the variations on the biomechanical properties of human menisci by degeneration state. The test was carried out for 20 s, as in the present study, and the same indenter and test setup was employed. The values of the instantaneous modulus ranged from 0.1 MPa to 1.6 MPa, results which are completely in line with those obtained in the current work.

The limitations present in *in vitro* studies are significant in this work, such as the absence of the surrounding soft tissues present in a healthy knee, elements that play an important role in the articular biomechanics of the joint. The stress-relaxation tests were performed under unconfined conditions and using isolated meniscus without attaching them to the anatomical root insertion in the tibia. This approach is widely accepted in the study of the compressive properties of the menisci (Chia and Hull, 2008b; Danso et al., 2015; Fischenich et al., 2015; Kwok et al., 2014; Seitz et al., 2021; Warnecke et al., 2020). Stress-relaxation tests are typically conducted for the characterization of the compressive properties of the menisci and, in general, of soft biological tissues. In this sense, it is preferable to perform the stress-relaxation test during the enough relaxation time to achieve the equilibrium state of the tissue allowing the assessment of the viscoelastic effect on the computed properties (Chia and Hull, 2008b; Coluccino et al., 2017; Danso et al., 2015; Pordzik et al., 2020b). As already mentioned, this point is one of the main limitations in the present study, where the relaxation time was 20 s, not enough to achieve the equilibrium state of the meniscal tissue, which is typically reached after relaxation times between 30 min and 60 min (Chia and Hull, 2008b; Danso et al., 2015; Warnecke et al., 2020). However, the assessment of the viscoelastic effect on the compressive properties was not an objective of this study but rather to assess the variations in the compressive properties as a function of the traction load applied in the circumferential direction. In this respect, the procedure and selected relaxation time followed the methodology of other works in the literature (Pordzik et al., 2020b; Seitz et al., 2021). The use of a single stitch to replicate the meniscal root reinsertion and to pull the meniscal horn in the circumferential direction during the stress-relaxation test was selected to avoid non uniform and non-controllable load distribution between more suture. The use of a single stitch is an approach followed by previous works (Peña-Trabalon et al., 2024, 2023). The load-to-failure test was conducted at a displacement rate of 0.1 mm/s, representative of quasi-static displacement and lower than what is common in daily knee movements (Prado-Novoa et al., 2022). This deliberate choice aimed to minimize the potential impact of viscous effects on the test, a characteristic not specifically addressed within the scope of this study.

6.5 Conclusions

The maximum force, relaxation modulus, and instantaneous modulus measured in unconfined indentation tests of sutured meniscal horns under suture

traction of 10N and 20N in the direction of the meniscal circumferential fibrils were more than double the values found in the scenario with no suture traction.

No differences were found between the compressive properties obtained in load levels higher than the value corresponding to the toe zone.

6.6 References

Berni, M., Marchiori, G., Cassiolas, G., Grassi, A., Zaffagnini, S., Fini, M., Lopomo, N.F., Maglio, M., 2021. Anisotropy and inhomogeneity of permeability and fibrous network response in the pars intermedia of the human lateral meniscus. Acta Biomater 135, 393–402. https://doi.org/10.1016/J.ACTBIO.2021.08.020

Boschetti, F., Peretti, G.M., 2008. Tensile and compressive properties of healthy and osteoarthritic human articular cartilage. Biorheology 45, 337–344. https://doi.org/10.3233/BIR-2008-0479

Bruce, R., David, M., Burr, B., Sharkey, N.A., Fyhrie, D.P., 2015. Skeletal Tissue Mechanics, Second. ed. Springer, New York. https://doi.org/10.1007/978-1-4939-3002-9

Cerminara, A.J., LaPrade, C.M., Smith, S.D., Ellman, M.B., Wijdicks, C.A., LaPrade, R.F., 2014. Biomechanical Evaluation of a Transtibial Pull-out Meniscal Root Repair Challenging the Bungee Effect. American Journal of Sports Medicine 42, 2988–2995. https://doi.org/10.1177/0363546514549447

Chia, H.N., Hull, M.L., 2008. Compressive moduli of the human medial meniscus in the axial and radial directions at equilibrium and at a physiological strain rate. Journal of Orthopaedic Research 26, 951–956. https://doi.org/10.1002/JOR.20573

Coluccino, L., Peres, C., Gottardi, R., Bianchini, P., Diaspro, A., Ceseracciu, L., 2017. Anisotropy in the Viscoelastic Response of Knee Meniscus Cartilage. J Appl Biomater Funct Mater 15, 77–83. https://doi.org/10.5301/JABFM.5000319/ASSET/IMAGES/LARGE/10.5301_JABFM.5000319-FIG4.JPEG

Danso, E.K., Mäkelä, J.T.A., Tanska, P., Mononen, M.E., Honkanen, J.T.J., Jurvelin, J.S., Töyräs, J., Julkunen, P., Korhonen, R.K., 2015. Characterization of site-specific biomechanical properties of human meniscus—

Importance of collagen and fluid on mechanical nonlinearities. J Biomech 48, 1499–1507. https://doi.org/10.1016/J.JBIOMECH.2015.01.048

Faul, F., Erdfelder, E., Lang, A.G., Buchner, A., 2007. G*Power 3: a flexible statistical power analysis program for the social, behavioral, and biomedical sciences. Behav Res Methods 39, 175–191. https://doi.org/10.3758/BF03193146

Fischenich, K.M., Lewis, J., Kindsfater, K.A., Bailey, T.S., Haut Donahue, T.L., 2015. Effects of degeneration on the compressive and tensile properties of human meniscus. J Biomech 48, 1407–1411. https://doi.org/10.1016/J.JBIOMECH.2015.02.042

Hayes, W.C., Keer, L.M., Herrmann, G., Mockros, L.F., 1972. A mathematical analysis for indentation tests of articular cartilage. J Biomech 5, 541–551. https://doi.org/10.1016/0021-9290(72)90010-3

Joshi, M.D., Suh, J. -K, Marui, T., Woo, S.L. -Y, 1995. Interspecies variation of compressive biomechanical properties of the meniscus. J Biomed Mater Res 29, 823–828. https://doi.org/10.1002/JBM.820290706

Jurvelin, J.S., Räsänen, T., Kolmonens, P., Lyyra, T., 1995. Comparison of optical, needle probe and ultrasonic techniques for the measurement of articular cartilage thickness. J Biomech 28, 231–235. https://doi.org/10.1016/0021-9290(94)00060-H

Kim, Y.M., Rhee, K.J., Lee, J.K., Hwang, D.S., Yang, J.Y., Kim, S.J., 2006. Arthroscopic pullout repair of a complete radial tear of the tibial attachment site of the medial meniscus posterior horn. Arthroscopy 22, 795.e1-795.e4. https://doi.org/10.1016/J.ARTHRO.2005.12.040

Kwok, J., Grogan, S., Meckes, B., Arce, F., Lal, R., D'Lima, D., 2014. Atomic force microscopy reveals age-dependent changes in nanomechanical properties of the extracellular matrix of native human menisci: implications for joint degeneration and osteoarthritis. Nanomedicine 10, 1777–1785. https://doi.org/10.1016/J.NANO.2014.06.010

Lai, J.H., Levenston, M.E., 2010. Meniscus and cartilage exhibit distinct intra-tissue strain distributions under unconfined compression. Osteoarthritis Cartilage 18, 1291–1299. https://doi.org/10.1016/J.JOCA.2010.05.020

Leslie, B.W., Gardner, D.L., McGeough, J.A., Moran, R.S., 2000. Anisotropic response of the human knee joint meniscus to unconfined

compression. http://dx.doi.org/10.1243/0954411001535651 214, 631–635. https://doi.org/10.1243/0954411001535651

Martin Seitz, A., Galbusera, F., Krais, C., Ignatius, A., Dürselen, L., 2013. Stress-relaxation response of human menisci under confined compression conditions. J Mech Behav Biomed Mater 26, 68–80. https://doi.org/10.1016/J.JMBBM.2013.05.027

Messner Karola, Gao, J., 1998. The menisci of the knee joint. Anatomical and functional characteristics, and a rationale for clinical treatment. J Anat 193, 161–178. https://doi.org/10.1046/J.1469-7580.1998.19320161.X

Moon, H.-K., Koh, Y.-G., Kim, Y.-C., Park, Y.-S., Jo, S.-B., Kwon, S.-K., 2010. Prognostic Factors of Arthroscopic Pull-out Repair for a Posterior Root Tear of the Medial Meniscus. Am J Sports Med 40(5), 1138–1143. https://doi.org/10.1177/0363546511435622

Morejon, A., Norberg, C.D., De Rosa, M., Best, T.M., Jackson, A.R., Travascio, F., 2021. Compressive Properties and Hydraulic Permeability of Human Meniscus: Relationships With Tissue Structure and Composition. Front Bioeng Biotechnol 8, 622552. https://doi.org/10.3389/FBIOE.2020.622552/BIBTEX

Moyer, J.T., Abraham, A.C., Haut Donahue, T.L., 2012. Nanoindentation of human meniscal surfaces. J Biomech 45, 2230–2235. https://doi.org/10.1016/J.JBIOMECH.2012.06.017

Peña-Trabalon, A., Perez-Blanca, A., Moreno-Vegas, S., Belen Estebanez-Campos, M., Prado-Novoa, M., 2024. Assessment of Surrogate Models for Research on Resistance and Deformation of Repairs of the Human Meniscal Roots: Porcine or Older Human Models? Applied Sciences 2024, Vol. 14, Page 670 14, 670. https://doi.org/10.3390/APP14020670

Peña-Trabalon, A., Perez-Blanca, A., Moreno-Vegas, S., Estebanez Campos, M.B., Prado-Novoa, M., 2023. Age influence on resistance and deformation of the human sutured meniscal horn in the immediate postoperative period. Front Bioeng Biotechnol 11. https://doi.org/10.3389/FBIOE.2023.1249982/FULL

Perez-Blanca, A., Prado Nóvoa, M., Lombardo Torre, M., Espejo-Reina, A., Ezquerro Juanco, F., Espejo-Baena, A., 2018. The role of suture cutout in the failure of meniscal root repair during the early post-operative period: a

biomechanical study. Int Orthop 42, 811–818. https://doi.org/10.1007/S00264-018-3799-9/FIGURES/5

Pordzik, J., Bernstein, A., Mayr, H.O., Latorre, S.H., Maks, A., Schmal, H., Seidenstuecker, M., 2020a. Analysis of Proteoglycan Content and Biomechanical Properties in Arthritic and Arthritis-Free Menisci. Applied Sciences 2020, Vol. 10, Page 9012 10, 9012. https://doi.org/10.3390/APP10249012

Pordzik, J., Bernstein, A., Watrinet, J., Mayr, H.O., Latorre, S.H., Schmal, H., Seidenstuecker, M., 2020b. Correlation of Biomechanical Alterations under Gonarthritis between Overlying Menisci and Articular Cartilage. Applied Sciences 2020, Vol. 10, Page 8673 10, 8673. https://doi.org/10.3390/APP10238673

Prado-Novoa, M., Perez-Sanchez, L., Estebanez, B., Moreno-Vegas, S., Perez-Blanca, A., 2022. Influence of Loading Conditions on the Mechanical Performance of Multifilament Coreless UHMWPE Sutures Used in Orthopaedic Surgery. Materials 2022, Vol. 15, Page 2573 15, 2573. https://doi.org/10.3390/MA15072573

Proffen, B.L., McElfresh, M., Fleming, B.C., Murray, M.M., 2012. A comparative anatomical study of the human knee and six animal species. Knee 19, 493–499. https://doi.org/10.1016/J.KNEE.2011.07.005

Seitz, A.M., Osthaus, F., Schwer, J., Warnecke, D., Faschingbauer, M., Sgroi, M., Ignatius, A., Dürselen, L., 2021. Osteoarthritis-Related Degeneration Alters the Biomechanical Properties of Human Menisci Before the Articular Cartilage. Front Bioeng Biotechnol 9. https://doi.org/10.3389/FBIOE.2021.659989/FULL

Stärke, C., Kopf, S., Lippisch, R., Lohmann, C.H., Becker, R., 2013. Tensile Forces on Repaired Medial Meniscal Root Tears. Arthroscopy: The Journal of Arthroscopic & Related Surgery 29, 205–212. https://doi.org/10.1016/J.ARTHRO.2012.09.004

Tissakht, M., Ahmed, A.M., 1995. Tensile stress-strain characteristics of the human meniscal material. J Biomech 28, 411–422. https://doi.org/10.1016/0021-9290(94)00081-E

Warnecke, D., Balko, J., Haas, J., Bieger, R., Leucht, F., Wolf, N., Schild, N.B., Stein, S.E.C., Seitz, A.M., Ignatius, A., Reichel, H., Mizaikoff, B., Dürselen, L., 2020. Degeneration alters the biomechanical properties and

structural composition of lateral human menisci. Osteoarthritis Cartilage 28, 1482–1491. https://doi.org/10.1016/J.JOCA.2020.07.004

7

Improved computational prediction of sutured meniscus behavior under combined axial and circumferential loading: Importance of experimental conditions in compression material properties

From previous chapters of this thesis, it has been possible to characterise the mechanical behaviour of meniscal tissue around the suture hole of a repaired human meniscus when subjected to isolated circumferential tensile loading and isolated axial compression loading. Likewise, to examine the effect of loads in a physiological situation, this tissue has been characterised under combined circumferential tensile and axial compression loads, as occurs naturally in the human knee. This experimental work can be used to develop a material model that reflects the behaviour of the tissue in the area affected by its interface with the suture. Computational models of the sutured meniscus could incorporate such a material model to analyse the performance of different repair techniques in this critical area. However, the material model must be contrasted before the results can be trusted. This chapter is devoted to evaluating the influence of the experimental approach employed during indentation tests conducted to ascertain the compressive properties of meniscal tissue on the response of a FE model of the sutured meniscal horn. Having completed objectives 1 to 5 of this thesis, this chapter addresses the last of the objectives of this work set out in Section 1.2.

7.1 Introduction

As discussed in previous chapters, the surgical management of meniscal root detachment has evolved from clinical meniscectomy to meniscal root repair, employing various techniques (Feucht et al., 2014; Laprade et al., 2015b). Among these, transtibial fixation (Ahn et al., 2007; Cerminara et al., 2014; Feucht et al., 2013; Kim et al., 2006; Petersen and Zantop, 2006) and *in situ* fixation (Balke et al., 2018; Cuéllar et al., 2017; Espejo-Reina et al., 2022; Kopf et al., 2011; Padalecki et al., 2014; Petersen et al., 2014; Zantop et al., 2004) are the most widely used. As a mean for fixation, both alternatives apply sutures through the base of the meniscal horn at the root interface area. Aiming to improve the clinical outcomes, different suturing materials and methodologies have been proposed (Anz et al., 2014; Kopf et al., 2011; Mitchell et al., 2016; Vertullo et al., 2021). However, despite the advancements in these techniques, neither method fully restores the natural biomechanics of the human knee (Espejo-Reina et al., 2023, 2022; J. H. Kim et al., 2011; Lee et al., 2009; Moon et al., 2010; Seo et al., 2010) and further research is necessary.

The effectiveness of meniscal root reconstruction can be evaluated using *in vitro* studies or computational techniques. The main drawback of experimental *in vitro* studies is that tests can be conducted on a limited number of cadaveric specimens of low availability. Consequently, published studies have predominantly focused on comparing specific suturing techniques, reporting on parameters such as displacement under subcritical cyclic loading, peak load resistance, and the overall strength of the repair (Nakama et al., 2019; Robinson et al., 2018). Conversely, computational modelling allows countless comparisons of different options. However, efforts to explore the behavior of reconstructed meniscal root using this approach have been limited, with only a few models addressing this issue (D'lima et al., 2011; Steineman et al., 2020). These studies typically incorporate meniscal tissue models that omit the interface with the suture thread and often simplify the thread itself as a linear elastic element. However, simplification fails to capture the more complex behavior observed in experimental studies (Cardoso Gomide et al., 2019), underscoring the need for more sophisticated models that adequately represent the mechanical effects of the interactions between the suture and the meniscal tissue.

Existing material models describing meniscus behavior focus on the healthy meniscus and vary in complexity, from simple linear representations (Bao et al.,

2013; Peña et al., 2006; Zielinska and Haut Donahue, 2006) to more intricate non-linear models (Freutel et al., 2015; Seyfi et al., 2018). Validation of these models typically involves their implementation in computational FE frameworks, where the simulation results are compared against experimental data to ensure accuracy (Danso et al., 2015; Freutel et al., 2015; LeRoux and Setton, 2002). However, none of these models considered the effect of suture perforation through tissue on the response of the meniscal horn to suture loading. Such perforations are expected to have a notorious impact on the stress field around the suture-tissue interface, which has previously been identified as a potential major contributor to clinical repair failures (Cerminara et al., 2014; Steineman et al., 2020). Despite the possible influence of this effect on the accurate prediction of the biomechanical response of root repair, a knowledge gap exists which also extends to the broader field of meniscal tear repair in other meniscal regions. Adding experimental data to characterize the mechanical behavior of the tissue at the sutured area under various loading conditions is an essential piece of information in contributing to cover this gap.

In Chapter 6, substantial discrepancies were identified in the set of parameters that characterize the mechanical compression properties of the tissue at the sutured area when circumferential traction was applied during indentation tests in comparison to isolated compressive indentations. In light of the above, it is pertinent to consider possible benefits in incorporating the recently identified parameters into a material model of the meniscal tissue influenced by the suture.

The central hypothesis guiding this research is that the inclusion of axial compressive properties that account for the circumferential tensile effect will enhance the accuracy of a FE model's predictions regarding the behavior of the sutured meniscus under combined loading scenarios.

7.2 Materials and methods

A set of FE models of a sutured meniscal horn was developed based on a randomly selected meniscal horn specimen from those tested in Chapter 6. These models integrated the compressive properties determined from indentation tests conducted at varying levels of suture tension. The purpose of the FE models was to evaluate how the experimental conditions of the indentation test, designed to calculate the Young's modulus (E) in axial compression of the meniscus tissue

near the puncture site, affected the initial linear elastic response under compressive loading.

7.2.1 Development of the Finite Element models

The experimental settings of the indentation study described in Section 6.2.3.1 of Chapter 6 were replicated in the models, and the maximum force at each measurement point was calculated for different traction conditions, T (unloaded, 10 N, or 20 N in the suture). Subsequently, the computed force values were compared with the corresponding experimental forces, $F^{i,T}$, obtained under the same conditions as described in Chapter 6. The *in silico* tests utilized the compressive Young's modulus, E, derived from the experimental IM in the absence of suture traction and under 20N suture tension. This level of suture tension was chosen as the most extreme loads analysed, although in Section 6.3.2 of Chapter 6 it was noted that there were no significant differences in the IM values obtained at 10 N and 20 N of circumferential tensile load.

The geometry of the meniscal horn sample was reconstructed in SolidWorks® (SolidWorks® 2023, Dassault Systèmes, France), a software for 3D modelling of components and assemblies and 2D drawings, using the dimensions measured before the experimental testing as it was explained in Section 6.2.1 of Chapter 6 and the coordinates of the indentation points. A suture hole with a diameter of 0.5 mm was perforated at the corresponding location of the experimental specimen. This geometric model was then exported to the FE simulation software Abaqus® (Abaqus® Standard 2023, Dassault Systèmes, France), where the spherical indenter tip, a 2 mm of diameter ruby ball, was incorporated into the model prior to the definition of the finite element simulations (Figure 7.1).

The mesh was automatically generated using the free meshing algorithm available in Abaqus® (Abaqus® Standard 2023, Dassault Systèmes, France). Second-order tetrahedral elements were selected (Figure 7.2), with average element sizes of 0.58 mm for the meniscal horn and 0.14 mm for the indenter tip. The defined element sizes introduced a minimum of three elements over the smallest dimension of the modelled solids and were considered appropriate for the comparative analysis carried out. This meshing strategy resulted in a total of 22,878 elements for the meniscal horn and 2,208 elements for the indenter tip. The indenter tip was modeled as an isotropic linear elastic material characterized by $E = 345000\ MPa$ and $\mu = 0.3$ ("Ruby Sapphire Balls | Salem Specialty Ball,").

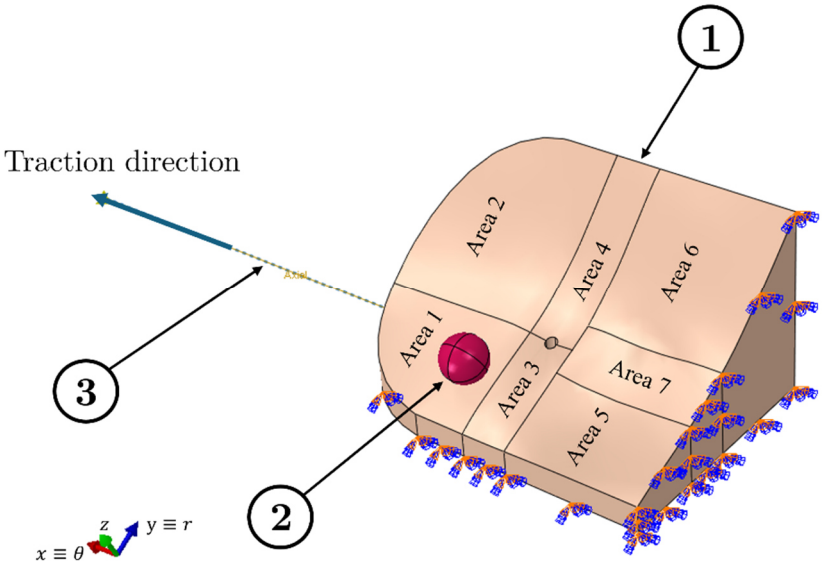

Figure 7.1. Representation of the modelled meniscal horn with the specified boundary conditions. The seven areas where distinct compression modulus were assigned are illustrated: (1) meniscal horn model incorporating the suture hole; (2) modelled indenter tip; (3) suture thread. The blue arrow indicates the direction of traction. The indentation direction matches the Z-axis of the orientation system depicted.

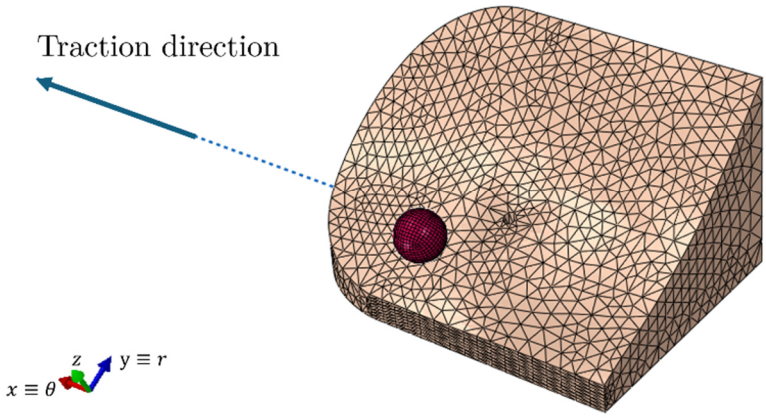

Figure 7.2. Meshes of the sutured meniscal horn and the tip of the indenter. A linear elastic axial spring modelled the suture. The blue arrow indicates the traction direction.

The UHWPE suture thread was modeled as a linear elastic axial spring aligned with the direction of traction. The material properties of the suture were defined using a spring constant $K_{suture} = 58.58\, N/mm$, based on prior mechanical testing of similar suture materials (Prado-Novoa et al., 2022).

Two distinct strategies were employed to characterize the material properties of the meniscal tissue at the sutured horn, utilizing orthotropic material models with transverse isotropy in the plane normal to the circumferential direction, θ.

- **Strategy 1**: The meniscal horn was segmented into seven distinct regions (Figure 7.1) surrounding the experimental indentation sites. Each region was assigned mechanical properties based on two distinct property sets. For Property Set 1, the Young's modulus values in the axial (z) and radial (r) directions were derived from the IM obtained from indentation tests performed under no traction condition (0 N) in each region (Table 7.1). For Property Set 2, the Young's modulus values were based on the instantaneous modulus from indentation tests conducted under the maximum traction condition of 20 N in each region (Table 7.1). Other material properties, including $E_\theta = 140\ MPa;\ G_{z\theta} = G_{r\theta} = 50MPa;\ \upsilon_{z\theta} = \upsilon_{r\theta} = 0.3;$ and $\upsilon_{rz} = 0.2$ were obtained from existing literature (Vaziri et al., 2008).

- **Strategy 2**: An alternative approach involved applying a uniform material model to the entire meniscal horn, without subdividing it into regions. Two property sets were utilized for this global model. Property Set 3 utilized Young's modulus value in the z and r directions obtained by averaging the instantaneous modulus data obtained at every indentation point from the tests of all specimens under pure compression conditions (Table 7.1). Property Set 4 employed Young's modulus value as the mean instantaneous modulus value derived from indentation tests of all specimens conducted under the maximum traction level of 20 N (Table 7.1). The remaining mechanical properties for both Property Sets 3 and 4 were consistent with those used in the first strategy.

The displacement of the caudal surface of the meniscal horn in contact with the 3D printed support was constrained in the indentation direction, allowing the displacements in the other two axis. Following the experimental procedure explained in Section 6.2.3.1 of Chapter 6, the surface representing the cutting plane is completely constrained simulating the effect of the adhesive (Figure 6.6)

Following a non-linear approach with an automatic time incrementation and a direct method equation solver, the simulations were executed in a two-step process:

- **Step 1**: A linear ramp displacement was applied to the free end of the suture, directly acting on the suture hole to impose the desired tensile load on the circumferential fibers of the meniscal horn. This phase replicated the tensile effect of the traction device depicted in Figure 6.3. The maximum displacement applied at each testing condition was adjusted to match the corresponding experimental force, resulting in: 0 mm for the unloaded state, 0.23 mm for the 10 N traction level, and 0.44 mm for the 20 N traction level.

- **Step 2**: While maintaining the final displacement of step 1, a 0.5 mm indentation was executed by placing the indenter tip on a designated measurement point on the meniscal horn and applying a ramp displacement of the indenter tip in the direction of indentation, while restricting any other ruby ball movements. The contact between the indenter tip and the cranial surface of the meniscal horn was modeled as a Surface-to-Surface interaction with hard contact behavior. This indentation procedure was then applied systematically to each measurement point.

In total, 84 Finite Element models were simulated, encompassing four different material property sets, three traction levels, and seven indentation points.

7.2.2 Computational indentation test analysis

The compressive force required to achieve a vertical displacement of 0.5 mm by the indenter tip was determined by calculating the reaction force exerted on the indenter. This computed force was then compared to the maximum experimental force measured at the corresponding point and under the same loading conditions, denoted as $F^{i,T}$.

To evaluate the accuracy of the mechanical property sets defined in the FE models, the differences between the maximum forces recorded in the simulated and experimental indentation tests were analyzed. This comparison specifically focused on validating the appropriateness of the instantaneous modulus, used as the Young's modulus, in accurately representing the material behavior under the given conditions.

For the finite element models of the specific sample developed using the first strategy, *S1*, the error at each traction level was calculated as the mean absolute difference between the simulated and experimental maximum indentation forces across the seven measurement points. This error was expressed relative to the mean experimental force for the corresponding traction level:

$$Error_{s1}^{T} = \frac{\sum_{i=1}^{7} \left| F_{exp,j}^{i,T} - F_{sim,j}^{i,T} \right|}{\sum_{i=1}^{7} F_{exp,j}^{i,T}} \tag{7.1}$$

where i denotes the measurement point; $T = 0N, 20N$ represents the traction level; j indicates the modelled specimen; exp refers to experimental values and sim refers to simulated ones.

For the finite element models developed using the second strategy, *S2*, the error for each traction level was determined as the mean absolute difference between the simulated and experimental maximum indentation forces at the seven measurement points. This difference was compared to the global mean experimental force obtained across all samples:

$$Error_{s2}^{T} = \frac{\sum_{i=1}^{7} \left| F_{exp,j}^{i,T} - F_{sim,j}^{i,T} \right|}{(\sum_{j=1}^{M} \sum_{i=1}^{7} F_{exp,j}^{i,T})/M} \tag{7.2}$$

where M=27 is the number of samples.

7.3 Results

In this section, the comparison between the experimental and simulated maximum forces are shown with the different errors explained in Section 7.2.2.

The results shown in this chapter correspond to mean values. For all values, see appendix D.

7.3.1 Computational results

Table 7.1 lists the experimentally computed instantaneous modulus in the unloaded and 20 N traction loading conditions for each indentation point of the specific specimen selected for computational modelling and the mean instantaneous modulus obtained after testing all the specimens ($n = 27$) in Chapter 6.

Table 7.1. Columns 1 to 7 show IM values from the indentation test at the seven measurement points of the modelled specimen under suture traction levels 0 and 20 N. Column 8 displays mean and SD values of IM pooled for the twenty-seven specimens tested also at both traction levels.

	Modelled specimen							**Pooled mean (n=27)**
	1	**2**	**3**	**4**	**5**	**6**	**7**	
IM^0 (MPa)	0.209	0.177	0.504	0.168	1.712	0.268	1.044	0.651 (0.20)
IM^{20} (MPa)	1.374	0.531	1.133	0.684	2.051	0.645	3.011	1.450 (0.30)

Table 7.2 summarizes the prediction errors for the maximum force in the indentation tests as simulated by the FE models across seven measurement points. The errors are presented in two columns:

- **Column 1** displays the errors for FE models that incorporated specimen-specific material compression properties at each indentation location, corresponding to property sets 1 and 2.

- **Column 2** shows the errors for FE models in which Young's modulus was set to the mean IM derived from tests on 27 specimens under various loading conditions, corresponding to property sets 3 and 4.

Table 7.2. Errors between experimental and simulated $\boldsymbol{F^T}$ values for the four property sets considered.

	$\boldsymbol{Error^T_{S1}}$	$\boldsymbol{Error^T_{S2}}$
Error of $F^{i,0}_{max}$ with $IM^{i,0}$	0.30	0.63
Error of $F^{i,0}_{max}$ with $IM^{i,20}$	1.07	1.24
Error of $F^{i,10}_{max}$ with $IM^{i,0}$	0.34	0.50
Error of $F^{i,10}_{max}$ with $IM^{i,20}$	0.23	0.31
Error of $F^{i,20}_{max}$ with $IM^{i,0}$	0.46	0.49
Error of $F^{i,20}_{max}$ with $IM^{i,20}$	0.09	0.27

For both types of material models, computed errors were lower when the axial Young's modulus was derived from test conducted under similar traction conditions, i.e. with or without applied circumferential traction. In instances where traction was applied, a reduction in error was observed for both loading

level. As expected, errors in Column 1 are smaller, indicating a higher level of accuracy using specimen-specific Young modulus. However, the improvement in prediction accuracy observed extend also to the models represented in Column 2, which use mean properties.

7.4 Discussion

The findings of this study indicate that using compression properties obtained from indentation tests that account for the circumferential traction conditions imposed by suture improves the predictive accuracy of a material model that represents the behavior of the sutured meniscal horn tissue. Specifically, when determining the Young's modulus in axial compression using the instant indentation modulus, the simulations achieve higher accuracy when the indentation tests incorporate the traction condition present in the modeled scenario.

The human meniscus is subjected to physiological compressive loads resulting from tibiofemoral contact, combined with circumferential traction, particularly in the horn region. This circumferential traction is either due to the meniscal root attachments in a healthy meniscus or from sutures in the case of surgical repair. FE models are extensively used to analyze the physiological performance of the meniscus under these conditions (Donahue et al., 2002; Imeni et al., 2020; LeRoux and Setton, 2002; Vaziri et al., 2008). In this study, FE models were developed to simulate a sutured meniscal horn using a simplified elastic orthotropic material model. This material model, characterized by a limited number of parameters, was employed to explore the variability in mechanical response associated with different values of compression Young's modulus, E.

Given that no significant differences were observed in Chapter 6 between the instantaneous modulus for 10 N and 20 N of suture traction, the Young's modulus for axial compression was derived from the IM under two conditions: with no suture-induced traction and with maximum suture-induced traction. The IM obtained under the 20 N traction condition was selected for analysis, as it represents the highest loading level tested. Indentation tests are frequently utilized to determine the Young's modulus of axial compression for the meniscus in FE models (Danso et al., 2015; Fischenich et al., 2015; Pordzik et al., 2020b; Seitz et al., 2021), and this approach is also commonly applied to other soft

biological tissues (Choi and Zheng, 2005; Hori and Mockros, 1976; Iivarinen et al., 2011).

Material properties not explicitly addressed in this study were sourced from existing literature (Donahue et al., 2002; Imeni et al., 2020; Vaziri et al., 2008). It is important to highlight that other studies frequently report axial Young's modulus values that are up to two orders of magnitude higher than those employed in our models. These higher values are generally obtained from tensile tests, where the stiffness of collagen fibrils plays a dominant role in the results (Danso et al., 2015). In contrast, our Finite Element models were specifically designed to simulate axial compression. Therefore, axial Young's modulus was determined using data from indentation tests, ensuring consistency with the magnitude of values reported in similar studies (Danso et al., 2015; Fischenich et al., 2015; Seitz et al., 2021).

To our knowledge, previous meniscal indentation tests have typically been conducted on specimens that were not subjected to simultaneous traction loads. In contrast, this FE analysis revealed that the accuracy of predictions for a sutured meniscal specimen, under both isolated compression and combined with suture-induced circumferential traction, improved when using material models that incorporate compression properties derived from indentation tests conducted under similar loading conditions. The circumferential stress in the simulations surpassed the toe region of the load-deformation curve observed in load-to-failure tests of Chapter 6. It is noteworthy that the maximum physiological loads experienced by meniscal roots during daily activities, though not extensively studied, have been reported to exceed the F_{toe} value identified in the load-to-failure test (Espejo-Reina et al., 2023; Stärke et al., 2013). Consequently, our findings of a more accurate estimate of Young's modulus for finite element models of sutured meniscal horns apply to simulations of physiological conditions that involve both axial compression and circumferential traction beyond the toe region of the load-deformation curve, regardless of the value of traction applied after over the toe force, due to the absence of differences in the IM between circumferential load values that lie in the linear zone of the load-deformation curve exceeding the toe force.

Two Finite Element models were developed for the same meniscus: one in which Young's modulus for axial compression was determined from tests conducted specifically at the location of the modeled specimen, and another in

which Young's modulus was set to the average value derived from tests on 27 different menisci. The model utilizing specimen-specific data demonstrated smaller errors when compared to the experimental results for that particular specimen, indicating higher accuracy. However, the model using the average Young's modulus value offers greater applicability in clinical settings, as current technology does not permit in vivo indentation testing of each patient's meniscus. This broader applicability makes the average-based model more practical for general use despite the trade-off in precision.

7.5 Conclusions

The computational simulations indicated that the tissue response around the suture hole, when subjected to combined axial compression and suture-induced circumferential traction beyond F_{toe}, is more accurately represented using material models with compressive properties derived from indentation tests conducted under suture traction conditions. This modeling approach yielded more precise predictions compared to models that relied solely on pure axial compression test data.

7.6 References

Ahn, J.H., Wang, J.H., Yoo, J.C., Noh, H.K., Park, J.H., 2007. A pull out suture for transection of the posterior horn of the medial meniscus: Using a posterior trans-septal portal. Knee Surgery, Sports Traumatology, Arthroscopy 15, 1510–1513. https://doi.org/10.1007/S00167-007-0310-3/FIGURES/6

Anz, A.W., Branch, E.A., Saliman, J.D., 2014. Biomechanical Comparison of Arthroscopic Repair Constructs for Meniscal Root Tears. Am J Sports Med 42 (11), 2699–2706. https://doi.org/10.1177/0363546514549445

Balke, M., Akoto, R., Offerhaus, C., Hoeher, J., 2018. Suture Anchor Refixation of Meniscal Root Tears Without an Additional Portal. Arthrosc Tech 7, e511–e515. https://doi.org/10.1016/J.EATS.2018.01.003

Bao, H.R.C., Zhu, D., Gong, H., Gu, G.S., 2013. The effect of complete radial lateral meniscus posterior root tear on the knee contact mechanics: A finite element analysis. Journal of Orthopaedic Science 18, 256–263. https://doi.org/10.1007/S00776-012-0334-5/TABLES/3

Cardoso Gomide, L., De Oliveira Campos, D., Amaral Araújo, C., Lima Menegaz, G., Silva Cardoso, R., Crosara Saad, S., 2019. Mechanical study of the properties of sutures used in orthopaedics surgeries. Rev. Bras. Ortop. 54, 247–252. https://doi.org/10.1016/J.RBO.2018.02.001/ID/OR170225-10

Cerminara, A.J., LaPrade, C.M., Smith, S.D., Ellman, M.B., Wijdicks, C.A., LaPrade, R.F., 2014. Biomechanical Evaluation of a Transtibial Pull-out Meniscal Root Repair Challenging the Bungee Effect. American Journal of Sports Medicine 42, 2988–2995. https://doi.org/10.1177/0363546514549447

Choi, A.P.C., Zheng, Y.P., 2005. Estimation of Young's modulus and Poisson's ratio of soft tissue from indentation using two different-sized indentors: Finite element analysis of the finite deformation effect. Med Biol Eng Comput 43, 258–264. https://doi.org/10.1007/BF02345964/METRICS

Cuéllar, Adrián, Cuéllar, Asier, Sánchez, A., Cuéllar, R., 2017. Posterior Lateral Meniscus Root Reattachment With Suture Anchors: An Arthroscopic Technique. Arthrosc Tech 6, e1919–e1925. https://doi.org/10.1016/J.EATS.2017.07.011

Danso, E.K., Mäkelä, J.T.A., Tanska, P., Mononen, M.E., Honkanen, J.T.J., Jurvelin, J.S., Töyräs, J., Julkunen, P., Korhonen, R.K., 2015. Characterization of site-specific biomechanical properties of human meniscus—Importance of collagen and fluid on mechanical nonlinearities. J Biomech 48, 1499–1507. https://doi.org/10.1016/J.JBIOMECH.2015.01.048

D'lima, D.D., Chen, P.C., Kessler, O., Hoenecke, H.R., Colwell, C.W., 2011. Effect of Meniscus Replacement Fixation Technique on Restoration of Knee Contact Mechanics and Stability. MCB 8, 123–134.

Donahue, T.L.H., Hull, M.L., Rashid, M.M., Jacobs, C.R., 2002. A Finite Element Model of the Human Knee Joint for the Study of Tibio-Femoral Contact. J Biomech Eng 124, 273–280. https://doi.org/10.1115/1.1470171

Espejo-Reina, A., Prado-Novoa, M., Espejo-Baena, A., Estebanez, B., Perez-Blanca, A., 2023. Improved tibiofemoral contact restoration after transtibial reinsertion of the anterior root of the lateral meniscus compared to in situ repair: a biomechanical study. Int Orthop 1, 3. https://doi.org/10.1007/s00264-023-05769-y

Espejo-Reina, A., Prado-Novoa, M., Espejo-Baena, A., Peña-Trabalon, A., Perez-Blanca, A., 2022. Biomechanical consequences of anterior root detachment

of the lateral meniscus and its reinsertion. Sci Rep 12, 6182. https://doi.org/10.1038/S41598-022-10229-5

Feucht, M.J., Grande, E., Brunhuber, J., Burgkart, R., Imhoff, A.B., Md, §, Braun, S., 2013. Biomechanical Evaluation of Different Suture Techniques for Arthroscopic Transtibial Pull-out Repair of Posterior Medial Meniscus Root Tears. Am J Sports Med 41, 2784–2790. https://doi.org/10.1177/0363546513502464

Feucht, M.J., Grande, E., Brunhuber, J., Rosenstiel, N., Burgkart, R., Imhoff, A.B., Braun, S., 2014. Biomechanical comparison between suture anchor and transtibial pull-out repair for posterior medial meniscus root tears. American Journal of Sports Medicine 42, 187–193. https://doi.org/10.1177/0363546513502946/ASSET/IMAGES/LARGE/10.1177_0363546513502946-FIG2.JPEG

Fischenich, K.M., Lewis, J., Kindsfater, K.A., Bailey, T.S., Haut Donahue, T.L., 2015. Effects of degeneration on the compressive and tensile properties of human meniscus. J Biomech 48, 1407–1411. https://doi.org/10.1016/J.JBIOMECH.2015.02.042

Freutel, M., Galbusera, F., Ignatius, A., Dürselen, L., 2015. Material properties of individual menisci and their attachments obtained through inverse FE-analysis. J Biomech 48, 1343–1349. https://doi.org/10.1016/J.JBIOMECH.2015.03.014

Hori, R.Y., Mockros, L.F., 1976. Indentation tests of human articular cartilage. J Biomech 9, 259–268. https://doi.org/10.1016/0021-9290(76)90012-9

Iivarinen, J.T., Korhonen, R.K., Julkunen, P., Jurvelin, J.S., 2011. Experimental and computational analysis of soft tissue stiffness in forearm using a manual indentation device. Med Eng Phys 33, 1245–1253. https://doi.org/10.1016/J.MEDENGPHY.2011.05.015

Imeni, M., Seyfi, B., Fatouraee, N., Samani, A., 2020. Constitutive modeling of menisci tissue: a critical review of analytical and numerical approaches. Biomech Model Mechanobiol 19, 1979–1996. https://doi.org/10.1007/S10237-020-01352-1/TABLES/5

Kim, J.H., Chung, J.H., Lee, D.H., Lee, Y.S., Kim, J.R., Ryu, K.J., 2011. Arthroscopic Suture Anchor Repair Versus Pullout Suture Repair in Posterior Root Tear of the Medial Meniscus: A Prospective Comparison Study.

Arthroscopy: The Journal of Arthroscopic & Related Surgery 27, 1644–1653. https://doi.org/10.1016/J.ARTHRO.2011.06.033

Kim, Y.M., Rhee, K.J., Lee, J.K., Hwang, D.S., Yang, J.Y., Kim, S.J., 2006. Arthroscopic pullout repair of a complete radial tear of the tibial attachment site of the medial meniscus posterior horn. Arthroscopy 22, 795.e1-795.e4. https://doi.org/10.1016/J.ARTHRO.2005.12.040

Kopf, S., Colvin, A.C., Muriuki, M., Zhang, X., Harner, C.D., 2011. Meniscal root suturing techniques: Implications for root fixation. American Journal of Sports Medicine 39, 2141–2146. https://doi.org/10.1177/0363546511413250/ASSET/IMAGES/LARGE/10.1177_0363546511413250-FIG2.JPEG

Laprade, R.F., Laprade, C.M., James, E.W., 2015. Recent advances in posterior meniscal root repair techniques. Journal of the American Academy of Orthopaedic Surgeons 23, 71–76. https://doi.org/10.5435/JAAOS-D-14-00003

Lee, J.H., Lim, Y.J., Kim, K.B., Kim, K.H., Song, J.H., 2009. Arthroscopic Pullout Suture Repair of Posterior Root Tear of the Medial Meniscus: Radiographic and Clinical Results With a 2-Year Follow-up. Arthroscopy: The Journal of Arthroscopic & Related Surgery 25, 951–958. https://doi.org/10.1016/J.ARTHRO.2009.03.018

LeRoux, M.A., Setton, L.A., 2002. Experimental and Biphasic FEM Determinations of the Material Properties and Hydraulic Permeability of the Meniscus in Tension. J Biomech Eng 124, 315–321. https://doi.org/10.1115/1.1468868

Mitchell, R., Pitts, R., Kim, Y.M., Matava, M.J., 2016. Medial Meniscal Root Avulsion: A Biomechanical Comparison of 4 Different Repair Constructs. Arthroscopy: The Journal of Arthroscopic & Related Surgery 32, 111–119. https://doi.org/10.1016/J.ARTHRO.2015.07.013

Moon, H.-K., Koh, Y.-G., Kim, Y.-C., Park, Y.-S., Jo, S.-B., Kwon, S.-K., 2010. Prognostic Factors of Arthroscopic Pull-out Repair for a Posterior Root Tear of the Medial Meniscus. Am J Sports Med 40(5), 1138–1143. https://doi.org/10.1177/0363546511435622

Nakama, G.Y., Aman, Z.S., Storaci, H.W., Kuczmarski, A.S., Krob, J.J., Strauss, M.J., 2019. Different Suture Materials for Arthroscopic Transtibial Pull-out Repair of Medial Meniscal Posterior Root Tears: A Human

Biomechanical Study. Orthop J Sports Med 7. https://doi.org/10.1177/2325967119873274/ASSET/IMAGES/LARGE/10.1177_2325967119873274-FIG6.JPEG

Padalecki, J.R., Jansson, K.S., Smith, S.D., Dornan, G.J., Pierce, C.M., Wijdicks, C.A., Laprade, R.F., 2014. Biomechanical consequences of a complete radial tear adjacent to the medial meniscus posterior root attachment site: In situ pull-out repair restores derangement of joint mechanics. American Journal of Sports Medicine 42, 699–707. https://doi.org/10.1177/0363546513499314

Peña, E., Calvo, B., Martínez, M.A., Doblaré, M., 2006. A three-dimensional finite element analysis of the combined behavior of ligaments and menisci in the healthy human knee joint. J Biomech 39, 1686–1701. https://doi.org/10.1016/J.JBIOMECH.2005.04.030

Petersen, W., Forkel, P., Feucht, M.J., Zantop, T., Imhoff, A.B., Brucker, P.U., 2014. Posterior root tear of the medial and lateral meniscus. Arch Orthop Trauma Surg 134, 237–255. https://doi.org/10.1007/S00402-013-1873-8/TABLES/3

Petersen, W., Zantop, T., 2006. Avulsionsverletzung des außenmeniskushinterhorns. Arthroskopische refixationstechnik. Unfallchirurg 109, 984–987. https://doi.org/10.1007/S00113-006-1193-3/FIGURES/4

Pordzik, J., Bernstein, A., Watrinet, J., Mayr, H.O., Latorre, S.H., Schmal, H., Seidenstuecker, M., 2020. Correlation of Biomechanical Alterations under Gonarthritis between Overlying Menisci and Articular Cartilage. Applied Sciences 2020, Vol. 10, Page 8673 10, 8673. https://doi.org/10.3390/APP10238673

Prado-Novoa, M., Perez-Sanchez, L., Estebanez, B., Moreno-Vegas, S., Perez-Blanca, A., 2022. Influence of Loading Conditions on the Mechanical Performance of Multifilament Coreless UHMWPE Sutures Used in Orthopaedic Surgery. Materials 2022, Vol. 15, Page 2573 15, 2573. https://doi.org/10.3390/MA15072573

Robinson, J.R., Frank, E.G., Hunter, A.J., Jermin, P.J., Gill, H.S., 2018. The Strength of Transosseous Medial Meniscal Root Repair Using a Simple Suture Technique Is Dependent on Suture Material and Position. American Journal of Sports Medicine 46, 924–932. https://doi.org/10.1177/0363546517749807/ASSET/IMAGES/LARGE/10.1177_0363546517749807-FIG7.JPEG

Supplier of Precision Balls, n.d. Ruby Sapphire Balls | Salem Specialty Ball [WWW Document]. URL https://www.salemball.com/ruby-sapphire-balls/ (accessed 15.3.24).

Seitz, A.M., Osthaus, F., Schwer, J., Warnecke, D., Faschingbauer, M., Sgroi, M., Ignatius, A., Dürselen, L., 2021. Osteoarthritis-Related Degeneration Alters the Biomechanical Properties of Human Menisci Before the Articular Cartilage. Front Bioeng Biotechnol 9. https://doi.org/10.3389/FBIOE.2021.659989/FULL

Seo, H.S., Lee, S.C., Jung, K.A., 2010. Second-Look Arthroscopic Findings After Repairs of Posterior Root Tears of the Medial Meniscus. https://doi.org/10.1177/0363546510382225 39, 99–107. https://doi.org/10.1177/0363546510382225

Seyfi, B., Fatouraee, N., Imeni, M., 2018. Mechanical modeling and characterization of meniscus tissue using flat punch indentation and inverse finite element method. J Mech Behav Biomed Mater 77, 337–346. https://doi.org/10.1016/J.JMBBM.2017.09.023

Stärke, C., Kopf, S., Lippisch, R., Lohmann, C.H., Becker, R., 2013. Tensile Forces on Repaired Medial Meniscal Root Tears. Arthroscopy: The Journal of Arthroscopic & Related Surgery 29, 205–212. https://doi.org/10.1016/J.ARTHRO.2012.09.004

Steineman, B.D., LaPrade, R.F., Haut Donahue, T.L., 2020. Nonanatomic placement of posteromedial meniscal root repairs: A finite element study. J Biomech Eng 142. https://doi.org/10.1115/1.4045893/1072350

Vaziri, A., Nayeb-Hashemi, H., Singh, A., Tafti, B.A., 2008. Influence of meniscectomy and meniscus replacement on the stress distribution in human knee joint. Ann Biomed Eng 36, 1335–1344. https://doi.org/10.1007/S10439-008-9515-Y/FIGURES/5

Vertullo, C.J., Cadman, J., Dabirrahmani, D., Appleyard, R., 2021. Biomechanical Comparison of an All-Inside Meniscal Repair Device Construct Versus Pullout Sutures for Arthroscopic Transtibial Repair of Posterior Medial Meniscus Root Tears A Matched-Pair Cadaveric Study. Orthop J Sports Med 9(4), 23259671211000464. https://doi.org/10.1177/23259671211000464

Zantop, T., Eggers, A.K., Weimann, A., Hassenpflug, J., Petersen, W., 2004. Initial Fixation Strength of Flexible All-Inside Meniscus Suture Anchors

in Comparison to Conventional Suture Technique and Rigid Anchors Biomechanical Evaluation of New Meniscus Refixation Systems and the. https://doi.org/10.1177/0363546503260749

Zielinska, B., Haut Donahue, T.L., 2006. 3D Finite Element Model of Meniscectomy: Changes in Joint Contact Behavior. J Biomech Eng 128, 115–123. https://doi.org/10.1115/1.2132370

8

Conclusions and Future Works

This thesis aims to the general objective of to contribute to the advancement of the scientific understanding of the biomechanics of the sutured human meniscal horn when subjected to physiological loads, with the goal of contributing to the improvement of the surgical treatment of meniscal root avulsions.

Firstly, a review was conducted of the most important anatomical, physiological and mechanical aspects to highlight the importance of the meniscus and its articular connections, with special attention to the role played by the meniscal roots as the main restrictors of meniscal movement. Likewise, the consequences of a complete tear of the roots were presented, along with a review of the repair techniques currently applied.

The experimental and computational work presented in the next chapters of thesis aims to fulfill the six specific objectives listed in section 1.2 of Chapter 1.

8.1 Conclusions of the thesis

The main conclusions derived from the experimental works performed by subjecting the menisci to traction load-to-failure tests in the direction of their circumferential fibers can be summarized as follows:

- At the tissue level, meniscal horns from individuals over 75 years old demonstrate increased elasticity and decreased tissue resistance to cut-out at the suture hole compared to those from younger specimens.

- At the specimen level, aging is associated with a thickening of the meniscal horns which may influence the overall mechanical performance of the menisci in the context of root surgical repair. Indeed, menisci from donors over 75 years old show comparable resistance to younger specimens, in terms of the force necessary to initiate tearing and the maximum force in

a load-to-failure test, probably due to the fact that this age-related thickening compensates for the decreased tissue resistance.

Regarding the suitability of porcine or older human models as a surrogate for the human meniscus at the age considered routinely eligible for root surgical repair, this thesis has concluded that:

- Neither porcine nor cadaveric menisci from donors over 75 years old serve as an accurate overall model for replicating the behavior of the adult human meniscus under the age of 75. Differences in elasticity, thickness, and resistance limit the ability of these models to accurately represent the mechanical properties of younger human menisci, and each model offers advantages depending on the study's objectives.

- The older human meniscus is a more appropriate surrogate for investigating the resistance of sutured meniscal root at the specimen level, particularly in relation to cut-out resistance.

- The porcine model provides a more accurate representation around the suture site of deformation-related properties at the tissue level.

After subjecting human meniscus samples to experimental pure unconfined indentation tests and indentation tests that included suture-induced tensile loads in the circumferential direction, it can be stated that:

- The compressive properties of the sutured human meniscal horns are significantly affected by the presence of circumferential tensile loads.

- The maximum force during relaxation, the instantaneous modulus, and the relaxation modulus more than double their values when suture-induced traction is involved in the test compared to the unloaded condition.

- No differences are observed in the compressive properties when suture-induced circumferential traction is applied at different load levels exceeding those corresponding to the toe region of the stress-strain curve obtained in traction load-to-failure tests in the direction of their circumferential fibers.

- No correlation is found between the compressive and tensile properties studied.

The main conclusions derived from the development and validation of the computational model of sutured meniscus can be summarised as follows:

- Computational simulations show that the compressive behavior of the tissue around the suture hole under combined axial compression and suture-generated circumferential traction, is more accurately predicted with material models that use compressive properties obtained from indentation tests involving suture traction, rather than from pure axial compression tests.

8.2 Future works

This thesis has explored aspects related to the mechanical behavior of the sutured meniscal horn. Understanding this field is essential for improving the surgical treatment of meniscal root avulsion, a clinical procedure with significant room for improvement, as current solutions have been shown to be insufficient in completely restoring the biomechanics of the natural knee.

Therefore, some research topics are proposed to further advance the general objective of this thesis:

- Experimental research in the possible variability between experimental outcomes of porcine models in the field of meniscal research specifically porcine specimens with differences in specie, breed, diet, housing conditions and other factors that may introduce significant variability, even within the same species. This topic is considered important since porcine models are used by this research group and many others, given their low economic cost and the greater availability of specimens. However, it is necessary to verify that the results offered by the different researchers are not altered by variables such as those mentioned above.

- Clinical research on the efficacy and performance of meniscal root repair in patients aged 55 to 75 years. The proposed study would involve a prospective clinical investigation comparing the outcomes of meniscal root repair between patients currently considered routinely eligible for this surgical intervention (<55 years) and those in the 55-75 age group . This comparison aims to corroborate one of the main biomechanical conclusions of this thesis.

This study is important because the in-vitro experiments in this thesis found no significant biomechanical differences between young and middle-aged specimens. However, these experiments lacked the inherent limitations of in-vivo studies, as detailed in Chapter 4, particularly because critical biological factors influencing the healing process could not be accounted for.

This work would be essential for the scientific community to establish a clearer consensus on increasing the upper age limit for patients undergoing this type of repair, which could significantly improve the quality of life in an increasingly active older population.

- Development of a specific material model to accurately reflect the tensile and deformation behavior of the suture-affected meniscal horn tissue under various loading conditions, specifically adjusted to physiological loading.

The material model could be based on the experimental data obtained from the load-to-failure and indentation tests performed in this thesis. However, it is recommended to add further experimental data, particularly by performing indentation tests under a wider range of loading conditions on the suture. In Chapter 6 of this thesis, no differences were found in the compressive properties of the meniscal specimens when subjected to circumferential tensions induced by 10N and 20N of suture traction. It was hypothesized that this was because both conditions induced stress states that exceeded the well-known toe zone of the stress-strain curve from circumferential traction tests. This toe zone is considered where the straightening and alignment of meniscal fibers occur prior to their stretching. As noted in the corresponding chapter, this hypothesis must be confirmed before it can be included in a material model, and for this purpose, tests under a broader range of loading conditions are required. This point is critical because physiological stress states associated with daily activities have been reported to be above this toe zone.

For this work, the use of inverse FE models that calibrate the material model through optimal parameter estimation, thereby minimizing discrepancies between simulated and experimental results, is proposed. Among the various techniques available for this task, genetic algorithms stand out for their effectiveness in optimizing material model parameters

by iteratively reducing the error between experimental and simulation data without falling into local minima.

- Development of an FE model of a human meniscus with suture-repaired root, representative of individuals under 75 years of age, which, from a biomechanical perspective, is the age range conducive to clinical repair according to the conclusions of this thesis.

  Existing human meniscus FE models typically incorporate material properties derived from experimental studies on older human or animal models, primarily due to their greater availability. However, as demonstrated in this thesis, the biomechanical properties obtained with these surrogate models are not fully representative of meniscal tissue behavior in younger populations, who are candidates for surgical repair.

  Furthermore, the experimental studies that quantify meniscal mechanical properties published in the scientific literature have been performed on healthy specimens, without accounting for the impact of suturing. The improvement in FE model predictions that could be achieved by applying different material models, or adjusting parameters within the same model, to areas affected or unaffected by the suture should be assessed.

  Finally, age-related anatomical changes in human menisci, specifically thickening in the meniscal root zone, have also been demonstrated in this thesis. It is proposed to include at least one of the following approaches in the FE model:

  - Modeling a representative geometry of the younger meniscus. This would require better characterization of its dimensions in the age range below 75 years. In this thesis, only the thickness in the suture area has been analyzed, as this was the variable expected to have the greatest impact on cut-out resistance and deformation around the suture hole. However, in a complete meniscal model, other dimensions could be crucial due to their important influence on the distribution of pressures on the cartilages and the tibiofemoral contact area.

  - Defining a parametric geometry based on dimensions that can currently be measured in vivo, through ultrasound, MRI, or CT scans. This approach would aim to develop a patient-specific model tailored to the individual's anatomy, since in-vivo measurement of mechanical properties remains an unsolved issue (although some research groups are working on this topic).

The proposed FE model aims to provide a more accurate and realistic computational framework for studying the post-repair biomechanical behavior of human meniscal tissue and evaluating the impact of various surgical technique modifications, with the ultimate goal of optimizing surgical outcomes.

- Development of a comprehensive FE model of the repaired human knee, incorporating a meniscus FE model with a suture-repaired root representative of individuals under 75 years of age. This model would integrate the mechanical behavior of the surgical suture, both with and without a previous loading history, which has been another line of research in BIOCLINA.

This model is especially important because it will allow, on the one hand, the computational study of biomechanical effects that cannot be analyzed in isolated meniscus-suture models, such as the influence of surrounding tissues on different surgical techniques. On the other hand, it will enable the analysis of how different surgical repairs impact the joint as a whole, such as: modification of knee kinematics, ability to restore natural contact biomechanics, which greatly influences cartilage loading and its role in the development of early osteoarthritis, and other factors. Key parameters to be analyzed from the FE model include variations in mean and peak contact pressures and contact area, metrics typically examined in in-vitro studies; meniscal extrusion, a common clinical indicator of meniscal dysfunction; and the impact of potential repair failures, whether due to tissue cut-out or non-anatomical repairs.

Ultimately, this FE model will serve as a critical tool for studying the biomechanical behavior of repaired meniscal tissue within the context of the human knee under physiological loading conditions, providing insights into improving clinical outcomes.

APPENDIX A

Results of Chapter 3

The results obtained from the experimental load-to-failure test with sutured porcine meniscal horns in Chapter 3 are presented below.

A.1 Geometrical data of the specimens

Geometric parameters were initially measured for the porcine specimens in this study in a plane normal to the direction of loading containing the suture point. These measurements refer to the thicknesses at the orifice, $\boldsymbol{e_o}$; at the outer edge of the meniscus horn, $\boldsymbol{e_e}$; and at the inner edge, $\boldsymbol{e_i}$. The distances between the suture hole and the outer edge, $\boldsymbol{d_{oe}}$, and between both edges, $\boldsymbol{d_{ei}}$, were also measured. Distance between Point 1 and Point 2, $\boldsymbol{d_{12}}$, was also recorded for the study of deformation around the suture hole during the test. Finally, the distance between the Point 1 and the tip of the meniscal horn, $\boldsymbol{d_{h1}}$, and the distance between the base of the meniscus clamped in the jaw and the tip of the meniscus, $\boldsymbol{d_h}$, were measured too.

Table A.1. Values in mm of the measurements taken for each porcine specimen tested.

	e_i	e_o	e_e	d_{oe}	d_{ei}	d_{12}	d_{h1}	d_h
C1 MA	1.49	7.15	10.41	8.3	18.36	4.00	8.31	23.02
C3 MA	0.80	5.44	9.78	9.72	19.21	2.49	15.86	26.34
C3 LP	1.10	6.46	8.18	8.82	18.89	2.64	20.95	30.51
C4 MA	0.59	4.62	8.07	7.68	14.69	2.58	14.84	24.44
C4 LP	0.70	4.91	9.47	10.21	17.13	2.40	13.17	27.22
C5 MA	0.66	3.87	8.23	9.62	14.93	2.78	16.94	26.96
C5 LP	0.68	3.80	9.12	11.04	20.6	2.81	23.78	34.86
C6 MP	0.39	2.68	7.02	10.14	17.6	2.47	8.39	18.77
C6 LP	0.78	5.10	6.41	9.69	17.5	2.63	12.88	22.82
C7 MP	0.54	4.08	9.04	10.68	19.55	2.67	10.71	21.83
C7 LP	1.05	6.17	9.95	8.57	17.04	2.91	15.76	27.35
C8 MA	1.10	4.80	8.93	8.27	15.34	2.80	12.74	24.08
C8 LP	0.49	5.74	10.55	8.90	15.67	2.83	17.45	29.28

C9 LA	1.00	6.34	11.65	7.49	16.11	1.18	13.03	17.76
C9 MP	0.65	3.58	7.99	10.04	17.73	1.89	13.89	22.09
C10 MA	1.06	5.26	8.42	6.55	11.87	2.35	9.10	18.40
C11 LP	0.60	5.74	10.04	7.96	18.20	3.41	12.94	20.76
C12 MA	0.46	4.20	8.70	7.70	13.20	2.20	10.00	18.00
C12 LP	0.80	4.60	8.20	9.46	17.50	2.70	16.20	32.00
C13 LA	0.30	4.70	11.2	12.20	18.60	2.80	12.00	20.00
C14 MA	0.40	3.90	8.00	6.50	14.60	2.40	8.00	19.00
C14 LP	0.40	6.50	8.00	8.90	18.30	2.50	7.00	17.00

C: porcine; M: medial; L: lateral; A: anterior; P: posterior.

A.2 Results of the load-to-failure test

Specimen and tissue level parameters described computed for all the tested porcine specimens. These parameters mainly focus on the meniscal cut-out force, F_c, the meniscal ultimate force, F_u, the tissue cut-out resistance, S_c, and the tissue equivalent stiffness modulus, m_s.

Table A.2. Values of the specimen cut-out force, $\boldsymbol{F_c}$; specimen ultimate force, $\boldsymbol{F_u}$; tissue cut-out resistance, $\boldsymbol{S_c}$; and tissue equivalent stiffness modulus, $\boldsymbol{m_s}$ of all the porcine meniscal horns at the suture insertion point area.

	$\boldsymbol{F_c}$ (N)	$\boldsymbol{F_u}$ (N)	$\boldsymbol{S_c}$ (MPa)	$\boldsymbol{m_s}$ (MPa)
C1 MA	108.40	151.40	30.28	97.90
C3 MA	191.40	200.20	70.37	112.80
C3 LP	115.20	205.10	35.67	80.22
C4 MA	175.78	197.30	76.10	130.20
C4 LP	187.50	220.70	76.22	80.13
C5 MA	168.00	169.90	86.60	139.10
C5 LP	255.90	278.30	134.68	218.00
C6 MP	155.11	168.90	128.19	197.70
C6 LP	201.78	185.50	88.11	203.30
C7 MP	99.82	119.14	54.25	141.10
C7 LP	186.67	327.10	67.15	82.29
C8 MA	205.11	232.42	94.96	87.72
C8 LP	209.44	379.88	81.18	58.50
C9 LA	148.67	224.61	52.16	39.82
C9 MP	111.78	105.50	69.43	79.55
C10 MA	108.51	117.18	45.79	43.53
C11 LP	149.40	168.00	52.06	96.17
C12 MA	104.50	120.10	49.76	59.48

C12 LP	291.00	309.60	126.52	167.10
C13 LA	197.30	197.30	83.96	56.27
C14 MA	144.50	145.50	74.10	136.90
C14 LP	199.20	303.70	61.29	141.70

M: medial; L: lateral; A: anterior; P: posterior.

A.3 Load-displacement curves

Load-displacement curves of all the porcine specimen tested are shown in Figure A.1. The load was recorded by the load cell of the testing machine and the displacement refers to the displacement between Point 1 and Point 2 marked on the cranial meniscal surface.

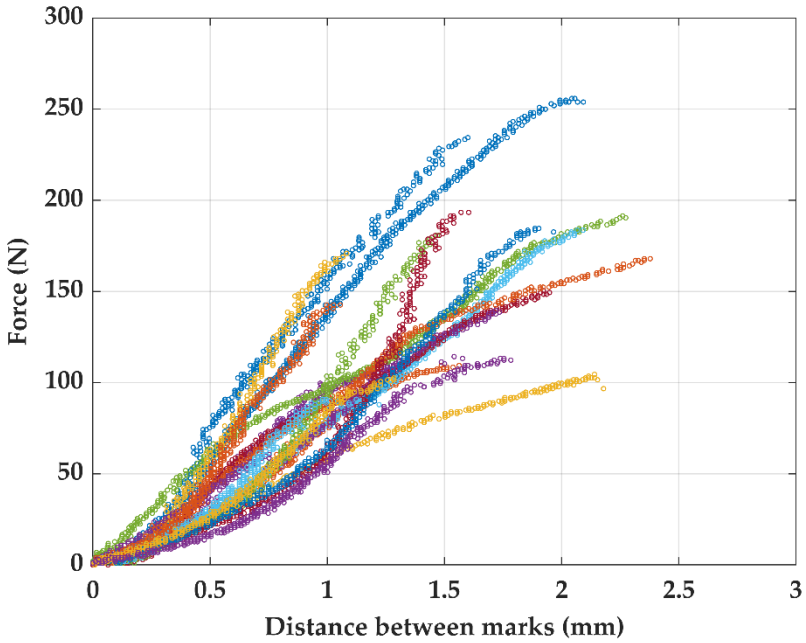

Figure A.1. Load-displacement curves until the initiation of tissue cut-out of all the sutured porcine specimens tested in the load-to-failure test under circumferential traction induced by the suture.

A.4 Stress-strain curves

Stress-strain curves of all the porcine specimen tested are shown in Figure A.2 with a magnification in the strain range of [0-0.3], where the tissue equivalent stiffness modulus, m_s, was computed.

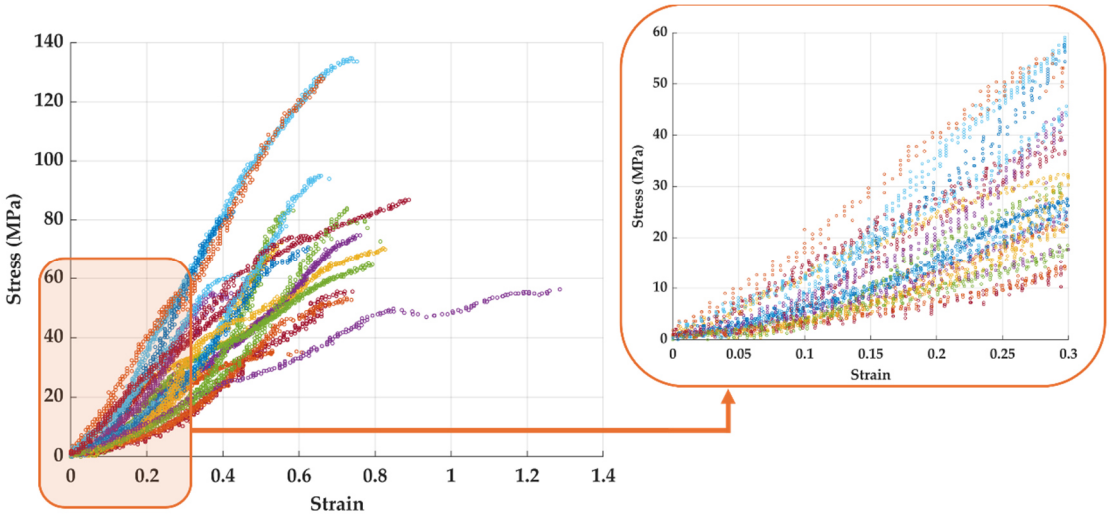

Figure A.2. Stress-strain curves with a magnification in $\boldsymbol{\varepsilon = [0 - 0.3]}$ of all the sutured porcine specimens tested in the load-to-failure test under circumferential traction induced by the suture.

APPENDIX B

Results of Chapter 4

The results obtained in the experimental load-to-failure test with sutured human meniscal horns from the three age groups tested in Chapter 4 are presented below.

B.1 Geometrical data of the specimens

Geometric parameters were initially measured for the human specimens in this study in a plane normal to the direction of loading containing the suture point. These measurements refer to the thicknesses at the orifice, e_o; at the outer edge of the meniscus horn, e_e; and at the inner edge, e_i. The distances between the suture hole and the outer edge, d_{oe}, and between both edges, d_{ei}, were also measured. Distance between Point 1 and Point 2, d_{12}, was also recorded for the study of deformation around the suture hole during the test. Finally, the distance between the Point 1 and the tip of the meniscal horn, d_{h1} , and the distance between the base of the meniscus clamped in the jaw and the tip of the meniscus, d_h, were measured too.

Table B.1. Values in mm of the measurements taken for each young human specimen tested.

	Age	e_i	e_o	e_e	d_{oe}	d_{ei}	d_{12}	d_{h1}	d_h
Y1 LA	28	0.45	1.92	3.28	7.33	11.71	2.30	12.41	25.00
Y1 MP	28	0.72	2.67	3.10	8.13	12.99	2.00	8.90	22.00
Y2 MA	28	1.00	2.61	3.38	6.72	12.37	2.70	12.26	24.00
Y3 LA	33	0.35	1.89	1.87	5.24	11.52	2.59	16.42	26.09
Y3 MA	33	0.48	1.89	3.52	5.97	9.80	2.99	23.31	31.79
Y4 LP	33	0.43	2.68	4.25	5.17	12.55	3.14	8.24	20.51
Y4 MP	33	0.42	1.80	3.90	10.09	15.60	2.27	10.96	18.05
Y5 LA	37	0.85	3.78	4.81	6.60	11.11	2.24	19.41	32.87
Y5 MP	37	0.60	2.89	4.08	6.10	15.31	2.23	17.58	27.14
Y6 LP	37	0.70	2.66	3.53	5.60	9.40	2.36	15.31	23.43
Y7 LA	41	0.59	4.62	8.07	8.83	14.00	1.80	20	27.00
Y7 MA	41	0.70	2.42	3.51	6.53	9.70	2.05	25.14	34.34

Y8 LP	41	0.72	2.40	4.04	6.16	10.04	2.50	7.97	22.87
Y8 MP	41	0.52	2.73	2.74	7.61	15.10	3.33	10.28	21.13
Y9 LA	41	0.45	1.56	2.65	6.71	11.38	2.70	16.00	26.00
Y9 MP	41	0.29	2.10	2.61	11.03	16.30	3.05	11.6	21.52
Y10 LP	41	0.42	2.46	3.46	7.48	12.92	3.29	11.09	24.10
Y10 MA	41	0.50	3.02	4.31	4.95	10.64	2.85	15.62	22.70
Y11 LP	47	0.61	3.12	3.50	4.54	9.68	2.63	17.00	27.00
Y11 MA	47	0.44	3.12	3.42	9.69	12.62	2.55	15.00	27.00
Y12 LA	47	0.56	2.29	3.24	7.44	14.00	3.14	15.00	24.74
Y12 MP	47	0.55	2.75	3.00	10.00	18.64	2.85	10.00	23.23

Y: young; M: medial; L: lateral; A: anterior; P: posterior.

Table B.2. Values in mm of the measurements taken for each middle-aged human specimen tested.

	Age	e_i	e_o	e_e	d_{oe}	d_{ei}	d_{12}	d_{h1}	d_h
MA1 MA	57	0.83	2.84	3.53	6.17	10.64	2.44	11.00	23.00
MA1 MP	57	0.92	3.38	5.26	7.48	11.47	3.15	8.00	24.00
MA2 LA	57	0.72	3.88	3.49	8.49	18.25	2.56	15.00	23.00
MA2 LP	57	1.24	3.36	4.85	8.65	15.86	3.30	6.13	16.00
MA3 MA	58	0.80	3.23	3.82	4.03	7.38	2.00	14.34	30.66
MA4 MA	60	0.53	3.22	4.97	6.69	11.64	3.07	16.00	28.00
MA4 MP	60	0.78	3.09	2.35	15.25	25.43	2.81	6.97	18.00
MA5 LA	60	0.74	3.61	3.38	5.00	11.94	2.76	8.78	16.18
MA5 LP	60	0.70	2.14	3.64	5.13	10.59	7.38	21.00	20.00
MA6 MA	60	0.60	3.03	4.83	4.64	8.95	2.63	8.96	22.00
MA6 MP	60	0.90	2.12	3.80	9.10	16.58	2.57	11.30	22.00
MA7 LP	64	0.41	2.10	4.06	6.36	8.78	2.53	5.00	18.00
MA7 MA	64	0.56	2.22	3.20	5.13	8.53	2.36	15.00	26.00
MA8 LP	64	0.90	2.07	3.81	4.93	9.77	2.18	5.00	25.00
MA8 MP	64	0.48	2.70	3.76	5.00	10.97	2.33	8.00	20.00
MA9 LA	65	0.55	2.59	2.76	5.25	10.00	2.64	12.00	25.00
MA9 LP	65	0.92	3.50	3.96	5.88	9.80	2.25	15.00	23.00
MA10 LA	67	0.58	2.87	3.79	6.57	11.61	2.23	13.42	28.36
MA10 MA	67	0.69	2.56	3.39	8.19	10.66	2.54	12.26	27.42
MA11 LP	67	0.6	4.29	5.29	7.47	12.91	1.95	13.68	26.89
MA11 MP	67	0.49	2.39	3.73	10.06	17.89	2.35	15.26	29.20
MA12 MP	67	0.45	2.79	4.44	8.55	12.99	2.15	13.75	28.54
MA12 LA	67	0.40	3.10	4.61	9.22	13.45	2.04	14.05	30.10

MA: middle-aged; M: medial; L: lateral; A: anterior; P: posterior.

Table B.3. Values in mm of the measurements taken for each old human specimen tested.

	Age	e_i	e_o	e_e	d_{oe}	d_{ei}	d_{12}	d_{h1}	d_h
O1 LP	82	1.45	3.10	3.71	8.83	15.77	2.95	9.26	18.97
O1 MA	82	0.84	2.40	2.80	8.46	10.61	2.84	18.00	30.00
O2 LA	82	0.71	4.78	4.51	5.86	13.30	2.52	6.14	13.61
O2 MP	82	0.94	3.32	5.97	8.16	18.51	2.43	11.66	20.13
O3 LP	82	0.70	3.57	3.50	7.00	13.33	2.00	10.90	14.92
O3 MA	82	0.53	3.99	3.90	4.15	8.87	2.81	11.48	20.15
O4 LA	83	0.45	4.34	4.00	8.20	11.26	2.40	12.16	18.21
O4 MP	83	0.55	2.20	3.74	8.59	14.29	2.21	9.21	18.78
O5 LP	83	0.55	4.52	5.19	8.34	13.71	2.00	9.70	15.57
O5 MA	83	0.60	3.68	4.08	3.41	7.43	2.49	10.35	18.22
O6 LP	83	0.58	3.41	3.51	11.24	17.49	2.00	14.00	28.00
O6 MA	83	1.13	3.26	2.20	8.00	12.80	2.81	19.74	33.00
O7 LP	88	0.99	2.99	3.39	5.70	10.48	1.96	10.55	26.14
O7 MP	88	0.78	4.05	6.80	8.06	14.15	1.70	7.70	22.52
O8 MA	88	0.89	2.17	4.37	9.01	14.17	2.75	28.26	42.54
O9 MA	90	0.79	2.36	1.42	7.79	13.52	2.36	27.53	38.00
O10 LP	91	0.79	2.53	4.45	7.77	13.05	4.00	8.00	32.63
O10 MP	91	0.86	2.44	5.14	9.57	11.28	3.49	14.99	32.27
O11 MA	91	0.51	3.42	3.43	5.16	8.96	3.14	19.48	44.78
O12 LP	91	0.94	5.00	6.44	10.51	15.19	3.00	9.00	18.00
O13 LP	95	1.04	3.55	4.32	11.25	14.91	1.94	14.53	21.98

O: old; M: medial; L: lateral; A: anterior; P: posterior.

B.2 Results of the load-to-failure test

Specimen and tissue level parameters described computed for all the tested human specimens. These parameters mainly focus on the meniscal cut-out force, F_c, the meniscal ultimate force, F_u, the tissue cut-out resistance, S_c, and the tissue equivalent stiffness modulus, m_s.

Table B.4. Values of the specimen cut-out force, F_c; specimen ultimate force, F_u; tissue cut-out resistance, S_c; and tissue equivalent stiffness modulus, m_s of all the young human meniscal horns at the suture insertion point area.

	F_c (N)	F_u (N)	S_c (MPa)	m_s (MPa)
Y1 LA	41.99	41.99	43.74	122.30
Y1 MP	91.80	135.70	68.76	109.00
Y2 MA	23.44	49.80	17.96	103.30

Y3 LA	40.04	43.95	42.60	42.27
Y3 MA	78.13	83.01	82.24	193.30
Y4 LP	66.41	111.30	49.56	80.93
Y4 MP	68.36	104.50	75.96	105.40
Y5 LA	64.45	64.45	34.10	57.70
Y5 MP	50.78	126.95	35.02	102.50
Y6 LP	41.02	43.95	30.84	39.01
Y7 LA	24.41	41.99	28.48	99.06
Y7 MA	38.09	38.09	31.48	101.80
Y8 LP	34.18	34.18	86.60	128.60
Y8 MP	76.17	90.82	55.60	134.20
Y9 LA	36.13	41.99	46.32	157.90
Y9 MP	82.03	102.50	78.12	121.70
Y10 LP	36.13	50.78	29.37	91.66
Y10 MA	83.01	116.20	54.97	305.60
Y11 LP	72.27	92.77	46.33	105.70
Y11 MA	66.41	77.15	42.57	51.90
Y12 LA	51.76	77.15	45.21	104.10
Y12 MP	105.5	140.60	76.73	140.40

Y: young; M: medial; L: lateral; A: anterior; P: posterior.

Table B.5. Values of the specimen cut-out force, $\boldsymbol{F_c}$; specimen ultimate force, $\boldsymbol{F_u}$; tissue cut-out resistance, $\boldsymbol{S_c}$; and tissue equivalent stiffness modulus, $\boldsymbol{m_s}$ of all the middle-aged human meniscal horns at the suture insertion point area.

Specimen	$\boldsymbol{F_c}$ **(N)**	$\boldsymbol{F_u}$ **(N)**	$\boldsymbol{S_c}$ **(MPa)**	$\boldsymbol{m_s}$ **(MPa)**
MA1 MA	47.85	51.76	33.70	88.07
MA1 MP	71.29	71.29	42.18	79.00
MA2 LA	87.89	87.89	45.30	61.56
MA2 LP	70.31	74.22	41.85	89.60
MA3 MA	53.17	81.05	36.67	99.74
MA4 MA	81.05	84.96	50.34	70.07
MA4 MP	100.60	116.20	65.11	97.12
MA5 LA	62.50	69.34	34.63	69.03
MA5 LP	52.73	66.41	49.28	138.50
MA6 MA	76.17	78.13	50.28	56.37
MA6 MP	83.98	95.70	79.23	255.80
MA7 LP	58.59	64.45	55.80	170.10
MA7 MA	55.66	56.64	50.14	123.90
MA8 LP	25.39	25.39	24.53	44.43

MA8 MP	68.36	69.34	50.64	64.00
MA9 LA	49.80	49.80	38.46	48.82
MA9 LP	46.88	48.83	26.79	58.02
MA10 LA	47.26	52.73	36.63	234.90
MA10 MA	44.49	44.92	38.69	143.80
MA11 LP	64.02	65.43	33.17	66.46
MA11 MP	55.33	131.84	51.23	144.90
MA12 MP	70.53	106.44	50.38	134.30
MA12 LA	59.68	76.17	42.63	145.70

MA: middle-aged; M: medial; L: lateral; A: anterior; P: posterior.

Table B.6. Values of the specimen cut-out force, $\boldsymbol{F_c}$; specimen ultimate force, $\boldsymbol{F_u}$; tissue cut-out resistance, $\boldsymbol{S_c}$; and tissue equivalent stiffness modulus, $\boldsymbol{m_s}$ of all the old human meniscal horns at the suture insertion point area.

	$\boldsymbol{F_c}$ (N)	$\boldsymbol{F_u}$ (N)	$\boldsymbol{S_c}$ (MPa)	$\boldsymbol{m_s}$ (MPa)
O1 LP	19.53	31.25	12.60	41.82
O1 MA	45.90	45.90	38.25	119.10
O2 LA	77.15	83.01	32.28	46.07
O2 MP	73.24	113.30	44.12	42.21
O3 LP	36.13	59.57	20.24	30.52
O3 MA	55.66	76.17	27.90	65.76
O4 LA	62.50	64.45	28.80	48.28
O4 MP	80.08	85.94	72.80	60.23
O5 LP	31.25	82.03	13.83	23.12
O5 MA	61.52	74.22	33.43	95.55
O6 LP	66.41	81.05	38.84	25.36
O6 MA	71.29	74.22	43.74	35.51
O7 LP	41.02	43.95	27.34	69.88
O7 MP	68.36	115.00	33.67	30.66
O8 MA	31.25	44.92	28.67	73.62
O9 MA	34.18	42.97	28.97	36.01
O10 LP	62.50	80.08	49.21	121.40
O10 MP	59.57	83.01	48.83	113.10
O11 MA	51.76	51.76	30.27	74.09
O12 LP	52.73	73.24	21.09	16.47
O13 LP	62.50	74.22	35.21	38.29

O: old; M: medial; L: lateral; A: anterior; P: posterior.

B.3 Load-displacement curves

Load-displacement curves of all young, middle-aged and old human specimen tested are shown in Figure B.1, Figure B.2 and Figure B.3, respectively. The load was recorded by the load cell of the testing machine and the displacement refers to the displacement between Point 1 and Point 2 marked on the cranial meniscal surface.

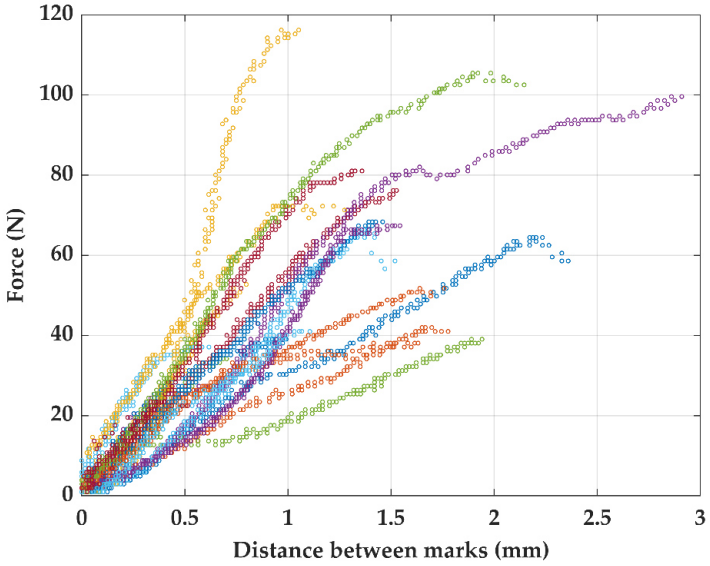

Figure B.1. Load-displacement curves until the initiation of tissue cut-out of all the sutured young human specimens tested in the load-to-failure test under circumferential traction induced by the suture.

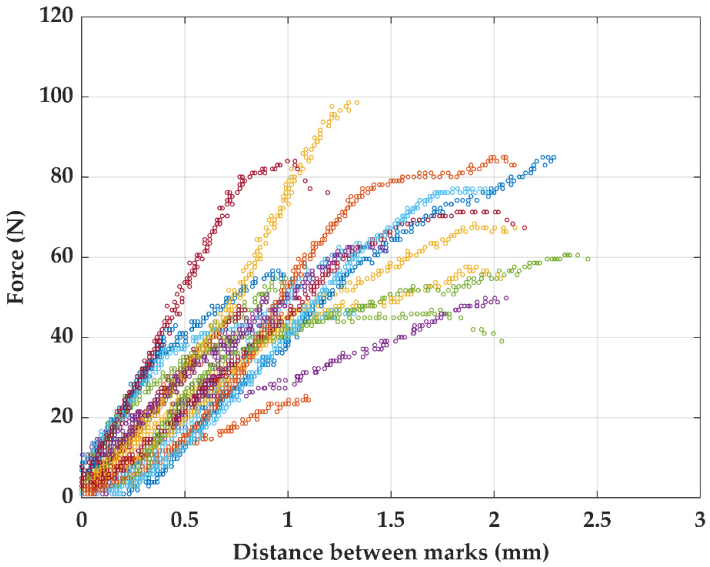

Figure B.2. Load-displacement curves until the initiation of tissue cut-out of all the sutured middle-aged human specimens tested in the load-to-failure test under circumferential traction induced by the suture.

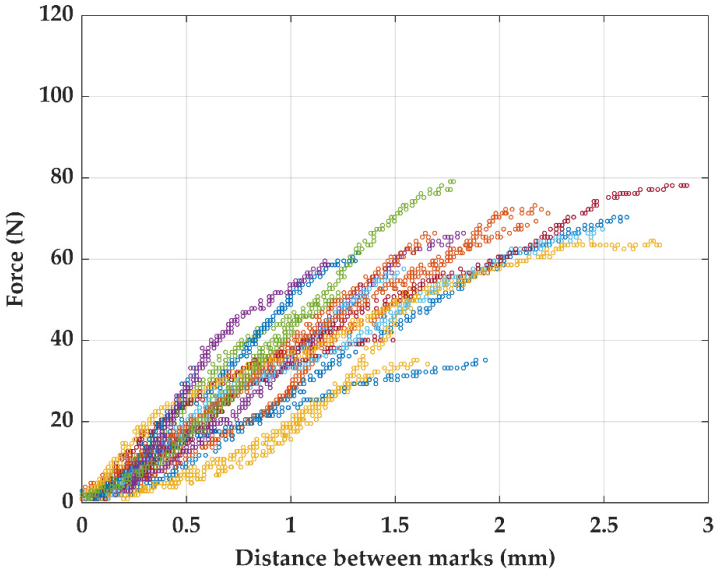

Figure B.3. Load-displacement curves until the initiation of tissue cut-out of all the sutured old human specimens tested in the load-to-failure test under circumferential traction induced by the suture.

B.4 Stress-strain curves

Stress-strain curves of all young, middle-aged and old human specimen tested are shown in Figure B.4, Figure B.5 and Figure B.6, respectively. A magnification in the strain range of [0-0.3], where the tissue equivalent stiffness modulus, m_s, is computed can be observed too.

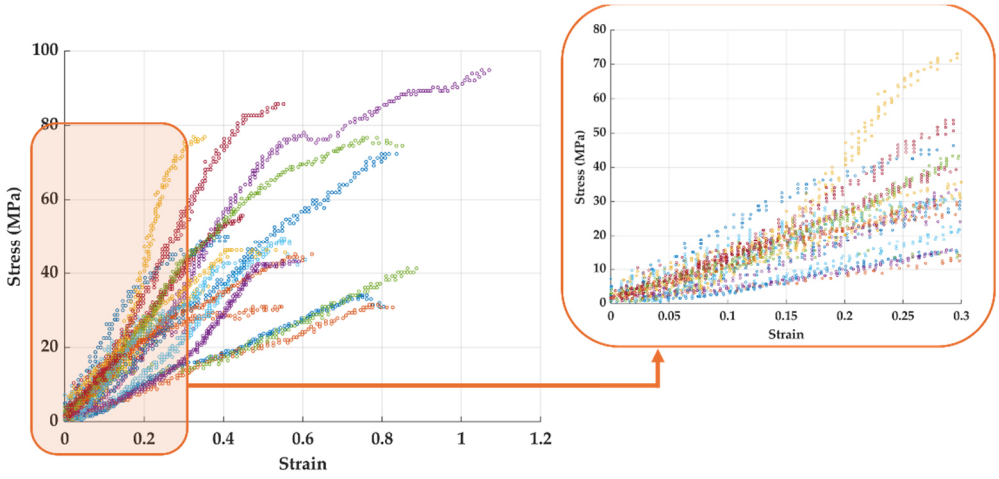

Figure B.4. Stress-strain curves with a magnification in $\boldsymbol{\varepsilon = [0 - 0.3]}$ of all the sutured young human specimens tested in the load-to-failure test under circumferential traction induced by the suture.

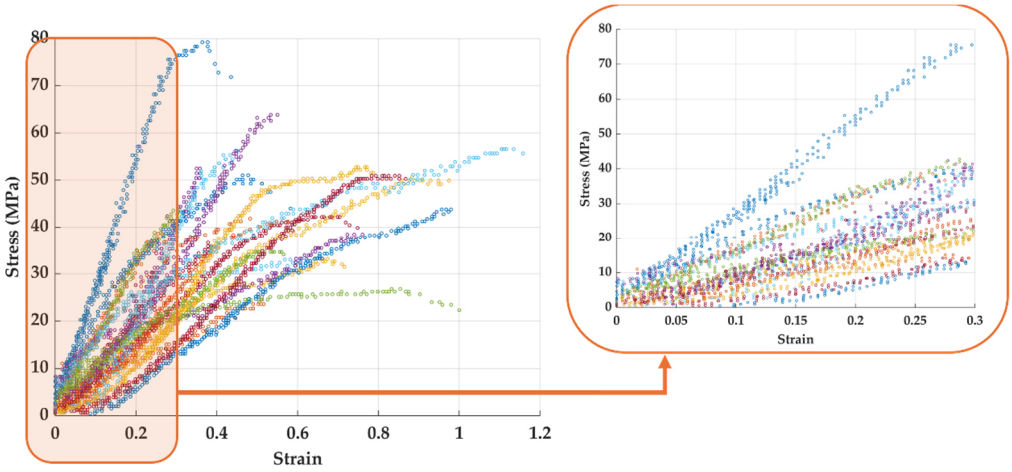

Figure B.5. Stress-strain curves with a magnification in $\boldsymbol{\varepsilon = [0 - 0.3]}$ of all the sutured middle-aged human specimens tested in the load-to-failure test under circumferential traction induced by the suture.

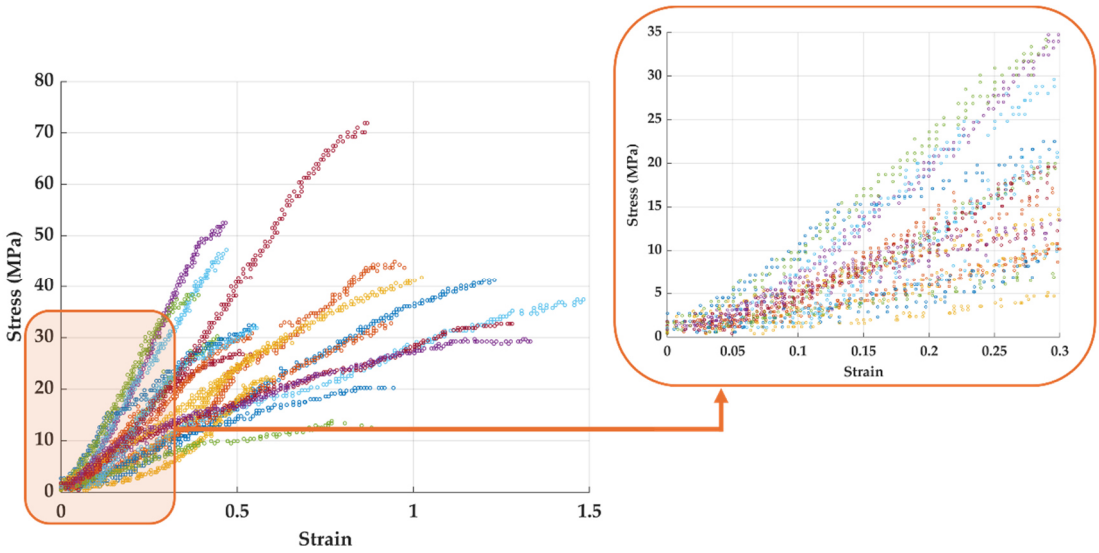

Figure B.6. Stress-strain curves with a magnification in $\boldsymbol{\varepsilon = [0 - 0.3]}$ of all the sutured old human specimens tested in the load-to-failure test under circumferential traction induced by the suture.

APPENDIX C

Results of Chapter 6

The results obtained in the experimental indentation test with sutured human meniscal horns tested in Chapter 6 are presented below.

C.1 Geometrical data of the specimens

Geometric parameters were initially measured for the human specimens in this study in a plane normal to the direction of loading containing the suture point. These measurements refer to the thicknesses at the orifice, $\boldsymbol{e_o}$; at the outer edge of the meniscus horn, $\boldsymbol{e_e}$; and at the inner edge, $\boldsymbol{e_i}$. The distances between the suture hole and the outer edge, $\boldsymbol{d_{oe}}$, and between both edges, $\boldsymbol{d_{ei}}$, were also measured. Distance between Point 1 and Point 2, $\boldsymbol{d_{12}}$, was also recorded for the study of deformation around the suture hole during the test. Finally, the distance between the Point 1 and the tip of the meniscal horn, $\boldsymbol{d_{h1}}$, and the distance between the base of the meniscus clamped in the jaw and the tip of the meniscus, $\boldsymbol{d_h}$, were measured too.

Table C.1. Values in mm of the measurements taken for each human specimen tested**.**

	$\boldsymbol{e_i}$	$\boldsymbol{e_o}$	$\boldsymbol{e_e}$	$\boldsymbol{d_{oe}}$	$\boldsymbol{d_{ei}}$	$\boldsymbol{d_{12}}$	$\boldsymbol{d_{h1}}$	$\boldsymbol{d_h}$
H1 MA	0.30	3.50	6.51	8.84	14.42	2.48	8.85	16.80
H1 MP	0.94	4.54	5.54	6.91	12.41	3.18	11.31	17.10
H2 MP	1.01	3.04	4.84	4.30	10.39	2.07	8.44	20.22
H2 MA	0.39	3.78	4.92	12.48	16.83	2.74	6.79	17.40
H3 LP	0.59	2.98	6.61	6.71	12.15	1.95	4.65	15.66
H3 LA	0.95	4.02	4.54	6.26	12.50	4.13	4.13	12.22
H4 LP	1.11	3.64	7.65	7.64	11.74	2.34	14.94	18.58
H4 LA	0.50	4.36	5.49	9.40	15.11	2.88	7.40	13.42
H5 MA	0.32	3.14	5.12	5.30	11.27	3.52	21.27	34.61
H6 LA	0.92	2.40	3.66	5.91	8.87	3.41	7.45	16.90
H7 MP	0.87	5.71	6.44	8.94	15.44	3.05	11.54	17.01
H8 LA	0.71	2.44	4.60	3.91	6.16	3.83	7.26	19.89

H9 LA	0.44	3.30	6.83	6.41	17.11	2.26	10.62	16.75
H9 LP	0.88	4.27	5.46	6.15	11.31	2.14	8.78	14.68
H10 LA	1.05	4.17	4.91	5.09	7.38	2.31	9.56	17.31
H11 MP	0.47	5.54	8.17	7.52	14.28	2.34	12.21	24.25
H11 MA	1.21	4.13	5.68	4.14	10.49	2.52	10.92	21.77
H12 LA	0.62	3.27	4.82	6.09	10.56	2.64	13.04	23.83
H12 LP	0.49	3.43	5.38	6.08	10.49	2.64	8.41	18.85
H13 MA	1.10	5.53	6.94	8.03	10.83	2.43	13.85	25.94
H13 MP	0.97	3.28	5.68	7.08	11.27	2.48	8.38	22.33
H14 LP	0.96	3.88	5.05	6.85	10.17	2.86	11.43	21.89
H14 LA	0.22	3.93	4.29	6.16	10.04	2.57	12.96	21.87
H15 LP	0.46	3.72	6.74	9.45	19.94	2.56	8.20	21.92
H15 LA	0.46	1.75	3.96	7.09	9.32	3.02	8.72	23.19
H16 LA	0.47	3.37	6.07	8.11	12.80	3.30	5.98	18.45
H16 LP	0.60	4.84	6.30	6.19	8.90	2.82	8.57	17.03

H: human; M: medial; L: lateral; A: anterior; P: posterior.

C.2 Results of the indentation test

Compressive parameters obtained from the indentation tests and computed for all the tested human specimens in the three tensile states: unloaded, 10 N and 20 N are shown in Table C.2, Table C.3 and Table C.4, respectively. These parameters mainly focus on the maximum indentation force, F, the instantaneous modulus, IM, the relaxation modulus, E_{t20} and the relaxation stress percentage, $\Delta\sigma_{relax}$.

Table C.2. Values of the maximum indentation force, $\boldsymbol{F}$; the instantaneous modulus, $\boldsymbol{IM}$; the relaxation modulus, $\boldsymbol{E_{t20}}$ and the relaxation stress percentage, $\boldsymbol{\Delta\sigma_{relax}}$ of all the human meniscal horns at the suture insertion point area in the unloaded state.

	$\boldsymbol{F}$ (N)	$\boldsymbol{IM}$ (MPa)	$\boldsymbol{E_{t20}}$ (MPa)	$\boldsymbol{\Delta\sigma_{relax}}$ (%)
H1 MA	0.196	0.223	0.170	67.870
H1 MP	0.506	0.571	0.350	61.040
H2 MP	0.250	0.257	0.250	60.240
H2 MA	0.199	0.230	0.170	65.150
H3 LP	0.645	0.692	0.320	41.780
H3 LA	0.448	0.510	0.310	57.770
H4 LP	0.228	0.265	0.260	64.920
H4 LA	0.467	0.541	0.420	64.870
H5 MA	0.602	0.670	0.390	53.390
H6 LA	0.265	0.274	0.180	66.120

H7 MP	0.126	0.148	0.150	66.940
H8 LA	1.872	1.709	0.370	47.010
H9 LA	0.914	1.046	0.700	58.37
H9 LP	0.343	0.409	0.440	71.060
H10 LA	0.415	0.446	0.290	60.240
H11 MP	0.256	0.297	0.320	74.210
H11 MA	0.719	0.893	0.930	59.600
H12 LA	0.548	0.583	0.230	53.360
H12 LP	1.609	1.284	0.440	44.940
H13 MA	0.416	0.501	0.390	55.630
H13 MP	0.176	0.206	0.210	70.600
H14 LP	0.633	0.676	0.410	63.880
H14 LA	1.279	1.435	0.600	48.730
H15 LP	0.267	0.305	0.210	54.540
H15 LA	2.746	2.302	0.450	47.640
H16 LA	0.586	0.589	0.260	59.230
H16 LP	0.460	0.503	0.310	62.650

H: human; M: medial; L: lateral; A: anterior; P: posterior.

Table C.3. Values of the maximum indentation force, $\boldsymbol{F}$; the instantaneous modulus, $\boldsymbol{IM}$; the relaxation modulus, $\boldsymbol{E_{t20}}$ and the relaxation stress percentage, $\boldsymbol{\Delta\sigma_{relax}}$ of all the human meniscal horns at the suture insertion point area under 10 N in the circumferential direction.

	$\boldsymbol{F}$ (N)	$\boldsymbol{IM}$ (MPa)	$\boldsymbol{E_{t20}}$ (MPa)	$\boldsymbol{\Delta\sigma_{relax}}$ (%)
H1 MA	0.610	0.687	0.439	65.769
H1 MP	1.120	1.089	0.765	60.578
H2 MP	0.820	0.983	0.782	53.333
H2 MA	0.410	0.463	0.312	58.541
H3 LP	1.480	1.566	0.745	42.425
H3 LA	0.780	0.880	0.469	53.085
H4 LP	0.440	0.509	0.814	53.138
H4 LA	1.760	2.011	1.284	57.851
H5 MA	1.800	1.969	1.020	51.407
H6 LA	0.770	0.789	0.402	57.343
H7 MP	0.430	0.494	0.412	62.160
H8 LA	2.060	1.912	0.650	54.179
H9 LA	1.320	1.505	1.075	63.405
H9 LP	0.940	1.118	1.070	63.733
H10 LA	0.880	1.004	0.835	59.925

H11 MP	0.910	1.062	1.079	65.952
H11 MA	1.570	1.935	1.919	53.772
H12 LA	1.010	1.080	0.476	48.072
H12 LP	3.640	2.625	0.739	45.047
H13 MA	0.941	1.137	0.863	47.611
H13 MP	0.739	0.848	0.666	61.365
H14 LP	1.824	1.941	0.912	54.071
H14 LA	1.615	1.781	0.670	45.639
H15 LP	0.294	0.338	0.256	55.023
H15 LA	4.840	4.038	1.021	49.174
H16 LA	1.100	1.105	0.564	60.305
H16 LP	0.828	0.905	0.581	63.320

H: human; M: medial; L: lateral; A: anterior; P: posterior.

Table C.4. Values of the maximum indentation force, $\boldsymbol{F}$; the instantaneous modulus, $\boldsymbol{IM}$; the relaxation modulus, $\boldsymbol{E_{t20}}$ and the relaxation stress percentage, $\boldsymbol{\Delta\sigma_{relax}}$ of all the human meniscal horns at the suture insertion point area under 20 N in the circumferential direction.

	$\boldsymbol{F}$ (N)	$\boldsymbol{IM}$ (MPa)	$\boldsymbol{E_{t20}}$ (MPa)	$\boldsymbol{\Delta\sigma_{relax}}$ (%)
H1 MA	0.603	0.687	0.510	64.856
H1 MP	1.102	1.087	0.733	61.256
H2 MP	0.990	1.185	0.978	52.135
H2 MA	0.405	0.465	0.337	58.418
H3 LP	1.272	1.329	0.639	42.808
H3 LA	0.971	1.089	0.577	53.826
H4 LP	0.483	0.562	0.980	56.256
H4 LA	1.828	2.089	1.367	58.269
H5 MA	1.819	2.018	1.081	48.143
H6 LA	0.949	0.964	0.470	55.953
H7 MP	0.436	0.505	0.419	59.706
H8 LA	2.972	2.834	1.163	51.545
H9 LA	1.427	1.621	1.023	58.989
H9 LP	1.145	1.366	1.271	61.601
H10 LA	0.956	1.077	0.788	56.934
H11 MP	1.264	1.486	1.523	65.883
H11 MA	1.852	2.299	2.415	54.973
H12 LA	1.257	1.347	0.627	48.567
H12 LP	4.065	3.098	1.080	51.143
H13 MA	0.765	0.922	0.703	49.489

H13 MP	0.884	1.007	0.743	60.419
H14 LP	2.559	2.711	1.138	51.728
H14 LA	1.675	1.847	0.684	44.502
H15 LP	0.362	0.415	0.288	50.978
H15 LA	3.377	2.812	0.971	56.398
H16 LA	1.360	1.364	0.697	59.926
H16 LP	0.869	0.947	0.576	60.507

H: human; M: medial; L: lateral; A: anterior; P: posterior.

C.3 Results of the load-to-failure test

Tensile parameters from the load-to-failure tests for all the tested human specimens are shown in Table C.5. These parameters mainly focus on the tissue equivalent stiffness modulus, m_s, the toe force, F_{toe}, and the force achieved at $\varepsilon = 0.4$, $F_{\varepsilon=0.4}$.

Table C.5. Values of the equivalent stiffness modulus, $\boldsymbol{m_s}$; the toe force, $\boldsymbol{F_{toe}}$, and the force achieved at $\boldsymbol{\varepsilon = 0.4}$, $\boldsymbol{F_{\varepsilon=0.4}}$ of all the human meniscal horns at the suture insertion point area.

Specimen	m_s (MPa)	F_{toe} (N)	$F_{\varepsilon=0.4}$ (N)
H1 MA	7.880	10.710	9.087
H1 MP	11.220	17.710	18.190
H2 MP	19.820	6.509	23.150
H2 MA	18.260	10.800	21.130
H3 LP	17.280	10.710	12.400
H3 LA	20.520	11.250	12.425
H4 LP	28.450	8.852	32.892
H4 LA	24.110	8.744	33.500
H5 MA	120.300	6.620	42.290
H6 LA	98.100	6.503	41.740
H7 MP	36.000	6.965	38.120
H8 LA	111.600	8.867	37.900
H9 LA	8.670	6.440	17.220
H9 LP	36.000	4.063	29.930
H10 LA	30.470	5.245	30.245
H11 MP	26.430	9.024	48.310
H11 MA	29.570	6.674	34.730
H12 LA	43.470	7.494	36.400
H12 LP	52.580	7.628	45.020

H13 MA	33.820	9.350	57.190
H13 MP	20.660	6.372	28.350
H14 LP	24.560	8.644	27.180
H14 LA	50.300	7.529	42.110
H15 LP	35.210	6.632	23.530
H15 LA	27.260	5.392	17.620
H16 LA	120.600	8.754	36.105
H16 LP	34.550	8.606	35.620

H: human; M: medial; L: lateral; A: anterior; P: posterior.

C.4 Load-displacement curves

Load-displacement curves of all the porcine specimen tested are shown in Figure C.1. The load was recorded by the load cell of the testing machine and the displacement refers to the displacement between Point 1 and Point 2 marked on the cranial meniscal surface.

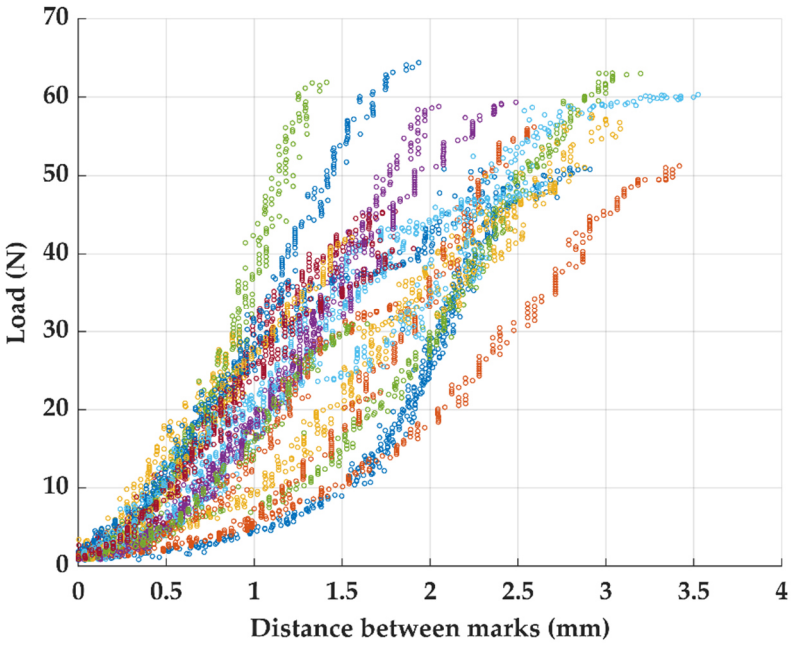

Figure C.1. Load-displacement curves until the initiation of tissue cut-out of all the sutured human specimens tested in the load-to-failure test under circumferential traction induced by the suture.

C.5 Stress-strain curves

Stress-strain curves of all the porcine specimen tested are shown in Figure C.2 with a magnification in the strain range of [0-0.4], where the tissue equivalent stiffness modulus, m_s, was computed.

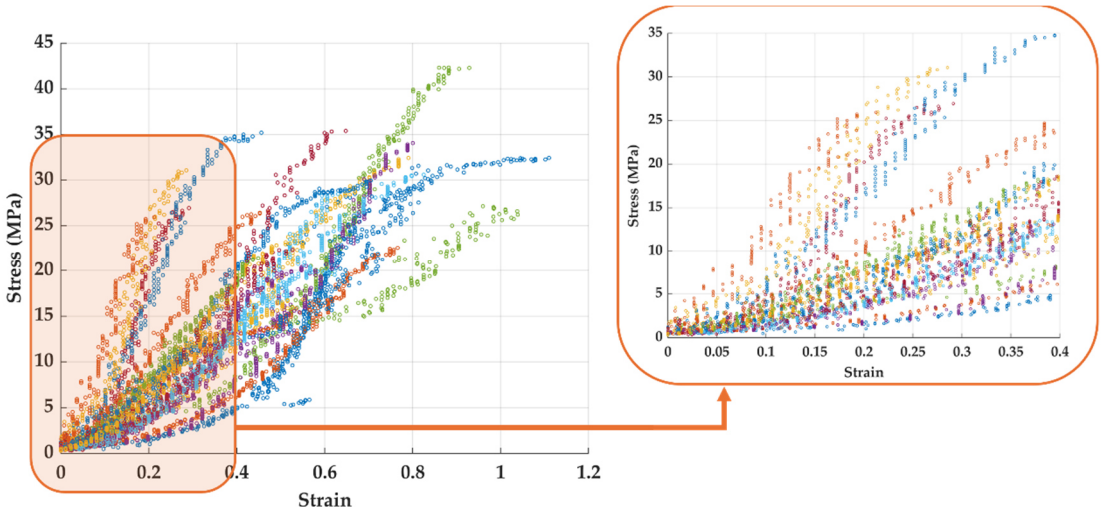

Figure C.2. Stress-strain curves with a magnification in $\boldsymbol{\varepsilon = [0 - 0.4]}$ of all the sutured human specimens tested in the load-to-failure test under circumferential traction induced by the suture.

APPENDIX D

Results of Chapter 7

The results obtained in the computational indentation test with sutured human meniscal horns tested in Chapter 7 are presented below.

D.1 Results of the indentation test

The values of the maximum indentation force, F, of each measurement point at the three tensile states of the elected human meniscal horn specimen for computational modelling after the indentation test are shown in Table D.1.

Table D.1. Values of the maximum indentation force at the three circumferential tensile states of each measurement point in the suture area of the human meniscal horn used for computational modelling.

	1	**2**	**3**	**4**	**5**	**6**	**7**
$F_{exp}^{i,0}$ **(N)**	0.200	0.149	0.482	0.141	1.639	0.224	1.000
$F_{exp}^{i,10}$ **(N)**	1.233	0.379	1.048	0.407	1.629	0.372	2.005
$F_{exp}^{i,20}$ **(N)**	1.315	0.445	1.085	0.537	1.964	0.540	2.883

exp: experimental; i: measurement point.

D.2 Results of the computational modelling

The values of the maximum indentation force, F, obtained from the computational model of the elected human meniscal horn specimen at each measurement point in the three tensile states using specimen-specific material compression properties at each indentation location, corresponding to property sets 1 and 2 are shown in Table D.2 and Table D.3, respectively.

Table D.2. Values of the computational maximum indentation force at the three circumferential tensile states of each measurement point in the suture area of the human meniscal horn used for computational modelling incorporating specimen-specific material compression properties under 0 N of circumferential tensile loading at each indentation location.

	1	**2**	**3**	**4**	**5**	**6**	**7**
$F_{sim}^{i,0}$ **(N) with** $IM^{i,0}$	0.315	0.271	0.607	0.363	1.305	0.419	1.027
$F_{sim}^{i,10}$ **(N) with** $IM^{i,0}$	0.388	0.331	0.565	0.331	1.435	0.371	1.231
$F_{sim}^{i,20}$ **(N) with** $IM^{i,0}$	0.388	0.281	0.507	0.360	1.517	0.394	1.283

sim: simulated; i: measurement point.

Table D.3. Values of the computational maximum indentation force at the three circumferential tensile states of each measurement point in the suture area of the human meniscal horn used for computational modelling incorporating specimen-specific material compression properties under 20 N of circumferential tensile loading at each indentation location.

	1	**2**	**3**	**4**	**5**	**6**	**7**
$F_{sim}^{i,0}$ **(N) with** $IM^{i,20}$	1.006	0.542	1.153	0.748	1.641	0.756	2.080
$F_{sim}^{i,10}$ **(N) with** $IM^{i,20}$	1.284	0.671	1.087	0.674	1.818	0.664	2.531
$F_{sim}^{i,20}$ **(N) with** $IM^{i,20}$	1.297	0.565	0.985	0.736	1.933	0.705	2.646

sim: simulated; i: measurement point.

The values of the maximum indentation force, F, obtained from the computational model of the elected human meniscal horn specimen at each measurement point in the three tensile states in which Young's modulus in all the indentation areas was set to the mean IM derived from the tests on the 27 specimens, corresponding to property sets 3 and 4 are shown in Table D.4 and Table D.5, respectively.

Table D.4. Values of the computational maximum indentation force at the three circumferential tensile states of each measurement point in the suture area of the human meniscal horn used for computational modelling incorporating the Young´s modulus in axial and radial direction in all the indentation areas as the mean $\boldsymbol{IM}$ under 0 N of circumferential tensile loading derived from the tests on the 27 specimens.

	1	**2**	**3**	**4**	**5**	**6**	**7**
$F_{sim}^{i,0}$ **(N) with** IM^{0}	0.532	0.558	0.522	0.644	0.784	0.660	0.818
$F_{sim}^{i,10}$ **(N) with** IM^{0}	0.640	0.854	0.504	0.771	0.760	0.768	0.796
$F_{sim}^{i,20}$ **(N) with** IM^{0}	0.642	0.735	0.506	0.733	0.912	0.708	1.050

sim: simulated; i: measurement point.

Table D.5. Values of the computational maximum indentation force at the three circumferential tensile states of each measurement point in the suture area of the human meniscal horn used for computational modelling incorporating the Young´s modulus in axial and radial direction in all the indentation areas as the mean ***IM*** under 20 N of circumferential tensile loading derived from the tests on the 27 specimens.

	1	**2**	**3**	**4**	**5**	**6**	**7**
$F_{sim}^{i,0}$ **(N) with** IM^{20}	1.055	1.044	1.308	1.256	1.340	1.308	1.387
$F_{sim}^{i,10}$ **(N) with** IM^{20}	1.290	1.251	1.176	1.081	1.582	1.150	1.795
$F_{sim}^{i,20}$ **(N) with** IM^{20}	1.337	1.110	1.092	1.085	1.892	1.225	2.199

sim: simulated; i: measurement point.

APPENDIX E

Dissemination of the thesis results

The main contributions resulting from this thesis are set out in this appendix.

E.1 Publication in Q1: Age influence on resistance and deformation of the human sutured meniscal horn in the immediate postoperative period

This article is published in the journal Frontiers in Bioengineering and Biotechnology, year 2024, volume 11, 1249982. The journal is indexed in the JCR at 41/174 (Q1) in the year of publication, with an impact factor of 4.3.

It contains the most relevant results of the work presented in Chapter 4 of the thesis, which analyses the influence of age on the mechanical properties that characterise the behaviour of meniscal tissue around the suture hole of human meniscal horns undergoing meniscal root repair by suturing.

The first page of the publication is included on the following page.

frontiers | Frontiers in Bioengineering and Biotechnology

TYPE Original Research
PUBLISHED 05 January 2024
DOI 10.3389/fbioe.2023.1249982

OPEN ACCESS

EDITED BY
Francesco Travascio,
University of Miami, United States

REVIEWED BY
Dong Jiang,
Peking University Third Hospital, China
Giovanni Solitro,
Louisiana State University Health Shreveport, United States

*CORRESPONDENCE
Alejandro Peña-Trabalon,
alejandropt98@uma.es

RECEIVED 29 June 2023
ACCEPTED 18 December 2023
PUBLISHED 05 January 2024

CITATION
Peña-Trabalon A, Perez-Blanca A, Moreno-Vegas S, Estebanez Campos MB and Prado-Novoa M (2024), Age influence on resistance and deformation of the human sutured meniscal horn in the immediate postoperative period. *Front. Bioeng. Biotechnol.* 11:1249982. doi: 10.3389/fbioe.2023.1249982

Age influence on resistance and deformation of the human sutured meniscal horn in the immediate postoperative period

Alejandro Peña-Trabalon*, Ana Perez-Blanca, Salvador Moreno-Vegas, M. Belen Estebanez Campos and Maria Prado-Novoa

Clinical Biomechanics Laboratory of Andalusia (BIOCLINA), University of Malaga, Málaga, Spain

Introduction: To preserve knee function, surgical repair is indicated when a meniscal root disinsertion occurs. However, this surgery has not yet achieved complete recovery of the joint´s natural biomechanics, with the meniscus-suture interface identified as a potentially determining factor. Knowing the deformation and resistance behavior of the sutured meniscal horn and whether these properties are preserved as the patient ages could greatly contribute to improving repair outcomes.

Methods: A cadaveric experimental study was conducted on human sutured menisci classified into three n = 22 age groups (young ≤55; 55 < middle-aged ≤75; 75 < old) were subjected to load-to-failure test by suture pulling. Meniscal thickness at the suture hole was measured and the applied traction force and tissue deformation in the suture area in the direction of traction were recorded during the test. The traction load that initiated the meniscal cut-out, F_c, maximum load borne by the meniscus, F_u, tissue stress at the cut-out initiation, S_c, and equivalent stiffness modulus at the suture area, m_s, were calculated.

Results: At the tissue level, the resistance in terms of S_c decrease with age (young: 47.2 MPa; middle-aged: 44.7 MPa; old: 33.8 MPa) being significantly different between the young and the old group (p = 0.015). Mean meniscal thickness increased with age (young: 2.50 mm; middle-aged: 2.92 mm; old: 3.38 mm; p = 0.001). Probably due to thickening, no differences in resistance were found at the specimen level, i.e., in F_c (overall mean 58.2 N) and F_u (overall mean 73.6 N). As for elasticity, m_s was lower in the old group than in the young group (57.5 MPa vs. 113.6 MPa, p = 0.02) and the middle-aged one (57.5 MPa vs. 108.0 MPa, p = 0.04).

Conclusion: Regarding the influence of age on the sutured meniscal horn tissue, *in vitro* experimentation revealed that meniscal horn specimens older than 75 years old had a more elastic tissue which was less resistant to cut-out than younger menisci at the suture hole area. However, a thickening of the meniscal horns with age, which was also found, leveled out the difference in the force that initiated the tear, as well as in the maximum force borne by the meniscus in the load-to-failure test.

KEYWORDS

human meniscal tissue, meniscal root detachment, suture, age influence, tissue resistance

E.2 Publication in Q1: Assessment of surrogate models for research on resistance and deformation of repairs of the human meniscal roots: Porcine or older human models?

This article is published in the journal Applied Sciences, year 2024, volume 14(2), 670. The journal is indexed in the JCR at 44/179 (Q1) in the year of publication, with an impact factor of 2.5.

It contains the most relevant results of the work presented in chapter 5 of the thesis, in which the use of porcine meniscal models or aged human specimens as surrogates for young human specimens is analysed when the objective is related to the resistance and/or deformation of the meniscal tissue around the suture hole once the meniscal horns have undergone suture repair.

The first page of the publication is included on the following page.

applied sciences

MDPI

Article

Assessment of Surrogate Models for Research on Resistance and Deformation of Repairs of the Human Meniscal Roots: Porcine or Older Human Models?

Alejandro Peña-Trabalon, Ana Perez-Blanca, Salvador Moreno-Vegas, M. Belen Estebanez-Campos and Maria Prado-Novoa *

Laboratory of Clinical Biomechanics of Andalusia (BIOCLINA), 29071 Málaga, Spain; alejandropt98@uma.es (A.P.-T.); anaperez@uma.es (A.P.-B.); belen@uma.es (M.B.E.-C.)
* Correspondence: maria.prado@uma.es

Featured Application: This study provides data and rationales to aid researchers in the selection of surrogate models for in vitro assessments of surgically repaired meniscal roots. The results are potentially applicable in experimental in vitro investigations aimed at evaluating the performance of surgical repair both in existing approaches and emerging techniques. It could also be of interest for studies seeking to adjust material models of the meniscal tissue around the suture area for incorporation into computational models.

Abstract: Meniscal root repair is not routinely recommended for patients over 75 years old, yet surrogate age-unrestricted human or porcine models are used for its evaluation. This study assesses the suitability of older human or porcine meniscus models for in vitro testing of the sutured meniscal horn. Three groups of menisci underwent a load-to-failure test with continuous monitoring of the traction force and deformation around the suture: human < 75 years, human ≥ 75 years, and porcine. Both surrogate models were compared to the younger group. The porcine group exhibited a 172.1%-higher traction force before tearing ($p < 0.001$) and a 174.1%-higher ultimate force ($p < 0.001$), without there being differences between the human groups. At tissue level, the older group had a 28.7%-lower cut-out stress ($p = 0.012$) and the porcine group had a 57.2%-higher stress ($p < 0.001$). Regarding elasticity at the sutured area, a 48.1%-greater deformation rate was observed in the older group ($p < 0.001$), without difference for the porcine group. In conclusion, neither the porcine nor the older human model demonstrated a clear advantage as a surrogate model for young human sutured meniscal horns. The older human meniscus is preferable for resistance at the specimen level, while the porcine model better represents deformation in the sutured zone.

Keywords: meniscal repair; surrogate models; human meniscal tissue; meniscal root detachment; suture; resistance; deformation

Citation: Peña-Trabalon, A.; Perez-Blanca, A.; Moreno-Vegas, S.; Estebanez-Campos, M.B.; Prado-Novoa, M. Assessment of Surrogate Models for Research on Resistance and Deformation of Repairs of the Human Meniscal Roots: Porcine or Older Human Models? *Appl. Sci.* **2024**, *14*, 670. https://doi.org/10.3390/app14020670

Academic Editors: Cecilia Surace and Alice Berardo

Received: 29 November 2023
Revised: 8 January 2024
Accepted: 10 January 2024
Published: 12 January 2024

1. Introduction

The menisci of the knee are fixed by ligamentous attachments that retain them in the intra-articular zone while allowing the necessary mobility (up to 10 mm [1]) to be placed between the tibia and femur at the contact area, which shifts during flexion–extension. The meniscal roots are the only ligamentous attachments with direct insertion into the bone, playing a crucial role in meniscal function. Complete meniscal root avulsion has been shown to cause significant changes in the contact biomechanics of the knee, increasing pressure and decreasing the contact area on the cartilage of the affected compartment, changes that may be similar to those observed for total meniscectomy [2–4]. Biomechanical studies have also highlighted the role of meniscal roots as secondary stabilizers of knee kinematics, contributing to the restriction of anteroposterior translation and internal–external rotation [5–7]. From a clinical point of view, a meniscal root detachment can

E.3 Contribution to an international congress: 27th Congress of the European Society of Biomechanics (ESB), 26 - 29 June 2022, Porto, Portugal.

A contribution was presented at the European Society of Biomechanics (ESB) Congress: Lateral meniscus anterior root avulsion increases contact pressures: a Finite Element study, which provides a first meniscus model, with which changes on joint contact biomechanics when lateral meniscus anterior root avulsion occurs, are computationally analysed.

The first page of the contribution is included on the following page.

LATERAL MENISCUS ANTERIOR ROOT AVULSION INCREASES CONTACT PRESSURES: A FINITE ELEMENT STUDY

Peña-Trabalón A. (1), Moreno-Vegas S. (1), Estebanez B. (1), Prado-Novoa M. (1), Espejo-Reina A. (1, 2), García-Vacas F. (1), Perez-Blanca A. (1)

1. Clinical Biomechanics Laboratory of Andalusia, University of Malaga, Spain
2. Vithas Malaga Hospital, Spain

Introduction

Deleterious consequences of posterior meniscal root detachment have been related to variations in contact pressure (CP) distribution seen in biomechanical investigations. However, little is known about the biomechanical effects of lateral anterior root avulsions (ARA), despite clinical studies reporting it as a lesion concomitant with anterior cruciate ligament (ACL) injuries and tibial fractures [1,2] and as an iatrogenic injury during ACL reconstructions [3,4]. This work analyzes variations in CP due to lateral meniscus (LM) ARA using a knee finite element model (FEM).

Methods

A human cadaveric specimen was used to create and validate a knee FEM to compute the tibio-femoral CP distribution in three conditions of the LM: intact, with ARA and with posterior root avulsion (PRA).
Meniscus, cartilages, femur and tibia were segmented from MRI data (T1, thickness=3.5mm) using 3D Slicer®. From the point clouds extracted, solid models were built and assembled in Solidworks®. Cartilage models were refined using a 3D Laser Scanner (Picza LPX-1200, Roland DG, Hamamatsu, Japan). From the assembly, a FEM was defined in Abaqus®. Ligament insertions were identified in MRI images (Figure 1).

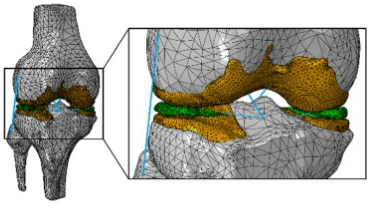

Figure 1: Knee FEM developed in Abaqus®.

Bones were assumed rigid. Meshes of cartilages and menisci were created using 1.5mm second order tetrahedral elements. Linear isotropic elastic materials were applied to the menisci (E = 59MPa) and cartilages (E = 5MPa). Menisci root and ligaments were modelled as nonlinear elastic axial springs with material properties extracted from the literature [5,6]. Surface-to-surface contact was defined at all menisci/cartilage and cartilage/cartilage interfaces.
To validate the model, the same specimen with intact menisci was subjected to an experimental axial compression test with the knee in extension under a 1000N load. A pressure sensor (K-scan 4000, Tekscan Inc., Boston, MA) placed between menisci-tibial cartilage captured the CP.
Boundary conditions were replicated in the FEM and CP given by the two methods were compared. The validated model was used to compute the CP distributions in the three pre-stablished conditions of the lateral meniscus.

Results

In the intact condition, the CP distributions of experimental and FEM methods were similar (Figure 2). In ARA and PRA, the CP increases and the contact area decreases (Table 1).

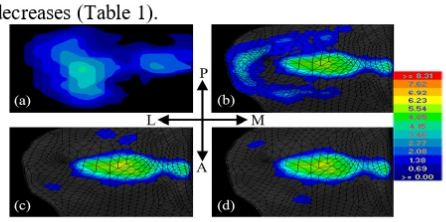

Figure 2: Tibial cartilage CP: (a) Intact experimental; (b) Intact FEM; (c) ARA FEM; (d) PRA FEM.

FEM	Pmax	Pavg	Contact Area
Intact	6.40MPa	1.02MPa	578.28mm^2
ARA	6.92MPa	2.00MPa	387.01mm^2
PRA	6.81MPa	1.98MPa	367.49mm^2

Table 1: FEM contact area, maximum and average pressures in the three conditions of the lateral meniscus.

Discussion

Changes observed in knee contact biomechanics after lateral meniscus ARA indicated potential for similar cartilage damage than observed after a PRA. Since most daily activities and sports are done in low flexion angles in which anterior roots bear most of the load, an ARA could be even more critical. Therefore, special attention should be paid to diagnostic and treatment of this injury.

References

1. Krych A. et al, J Am Acad Orthop Surg, 28:491-9, 2020.
2. Menge TJ. et al, J Orthop Res, 47(5), 2018.
3. Kodama Y. et al, J Orthop Res, 28(11), 2020.
4. Kodama Y. et al, KSSTA, 28:3517-23, 2020.
5. Orozco, G.A. et al, Sci Rep, 8:2323, 2018.
6. Peña, E. et al, Clin Biomech, 20:498-507, 2005.

Acknowledgements

This work was supported by MCIU/AEI/FEDER, EU Grant RTI2018-094339-B-I00 and the University of Malaga.

E.4 Contribution to an international congress: XV Iberoamerican Congress of Mechanical Engineering (CIBIM), 22 - 24 November 2022, Madrid, Spain.

A contribution was presented at the Iberoamerican Congress of Mechanical Engineering (CIBIM): Biomechanical effects of avulsion of the anterior root of the lateral meniscus and influence of collateral ligaments on its extrusion: a Finite Element study, which provides further insight into the influence of modelling collateral ligaments as axial springs or as solid elements on meniscal extrusion when an anterior root tear of the lateral meniscus occurs. This is studied by making use of the finite element model initially developed.

The first page of the contribution is included on the following page.

XV Congreso Iberoamericano de Ingeniería Mecánica
XV Congresso Ibero-americano de Engenharia Mecânica
Madrid, España, 22-24 de noviembre de 2022

Efectos biomecánicos de la avulsión de la raíz anterior del menisco lateral e influencia de los ligamentos colaterales en su extrusión: un estudio de elementos finitos

Alejandro Peña-Trabalon[1,2,3], Salvador Moreno-Vegas [2,3,5], Maria Belen Estebanez Campos[1,2,6], Maria Prado-Novoa[1,2,7], Ana Perez-Blanca[1,2,8]

[1]Universidad de Málaga, España.
[2] Laboratorio de Biomecánica Clínica de Andalucía (BIOCLINA), España. Email: bioclina@uma.es
[3]Instituto de Investigación Biomédica de Málaga (IBIMA), España.
[4]alejandropt98@uma.es
[5]smorenov@uma.es
[6]belen@uma.es
[7]maria.prado@uma.es
[8]anaperez@uma.es

Resumen

Este trabajo aborda el estudio de las variaciones en las áreas y presiones de contacto cuando se produce una avulsión de la raíz anterior del menisco lateral, la cual está muy poco estudiada comparativamente con la avulsión de la raíz posterior, y el efecto sobre la extrusión de este menisco cuando se modela el ligamento colateral lateral como elemento sólido, frente a su tratamiento como muelle axial elástico no-lineal. Se desarrolló un Modelo de Elementos Finitos validado experimentalmente, incorporando este ligamento como banda sólida y como muelle axial. La avulsión de la raíz anterior implica un aumento de las presiones de contacto medias y máxima, y una disminución del área de contacto, alteraciones similares sobre los parámetros de contacto a cuando se produce una avulsión de la raíz posterior, siendo más crítica la primera, debido a que la mayor parte de la carga de actividades diarias recae sobre ella. Incorporar el ligamento como banda sólida supone significativas variaciones sobre la extrusión meniscal, así como sobre los parámetros de contacto.

Palabras clave: Ligamento Colateral Lateral; Menisco Lateral; Extrusión; Modelo Elementos Finitos.

Abstract

This work deals with the study of the variations in the contact areas and pressures when an anterior root avulsion of the lateral meniscus occurs, which is very little studied compared to the avulsion of the posterior root, and the effect on the extrusion of the lateral meniscus. this meniscus when the lateral collateral ligament is modeled as a solid element, as opposed to its treatment as a non-linear elastic axial spring. An experimentally validated Finite Element Model was developed, incorporating this ligament as a solid band and as an axial spring. Anterior root avulsion involves an increase in medium and maximum contact pressures, and a decrease in the contact area, similar changes on contact parameters to when a posterior root avulsion occurs, being more critical the first, because most of the load of daily activities falls on it. Incorporating the ligament as a band supposes significant variations on the meniscal extrusion, as well as on the contact parameters.

Keywords: Lateral Collateral Ligament; Lateral Meniscus; Extrusion; Finite Element Model.

E.5 Contribution to an international congress: 28th Congress of the European Society of Biomechanics (ESB), 9 - 12 July 2023, Maastricht, Netherlands.

A contribution was presented at the European Society of Biomechanics (ESB) Congress: Age influence on cut-out resistance of sutured meniscus: An experimental cadaveric study, which disseminates the results obtained after the experimental tests of Chapter 4, concerning the effect of age on the parameters that mechanically characterize the resistance of the human meniscal horn repaired by suturing establishing a division into two age groups.

The first page of the contribution is included on the following page.

AGE INFLUENCE ON CUT-OUT RESISTANCE OF SUTURED MENISCUS: AN EXPERIMENTAL CADAVERIC STUDY

A. Peña-Trabalon (1), B. Estebanez-Campos (1), S. Moreno-Vegas (1), A. Perez-Blanca (1), M. Prado-Novoa (1)

1. Clinical Biomechanics Laboratory of Andalusia (BIOCLINA), University of Malaga, Spain

Introduction

Surgical treatment of meniscal root detachment is changing from partial meniscectomy to root reinsertion with sutures [1] due to alterations in the knee joint contact biomechanics and early cartilage loss development [2]. Suture fixation techniques of meniscal roots can be grouped into transtibial [3] and *in situ* fixations [4], both techniques pierce the meniscal horn to pass a suture thread through the hole and reconnect meniscus to bone. Despite its importance for the survival of the repair, few works focus on determining the resistance of meniscal tissue cut-out by direct thread traction on the suture hole and, as far as we are aware, the influence of age on this resistance has not been yet studied.

Methods

This study tested 44 half human meniscal horns (resulting from splitting the meniscus perpendicularly to its transverse plane in two) of different age group: young $\leq$ 60; 60 < old. They were sutured with Nº2 UHPW thread using a simple stitch. Two ink points at the suture hole area were marked on the meniscus surface aligned with the direction of the longitudinal meniscal root fibers. A displacement-controlled load-to-failure test was conducted using an universal testing machine. The meniscal horn was fixed with its longitudinal root fibers aligned with the suture thread and the traction direction (Figure 1). During testing, the marks were continuously recorded using a video camera synchronized with the testing bench. Using a custom videogrammetry software, evolution of the distances between marks was computed and used to determine the start of meniscal tissue cut-out at the suture hole.

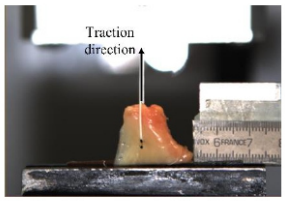

Figure 1: Meniscal horn located in the testing machine.

Meniscal horn tissue cut-out resistance, S_c, was:

$$S_c = \frac{F_c}{d \cdot t} \qquad (1)$$

where F_c is the traction at cutting time, and $d \cdot t$, the projected suture-tissue contact area at the hole, where d is the thread diameter, and t, horn thickness at the hole.

Two-tailed independent measure t tests were conducted to evaluate differences between groups. P values ≤ 0.05 were regarded as significant.

Results

For tissue cut-out resistance, S_c, no significant differences between groups were found for lateral meniscus specimens. For medial meniscus, the young group needed a higher stress level to start tissue cut-out (Figure 2a). For each age group, average resistance was higher in medial specimens than in the lateral ones.

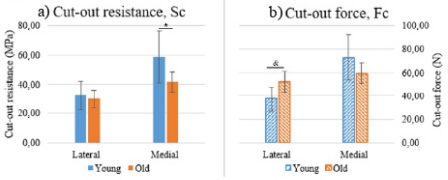

*Figure 2: Meniscal horn tissue at cut-out. Significant differences, *: p=0.032; &: p=0.038.*

Regarding specimen resistance, F_c, for the lateral meniscus significant higher values were found for the old group, due to its higher thickness. No differences were found for the medial meniscus (Figure 2b). Medial meniscus showed higher average F_c than lateral ones.

Discussion

Medial meniscal horn showed more tissue and specimen resistance for both groups. At the lateral horn, no differences were found for S_c between age groups, but due to its age-thickening, F_c was significantly higher for the older group. However, at the medial horn the opposite was found. The older tissue was less resistant, but due to a lower age-thickening, its F_c did not result significantly different. Therefore, from a biomechanical point of view there is no reason to not repair detachments of older lateral meniscus roots using suture techniques, as currently done with younger menisci.

References

1. LaPrade R.F. et al, JAAOS, 23(2):71-76, 2015.
2. Perez-Blanca A. et al, Arthroscopy, 32:624-633, 2015.
3. Ahn J. et al, Knee Surg Sports Traumatol Arthrosc, 15:1510-1513, 2007.
4. Cuellar A. et al, Arthroscopy Techniques, 6(5):e1919-e1925, 2017.

Acknowledgements

This work was supported by the project UMA20-FEDERJA-116, Junta de Andalucía (grant P20-00294) and the University of Málaga.

E.6 Contribution to a national congress: XII Spanish Chapter of the European Society of Biomechanics (ESB), 2 - 3 November 2023, Málaga, Spain.

A contribution was presented at the Spanish Chapter of the European Society of Biomechanics (ESB): Influence of age on the resistance of sutured meniscal horn: An experimental cadaveric study, which disseminates the results obtained after the experimental tests in Chapter 4, concerning the influence of age on the mechanical parameters characterising the behaviour of meniscal tissue of sutured human meniscal horns in terms of strength, establishing a division into three age groups, different from the one shown in contribution E.5.

The first page of the contribution is included on the following page.

XII Reunión del Capítulo Español de la Sociedad Europea de Biomecánica (ESB)
2 - 3 de noviembre de 2023, Málaga

INFLUENCIA DE LA EDAD EN LA RESISTENCIA DEL CUERNO MENISCAL SUTURADO: ESTUDIO CADAVÉRICO EXPERIMENTAL

Peña-Trabalon A.[1], Estebanez-Campos B.[1], Moreno-Vegas S.[1], Perez-Blanca A.[1], Prado-Novoa M.[1]

[1] Laboratorio de Biomecánica Clínica de Andalucía (BIOCLINA), Universidad de Málaga, España, alejandropt98@uma.es

Introducción

El tratamiento quirúrgico del desprendimiento de la raíz meniscal está cambiando de la meniscectomía parcial, a la reparación de la raíz con suturas.[1] Las técnicas de fijación con suturas de las raíces meniscales pueden agruparse en transtibiales[2] y fijaciones *in situ*.[3] Sin embargo, ambas técnicas perforan el cuerno meniscal para reinsertar la raíz meniscal al hueso. Pocos trabajos se centran en determinar la resistencia al corte del tejido meniscal por tracción directa del hilo en el orificio de sutura y, que sepamos, aún no se ha estudiado la influencia de la edad en esta resistencia.

Materiales y métodos

Se analizaron 66 cuernos meniscales de diferentes grupos de edad, sin signos de degeneración avanzada (<grado 3, Pauli et al. [4]): jóvenes ≤ 55; 55 < mediana edad ≤ 75; edad avanzada > 75. Se realizó una sutura simple con hilo UHMWPE Nº2. En la superficie de cada menisco y alineados con las fibras longitudinales de su raíz, se marcaron con tinta dos puntos en la zona del orificio de sutura. El cuerno meniscal se fijó con sus fibras longitudinales alineadas con el hilo de sutura y la dirección de carga (Figura 1). Se realizó un ensayo de tracción a rotura controlado por desplazamiento utilizando un banco de ensayos uniaxial. Durante el ensayo, las marcas se grabaron mediante una cámara de vídeo sincronizada con la máquina uniaxial. Utilizando un software de videogrametría de desarrollo propio, se calculó la evolución de las distancias entre las marcas y se utilizó para determinar el inicio del corte del tejido meniscal en el orificio de sutura.

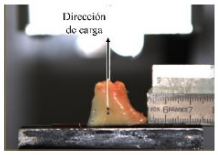

Figura 1: Cuerno meniscal en el banco de ensayos uniaxial.

La resistencia al corte del tejido del cuerno meniscal, S_c, se calculó como:

$$S_c = \frac{F_c}{d \cdot t} \qquad (1)$$

Donde F_c es la fuerza en el momento del corte y $d \cdot t$, el área proyectada de contacto sutura-tejido en el orificio, donde d es el diámetro del hilo, y t, el espesor del cuerno en el orificio.

Mediante una prueba ANOVA se buscaron diferencias globales con la edad, y cuando se encontraron, se realizaron comparaciones entre grupos mediante test de *t_student* con corrección de Bonferroni. Los valores $p \leq 0.05$ se consideraron significativos.

Resultados

En cuanto a la resistencia al corte del tejido, S_c, se encontraron diferencias significativas globales entre todos los grupos (p=0.012). El tejido de los meniscos jóvenes mostró una resistencia mayor a la de los meniscos de edad avanzada (p=0.015) y el de mediana edad reflejó una tendencia a ser más resistente que el de edad avanzada (p=0.061) (Figura 2a).

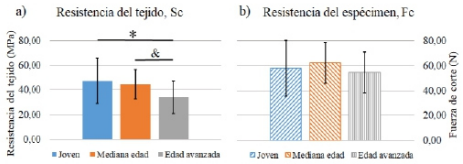

*Figura 2: (a) Resistencia al corte del tejido; (b) Resistencia del espécimen. Diferencias significativas, *:0.015; &: 0.061.*

En cuanto a la resistencia del espécimen, F_c, no se observaron diferencias significativas globales entre los grupos (Figura 2b).

Conclusión

Referente a la resistencia al corte del tejido meniscal en el entorno del orificio de sutura, S_c, los meniscos sin signos de degeneración avanzada tanto jóvenes como de mediana edad resultaron más resistentes que los de edad avanzada. Sin embargo, debido al engrosamiento de los especímenes con la edad, la resistencia del espécimen, F_c, se nivela. Por lo tanto, desde un punto de vista biomecánico, no hay razón para no reparar los desprendimientos de las raíces de los meniscos de edad avanzada mediante sutura, como se hace actualmente con los meniscos más jóvenes.

Agradecimientos

Este trabajo ha sido financiado por el proyecto UMA20-FEDERJA-116, la Junta de Andalucía (ayuda P20-00294) y la Universidad de Málaga.

Referencias

[1] LaPrade R.F. *et al.*, JAAS. 23(2): 71-76, 2015.
[2] Ahn J. *et al.*, Knee Surg Sports Traumatol Arthrosc. 15:1510-1513, 2007.
[3] Cuellar A. *et al.*, Arthroscopy Techniques. 6(5): e1919-e1925, 2017.
[4] Pauli C. et al, Osteoarthritis Cartilage. 19: 1132-41, 2011.

E.7 Contribution to an international congress: 29th Congress of the European Society of Biomechanics (ESB), 30 - 3 July 2024, Edinburgh, Scotland.

A contribution was presented at the European Society of Biomechanics (ESB) Congress: Compressive relaxation properties of human meniscus increase under combined traction and compression, which disseminates the results obtained after the experimental indentation tests of Chapter 6, concerning the effect of the incorporation of physiological tensile loads in circumferential direction during indentation on parameters characterizing the compression behaviour of the sutured meniscal tissue.

The first page of the contribution is included on the following page.

COMPRESSIVE RELAXATION PROPERTIES OF HUMAN MENISCUS INCREASE UNDER COMBINED TRACTION AND COMPRESSION

Alejandro Peña-Trabalon (1), Luisa de Roy (2), Ana Perez-Blanca (1), Maria Prado-Novoa (1), Andreas Martin Seitz (2)

1. Clinical Biomechanics Laboratory of Andalusia (BIOCLINA), University of Malaga, Spain
2. Institute of Orthopaedic Research and Biomechanics, Ulm University Medical Centre, Ulm, Germany

Introduction

Physiologically, the meniscal horns are subjected to a complex loading combination of compressive axial forces and internal circumferential tensile loading [1]. However, while the compressive properties of human menisci have been extensively studied [2-5], the impact of tensile loading on the compressive properties is unknown. Therefore, the aim of this study was to analyze the changes in the compressive relaxation properties of the meniscal horn under combined axial compression and circumferential traction.

Methods

The study included 27 human meniscal horns, derived from 16 patients (65 ± 6yrs; 10 female, 6 male), who underwent total knee replacement surgery. Each horn was sutured with Nº2 UHMWPE surgical thread using a simple stitch. In the cranial surface around the suture hole, seven measurement points were marked using a tissue marker. A multiaxial mechanical tester (MACH-1 v500css, Biomomentum Inc., Laval, QC, Canada) was employed to conduct a non-destructive indentation test using a spherical indenter of ∅2 mm (Figure 1) to determine the relaxation behavior under three conditions of traction induced by a single suture: unloaded, 10 N and 20 N. The pulling force is applied to the horn by a thread simulating a root repair by suturing. The test was run at contact velocity of 0.5 mm/s, contact criteria of 0.049 N, indentation amplitude of 0.5 mm, indentation velocity of 0.25 mm/s, and relaxation time of 20 s [4].

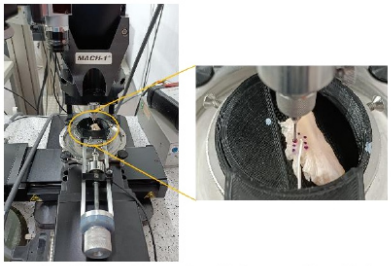

Figure 1: Sutured meniscal horn placed in the multiaxial mechanical tester.

For each traction condition two parameters where computed: the maximum force in the relaxation period (F_{max} *in* N) and the relaxation modulus at 20s (E_{t20} *in* MPa):

$$E_{t20} = \frac{\sigma_{t20}}{\varepsilon} = \frac{F_{t20}/A}{\Delta L/h} \quad (1)$$

with F_{t20} being the force at 20s, A the meniscus-indenter contact area after reaching the indentation amplitude, ΔL, and h the thickness of the sample. Differences between groups were evaluated by an ANOVA test. When a global significant difference was detected (p values ≤ 0.05), a Student´s t-test with Bonferroni correction was performed between the groups.

Results

Significant higher values for F_{max} (Figure 2a) and E_{t20} (Figure 2b) were found under simultaneous traction at 10N and 20N levels compared to the unloaded group.

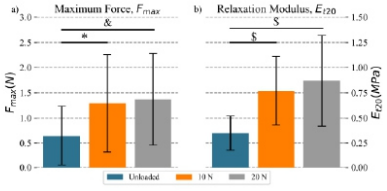

*Figure 2: Meniscal horn properties: a) Maximum force; b) Relaxation modulus. *: p=0.02; &: p=0.007; $: p<0.001.*

Between the two traction levels, 10N and 20N, no significant differences were found in any parameter.

Discussion

When applying 10 or 20N of traction, the values of the maximum force in the relaxation period and the relaxation modulus at 20 s of the meniscal horn are more than the double of the values in the no-traction state. Therefore, the values obtained with isolated compression should not be transferred to physiological loading conditions that involve combined traction and compression. This study focuses on suture-repaired meniscal roots, further research is needed to confirm whether the results are applicable to healthy meniscal roots with natural anchoring.

References

1. Messner, K. et al, J Anat, 193(2):161-178, 1998.
2. Fischenich, K. M. et al, J Biomech, 48(8):1407-1411, 2015.
3. Moyer, J. T. et al, J Biomech, 45:2230-2235, 2012.
4. Seitz, A. M. et al, Front Bioeng Biotechnol, 9:659989, 2021.
5. Sweigart, M.A. et al, Ann Biomed Eng, 32:1569-79, 2004.

Acknowledgements

This work was supported by the University of Málaga and the Ministry of Universities of the Spanish Government.

E.8 Contribution to an international congress: 29th Congress of the European Society of Biomechanics (ESB), 30 - 3 July 2024, Edinburgh, Scotland.

A contribution was presented at the European Society of Biomechanics (ESB) Congress: Method for assessing the breaking starting strength of meniscal horns from suture retention tests, which, using the results obtained in Chapter 3 with porcine meniscal specimens and Chapter 4 with human specimens, establishes a robust methodology to identify the instant of onset of tissue cut-out of the repaired meniscal tissue when it is subjected to suture-induced traction.

The first page of the contribution is included on the following page.

METHOD FOR ASSESSING THE BREAKING STARTING STRENGTH OF MENISCAL HORNS FROM SUTURE RETENTION TESTS

A. Peña-Trabalon (1), A. Perez-Blanca (1), B. Estebanez-Campos (1), S. Moreno-Vegas (1), M. Prado-Novoa (1)

1. Clinical Biomechanics Laboratory of Andalusia (BIOCLINA), University of Malaga, Spain

Introduction

Surgical repair of a detached meniscal root is performed via a transtibial or in situ technique, using sutures to fix the meniscus to restore knee biomechanics [1]. A critical aspect to prevent repair failure is the capacity of the tissue to hold the sutures subjected to forces throughout surgery and the postoperative period. Previously, visual inspection of video-monitored suture retention tests of meniscal horns [2] and other soft tissues [3], allowed the identification of a breaking starting point that initiates tissue damage, better representing its suture retention capacity than the final failure. In this scenario, it is key to quantifying the Breaking Starting Strength (BSS). Some studies have analyzed horn resistance at the tissue-suture interface [4-5], but a robust methodology for computing the BSS has not been described. This work proposes a method to identify the BSS directly from the load curves of suture retention tests. The methodology has been validated using meniscal horns in human and porcine models.

Methods

Eight porcine meniscal roots (5 months and 100 kg) and 60 human meniscal roots (62(20) years expressed as mean(SD)) were included in the study. A Nº2 UHMWPE thread was inserted in the meniscal horn at 5mm from its internal edge and its root junction using a single simple stitch. Following the positioning protocol described by Peña-Trabalon et al. [5], the sutured menisci were subjected to displacement-controlled Load-To-Failure (LTF) tests at 0.1mm/s (Figure 1b), while continuously video-monitored at 4 fps.

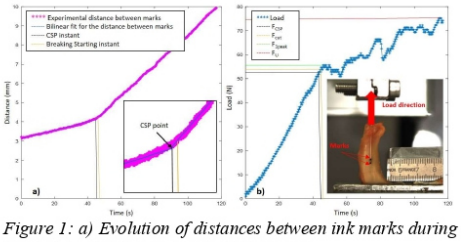

Figure 1: a) Evolution of distances between ink marks during the test. b) Test set-up and load evolution

Distances between two ink marks placed around the suture hole were computed using videogrametry [5]. The curve of the evolution of the distances between marks (Figure 1a) was approximated by a bilinear fit. The fitting process searched the optimal transition or change of slope point (CSP) and the slopes in both intervals to minimize the RMSE. Subsequently, the time coordinate of the CSP was used to determine the traction borne by the specimen at that instant, F_{csp}. Additionally, in the porcine group the breaking starting point was visually identified from the images in a cumbersome and subjective task and the load withstood by the specimen at that instant computed, F_{cut}.

From the load curve in the LTF test, the first peak load, F_{1peak}, and the ultimate load, F_U, were recorded. F_{1peak} was computed as the first point on the curve with a value greater than its two neighboring values, with a prominence higher than 2 and a width greater than 0.5ms. Peak width was calculated as the time distance between load curve intersections with a horizontal line under the peak at a distance equal to half its prominence. To focus on tissue strength, all forces were normalized by the horn thickness at the hole area (F^*_{csp}, F^*_{1peak}, F^*_U).

Results

In the porcine model, comparison of the observed F_{cut} and the computed F_{csp} confirmed to be virtually coincident (difference under 6.7%). In the human group, for the normalized force values (Table 1), difference between F^*_{csp} and F^*_{1peak} was 6.4%(5.1%), with F^*_{1peak}, always higher. F^*_U was also higher than F^*_{csp} with a notable larger difference of 15.6%(12.2%) and, more important, with a wide variation range of [0.61, 9]%.

Group	F^*_{csp}	F^*_{1peak}	F^*_U	Horn thickness
Porcine	30(3)	31(3)	33(4)	3.3(0.4)
Human	22(8)	23(8)	26(10)	2.9(0.7)

Table 1: Forces normalized by the horn thickness in N/mm and thickness of the meniscal horn at the suture area in mm. Values are expressed as mean (standard deviation).

Discussion

Our study found that the BSS of the meniscal horn can be determined from F_{csp} using a robust and automated algorithm with minimal errors, albeit requiring a videogrammetric system. Alternatively, F_{1peak} is proposed as a viable estimator that avoids the need for videogrammetric analysis, though it entails a mean overestimation of 6.4%, requiring consideration of a safety factor of this magnitude. In contrast, F_U is not a recommended estimator given its substantial overestimation of the breaking strength.

References

1. Perez-Blanca et al, Arthroscopy, 32:624-633, 2015.
2. Perez-Blanca et al, Int. Orthop., 42:811-818, 2018.
3. Pensalfini et al. JMBBM, 77: 711-717, 2018
4. Vertullo C. et al, Orthop. J. Sports Med., 9 (4), 2021.
5. Peña-Trabalón et al, Front. Bioeng. Biotechnol., 11:1-11, 2024.

Acknowledgements

This work was supported by the project UMA20-FEDERJA-116 and the University of Málaga.